A STUDY OF

IRRADIATION EFFECTS IN SOLIDS.

by

M. E. BROWN, B.Sc. Hons. (Rand).

A thesis submitted in fulfilment of the
requirements for the Degree of Doctor of Philosophy
of Rhodes University.

Department of Chemistry,
Rhodes University,
Grahamstown,
South Africa.

November, 1965.

A C K N O W L E D G E M E N T S.

The author wishes to express his appreciation to:

Prof. E.G. Prout, M.Sc., Ph.D.(S.A.), of Rhodes University, for his direction and keen interest in all aspects of the work and to thank him for valuable criticisms;

Mr. L. Nassimbeni, M.Sc.(Rhodes), for valuable advice and discussions on the X-ray crystallographic study;

Messrs. S. Harris, G. Ranftelshofer and F. van der Water, for technical assistance; and

Mrs. R. Heffer, Miss C. Kay, Mr. A. Sonemann and Mr. G. Walters, for assistance in preparation of this thesis.

The author also acknowledges financial assistance from the South African Council for Scientific and Industrial Research.

C O N T E N T S.

3.3./...

4./...

5.4./...

7.3./...

7.3.10.4./...

1. INTRODUCTION.

1.1 THE THERMAL DECOMPOSITION OF SOLIDS.

Absorption of heat quanta in solids results in increased atomic vibration. Only a few of the quanta correspond to the high-energy limit of the Boltzmann distribution and can lead to bond rupture. Under isothermal conditions heat quanta are distributed uniformly throughout the volume of the crystal. If this alone governed the start of thermal decomposition, decomposition could begin at any point in the crystal and would proceed by a first-order kinetic mechanism. Different positions in the crystal, however, are not equivalent in reactivity. Bond rupture takes place at those points in the lattice where, at a given instant, the bond is for some reason weaker than at other points. These active points are generally lattice imperfections, such as vacancies, interstitials, jogs in dislocations, Smekal cracks etc., as well as the crystal surface. The number of initial decomposition centres, or nuclei, formed in a given time will depend upon the number of these potential nucleus-forming sites as well as the activation energy for nucleus formation. The nature of the nuclei formed is not always clearly defined, but it is generally accepted that they are composed of solid reaction product.

The difference in molecular dimensions of the product phase will result in the development of strain in the reactant lattice. A consequence of this strain is that small fragments of the new phase will be more unstable than larger fragments and further reaction will tend to occur at the interface, rather than to lead to the initiation of a very large number of fresh nuclei. The product phase thus spreads outwards from the nuclei.

Mathematical/...

Mathematical analyses of the experimental rate/time, pressure/time, or α/time curves (where α is the fraction of compound decomposed), can provide information on the process of nucleation, the shape of the nuclei formed and their mode of growth. In barium azide, for example, the nucleation process has been observed directly [1].

The applicability of a mathematical relationship, derived on the assumption of a specific process, to a portion of the curve, is not proof that the assumed mechanism actually occurs. Further evidence has often to be sought in the general chemical and physical properties of the solid (e.g. crystal structure, macroscopic chemical reactions, conductivity, etc.).

The pressure/time plot for the isothermal decomposition of a solid which decomposes, with the evolution of gas, to give a solid residue, is usually of sigmoid shape. The curve may be divided into two main sections:-

(i) The acceleratory section - which may or may not be preceded by an induction period and/or an initial burst of gas.

(ii) The decay section.

These divisions are usually associated with the production of nuclei, their growth and, beyond the point of inflexion, the overlap of nuclei and the shrinking of the reactant/product interface.

For the acceleratory period the extent of decomposition is given by the product of two terms, one of which describes the rate of nucleation, and the other the rate of growth.

Nucleation may occur according to the exponential law: $dN/dt = k N_o \exp(- kt)$ ..... (1.1) where

N_o/.....

N_o is the number of nucleus-forming sites. This equation is based on the assumption that decomposition of a single molecule or ion results in a nucleus. In the early stages of the reaction, and especially if the activation energy for nucleus formation is large (i.e. k is small):

$$dN/dt = kN_o \qquad \ldots\ldots \qquad (1.2)$$

i.e. the number of nuclei increases linearly with time.

For k very large: $N = N_o$ ..... (1.3)

i.e. nucleation is instantaneous.

Where more than one event is necessary for nucleus formation, the power law:

$$dN/dt = k't^n \qquad \ldots\ldots \qquad (1.4)$$

applies, where n is an integer. The events may be several successive decompositions at the same site, or several single decompositions at different sites, with resulting diffusion and aggregation to form an active nucleus.

n = 2, corresponds to two-dimensional growth e.g. barium styphnate monohydrate [2].

n = 3, corresponds to the formation of a fixed number of nuclei which grow three-dimensionally; or linear growth with time of two-dimensional nuclei, e.g. mercury fulminate [3].

n = 4, is the formation of compact, spherical nuclei which grow according to a linear law, e.g. ammonium chromates [4].

Garner and Hailes [5] derived the concept of linear branching chains to apply to mercury fulminate. Assuming a constant rate of nucleation and a constant branching coeffecient, k_2,

$$p = C \exp(k_2 t) \qquad \ldots\ldots \qquad (1.5)$$

Linear branching chains, however, would separate the crystal into mosiac blocks which would then decompose slowly. Branching plate-like nuclei of constant width are more acceptable. This corresponds to the spreading of the

reaction/...

reaction along the grain boundaries and dislocation network of the crystal (e.g. Silver oxalate [6]). Hill[7] has criticised the concept of "chains".

Prout and Tompkins [8] allowed for the interference of branching chains, and derived the Prout-Tompkins equation

$$\log [p/(p_f - p)] = k_2 t + C_2 \quad \ldots\ldots \quad (1.6)$$

where k_2 is the probability of the occurrence of branching, and p_f is the final pressure. One of the conditions of the equation is that $d\alpha/dt$ is a maximum (i.e. the inflexion point) at $\alpha = 0.5$. This analysis describes many solid decompositions (e.g. permanganates [9]).

A modification allowing for the inverse variation of the branching coefficient, k_2, with time was introduced by Prout and Tompkins [10] to describe the decomposition of $AgMnO_4$

$$\log [p/(p_f - p)] = k_2' \log t + C_2' \quad \ldots\ldots \quad (1.7)$$

Quite apart from the special case of branching nuclei, an analysis of random nucleation leading to the experimental law must allow for the ingestion of potential nucleation sites.

Avrami [11] dealt with the nucleation process in a study of the kinetics of phase change. He used the terms "nuclei" (germ nuclei) and "grains" (growth nuclei), for centres below and above the critical size for steady growth, respectively. The number of nuclei decreases in two ways with time. Some become activated for growth and others are ingested by growing grains. The nuclei ingested before activation are termed "phantom nuclei". The grains (phantom nuclei included), taken to full growth and neglecting impingement upon one another are referred to as "extended grains".

The type of grain interaction applicable to crystalline solids is the adherence of grains to grow at

common interfaces, while continuing to grow normally elsewhere.

If N_o is the number of nuclei randomly distributed/unit vol. at time t = o; N(t) the number of grains (growth nuclei) at time t; N'(t) the number of nuclei/unit vol. at t; and N"(t) the number of nuclei ingested/unit vol. at t, then:

$$-dN' = dN + dN'' \quad \ldots\ldots \quad (1.8)$$

$$dN = k_1 N' \, dt \quad \ldots\ldots \quad (1.9)$$

$$dN'' = \frac{N'}{1-\alpha} \, d \quad \ldots\ldots \quad (1.10)^{12}$$

For dN" negligible, $N' = N_o \, e^{-k_1 t}$ ..... (1.11)

Allowing for ingestion:

$$\frac{dN'}{dt} + k_1 N' + \frac{N'}{1-\alpha} \frac{d\alpha}{dt} = 0 \quad \ldots\ldots \quad (1.12)$$

Re-arranging and integrating:

$$N' = N_o \, e^{-k_1 t} \, (1-\alpha) \quad \ldots\ldots \quad (1.13)$$

hence

$$dN/dt = k_1 N_o \, e^{-k_1 t} . \, (1-\alpha) \quad \ldots\ldots \quad (1.14)$$

Thus when α is small, i.e. at the beginning of the reaction, nucleation follows the exponential law.

$$N(t) = k_1 N_o \int_o^t e^{-k_1 y} \left[1 - \alpha(y)\right] dy \quad \ldots\ldots \quad (1.15)$$

For 3-dimensional growth:

$$\alpha = \frac{s k_1 N_o k_2^3}{V_o} \int_o^t e^{-k_1 y} \, (t-y)^3 \left[1-\alpha(y)\right] dy \quad (1.16)$$

s is a shape factor and

V_o is the final volume of product obtained from complete decomposition of w_o gm of original substance.

The problem of accounting for the fact that the fraction decomposed when grains overlap is less than the value of α based on calculations neglecting impingement, is tackled by the introduction of the "extended fractional decomposition", α_{ex}. This is obtained from calculation of

the/...

the extended volume, V_{ex}.

$$\alpha_{ex} = \frac{1}{V_o} \int_o^t v(t,y) \left[\frac{dN'}{dt}\right]_{t=y} dy \qquad \ldots\ldots\ldots \qquad (1.17)$$

$v(t,y)$ is the volume at time t, of a nucleus formed at time $t = y$.

$$v(t,y) = s \left[k_2 (t-y)\right]^3 \qquad \ldots\ldots\ldots \qquad (1.18)$$

where k_2 is the linear rate of isotropic growth.

Hence

$$\alpha_{ex} = \frac{s\, k_2^3\, k_1\, N_o}{V_o} \int_o^t e^{-ky} (t-y)^3 dy = \frac{V_{ex}}{V_o} \qquad (1.19)$$

The problem is thus to relate V_{ex} to the actual volume of the product, V.

If the distribution of nuclei is uniformly or even locally random, Avrami has shown that

$$V(t) = 1 - \exp\left(- V_{ex}(t)\right) \qquad \ldots\ldots\ldots \qquad (1.20)$$

Hence

$$d\alpha/d\alpha_{ex} = 1 - \alpha \qquad \ldots\ldots\ldots \qquad (1.21)$$

This satisfies the conditions:-

at $\alpha = o$, $d\alpha/dt = d\alpha_{ex}/dt$

at $\alpha = 1$, $d\alpha/dt = 0$, but $d\alpha_{ex}/dt$ is finite.

Thus

$$\alpha_{ex} = \int_o^{\infty} \frac{d\alpha}{1-\alpha} = \frac{s\, k_2^3\, k_1\, N_o}{V_o} \int_o^t e^{-k_1 t} (t-y)^3 dy \qquad (1.22)$$

or

$$-\log(1-\alpha) = \frac{6\, s\, N_o\, k_2^3}{V_o\, k_1^3} \left[e^{-k_1 t} - 1 + k_1 t - \frac{(k_1 t)^2}{2!} + \frac{(k_1 t)^3}{3!}\right] \qquad \ldots\ldots\ldots \qquad (1.23)$$

This is the most general solution for random nucleation followed by isotropic three-dimensional growth at a linear rate k_2.

For/...

For α very small, overlapping is negligible and $\alpha = \alpha_{ex}$ given above.

$$\alpha = \frac{6s\ N_o\ k_2^3}{V_o\ k_1^3}\left[e^{-k_1 t} - 1 + k_1 t - \frac{(k_1 t)^2}{2!} + \frac{(k_1 t)^3}{3!}\right] \quad \ldots\ldots\ (1.24)$$

Thus for $k_1 t$ small

$$\alpha = C.t^4 \quad \ldots\ldots\ (1.25)$$

If growth is plate-like, or for rapid nucleation and three-dimensional growth

$$\alpha = C't^3 \quad \ldots\ldots\ (1.26)$$

and for linear growth

$$\alpha = C''t^2 \quad \ldots\ldots\ (1.27)$$

In the decay period, when t is large

$$-\log(1-\alpha) = \left[\frac{s\ N_o\ k_2^3}{V_o}\right] t^3 = k\ t^3 \quad \ldots\ (1.28)$$

Erofeyev [13] derived a similar equation using a different treatment. First he derived a general kinetic equation

$$\alpha = 1 - \exp\left(-\int_o^t p\ dt\right) \quad \ldots\ldots\ (1.29)$$

where p is the probability of the reaction of an individual molecule in an interval dt. This equation involved no assumptions regarding the properties of the reacting system.

Differentiating:

$$d\alpha/dt = p \exp\left(-\int_o^t p\ dt\right) = p(1-\alpha) \quad \ldots\ (1.30)$$

$$\alpha/(1-\alpha) = p\ dt$$

$$-\ln(1-\alpha) = \int_o^t p\ dt \quad \ldots\ldots\ (1.31)$$

He then applied the general equation to the growth of reaction nuclei in solids. For 3-dimensional growth, in general, the probability p dt is proportional to the total volume of the spherical layers traced, at the instant t, around the nuclear centres that have arisen at the instant t_*. The radii of the spheres limiting the layers are:-

Y/...

$r = u(t-t_*)$ and $r + dr = u(t+dt - t_*)$

Accordingly

$$p\,dt = dt \int_0^t 4\pi u^3 (t - t_*)^2 \frac{dv}{dt}\, dt_* \quad \ldots\ldots \quad (1.32)$$

where dv/dt is the rate of formation of nuclei.

For a constant rate of nucleation, i.e. dv/dt = constant,

$$p\,dt = \text{const.}t^3\,dt$$

and $$\alpha = 1 - \exp(-kt^4) \quad \ldots\ldots \quad (1.33)$$

For cylindrical nuclei

$$\alpha = 1 - \exp(-kt^3) \quad \ldots\ldots \quad (1.34)$$

For flat nuclei

$$\alpha = 1 - \exp(-kt^2) \quad \ldots\ldots \quad (1.35)$$

In general, according to the shape of the nucleus

$$\alpha = 1 - \exp(-kt^n) \quad \ldots\ldots \quad (1.36)$$

This in known as the AVRAMI-EROFEYEV EQUATION.

In the decay period, overlap of compact nuclei results in a contracting interface. If this remains intact the Avrami-Erofeyev equation may still hold. Because of the difference in molecular volume between product and reactant phases, the interface may collapse leaving isolated blocks of material in which no nuclei are present. The same condition may arise from extensive growth of plate-like nuclei. In these isolated blocks, if each molecule has an equal probability of decomposing, the rate will be proportional to the amount of undecomposed material.

$$d\alpha/dt = k(1-\alpha) \quad \ldots\ldots \quad (1.37)$$

$$-\log(1-\alpha) = kt \quad \ldots\ldots \quad (1.38)$$

$$\log p_f/(p_f - p) = kt \quad \ldots\ldots \quad (1.39)$$

This is known as the UNIMOLECULAR DECAY LAW.

If the rate-controlling factor in the decay becomes the number of remaining unreacted molecules, not all of the molecules will be favourably situated next to a product

molecule, and

$$dp/dt = k'(p_f - p)\ P \qquad \ldots\ldots\ (1.40)$$

where P, the probability of the favoured situation, is determined by p/p_f. Thus

$$dp/dt = k'(p_f - p)\ p/p_f \qquad \ldots\ldots\ (1.41)$$

which on integration reduces to the Prout-Tompkins equation (1.6) with a constant k', different to that applying over the acceleratory period.

The rate-determining step may become the progression of the reactant/product interface. When the surface of a particle is covered with product and the interface progresses inwards, the rate will depend on the geometry of both the particle and the interface. This, for example, may be that of a contracting parallelopiped or a contracting sphere. When nucleation is confined to certain faces only, the mechanism may be that of a contracting rectangle or circle e.g. potassium hydrogen oxalate hemihydrate [14].

For a contracting sphere mechanism, assuming spherical particles of initial radius a, the fraction decomposed at time t is

$$\alpha = \frac{{}^4/_3\ \Pi a^3 - {}^4/_3\ \Pi\ (a-kt)^3}{{}^4/_3\ \Pi\ a^3}$$

$$= 1 - \left(\frac{a - kt}{a}\right)^3$$

$$= 1 - (1 - k't)^3 \qquad \ldots\ldots\ (1.43)$$

or

$$1 - (1 - \alpha)^{\frac{1}{3}} = k't \qquad \ldots\ldots\ (1.44)$$

which is the usual form of the CONTRACTING SPHERE EQUATION.

The nuclei however, may not cover the surface, and the rate of reaction can be governed by the spherical growth of single nuclei from points on the surface into the particle. Assuming a single nucleus per spherical particle, it can be

shown/...

shown that the rate would have a maximum at $\alpha = 0.593$.

Random nucleation followed by rapid surface growth has been treated by Jacobs and Tompkins [15] and leads to a linear function of log $(1 - \alpha)$ plotted against t.

e.g. dehydration of $CaCO_3.6H_2O$ [16].

Mathematical analyses thus supply information on the process of nucleaction, the approximate shape of the nuclei e.g. two or three-dimensional, and the mechanism by which they grow in size as the reaction progresses through the solid. Growth may be from a fixed number of centres, or from centres which are increasing in number as a power of time. The occurrence of branching chains of reaction can also be detected. The exact nature of the nuclei formed is however speculative.

1.2 CREATION OF NUCLEI.

Grinding [17] of a solid or e.g. in hydrates, scratching [18] the surface of the crystal can sometimes have a marked effect on the subsequent thermal decomposition. Similar effects can be caused by pre-irradiation. This similarity in the effects of mechanical damaging of the solid and pre-irradiation, suggests that pre-irradiation produces centres of damage, and that these centres are important in the processes of nucleation and growth. Irradiation of crystalline ionic solids by ultra-violet light, γ-rays and X-rays, can produce various imperfections in the crystal structure such as vacancies, interstitials, and thermal and displacement spikes, as well as extensive ionisation and exitation. The nature and concentration of these defects depend upon the energy and type of radiation used, as well as the structural characteristics of the solid.

1.3/.....

1.3 IRRADIATION AND THE PRODUCTION OF DEFECTS.

1.3.1 The Action of Light on Solids.[19]

In ionic solids all the energy states in the first band are occupied. This is the 'full band' and it is separated from the next band, which is completely empty, by several ev. Such substances are thus insulators apart from possible ionic conductivity. Irradiation of the solid, however, with light of a suitable wavelength may excite electrons into an empty band, and when this band is the conduction band, photoconductance is observed. The positive holes in the full band are readily mobile and contribute to the conductivity.

Inorganic salts show strong characteristic absorption peaks, frequently in the ultra-violet but sometimes in the visible regions. Fergusson [20] has shown that photoconductance is not observed in Na Cl at wavelengths greater than 1280Å, which corresponds to the peak of the second absorption band. Thus the first band must represent excitation levels below the conduction band. This excitation is the formation of excitons, where an exciton is an excited electron localised in the neighbourhood of its positive hole and moves as an entity [21].

Thus the immediate result of the absorption of radiation of appropriate wavelength is the production of excitons, or of free electrons and their conjugate positive holes.

Re-emission of radiation has not been observed in the first absorption band and excitons dissipate their energy by scattering and transfer of energy to imperfections [22,23]. Free electrons may return to the ground state accompanied by fluorescence or phosphorescence.

Alkali/...

Alkali halides on exposure to UV-light, X-rays or electron bombardment acquire a deep colour, characteristic of the salt, which fades gradually. Comparison of the absorption bands of the irradiated salts with those of salts doped with excess metal or halogen, gave information on the types of imperfection responsible for the absorption. F-centres have been shown to be electrons trapped at vacant anion sites [24,25], and V-centres have been identified with the interaction of positive holes and cation vacancies.

Under varying conditions of temperature and with appropriate wavelengths, more complex centres may be formed on irradiation, by further trapping of electrons and holes at F-centres and V-centres respectively, giving F'- and V'-centres. Combination of F-centres with further F-centres (R_2-centres), or with a single anion vacancy (R_1-centres) or with a cation/anion vacancy pair (M-centres); and the corresponding combinations of V-centres, all give rise to characteristic absorption bands.

The importance of these centres, formed on irradiation, and of the role of excitons and free electrons and holes, has been emphasised in their use in the explanation of mechanisms of photolysis and radiolysis. (see later).

1.3.2 Irradiation with Particles, γ-rays and X-rays.

The primary or direct effects of irradiation are ionisation, displacement and excitation, with or without displacement. Nuclear interaction with radiation, resulting in transmutation is a further possibility. The secondary effects are further excitation and disruption of the structure by electrons and atoms which have been knocked on.

Irradiation/...

Irradiation with heavy charged particles (protons, deuterons and α-particles), may be accompanied at very high energies (1000 Mev) by the emission of brehmsstrahlung. The main energy loss at lower energies is by inellastic collisions with the electrons of the stopping material.

Neutrons interact directly with atomic nuclei. The result varies from elastic collision to neutron capture, depending upon the energy of the neutrons and the nature of the nucleus.

Bombardment with high-energy electrons (10 to 100 Mev) causes the emission of X-rays by the target. Lower energy electrons interact by inelastic collisions with the electrons of the stopping material, causing excitation and ionisation.

Photons lose a relatively large amount of energy whenever they interact with matter. Some however are transmitted with their original direction and energy. As a result of the photo-electric, Compton and pair-production interactions [26], irradiation with γ-rays and with X-rays, is approximately equivalent to internal bombardment with fairly energetic electrons. Most of the energy of these electrons is dissipated in causing further ionisation. The range of secondary electrons ejected on ionisation is small and the overall result is 'spurs' of excited and ionised species.

Seitz [27] has estimated that the threshold energy for displacement (E_d) of an atom in a stable lattice site is of the order of 25 ev. Experiments on Cu [28] and Ge [29,30] metals showed that E_d is dependent on the lattice structure and the direction of displacement.

Vineyard et al [31-35] have used computer methods to study displacements in model structures. Their calculations

confirmed/....

confirmed many of the predictions of earlier cascade theories [36,37,38], viz. the existence of a threshold energy for displacement, the production of interstitials and vacancies and the occurrence of many replacement collisions for the formation of each interstitial. A focussing chain carries matter as well as energy in the fashion of a dynamic crowdion and the interstitial is produced near the end of the chain. Vacancies are left behind and may form clusters[39,40].

No allowance was made for the influence of thermal vibrations and of ionisation and excitation on the threshold and range of collisions.

Once the threshold energy is known the minimum energy required to produce displacements can be calculated for the various types of radiation and the corresponding interactions [41,42].

For γ-ray irradiation the energy of the photo-electric and pair-production recoil processes may be above the displacement threshold for light atoms. Such atoms however have small cross-sections for these processes and the effect is not important at normal gamma-ray energies.

Internal beta-irradiation by Compton electrons may produce atomic displacements. Dienes and Vineyard [43] have calculated that for γ-ray energies of approximately 1 Mev (Co^{60}), the number of atoms displaced /cm^3/sec.,(R_d), is a maximum for materials of low atomic number (Z), and decreases as Z increases. Assuming Seitz's value of 25 ev for E_d, R_d is zero at Z approximately 125. The cross-section for displacement by photo-electrons is insignificant in comparison to that of the Compton process.

Cleland, Crawford and Holmes [44] have observed displacement of atoms in Ge, irradiated using a Co^{60} source. The cross-section obtained for atomic displacement was in

fair agreement with that based on the Compton process.

Two basic mechanisms have been suggested for the conversion of electronic excitation energy into displacement energy.

Seitz [45] proposed that excitons or free electrons and holes, formed on irradiation move through the crystal until they encounter a lattice irregularity, at which point the energy is discharged into the lattice producing a local hot spot.[46] Jogs at dislocation lines are likely sites and the release of energy at a jog can induce dislocation climb i.e. vacancies can be "boiled off" at the jog. The migration of point defects may be increased by further absorption of excitons on the defect. Measurements on the pinning of dislocations in NaCl on irradiation with X-rays[47] have lent some support to this mechanism.

Varley [48,49,50] showed, from measurements of the formation of colour centres in alkali halides, that the observed cross-section for displacement was thirty times larger than for direct collision between electron and atom. He proposed a displacement mechanism involving multiple ionisation. Anions may be stripped of two or more electrons on irradiation, becoming temporarily positively charged. The electrons are dispersed and the ion is left in an unstable position surrounded by other positive ions. This may lead to ejection of the ion, under the influence of lattice vibrations, into an interstitial site, where it will eventually be neutralised. Objections to the mechanism have been raised on the basis of the lifetime of the doubly-ionised state. [51,52]

Mitchell at al [53] proposed a combination of the Seitz and Varley mechanisms. The Varley process was considered as occurring near dislocations, the interstitials

joining/...

joining the dislocation core and causing it to climb. This was supported to some extent by the work of Nowick [54] on the effect of dislocation density on the growth of F-centres under γ-irradiation. The presence of dislocations only affected the production rate in the second stage.

The possibility of double ionisation by an Auger-type process has been suggested [55,56,57]. An electron is removed from the K-shell by primary radiation.[58] An L-electron subsequently falls into this empty level and the energy of transition causes a further electron to be ejected from the L-shell via an internal conversion process [59]. The probability of an intra-atomic Auger process, or an Auger cascade when this is energetically possible, was calculated to be at least 0.9 for KCl and LiF [57]. It was stressed that multiple ionisation may occur in positive as well as negative ions. A de-excitation collision between e.g. a Cl^+ ion and a neighbouring Cl^- ion could release up to 9eV of kinetic energy to the two neutral Cl atoms. The probability of such a "mutual neutralisation" is difficult to calculate [60].

An investigation of the Auger-type process in the formation of colour centres in KCl [61], showed that the rate of formation of F-centres increased when the K-absorption edge had been crossed. No such change was reported for KBr [62]. Royce [63] suggested that this was due to the higher mass of the Br^- ion.

The possibility of two neighbouring single ionisations with the subsequent formation of, for example, a chlorine molecule, has been discussed [55,64,65].

Alkali halides doped with divalent cations are more easily coloured by ionising radiation, than normal crystals [66,67,68]. To account for this a further

mechanism/...

mechanism for the production of anion vacancies was suggested [69]. In NaCl for example, a positive hole created by ionising radiation can be captured on a Cl^- ion adjacent to an Na^+ vacancy. The Cl atom formed would tend to move into the vacancy and with one of the neighbouring Cl^- ions, form a Cl_2^- molecule. The energy released would assist the chlorine vacancy to escape.

1.4 Detection of Defects.

In principle all the physical properties of a crystal are determined by its precise atomic structure and thus depend on the presence or absence of imperfections or, more precisely, on the concentrations of imperfections [70,71,72]. Some properties are more sensitive than others, however.

Sensitive properties are those involving the movement of atoms or electrons, further non-fundamental optical absorption, and luminescence and magnetic properties of imperfections.

Less sensitive properties are the density, the lattice constant, the crystal structure, the fundamental optical absorption and the specific heat; all do not depend essentially on the presence of imperfections. In this group the imperfections are only indicated by the difference between the property of a 'perfect' and a 'less perfect' crystal, and precise analysis is required.

1.4.1 Effects involving the Movement of Atoms.

Whenever appreciable atomic migration occurs it has been found to be linked up with the presence of imperfections such as interstitials or vacancies, or associates. The migration may occur under the influence of a concentration gradient i.e. diffusion, or in an electric field i.e. ionic conduction. Diffusion may occur both with

neutral/...

neutral and with charged imperfections, while ionic conduction requires imperfections with an effective charge.

Dienes [73] calculated the activation energy (E_m) for the motion of a neutral vacancy pair in KCl as 0.38 ev, compared to 0.51 ev for an Na^+ vacancy and 0.56 ev for a Cl^- vacancy in NaCl [74]. In alkali halides at low defect concentrations the conductivity is proportional to the concentration of the defects multiplied by the mobility of the defects, the latter being proportional to T^{-1} exp $(-E_m/kT)$.

Additional information regarding atomic migration is obtained by measuring the pressure dependence of ionic conduction and diffusion [75]. This yields the 'activation volume' of diffusion which includes both the volume effects involved in the formation of defects and that involved in the actual migration process [76].

The ionic conductivity of alkali halides at temperatures well below the melting point is due only to the motion of positive ion vacancies [77].

At low temperatures in the extrinsic or structure-sensitive range, the conductivity is controlled by cation vacancies, either "frozen-in" the crystal or present as a result of divalent cation impurity; while at high temperature the conductivity is intrinsic i.e. it depends on the concentration of cation vacancies generated thermally by an equilibrium process which is independent of the past history of the specimen. Since high energy radiation introduces additional defects, the extrinsic conductivity might be expected to increase on irradiation. The opposite effect has, however, been reported for NaCl and KCl exposed to X-rays [78,79,80]. Haeke [81] found that the depression in conductivity of NaCl, which had been irradiated with X-rays,

was/...

was enhanced as the temperature decreased. A study of the effect of γ-rays and of reactor radiation on KCl [82], showed that particle bombardment, in contrast to photon irradiation, caused a marked increase in conductivity. A smaller increase was also observed after proton bombardment. It was suggested that the concentration of positive ion vacancies was increased without altering their mobility. For photon-irradiation, Seitz [83] has suggested that the initially free cation vacancies may be bound in immobile, complex defects such as V_2- and V_3-centres, and combinations of these centres with anion vacancies. This has been supported, with modifications in detail, by Smoluchowski [84] and Kabayashi [85].

Conduction by the movement of charged atomic imperfections can also be measured by dielectric loss [86].

1.4.2 Effects involving the movement of electrons.

Electronic conduction is not possible when the crystal is in its lowest energy state. It can occur, however, when free electrons or holes are produced either by intrinsic excitation or by ionisation of imperfections. Methods of investigation comprise the measurement of dark conductivity, of the Hall effect, and of the thermoelectric power [87].

1.4.3 Optical Effects.

The normal absorption of light by a solid may be modified in the presence of imperfections, by additional absorptions caused by the excitation and ionisation of the atomic imperfections themselves e.g. the F- and V- bands of the alkali halides. Additional information is obtained by studying the effects with polarised light. Dichroism points to assymetrical centres which may be either associates [88] or distorted single imperfections (Jahn-Teller effect)[89]. Levy [90] has reviewed the use of colour centres for the detection and measurement of defects.

If/...

If the absorption leads to ionisation, photo-conductivity will be observed and a study of the decay can yield information on the capture cross-section for electrons and holes, of the imperfections [91]. The return to the ground state of non-ionised excited centres may be accompanied by luminescence. The spectral distribution of the excitation of luminescence and that of the luminescence itself yield information about the energy levels of the system.

1.4.4 Magnetic Effects.

The magnetic properties of imperfect crystals are in general different from those of perfect crystals. In diamagnetic substances, electrons and holes give rise both to a diamagnetic and a paramagnetic contribution. Atomic imperfections give rise to a paramagnetic contribution if they contain electrons in unpaired states, and to diamagnetism for paired states. The effects are small and difficult to measure [92,93]. A more sensitive way of measuring effects of imperfections is the use of resonance techniques: paramagnetic resonance, nuclear resonance and cyclotron resonance [94,95].

Paramagnetic resonance is the resonance due to the precession round a magnetic field of the spin of the electrons in imperfections having unpaired electrons. It has been observed with free electrons and holes [96], as well as with atomic imperfections.

Interaction of the spin of the resonating electron and the nuclear spin of atoms in or near the imperfection gives rise to a fine structure which is of value in determining the precise nature of the imperfection. Associates are indicated by a complicated fine structure and/or anisotropy of the splitting factor. e.g. Measurements on the V- and H-centres produced in alkali halides by

irradiation/...

irradiation with X-rays at low temperature, have led to the suggestion that the centrès are respectively a Cl_2^- ion at two normal Cl^- lattice sites, and a Cl_2^- ion at the site of one Cl^- ion [97].

Greater detail may be obtained by using the technique of double resonance (ENDOR) [98]. Interaction between the unpaired electron and nuclear spins at various distances are obtained separately and the wave function of the electron in and near the imperfection may be mapped with great accuracy. e.g. F-centres in KCl [99,100]. The only drawbacks to paramagnetic resonance methods are that they apply only to imperfections with unpaired spins and that not all such centres will necessarily give rise to an observable resonance effect.

Nuclear resonance itself can give information concerning imperfections. The line width depends on the dipolar interaction of the nuclear spins and may, if the nucleus also possesses an electric quadrupole moment, depend on gradients in the crystal electric field caused by imperfections. It is not possible to observe resonance peaks of the imperfections themselves.

Cyclotron resonance [101], which is the resonance effect related to the diamagnetism of free electrons and holes, can be applied only under very stringent conditions, and may give information on the effective mass of carriers and the structure of bands.

Griffiths et al [102] have observed paramagnetic resonance in diamonds irradiated with fast neutrons or 1 Mev electrons but not with γ-rays or X-rays. This suggests that the creation of defects by atomic displacements is necessary for the observation of ESR in diamond.

Measurements/...

Measurements of electron spin resonance [103,104] together with those of magnetic susceptibility [105] have confirmed the model of the M-centre in alkali halides, as an association of two electrons and two anion vacancies.

1.4.5 Thermal Conductivity Effects.

Imperfections may play a part in heat conduction in two ways. Conduction may be increased if the imperfections, moving in a temperature gradient, transport energy in some form, while the intrinsic heat conductivity of a crystal i.e. the part carried by lattice vibrations may be decreased by the scattering of the phonons at imperfections. The latter effect is predominant at low temperatures and scattering at each type of imperfection has a typical temperature dependence [106]. The concentration of point imperfections in InSb was determined by the temperature dependence of the thermal conductivity [107]. Gebhardt [108] measured the thermal conductivity of alkali halides and concluded that the increased thermal resistance after X-irradiation was due to scattering by interstitial halogen atoms.

1.4.6 Effects on the Lattice Dimensions.

The presence of imperfections has a small effect on the lattice dimensions as well as on the density. Precise measurements are required to detect the effects. Lin [109] and Rabin [110] used a dilatometer to prove the formation of both anion and cation vacancies in alkali halides upon irradiation with X-rays. The formation of these imperfections under these conditions had previously been deduced from density measurements [111,112]. Wiegand [113], on measurements using precision X-ray diffraction techniques, postulated the formation even at room temperature, of interstitials in alkali halides. This was supported by

Nadeau [114] who measured the resistance to motion of dislocations in a LiF crystal.

1.4.7 The Field Ion Microscope.

Point imperfections and dislocations may be observed directly using the field ion microscope [115,116]. The crystal however, must be hot to have sufficient emission. The method has been applied so far to metals and to Si and Ge crystals [117].

1.4.8 Effects on the Diffraction of X-rays.

X-rays tend to exaggerate the perfection of crystals, and imperfections are, in general, difficult to detect and even more difficult to measure. This fact has allowed the progress of crystal structure analysis using real imperfect crystals, but has handicapped research into the finer detail of the solid state [118].

Departures from the regular periodic character in a lattice can give rise to anomalous X-ray effects such as diffuse scattering, decreased Bragg intensities and shifts in positions of diffraction maxima. Ways in which such departures can occur are:-

(1) Through thermal vibration of the atoms.

(2) Through the trapping of impurity atoms in the lattice.

(3) Through defects being present or being formed in the lattice.

The work on X-ray diffraction effects caused by the thermal vibration of atoms has been reviewed by James [119] and by Wooster [120]. There are many similarities in the X-ray effects caused by thermal motion and those caused by structural disorder. Much of the theory of thermal effects has been adapted and expanded to explain structural effects.

The/...

The study of structural disorder by X-ray diffraction methods has had several main themes [121]:-

(a) Stacking faults in layer structures e.g. micas.

(b) Defects in close-packed metals e.g. cobalt.

(c) Disorder in diamonds.

(d) Work-hardening and age-hardening in alloys.

(e) Various order-disorder problems in inorganic and metallic crystals.

Much of the work on solid solutions and the atomic size effect has formed the basis of theories of the effect of lattice defects, such as interstitials and vacancies, on the diffraction of X-rays.

Although some attention has been given to the scattering of X-rays by dislocations [122-128], the theories of X-ray diffraction by distorted lattices have been concerned mainly with imperfections at the unit-cell level.

Zachariasen [129] gave a general theory of X-ray diffraction by crystal imperfections, irrespective of their nature, and predicted a decrease in the effective scattering power per unit cell and the appearance of diffuse scattering around reciprocal lattice points (relps).

Huang's theoretical paper [130] on X-ray scattering by dilute solid solutions, formed the basis of much of the work that followed. Using a model of spherical centres of elastic distortion randomly distributed in an elastically isotropic lattice, he derived an expression for the intensity of the diffracted X-ray beam. He predicted:-

(a) An isotropic lattice expansion causing a shift in position of the Bragg maxima.

(b) Reduction in the intensities of the Bragg reflections by an 'artificial temperature factor' of the form $\exp(-B'(\sin^2\theta)/\lambda^2)$, where B' is a constant independent of temperature unlike the Debye-Waller factor B.

(c)/...

(c) Diffuse scattering about the relps, lemniscate in shape, with the axis parallel to the vector from the origin to the relp, and centre at the relp.

The Huang analysis is valid whether the pressure centres are on lattice sites or not, thus the predictions should hold for randomly distributed vacancies and interstitials. Eshelby [131] and Sampson and Tucker [132] modified the expression slightly to allow for the finite size of the elastic medium.

Ekstein [133] using a similar elastic model predicted diffuse scattering concentrated near relps and superimposed on the ordinary scattering by a regular crystal. The disorder scattering would tend towards zero at very low angles.

Matsubara [134] developed the atomistic counterpart of Ekstein's treatment. He considered a mono-atomic simple cubic lattice with a vacancy situated at the origin, and postulated minimum strain energy. For diffuse scattering to be observed, the number of lattice defects n, must exceed a certain value. This value can be estimated by comparison of the magnitude of displacement of atoms (U_o), with the mean square amplitude of thermal vibration of atoms (U^2).

$$\frac{I \text{ strain}}{I \text{ vibration}} = \frac{n}{N} \, 4\overline{II}^2 \, \frac{(U_o^2)}{\overline{U^2}} \quad \ldots\ldots\ldots \quad (1.45)$$

I strain = intensity of disorder diffuse scattering.
I vibration = intensity of thermal diffuse scattering.

In an actual case U_o may be several times larger than $(U^2)^{\frac{1}{2}}$, so that $n \gg N \times 10^{-3}$ will make the right-hand side $\gg 1$. The actual number may be less because the diffuse scattering due to defects is more directional and hence more intense than thermal diffuse scattering.

Cochran [135] in a treatment using Fourier transforms, replaced some atoms in the perfect crystal by atoms of a different scattering power at displaced positions. His results are equivalent to those of Zachariasen but are more easily applicable. He found that the diffuse intensity depends on the transform of the difference between the perfect and imperfect crystals, and that there is no diffuse intensity exactly at the relps.

Cochran and Kartha [136] extended this treatment to a solid containing a large number of randomly-distributed defects. Displacements of atoms by individual defects were superimposed to give a resultant displacement of each atom. These resultant displacements have a Gaussian distribution about the 'original' atomic positions. The expression derived for this situation includes an artificial temperature factor. As the concentration of defects increases, the diffuse regions around relps retain their shapes but decrease in intensity to the gain of other regions of reciprocal space.

For a non-random distribution of defects, the principle of superposition of displacements does not apply. Agglomeration into spheres, each of radius R_o, increases the diffuse intensity within roughly $(R_o)^{-1}$ of the relps, and decreases it elsewhere. The characteristic lemniscate shape is preserved while the lattice expansion and Bragg intensity effects are the same as for a random distribution.

Kanzaki [137] extended Matsubara's treatment by allowing for the volume change in the crystal caused by distortion around defects. The effects predicted other than the expansion of the lattice, were diminuition of the Laue and Bragg reflection intensities and diffuse scattering surrounding the relps.

For a cubic crystal isolated defects will give rise to lemniscate-shaped diffuse spots, while pairs of

defects/...

defects or an isolated interstitial in a dodecahedral position, will produce ellipsoidal diffuse reflections. Chang [138] has calculated the mechanical relaxation associated with paired point defects which form asymmetric centres of distortion in the lattice.

Modifications to the Huang treatment were made [139-141] to allow for the identities of the terminal and intervening atoms in the distorted lattice. This led to the prediction of a size-effect modulation of the diffuse scattering. These modulations would be sinusoidal and would increase in amplitude in reciprocal space, linearly with distance from the origin. Borie's expression [141] included Huang's artificial temperature factor and a term for the disorder diffuse scattering, identical in form to that for thermal diffuse scattering. This term conserves the intensity lost by the Bragg reflections as the disorder increases.

Thus in general, a crystal which has centres of distortion caused by atomic replacement (e.g. alloys) or atomic displacement (radiation or other damage), would be expected to show some or all of the following X-ray diffraction effects:-

(a) Reduction of the Bragg intensities by an artificial temperature factor which depends upon the defect concentration.

(b) A slowly varying background scattering.

(c) A lattice expansion which may or may not be istotropic, but which causes a shift in the positions of the Bragg maxima.

(d) Characteristic diffuse scattering, in the neighbourhood of Bragg directions, which is independent of temperature.

No line-broadening is predicted by these analyses. Dienes and Vineyard [142] propose that this is because of the mathematical approximations involved. Line-broadening may occur when the distortions are too large to satisfy the Huang-type treatment e.g. for large irradiation doses, or in treating thermal spikes, or when the mobility of point imperfections allows large clusters of defects to form. The diffraction effects in such cases, on Laue photographs, are:-

(a) Disappearance of higher-angle reflections

(b) Broadening of inner reflections, and

(c) Pronounced small-angle scattering, accompanied sometimes by extra reflections in the small-angle region. These extra reflections have been interpreted [143] as indicating that mosiac blocks in the crystal have been disoriented by more than 3°.

Guinier [144] in a general treatment of X-ray diffraction by an imperfect lattice, related line-broadening caused by distortion, to an 'apparent crystal size', L, using the Scherrer equation.

$$(2\theta) = \lambda/L \cos \theta \qquad \ldots\ldots \qquad (1.46)$$

(2θ) is the integral width of the line. If the line-broadening is due to the size of the crystal, L is independent of the order of reflection, but if L is dependent on the order, the broadening is caused by lattice distortion.

Further Guinier [145] stated that the nature of the diffuse scattering depends upon the degree of correlation between the fluctuations in structure factor from one unit cell to another. Even if the local imperfections are large, provided they are perfectly incoherent, the diffuse scattering will be very weak. This scattering is superimposed on the diffraction by the 'perfect average' lattice, and shows up experimentally as a haze, which is indistinguishable

from/...

from parasitic scattering found on all patterns, unless special precautions are taken. The diffuse scattering becomes more intense and is modulated if there is some correlation. In general there is correlation between neighbouring unit-cells, but this decreases as the distance between the unit cells under consideration increases.

If the correlation is periodic from cell to cell, the scattered intensity is then concentrated at two points which are symmetrical with respect to the nodes of the reciprocal lattice. All the intermediate cases are possible, with the Bragg reflections varying in breadth and the diffuse scattering varying in intensity and area over which it is spread.

For displacement disorder the intensity of the diffuse scattering is zero near the centre of reciprocal space and increases with an increase in radial distance. The opposite is true for substitution disorder.

Wooster [146] has given examples of types of diffuse X-ray reflections from crystals, using an optical diffractometer and masks [147]. He found that a single vacancy can give rise to a spherical reciprocal diffuse pattern about each relp. A disc of disturbed region of the lattice produces a streamer normal to the plane of the disc passing through each relp, and a rod of disturbed lattice produces a disc of diffuse reflection round about each relp. Thus by investigating the shape of the diffuse regions, conclusions may be drawn about the departure of the lattice from perfect regularity.

Tucker and Senio [148-150], using photographic methods, studied the X-ray diffraction effects shown by neutron-irradiated boron carbide, B_4C. The reaction:

$$B^{10} \xrightarrow[\text{neutrons}]{\text{thermal}} He^4 + Li^7$$

occurred/...

occurred and the product atoms dissipated through the lattice.

The structure of B_4C is based on an hexagonal unit cell with 12 B atoms and 3 C atoms per unit cell. The 3 C atoms form a linear chain parallel to the c-axis.

After irradiation the Bragg intensities were decreased by a strongly anisotropic artificial temperature factor. This was six times greater in the c_o direction than in the a_o direction. The lattice parameters a_o expanded 0.89% and c_o contracted 1.38%. Laue photographs showed decreased Laue intensities and diffuse reflections which did not disappear on reducing the temperature of the crystal to that of liquid nitrogen. The diffuse reflections had the shape of an ellipsoid, rather than that of Huang's lemniscate. These effects increased with increasing dose.

Electron density profiles through the linear C-C-C chain in the most heavily irradiated sample showed that the peak for the central C atom had been reduced by 47%, and that the two end C atoms had been displaced towards the centre. This effect was attributed to the displacement of central C atoms into interstitial positions. Annealing removed the effects except for an increased background owing to diffuse scattering from the remaining He^4 and Li^7 atoms and corresponding vacancies.

Studies on solid solutions have given support to the theories of diffraction by disordered lattices. Cu_3 Au, Co Pt, Ni Au and Li Mg [140,151] all show the predicted X-ray diffraction effects.

Borie [141] found all the effects predicted by Huang in a more detailed study of Cu_3 Au. The artificial temperature factor B' was approximately half the observed temperature factor B.

A/...

A comparative study of neutron-irradiated minerals[152] showed that not all substances will show diffraction effects even after heavy irradiation e.g. corundum (Al_2O_3) showed no detectable changes in powder pattern, while CaF_2 showed a lattice expansion of 0.08% and diamond an expansion of 0.9%. After the same dose the diffraction pattern of irradiated quartz (SiO_2) became so diffuse that line measurements were no longer possible.

Neutron-irradiated MgO did not show a very strong artificial temperature factor and had a lattice expansion of only 0.1% compared to that of silicon carbide (0.68%) for the same dose [150].

Studies on graphite [153] and quartz [154] confirm the fact that neutron-irradiation can cause sufficient displacement disorder to be detectable by X-ray diffraction methods.

Expansion of the lattice, and the corresponding decrease in density, of alkali halides on irradiation with X-rays and with γ-rays have been reported [155-159]. The magnitude of the effects is much smaller than those reported above (approximately 10^{-3}%), but this must be due to the nature of the compound rather than of the radiation, as Peisl [160] found lattice expansions of the same order in neutron-irradiated LiF. Results, however, do support the generation of interstitials, vacancies and other defects such as F-centres [161]. X-ray diffraction methods have been supplemented by electronic [162], photoelastic [163-165] and optical [166] techniques.

Several studies have been made of the effect of irradiation with X-rays and γ-rays on Rochelle salt, Na K $(C_4H_4O_6).4H_2O$ [167,168]. Marked changes occur in the ferroelectric properties at doses as low as 10^5 roëntgens. Toyoda et al [169] reported diffuse X-ray reflections from

gamma-irradiated Rochelle salt at higher doses. They noticed colouring and evolution of water during irradiation of the crystals. The intensities of the diffuse spots increased up to a point where the Laue spots split, and then became less marked. The diffuse scattering was distributed almost spherically around the relps and showed neither streaks nor fine structure. The defects caused by the elimination of water molecules from the lattice, which was reported to remain unchanged, were suggested as the origin of the diffuse reflections.

Boutin and Frazer [170] found that the radiation effects were similar to the effects of impurity substitution (Tl^+ or NH_4^+) in Rochelle salt. Using neutron-diffraction methods they studied the (0k0) reflection intensities as a function of radiation dosage. A condition of the orthorhombic $P2_12_12$ space group of the non-ferroelectric form is that (0k0) = 0, for k odd. This condition is removed for the $p2_1$ symmetry of the monoclinic ferroelectric form. On irradiation there was a marked decrease in the (050) reflection intensity with increasing dose. The (050) intensity of an irradiated crystal could be changed by application of a d.c. electric field, while that of an unirradiated crystal showed no change. Two basic types of radiation damage were proposed for the salt:-

(a) Stable damage centres, homogeneously distributed and producing effects at the unit cell level.

(b) Existing imperfections (e.g. dislocations) re-inforced by collection of diffusing damage products.

Krueger [171] et al were unable to detect changes in lattice parameters for neutron and γ-irradiated Rochelle salt. On irradiation a significant sharpening of the X-ray diffraction peaks occurred at first followed by increasing

diffuseness/...

diffuseness. This increase in perfection is similar to the increase in ordering of "ordered" Cu_3Au after pile-irradiation [172,173] and after electron bombardment [174]. Irradiation is thought to release pinned dislocations which then anneal out.

Krause reported an increase in lattice parameter of silver azide [175], AgN_3, on irradiation with X-rays. This substance is not purely ionic in structure and the increase was found to be in the direction of the weak Ag-N bonds.

Thallous azide [176], TlN_3, showed markedly anisotropic lattice constant changes on irradiation with X-rays and with UV-light. TlN_3 has a tetragonal unit cell and the structure is alternate layers of metal and azide ions perpendicular to [001]. The parameter change was in the direction perpendicular to the layers. The lattice constant increased with dose up to a "saturation" value. This value increased with increased X-ray intensity. Annealing caused the parameter to revert to its unirradiated value.

The wave-length of the UV-light used, determined the irradiation effect on TlN_3. Above 4000Å no changes in parameters were detected, while for wave-lengths less than 3600Å, the substance turned black within minutes and showed diffuse diffraction lines with low peak intensity. Krause related the lattice expansion to the chemical decomposition and suggested that the processes occurring were the formation of anion vacancies and F-centres, the production of interstitial metal atoms and the diffusion of N_2 through the lattice.

Keating and Krasner [177], using X-ray diffraction techniques, examined sodium azide powder which had been subjected to mechanical grinding, γ-irradiation and pile-irradiation. NaN_3 has a rhombohedral structure with alternate layers of Na^+ ions and N_3^- ions stacked in the direction of the long diagonal. Both γ- and reactor-irradiated samples showed similar line-broadening effects, characteristic of faulting and strain. The diffraction patterns resembled those of the ground material except for a displacement of the (00.9) reflection of the irradiated samples. This displacement was attributed to a contraction in the direction of the long dimension of the azide ion caused by radiolysis. No signs of decomposition were observed in the ground material. Annealing removed some of the faults and strain in both the ground and irradiated samples, and the lattice contraction disappeared. A significant fraction of the imperfections in the irradiated samples was stable however, even up to the ignition temperature.

Lattice defects such as dislocations affect X-ray intensities primarily by controlling the magnitudes of the extinction effects [178]. Qualitative observation of dislocations, small-angle boundaries and clusters of point defects can be made using topographic methods [179,180].

Point defects may also affect the extinction. Their main effect however, is to alter the electron density distribution in a crystal. When the concentration of point defects is sufficiently large to affect the intensities of Bragg reflections, electron density syntheses can be used to obtain quantitative information. The procedure is similar to that used for studying the distribution of valence electrons [181] and requires very accurate X-ray intensities.

Cochran [182] suggested that the difference synthesis could be used to study small departures from the electron density of ideally perfect crystals, if errors in extinction and atomic form factors were minimised. Ripples and series termination errors tend to subtract out.

Attard and Azároff [183] used this method to study the distribution of valence electrons in indium antimonide (InSb). The "core" corresponding to the electron density of the palladium atom, was subtracted from both the In and the Sb peaks. They were found to contain 3.5 and 4.6 electrons respectively.

Mohanty and Azároff [184] estimated the concentration of interstitial Zn atoms in zinc-doped zinc oxide crystals, as 10^{20} atoms/cm^2, by subtracting the electron density of a pure crystal from that of a doped crystal. The interstitial atoms were found to occupy normally empty octahedral sites at the corners of the unit cell. The concentration agreed with the measured lattice constant change of 0.027%.

A similar study on chlorine-doped cadmium sulphide [185] was less successful. Difficulties arose in the correction for extinction effects which were different for doped and pure crystals. Small peaks at the corners of the unit cell corresponded to a fraction of 1 in a 1000 interstitial atoms.

Mohanty and Azároff concluded that the concentration of interstitial atoms present in the doped ZnO (10^{20} atoms/cm^2) was just above the lower limit of detectability by the best X-ray diffraction methods available.

Azároff [186] pointed out that most ionic crystals with structures based on anion closest packing cannot accommodate sufficiently large defect concentrations to

produce/...

produce an effect on the intensities of the X-ray reflections. The results found for ZnO were largely due to the presence of a relatively "open" structure, where half of the tetrahedral voids and all of the octahedral voids in the anion closest packing are normally empty. The success of the difference synthesis method too, in measuring the charge transfer in InSb[183], was also largely due to the favourable conditions, such as the similarity of the atoms and the "averaging effect" of subtracting identical cores from both atoms. This success does not mean that point defect concentrations can be detected in all crystals in this way.

Prout and Woods [187,188] found no change in lattice parameters and no artificial temperature effect in an X-ray diffraction study of γ-irradiated (300 Mrad) silver permanganate. Comparative Fourier projections and electron density profiles for both unirradiated and irradiated $AgMnO_4$, showed no shifts in position, broadening or decrease in height of the Ag and Mn peaks on irradiation. The oxygen peaks were not resolved. Prout and Woods concluded that the absence of any of the effects predicted by Huang [130], in the diffraction patterns of the irradiated crystal, precluded the possibility of displacement of either Ag or Mn atoms to interstitial positions. This did not necessarily apply to the oxygen atoms, since their contribution to the structure factors was small, especially at high angles and any displacement of oxygen atoms would be difficult to detect. They proposed that γ-irradiation created centres of partially decomposed material, as a result of ionisation and bond-rupture in the MnO_4 group.

1.5 The Effects of Pre-irradiation on Thermal Decomposition.

The effects of pre-irradiation on the thermal decomposition of many crystalline solids, such as the permanganates, oxalates, perchlorates, bromates, dichromates and azides have been studied in considerable detail [189,190]. Such studies have lead to more detailed information on the processes of thermal decomposition, and conversely to information on the nature of radiation damage. Some of the effects noticed are:-

(a) Acceleration of the decomposition.

(b) Shortening of the induction period.

(c) Changes in activation energies.

(d) Changes in the mathematical analyses governing the p/t plots, and their extent of fit.

These effects may be permanent or may undergo ageing.

Some substances are insensitive to irradiation e.g. pre-irradiation of silver oxide with UV-light and with γ-rays does not affect its thermal decomposition [191].

Lead styphnate monohydrate [192] is affected only by neutron irradiation. Damage results from the reaction:

$$N^{14} + n \longrightarrow C^{14} + p$$

Dehydration does not alter the irradiation effect even though X-ray photographs show that recrystallisation follows dehydration. This suggests that the significant form of radiation damage is irreversibly altered styphnate units rather than displaced ions or vacancies. The reduced activation energy found for the initial process, represents the decomposition of the chemically altered styphnate group.

Prout/...

Prout [193], on the results of his study of the pre-irradiation of $KMnO_4$ with thermal neutrons, γ-rays and protons, proposed a mechanism for the activation of solids by pre-irradiation. During irradiation cations were thought to be displaced to interstitial positions by direct collision with compton or photoelectrons. The threshold radiation energy for displacement, assuming an atomic weight of 100 and the Seitz [2] value of 25eV, is 0.68 MeV. On heating, the point defects migrated and the Wigner energy released on recombination of the interstitials and vacancies [194,195], caused decomposition in small regions of the crystal. The centres of decomposed material grow and eventually fracture the crystal. The reaction proceeds in an accelerating manner by the Prout-Tompkins mechanism. The product molecules cover the surface and on reaching a certain critical thickness produce lateral strains which are relieved by cracks along which nuclear reaction is favoured. The reaction spreads through the solid by a system of branching planes of decomposed material. These ultimately interfere and after the time of maximum velocity, the rate is controlled by the number of unchanged reactant molecules which are contiguous to product molecules. The dependence of the length of the induction period on temperature for a fixed irradiation dose was used to obtain activation energies for the migration of point defects.

A detailed comparative study of pre-irradiation effects on the thermal decomposition of the permanganates of Li, K, Rb, Cs, Ag and Ba [196], showed no systematic decrease in the pre-irradiation effects for heavier cations. The pronounced effects for $CsMnO_4$, precluded the possibility of direct displacement of cations by interaction with Compton electrons. A modified Varley mechanism [49] was

proposed/...

proposed, with multiple ionisation of the MnO_4^- ion for light cations e.g. Li^+, and of the cation itself e.g. Cs^+. The resulting cation displacement is not then directly related to the identity of the cation. The Varley mechanism requires the expulsion of electrons into interstices and if this is hindered in any way, the radiation effect will be decreased.

Ammonium dichromate [197] showed only a very slight irradiation effect and this was attributed to the relative immobility of the NH_4^+ ion.

Pre-irradiation of the same series of permanganates with 200 kev X-rays [198], showed effects increasing through Li, K, Rb, Cs to Ag. The X-ray energy used precluded direct displacement for all but $LiMnO_4$ and this substance showed the smallest effect. Boldyriev [199,200] proposed that excitation and ionisation resulted in the radiolysis of the solid substance. The radiolysis products which appeared in the lattice, catalyses subsequent chemical reactions in which the irradiated solid may be involved, including thermal decomposition. The radiolysis-product interface causes deformations in the original substance and electronic and ionic stages of reaction will be favoured at these points. No detailed mechanism for the formation of radiolysis products in substances such as the permanganates, was given. Neither was the catalytic action elaborated. Displacement of ions as a secondary factor was not excluded.

Freeman and Anderson have reviewed the radiation-induced changes in the reactivity of ammonium perchlorate[201]. The unirradiated decomposition is characterised by the decomposition of only the strained material in the intermosaic grain boundaries at temperatures below 350°C [202] and the

decomposition/...

decomposition of the unstrained material forming the core of the mosaic blocks at higher temperatures [203]. Pre-irradiation with γ-rays and with X-rays shortens the induction period and accelerates the rate of decomposition. Possible causes [204] suggested for this enhanced reactivity were:-

(1) The presence of radiolysis products.

(2) Lattice defects caused by radiolysis, which act as reaction nuclei.

(3) The presence of electronic lattice defects.

The formation according to (3) of positive holes i.e. ClO_4 radicals was favoured. The ClO_4 then decomposes on heating. Microscopic studies showed that the initial reaction occurs primarily at the surface in unirradiated samples [205], but right throughout the irradiated crystal [206].

The transfer of electrons from ClO_4^- ions to interstitial NH_4^+ ions, was the rate-determining step suggested by Bircumshaw and Newman [205]. Both Cu^{++} and I^- were shown to act as bridges. Susceptibility to radiation damage was increased greatly by the presence of Ag^+ ions, although the doped sample decomposed in a similar manner to pure unirradiated material [207]. Measurements of electrical conductivity [208] supported an electron transfer process. EPR [209] and ESR [210] studies on irradiated NH_4ClO_4 established the presence of NH_3^+ ions and ClO_3 radicals. The ClO_3 radical apparently anneals to the ClO_3^- ion, while the NH_3^+ ion may also anneal.

The decomposition of ClO_3^--doped NH_4ClO_4 is similar to that of irradiated pure NH_4ClO_4 [211]. This was put forward as evidence that the decomposition originated at sites of radiation-induced reaction. The importance of lattice imperfections is emphasised by the reactivity of

the/...

the sublimate, which shows X-ray diffraction line-broadening, but no detectable ClO_3^- ions. [212]. The decomposition of the sublimate was very similar to that of irradiated NH_4ClO_4. Gentle grinding of the unirradiated substance does not however result in a similar decomposition.

Jach [213] found that the thermal decomposition of $KBrO_3$, although complicated by melting, approximated to a true solid state decomposition over the range 342 - 367°C. The decomposition mechanism suggested was based on the diffusion of Br^- ions, formed at the surface by decomposition of BrO_3^-, and K^+ ions to form regions of KBr lattice which introduce strains and cause cracks. Diffusion then becomes fast enough for eutectic formation, which is a function of both decomposition and diffusion rates. Grinding hastens the process.

Gamma-irradiated $KBrO_3$ showed melting over the whole temperature range. Towards the end of the decomposition the crystals broke into smaller crystallites which did not decompose further. Eutectic formation was thought to be enhanced by the radiolysis products present [214,215].

Haynes and Young [216] investigated the effect of reactor irradiation on the thermal decomposition of silver oxalate. The unirradiated decomposition was analysed in terms of an exponential law for the acceleratory period and the contracting-sphere mechanism for the decay. Pre-irradiation increased the rate in the acceleratory period, which was then better fitted by a cubic power law. There was no change in the decay. They suggested that irradiation "poisons" the branching process by converting branching points from "germ" into "growth" nuclei. These nuclei grow according to the cube law until they coalesce. After the contracting-sphere interface has been established,

the reaction proceeds irrespective of how the interface was formed.

Boldyriev [217] showed that pre-irradiation with UV-light or gamma-rays increased the rate of thermal decomposition of silver oxalate. The addition of a Cd impurity decreased the rate of decomposition of both unirradiated and irradiated specimens. Both grinding, and interruption and cooling in product gas, resulted in an increased rate of decomposition [218]. A general mechanism[219] was suggested. At the onset of irradiation widely differing bonds may break down in the solid. A corresponding excitation of electrons in different states of aggregation within the crystal will take place, and will be followed by the migration of electrons into the conduction band, accompanied by a sharp rise in conductivity. As energy is lost some electrons will revert to lower states, while others may return to electron traps. By altering the type and concentration of these traps the decomposition may be influenced.

Herley and Prout [220] reported an increase in the rate of the acceleratory reaction of lead oxalate after irradiation with gamma-rays. No radiolysis was detected.

Reactor-irradiation of uranyl oxalate [221] increased the maximum velocity and altered the shape of the acceleratory period of the subsequent thermal decomposition. Nucleation was thought to occur along the tracks of fission fragments which traverse the crystal. The reaction then continues in the form of "expanding cylinders" which eventually overlap with each other or the advancing interface formed at sub-grain boundaries.

More attention has been paid to the radiolysis of the azides (see section 1.6), than to the effects of

pre-irradiation/...

pre-irradiation on their thermal decomposition. The kinetic equations used to fit the p/t curves obtained from the thermal decomposition of the azides of K, Na, Ag, Cu, Tl, Ca, Sr, Ba and Pb, have been tabulated in a general review of the physics and chemistry of the inorganic azides.[222] In a later review, Gray [223] emphasised the importance of the excited N_3^{-*} ion in the mechanisms of both photochemical and thermal decomposition. The facts that the energy required to form an exciton diminishes in the order KN_3, TlN_3, AgN_3, CuN_3, while the energy to dissociate an exciton is much less for TlN_3 or AgN_3 than it is for KN_3, form the basis of correlations between azide stability and ionisation potential. Point defects, electron traps and dislocations and crystal surfaces play important parts in the various decomposition mechanisms suggested [224].

Pre-irradiation studies that have been carried out on the azides, include the work of Garner and Moon [225] on BaN_6. Bombardment at room temperature with the radiations from radium, had no effect on the subsequent thermal decomposition, but bombardment at the decomposition temperature, halved the induction period and increased the rate of decomposition four times. Similar results were found for SrN_6 after bombardment at room temperature [226] and after irradiation with UV-light [227]. Mercury fulminate showed no effect.

No change in the rate of thermal decomposition of KN_3 [228] was found after irradiation with UV-light, despite intense colouration. Damage was shown to bleach thermally, possibly by tunnelling of electrons from F-centres to positive holes.

Bowden and Singh [229] subjected the azides of Li, Pb, Ag and Cd and silver acetylide to bombardment by

electrons, thermal neutrons, fission products and X-rays. Neutron-irradiated LiN_3 showed a shortened induction period and increased acceleratory rate. The effect on the azides of Pb and Cd was less marked. AgN_3 melts on decomposing and showed no effect. No analysis was given of the p/t plots but the Prout-Tompkins equation appeared to fit the LiN_3 decomposition [230].

Boldyriev and Skorik [231] found that irradiation of BaN_6 with X-rays at the temperature of decomposition had a greater accelerating affect on the subsequent thermal decomposition, than pre-irradiation with the same dose at room temperature.

Jach [232] studied the effect of pile-irradiation on the thermal decomposition of α-lead azide. The induction period and acceleratory period were virtually removed, the maximum rate occurring at approximately zero-time instead of 40% decomposition as in the unirradiated solid. The changes in kinetics were attributed to the formation of a large number of nuclei. These grow rapidly over the surface at the decomposition temperature, and the decay reaction is a three-dimensional penetration of the interface. By analogy with the radiolysis of the nitrates, irradiation is thought to produce N_2 at internal and external surfaces and at imperfections such as dislocations. Prolonged irradiation causes decomposition at normal lattice sites and an internal build-up of gaseous N_2. This diffuses into pockets, causing rupture of the lattice and further radiolysis at the newly created surfaces. Vacancies and/or clusters of vacancies are left behind, where Pb metal may accumulate. The activation energy for the decay reaction of the irradiated azide was 11 kcal/mole less than for the unirradiated. This difference was attributed to the strains caused by the radiolysis products.

Prout and Moore have published preliminary results on the effect of γ-irradiation on the thermal decomposition of Barium azide [233] and of strontium azide [234]. Both azides show markedly decreased induction periods and increases in the rate of the acceleratory reactions. For unirradiated BaN_6, the analyses used were the Avrami-Erofeyev equation with $n = {}_4$, for the acceleratory period followed by a contracting sphere decay. The power law with n = 3, corresponding to three-dimensional growth of a fixed number of nuclei fitted the acceleratory period of unirradiated SrN_6, followed by the unimolecular decay. After irradiation (doses greater than 1 Mrad) the unimolecular decay still held, but the acceleratory period obeyed an exponential law. This indicated that formation of additional nuclei by chain mechanisms - possibly reaction chains along dislocation lines or sub grain boundaries - was occurring.

These various studies are examples of the approaches used in gaining information on details of solids from the manner in which they decompose on heating. The information is not always unambiguous and is therefore used to its greatest advantage in conjunction with the other techniques mentioned.

The degree of sensitivity of a solid to damage on irradiation varies over a wide range. Some substances decompose during irradiation whereas others are outwardly unchanged after irradiation, but display marked changes in the kinetics of their subsequent thermal decomposition. Many substances are hardly affected at all.

Tentative criteria for predicting whether a particular thermal decomposition will be affected by pre-irradiation were put forward by Prout [235]. These were that the substance should contain a simple metal cation and

should/...

should decompose according to a branching chain mechanism. Decomposition spikes should create strain sufficient to crack or fracture the solid and thus create new reaction surfaces.

1.6 Photolysis and Radiolysis.

The mechanism of radiolysis is often, but need not necessarily be, similar to that of thermal decomposition. When the mechanisms are similar, factors decreasing the radiation stability will also decrease the thermal stability. Consequently it is of importance to consider some of the work done on the photolysis and radiolysis of solids.

In the decomposition of solids under the influence of visible or ultra-violet light, the energy of the quantum is comparable to that of a chemical bond. Radiolysis that does occur is localised mainly at the surface e.g. by varying the wavelength of the light during the photolysis of barium azide, portions of the crystal surface differing in activity could be made to react separately [236].

For irradiation with γ-rays, X-rays and high-energy particles, the energies of the quanta are often far in excess of the bond energy. The probability of a process occurring then is determined not so much by the weakness of the chemical bond at individual sites in the lattice, as by the conditions that exist in the lattice for the restoration of a bond after it has been broken. In defective regions there is a greater probability of the destruction of excitons, accompanied by the release of energy. The removal of decomposition products too, is more rapid and recombination will be prevented. Other important factors include ionisation potentials of the ions and the free volume in the lattice [237]. For ionic salts containing complex anions or cations, specific effects

may appear owing to rupture of chemical bonds within the complex ions.

Alkali halides on exposure to UV-light, γ-rays, X-rays or electron bombardment acquire a deep colour characteristic of the salt, which fades gradually. A similar but permanent colouration occurs on heating the salt in the vapour of its alkali metal [238]. Kahn and Kittel [239] suggested a mechanism, based on density, paramagnetic and ESR measurements, whereby the excess metal atoms ionise and the electrons go into the conduction band of the salt, while the ions take up normal lattice sites on the surface. The resulting anion vacancies created, diffuse and trap mobile electrons forming F-centres. Exposure of KBr to bromine vapour leads to the formation of V-centres. The radiation produced F-centres are bleached thermally by a tunnelling effect which results in electrons combining with positive holes or V-centres. At high temperatures (400°C) colloidal particles of Na metal have been detected and are thought to be formed from the thermal aggregation of F-centres. At very high temperatures the F-centres are reformed showing that the process is reversible.

Photolysis of the silver halides and of the azides is however, irreversible. One of the basic problems is to explain how uniform illumination results in the observed growth of discrete nuclei. The Mott mechanism [240-242] assumed the crystal (of silver halide or barium azide) to be an ionic conductor with mobile metal cations. Irradiation produced conduction electrons and corresponding positive holes. The electrons were trapped at some unspecified 'sensitivity specks', possibly anion vacancies, and interstitial metal ions diffused and were neutralised at these traps. Further electrons were trapped by the metal

formed/...

formed and the speck grew by further neutralisation of metal ions etc. The positive holes diffused to the surface and neutralised surface anions.

In contrast to Mott, Mitchell [243], in dealing with the photographic process, proposed that the growth of the metal specks is by association of Ag atoms with Ag^+ ions, which then trap electrons and are neutralised. Further irradiation facilitates the redistribution and diffusion of Ag groups along sub-boundaries. Grimley and Mott [244] showed theoretically that massive Ag in contact with AgBr will acquire a positive charge owing to the attachment of interstitial Ag^+ ions. The lower limit to the size at which a group of Ag atoms will become positively charged was estimated at 3 Ag atoms and an Ag^+ ion [245].

Thomas and Tompkins [246,247] raised the objections that no photoconductance is observed in the decomposition of barium azide so electrons are not excited to the conduction band, and that the rate of growth of nuclei is too high for a mechanism depending on the transport of both ions and electrons. They suggested that excitons formed on irradiation are trapped at imperfections e.g. cation vacancies, and are stable for a certain time before reverting to the ground state. If before this happens, a second exciton is trapped forming a complex centre, reaction may occur:-

$$2N_3^{-*} \longrightarrow 3N_2 + 2e^- + 2 \text{ anion vacancies.}$$

The electrons and anion vacancies form F-centres, thus regenerating the trap. The F-centre aggregate eventually breaks away from the azide matrix to form a metallic nucleus. The nucleus then grows by transformation of lattice Ba^{+2} ions to Ba atoms occupying the lattice positions of the salt. On further growth "recrystallisation" to the normal metal

lattice/...

lattice takes place and the crystal becomes permeated with cracks through which N_2 can diffuse. Similar mechanisms were applied to the photolysis of KN_3 [248] and the radiolysis of $KClO_4$ [249] and NaN_3 [250] by X-rays.

Mechanisms suggested, vary for differing conditions of photolysis [251]. Baidins [252] proposed that irradiation could result in the ejection of electrons from macroscopic metal specks. If the electrons were trapped elsewhere, the metal would acquire a positive charge. The photoelectric threshold of Ba metal is 5000 Å, so the emission of photoelectrons at shorter wavelengths should be quite intensive. At longer wavelengths where the energy is insufficient to produce excitons in the bulk of the lattice, transitions may occur at special positions e.g. dislocations.

An internal transition of the azide ion [253], rather than exciton formation, was proposed for the photolysis of barium azide by UV-light [254].

The low-temperature colouration and decomposition of KN_3 is thought [255,256] to follow a decomposition scheme involving the production of excitons on UV-irradiation; the reaction of excitons with anion vacancies to yield F-centres and positive holes, and the bimolecular reaction of holes to yield N_2 at a rate proportional to the square of the irradiation intensity.

The photolysis of NaN_3 is different in that the rate of N_2 evolution is proportional to the first power of the irradiation intensity [257]. ESR evidence has been put forward [258] for the formation at low temperatures, not of F-centres, but of F_2^+ centres (an electron trapped at an anion divacancy). The mechanism suggested was:-

$$N_3^{-*} + \text{anion vacancy} \longrightarrow N_2 + N + F_2^+\text{-centre.}$$

Carlson/...

Carlson [259] however, showed that N is not trapped in the NaN_3 lattice during UV-irradiation, although it is found under X-irradiation.

The primary step in the radiolysis of nitrates[260,261] is thought to be:-

$$NO_3^- \longrightarrow NO_2^- + O$$

The reactions:-

$$NO_3^- \longrightarrow NO_3 + e \longrightarrow NO_2^- + O$$

have been considered [262] for barium nitrate.

Doigan and Davis [263] attempted to relate the radiolytic yield (G) to the polarising power of the cation in a series of nitrates. Hennig et al [264] attributed the variation in yield to the difference in "free space". (i.e. the difference between the actual volume of the crystal per ion pair and the combined volume of the ions calculated from standard ionic radii). The correlation shows several anomalies [265]. A similar correlation between free-space and chloride yields has been found in the radiolysis of perchlorates [266].

A number of techniques have been used to determine the reactions involved in the radiolysis of nitrates. Magnetic susceptibility measurements [264] showed that the oxygen liberated was present in the molecular, not atomic form. IR and X-ray studies [266] showed that while NO_2^- ions were formed at random sites, the O atoms combined at favourable sites. Hochandel and Davis [267] proposed that the oxygen atoms react with adjacent nitrate ions:-

$$NO_3^- + O \longrightarrow NO_2^- + O_2$$

The nitrates of lead, lithium and silver yield some oxide in addition to NO_2^- and O_2. Recent ESR studies [260] have detected, in addition, the presence of NO_3, NO_3^{-2}, NO_2 and O_2^-.

Johnson and Forten [268] measured the lattice expansions and heats of solution of γ-irradiated nitrates. The heat of solution is related to the strain induced in the lattice by oxygen pockets, where pressures of about 10^8 dynes/cm^2 may be reached initially. The expanded lattice permits diffusion of O_2 to more favourable sites for pocket formation. The strain is reduced but the lattice expansion is permanent.

A lack of similarity in the mechanisms governing the rates of the thermal decomposition and radiolysis of the alkali-metal bromates has been reported [269]. The thermal decompositions however are complicated by melting. The dependence of the radiolytic yield (G) on free space was similar to that of the nitrates, increasing through Li, Na, K, Rb and Cs. The mechanism suggested was the excitation or ionisation of the BrO_3^- ion followed by decomposition, directly or through intermediate stages, to Br^- and O_2. It was not established whether radiolysis occurred at random lattice sites or whether excitons migrated to lattice defects or special trapping centres. X-ray diffraction examinations proved insensitive to less than 5% decomposition.

The initial yield (G) values for the γ-radiolysis of the alkali-metal azides have been determined by titrimetric methods [270], and were found to be directly proportional to the free space in the lattices. The order of radiation stability did not correspond to that of thermal stability.

Logan and Moore [271] indicated that the important factors influencing G-values, are the extent of coupling of electronic states of the anion with crystal vibrations; the density of the vibrational states, and their average energies. These factors are related both to the polarizability of the cation and to the free space in the lattice. Electron trapping centres may also play a significant role [272].

2. OBJECTS OF THE RESEARCH.

The object of this research was to carry out a comparative study of the effects of high-energy radiation on the thermal decomposition of substances which are (a) insensitive and (b) sensitive to ultra-violet light.

An extensive study has been made of the thermal decomposition of pre-irradiated solids falling into class (a) above, in particular the permanganates. However there is no certainty with regard to the change(s) induced in the solid by irradiation prior to thermal decomposition. Obviously such knowledge would assist considerably in interpreting the kinetic data which would be obtained in the proposed research. One possible technique for determining the nature of the radiation damage in crystalline solids has already been outlined viz. X-ray diffraction methods. Consequently, an initial study similar to that of Senio and Tucker [148-150], but on a suitable permanganate was felt to be desirable. Prout and Woods [187,188] made such a study on $AgMnO_4$, but the presence of the heavy Ag atom in the molecule makes the detection of any positional changes in the oxygen atoms difficult, and consequently no attempt was made to do this. $KMnO_4$ is a more suitable permanganate and using improved methods for determining the intensities of the diffraction spots (see later), it was hoped to obtain more extensive and accurate information than had been found with $AgMnO_4$. The considerable changes in the thermal decomposition of $KMnO_4$ after pre-irradiation by γ-rays are also fully known [193].

Relatively little work has been done on the thermal decomposition of irradiated solids falling into class (b). It was hoped that by comparing the results from substances

in/...

in classes (a) and (b), that some information could be obtained on the problem of the characteristics which a solid must possess if the thermal decomposition of the solid is to be affected by pre-irradiation. (See Prout [235])

The thermal decompositions of nickel oxalate and of ammonium dichromate are not affected by pre-irradiation with ultra-violet light [273]. The effect of gamma-ray irradiation on ammonium dichromate has only been examined in a cursory fashion [274] and no such study has been made of nickel oxalate. Both these substances have the polyatomic anion which Prout suggested might be necessary for a pre-irradiation effect. Consequently, these two substances were chosen as being representative of class (a). The thermal decomposition of calcium azide is sensitive to pre-irradiation by UV-light and thus this substance was chosen as a member of class (b).

3. AN X-RAY DIFFRACTION STUDY OF GAMMA-IRRADIATED POTASSIUM PERMANGANATE.

3.1. PREVIOUS WORK.

3.1.1. Irradiated Permanganates.

The thermal decomposition of potassium permanganate[275] yields pressure-time plots which are sigmoid in form. The acceleratory and decay portions of the curve are described by the Prout-Tompkins equation:

$$\log (p/(p_f-p) = kt+c \quad \ldots\ldots \quad (3.1)$$

where p_f is the final pressure.

Pre-irradiation of $KMnO_4$ with thermal neutrons, gamma-rays and protons [276] shortens the induction period and increases the maximum velocity of the decomposition reaction. The Prout-Tompkins equation holds for both gamma- and pile irradiations up to a dose of approximately 50 Mrad. At higher doses, the Prout-Tompkins equation applied only over the decay period. The acceleratory period was fitted by:-

$$\log p = k't+c' \quad \ldots\ldots \quad (3.2)$$

Prout and Herley [277,278] studied the thermal decomposition of unirradiated $KMnO_4$ and $AgMnO_4$, and also of gamma-irradiated (10 Mrad) $KMnO_4$, by interrupting the decomposition and taking Laue photographs, at suitable intervals along the curve.

Prout and Woods [279,280] did a similar study of unirradiated and gamma-irradiated (300 Mrad) $AgMnO_4$.

Both the Prout-Tompkins equation and its modified form [281]:-

$$\log \; p/(p_f-p) = k''\log t+c'' \quad \ldots\ldots \quad (3.3)$$

are based on a mechanism that at the commencement of the acceleratory period, strain exists in the crystal at the interface between the product formed prior to the

acceleration/...

acceleration and the undecomposed material. This strain produces micro-cracks in the reactant surface and the reaction progresses inwards by a 'branching planes' mechanism [275,281,282].

The strain developed may result in the mechanical disruption of the crystal. This occurs in the decomposition of $KMnO_4$ but not of unirradiated $AgMnO_4$. Irradiated (300 Mrad) crystals of $AgMnO_4$ fractured at the start of the acceleratory reaction.

The lattice distortion expected for both substances during decomposition, was shown by the asterism of the diffraction spots on the Laues taken at intervals as the reactions proceeded. This was not exceptionally pronounced until immediately prior to acceleration, except for irradiated $AgMnO_4$ where the asterism does increase during the induction period. Unirradiated $AgMnO_4$ was the only study made beyond the start of the acceleratory period as the other crystals fragmented at this stage. Extreme asterism was visible just before fragmentation.

For irradiated (10 Mrad) $KMnO_4$, Prout and Herley [277] reported no marked differences from the unirradiated crystals.

Crystal structure analyses on unirradiated and irradiated $AgMnO_4$ [285,286], revealed no changes in the positions of the Ag and Mn atoms on irradiation. The oxygen atoms were not resolved in the analyses and no conclusions could be drawn about the effect of irradiation on their positions.

3.1.2/...

3.1.2 The Crystal Structure of $KMnO_4$

Mooney [283] determined the crystal structure of $KMnO_4$ from Laue and single-crystal oscillation photographs. He followed James and Wood [284] and Basche and Mark [285] in reporting that the unit cell is orthothombic, contains 4 molecules and has the symmetry

$$2\ Di - 16\ (V_h16)$$

in the Schoenflies notation. This corresponds to space group No. 62 Pnma.

Mooney's values for the lattice parameters were: $a = 9.09\text{Å}$ $b = 5.22\text{Å}$ $c = 7.41\text{Å}$.

A projection on the c-face i.e. a (hk0) projection was given with interatomic parameters referred to an origin which lies on a glide-plane when considering the projection on the b-face i.e. (h0l) projection. Intensities were estimated visually as strong, medium, weak etc.

Wyckoff [286,287] shifted the origin to a two-fold axis of symmetry. The atomic parameters in terms of this origin are given in TABLE 3.1. The origin is that required for use of the data relating to the space group No. 62 Pnma.[288]

TABLE 3.1

WYCKOFF			
ATOM	x	y	z
K	0.19	0.75	0.16
Mn	0.07	0.25	0.67
O_1	0.99	0.25	0.49
O_2	0.25	0.25	0.61
O_3	0.07	0.03	0.80
O_4	0.07	0.53	0.80

Ramaseshan et al [289] determined the crystal structure of $KMnO_4$ using anomalous scattering. Intensities were

measured/...

measured by comparison with a standard scale. Their final atomic parameters in fractional co-ordinates are given in TABLE 3.2. The mean Mn-O distance was 1.55Å and the O-O distance 2.55Å, with the exception of O_3-O_4 which was 2.44Å.

Their residual factor:

$$R = \frac{\sum \left| |F_o| - |F_c| \right|}{\sum |F_o|}$$

was stated as 17% for Cu k_α.

TABLE 3.2

RAMASESHAN			
ATOM	x	y	z
K	0.183	0.750	0.158
Mn	0.438	0.250	0.192
O_1	0.321	0.250	0.038
O_2	0.594	0.250	0.106
O_3	0.417	0.037	0.317
O_4	0.417	0.463	0.317

3.2 EXPERIMENTAL.

3.2.1 Preparation of Crystals.

Crystals were prepared from a saturated solution of B.D.H. Analar potassium permanganate. (33 gm/100 ml at 75°C). The solution was cooled to 50°C and the first batch of crystals discarded. The filtrate was cooled to room temperature and long needle crystals (0.1 to 0.2 mm width) of a high-degree of perfection were obtained. These were filtered rapidly, rinsed with alcohol and then ether, dried on paper and stored over silica-gel.

Smaller crystals were prepared by more rapid cooling, with stirring, to lower temperatures.

3.2.2/...

3.2.2 Irradiation.

Crystals of a variety of sizes, in evacuated Pyrex ampoules were irradiated in the Spent Fuel Facility at Harwell. (Temperature: 25°C; gamma-ray energy: 1.1 Mev; dose rate: 4 Mrad/hr.). Each ampoule received a dose of 500 Mrad.

After irradiation the crystals showed no visible signs of damage. The reflections from faces were still satisfactory for optical alignment. Two additional doses of 200 Mrad each, giving a total dose received of 900 Mrad, still did not result in disintegration of the crystals.

3.2.3 Apparatus and Equipment.

a) X-Ray generators.

Two generators were used in the project:

(i) A Philips PW 1009, employing a sealed X-ray tube, at a voltage of 40 kV and a tube current of 20 mA. A copper target was used.

(ii) A Hilger and Watts Microfocus generator, which has an X-ray tube which is continuously evacuated by an oil diffusion pump backed by a rotary oil pump. The generator was operated at 50 kV and 3 mA, and a demountable copper target was used.

b) Accessories.

The Laue camera and the rotation goniometer used were made by Unicam. The integrating Weissenberg goniometer was made by Stoë (Heidelberg). The Unicam goniometer has an optical goniometer.

3.2.4 Processing of X-ray films.

The films used were Kodak 'Kodirex', 'Industrex D' and 'Crystallex'. Development was at 20°C in Kodak D19b for 5 mins., with constant agitation. This was followed

by/...

by a rinse in a 3% acetic acid stop-bath and fixing in Kodak X-ray Fixer for 15 mins. The films were then washed for 2 hours and dried in a dust-free atmosphere at 20°C.

3.3 A COMPARISON OF THE CRYSTAL STRUCTURES OF UNIRRADIATED AND IRRADIATED $KMnO_4$.

Because of the disagreement between Mooney [283] and Ramaseshan [289] on the crystal structure of $KMnO_4$, the fact that Ramaseshan used the anomalous scattering technique for his determination, and the requirement that the comparison should be under standard conditions, it was necessary to determine the structure of the unirradiated substance as well as that of irradiated $KMnO_4$.

3.3.1 Preliminaries.

The Laue symmetry mmm and the absence of reflections when h = 2n (h00), and when l = 2n, (00l) check with the requirements of the assigned space group No. 62 Pnma [290].

On projection parallel to [010], this space group gives rise to plane group No. 8, p2gg [291,292].

Single-crystal rotation photographs established the needle axis as the b-axis.

The unit cell dimensions of the unirradiated crystal were checked and found to be:-

$$a = 9.132\text{Å} \; ; \quad b = 5.679\text{Å} \; ; \quad C = 7.405\text{Å}$$

(See Section 3.4).

3.3.2 The Measurement of Integrated Intensities.

Prout and Woods [279,280] in their study of irradiated $AgMnO_4$ and Nassimbeni [293] in his determination of the crystal structure of $CsMnO_4$, used the Dawton positive-print technique [294,295] for measuring intensities.

In/...

In this study of $KMnO_4$, Weissenberg photographs were taken using a Stoë integrating Weissenberg goniometer, and intensities measured by the "plateau method" [296]. The integrating mechanism gives the cylindrical camera a slight rotation about its axis and a slight translation parallel to its axis, at the end of each traverse.[297] The magnitude of these auxiliary motions, and hence the plateau size, is adjustable and is determined from the spot size on an ordinary Weissenberg photograph or the zero layer of a rotation photograph.

The multiple-film technique [298] was used to extend the range of the densities measured, as the linear density/exposure relationship holds only up to densities of approximately 1.2, with normal development.

3.3.2.1 The Weissenberg Photographs.

(a) Unirradiated $KMnO_4$: (Hilger generator - Stoë goniometer)

A preliminary rotation photograph checked the alignment of the crystal about the b-axis and gave an estimate of the spot size in the zero-layer as 0.1 mm x 1.3 mm. The integrating mechanism was set according to this spot size:-

Radial displacement:

Spot width 0.1 mm + plateau 0.2 mm = 0.3 mm
(1 scale division = 0.06 mm) Setting: 5 scale div.

Axial Displacement:

Spot length 1.3 mm + plateau 1.3 mm = 2.6 mm
(1 scale division = 0.1 mm) Setting: 26 scale div.

The sector scanned on traverse 60-60, speed 1, was 240°. Because of symmetry, one exposure enabled all reflections to be measured.

Conditions: Normal-beam, zero-layer ($1\frac{1}{2}$ mm setting on screens).

Exposure: 1728 counts with 3-film pack of Kodak Industrex D. (50 kV, 3 mA).

(b)/...

(b) Irradiated $KMnO_4$ (500 Mrad): (Philips generator - Stoë goniometer).

Spot size: 0.1 mm x 0.5 mm.

Setting: Radial: 5 scale div.
Axial: 12 scale div. (2 div. zero error)

Exposure: 432 counts (40 kV, 20 mA).

Both photographs received standard processing and were then indexed.

3.3.2.2 Measurement of Densities of Diffraction Spots.

(a) Procedure.

A modified Steinheil Densitometer [299] was used for measuring the densities of the spots on the Weissenberg photographs. The photo-emissive search-head and electronic photometer were supplied by Photovolt Corp., N.Y. The search-head was fitted with an opaque disc with a slit adjusted to a size slightly smaller than the plateau region on the enlarged, integrated spot.

Two possible ways of measuring the density are:-

(i) The lamp intensity is adjusted so that without the film being in position, the photometer reads zero density. The film is then moved into the beam and the density of the background next to the spot is read and subtracted from the reading of the density of spot plus background.

(ii) With a portion of the background next to the spot in the beam, the lamp is adjusted to zero density and the density of the spot read directly.

Both methods gave equivalent readings. Method (i) was used.

(b) Choice of Background.

The background reading was taken as near to the spot as possible without picking up any of the halation. In zero-

level/...

level Weissenberg photographs each strong reflection near the centre of the film is accompanied by a "radiation streak" [300,301]. The contribution to the density of the spot from the background streak varies so as to make it impossible to allow for it properly by subtraction of the background from top, side or below. Estimates were made from the density of the streak close to the spot.

(c) Doublets.

The densities of doublets were obtained by addition of the densities of the individual components.

For partial resolution the method of measurements depended upon the degree of overlap.

3.3.2.3 The Film-to-Film Factor [302].

The film-to-film factor (R) is the factor by which the intensity of the diffracted X-ray beam is reduced when passing through the film i.e. it is the ratio of the density of a spot on the film closer to the crystal, to the density of the same spot on the second film.

$$R_{a/b} = D_a/D_b \text{ for spot hOl.}$$

For other than zero-layer photographs, allowance has to be made for the variation of this factor with the angle of incidence of the diffracted beam. The factor is constant for all reflections on the same layer line.

Using a three-film pack, all density measurements were converted to the scale of the centre film using the film-to-film factors.

There was a variation in the densities of reflections having the same indices. This is owing to the variation of the absorption with the aspect of the crystal presented to the beam [303]. The shape only approximates to a cylinder. Densities of reflections

with/...

with the same indices were averaged to give the measured densities (D_m) tabulated in TABLE 3.3 for each reflection hOl.

TABLE 3.3

	UNIRRADIATED			IRRADIATED (500 Mrad)		
hOl	D_m	A*	$\|F_o\|$	D_m	A*	$\|F_o\|$
002	2.92	93	10.97	2.60	207	15.4
004	0.41	49	4.62	0.45	87	6.40
006	0.74	28	6.21	1.07	46	9.56
008	0.56	18	4.04	0.84	27	6.08
101	0.71	117	4.79	0.33	312	5.32
102	1.48	89	7.99	1.70	190	12.5
103	0.06	64	1.70			
104	0.41	47.5	4.60	0.45	84	6.41
105	0.17	36	3.03	0.20	61	4.27
106	0.06	28	1.78			
107	0.19	22	2.88	0.25	35	4.17
108	0.16	17.5	2.10	0.23	27	3.15
200	1.85	106	8.34	1.60	257	12.0
201	1.58	96.5	8.03	1.43	219	11.5
202	1.75	76.5	8.93	1.90	155	13.2
203	0.96	58.5	6.91	1.40	109	11.4
204	0.14	44	2.70	0.16	77	3.81
205	0.12	34	2.54	0.12	57	3.27
207	0.20	21	2.87	0.40	33	5.09
208	0.17	17.5	2.11	0.30	26	3.45
209	0.62	14.8	2.55	0.85	20	3.54
301	0.25	75	3.39	0.27	141	4.82
302	0.41	63	4.45	0.46	120	6.50
303	2.05	50.5	10.22	2.60	91	15.4
304	0.42	39.5	4.70	0.67	68	7.79
305	0.26	31.5	3.74	0.44	52	6.24
306	0.23	25	3.37	0.36	40	5.33
308	0.05	17	1.07	0.10	25	1.86
309	0.32	13.5	1.51	0.37	19	2.00
400	0.93	61	6.74	1.11	115	10.1
401	2.88	58.5	11.98	3.00	109	16.6
402	0.05	51.5	1.60			

TABLE 3.3/...

TABLE 3.3 (contd.)

	UNIRRADIATED			IRRADIATED (500 Mrad)		
hOl	D_m	A*	$\|F_o\|$	D_m	A*	$\|F_o\|$
403	0.93	42.8	7.00	1.40	74	11.3
404	0.05	35	1.64	0.10	59	3.00
405	0.98	28.5	7.18	1.60	46	11.7
407	0.66	19	4.71	1.40	29	8.52
501	0.19	46	3.15	0.18	81	4.05
503	0.67	36.8	6.06	0.98	61	9.42
504	0.25	34.3	3.89	0.45	50	6.27
506	0.20	21	2.86	0.40	33	5.08
507	0.05	17.5	1.16	0.07	26	1.69
508	0.24	15	1.77	0.38	21	2.67
600	0.31	37.5	4.06	0.36	64	5.69
601	0.29	36.5	3.94	0.34	62	5.53
602	0.29	34	3.96	0.34	57	5.52
603	0.08	30	2.06	0.06	49	2.28
604	0.04	26	1.42	0.05	42	2.02
607	0.06	16.3	1.10	0.07	24	1.45
608	0.48	13	1.75	0.56	19	2.35
701	0.05	30	1.64	0.05	49	2.19
702	0.68	28	5.98	1.02	45	9.25
703	0.09	25.3	2.12	0.13	41	3.24
704	0.34	22.3	3.89	0.65	36	6.83
705	0.10	19.5	1.89	0.20	30	3.33
707	0.23	14	1.61	0.33	21	2.44
800	0.92	24.8	6.72	1.30	40	10.2
802	0.35	23	4.01	0.53	37	6.26
806	0.83	15	3.46	1.50	22	5.75
902	0.05	19.3	1.33	0.10	30	2.35
904	0.06	17	1.18	0.12	25	2.05
905	0.41	15	2.41	0.69	22	3.89
1002	0.06	16.5	1.15	0.09	25	1.76
1003	0.05	15.5	0.93	0.09	23	1.54
1004	0.12	14	1.14	0.10	21	1.31
1101	0.04	14	0.68	0.13	21	1.55
1102	0.20	13.5	1.35	0.28	20	2.01
1103	0.90	13	2.09	1.80	18	3.80

3.3.3/...

3.3.3 CORRECTION OF INTENSITIES.

3.3.3.1. Extinction.

No correction was made for primary or secondary extinction, on the assumption that these effects would be approximately the same for both unirradiated and irradiated crystals.

The multiplicity factor of 4 was not included.

3.3.3.2. The Lorentz and Polarisation Corrections. $(Lp)^{-1}$

These corrections were applied in the standard way from values of sine θ/λ for copper radiation.

3.3.3.3. Absorption.

For rotation about the needle axis (b-axis), the shape of the crystal can be approximated to that of a cylinder, having a radius estimated from the mean cross-sectional dimensions.

For $KMnO_4$ (density = 2.703 gm/cc [304]), the linear absorption coefficient [305], μ = 376 cm^{-1}. Hence the optimum crystal size, t = 0.005 cm.

The actual sizes of the unirradiated and irradiated crystals corresponded to approximately cylindrical radii (R) of 0.010 cm and 0.0145 cm and values of μR of 3.8 and 5.5 respectively.

Graphs of the absorption factor A* against Sine θ were then plotted for these values of μR [306]. The values of A* corresponding to each reflection, hOl, were obtained from these graphs and are listed in TABLE 3.3.

The corrected densities $D_{corr.}$ were then calculated.

$$D_{corr.} = D_{m.}\ A^*\ (Lp)^{-1}$$

and hence the structure amplitudes

$$|F_{hOl}| = (D_{corr.\,hOl})^{\frac{1}{2}}$$

(See TABLE 3.3)

3.3.3.4./...

3.3.3.4. The Temperature Correction.

The Debye-Waller correction [307,308] was applied to the structure amplitudes $|F_{hOl}|$. This assumes that each atom of the crystal undergoes the same isometric motion.

$$|^{T}F|^{2} = |^{O}F|^{2} \exp(-2B \sin^{2}\theta/\lambda^{2})$$

where ^{O}F = structure factor at $0^{o}K$

^{T}F = structure factor at experimental temperature.

The value of B was found graphically [308,309].

See TABLE 3.4 and FIGURE 3.1

B = 2.2

This value was used for both unirradiated and irradiated structure determinations.

Values of the temperature factor [310], $\exp(-B \sin^{2}\theta/\lambda^{2})$ were used to calculate the temperature corrected values of the structure amplitudes.

The reciprocal temperature factors, t*, and the corrected observed structure amplitudes, $|F_u|$ and $|F_i|$, are given in TABLE 3.5.

TABLE 3.4

RANGE:(Sin θ)		$\sin^{2}\theta/\lambda^{2}$	$\langle I \rangle$	$\sum f^{2}$	$\ln(\langle I \rangle/\sum f^{2})$
1.	0-0.447	0.0424	40.54	3080	$\bar{5}.6026$
2.	0.447-0.632	0.1311	17.31	1283	$\bar{5}.6754$
3.	0.632-0.775	0.2147	5.503	855	$\bar{6}.9706$
4.	0.775-0.894	0.3007	2.742	633	$\bar{6}.5613$
5.	0.894-1.000	0.3664	2.600	518	$\bar{6}.6769$

TABLE 3.5/...

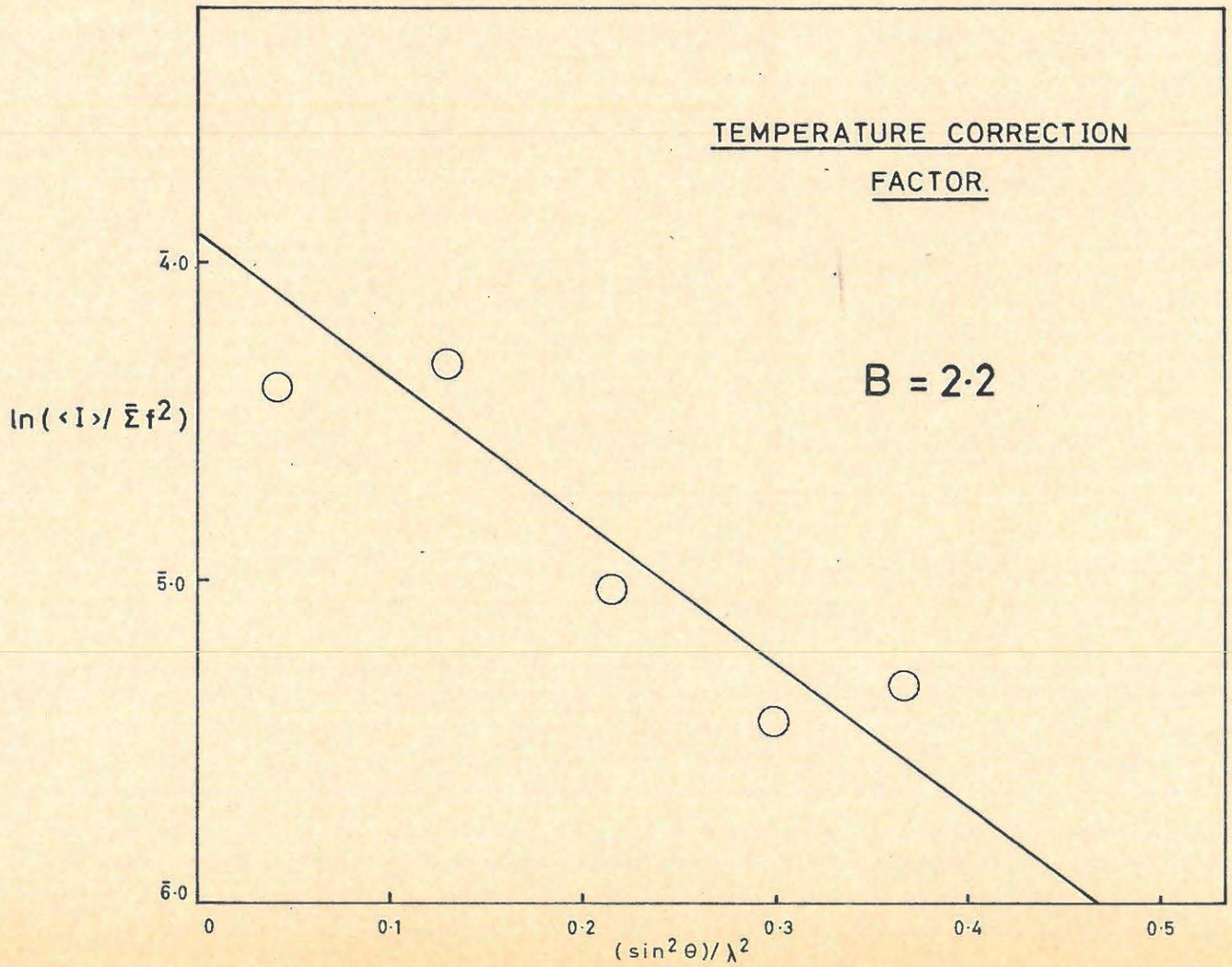
TEMPERATURE CORRECTION
FACTOR.
B = 2·2
ln (<I> / Σ̄ f²)
4̄·0
5̄·0
6̄·0
0
0·1
0·2
0·3
0·4
0·5
(sin² θ)/λ²

FIG. 3.1

TABLE 3.5.

h01	t*	$\|F_u\|$	$\|F_i\|$	h01	t*	$\|F_u\|$	$\|F_i\|$
002	1.037	11.4	16.0	407	1.812	8.53	15.4
004	1.174	5.42	7.51	501	1.188	3.74	4.81
006	1.422	8.83	13.6	503	1.290	7.82	12.2
008	1.901	7.68	11.6	504	1.397	5.43	8.76
101	1.018	4.88	5.42	506	1.695	4.85	8.61
102	1.050	8.39	13.1	507	1.946	2.26	3.29
104	1.188	5.46	7.62	508	2.268	4.01	6.06
105	1.290	3.91	5.51	600	1.271	5.16	7.35
107	1.661	4.78	6.93	601	1.290	5.08	7.13
108	1.901	3.99	5.99	602	1.330	5.27	7.34
200	1.027	8.57	12.3	603	1.397	2.88	3.19
201	1.037	8.33	11.9	604	1.502	2.13	3.03
202	1.066	9.52	14.1	607	2.096	2.31	3.04
203	1.124	7.77	12.8	608	2.392	4.19	5.62
204	1.203	3.25	4.58	701	1.397	2.29	3.06
205	1.309	3.32	4.28	702	1.447	8.65	13.4
207	1.661	4.77	8.45	703	1.531	3.25	4.96
208	1.946	4.11	6.71	704	1.626	6.33	11.1
209	2.331	5.94	8.25	705	1.773	3.35	5.90
301	1.074	3.64	5.18	707	2.268	3.65	5.53
302	1.101	4.90	7.16	800	1.531	10.3	15.6
303	1.160	11.9	17.9	802	1.592	6.38	9.97
304	1.253	5.89	9.76	806	2.208	7.64	12.7
305	1.374	5.14	8.57	902	1.773	2.36	4.17
306	1.531	5.16	8.16	904	1.992	2.35	4.08
308	1.992	2.13	3.71	905	2.208	5.32	8.59
309	2.392	3.61	4.78	1002	2.045	2.35	3.60
400	1.112	7.49	11.2	1003	2.151	2.00	3.31
401	1.124	13.5	18.7	1004	2.268	2.59	2.97
403	1.220	8.54	13.8	1101	2.268	1.54	3.52
404	1.309	2.15	3.93	1102	2.331	3.15	4.69
405	1.422	10.2	16.6	1103	2.463	5.15	9.36

3.3.4./...

3.3.4. ANALYSIS OF RESULTS.

3.3.4.1. Approach.

At this stage since the phases are unknown, a Patterson analysis [311,312] is often carried out using the structure amplitudes. However the approach used was to assume that Mooney's structure gave the approximate positions of the K and Mn atoms. This structure was then refined by Fourier and Difference syntheses, and finally an electron-density projection $\rho(x,z)$ for unirradiated $KMnO_4$ was plotted.

Intensity measurements made on the irradiated (500 Mrad) $KMnO_4$ were normalised with the unirradiated intensities and a similar electron-density projection calculated.

The two projections were compared by taking sectional electron-density profiles and also by performing an Irradiated - Unirradiated Difference synthesis.

All syntheses were carried out using Beevers - Lipson strips [313] for the summations and determining the electron-density at intervals of 1/60th of the unit cell. The method was as described by Buerger [314] for the plane group p2gg, and as used by Nassimbeni [315] in determining the structure of $CsMnO_4$.

3.3.4.2. Unirradiated $KMnO_4$.

Using Mooney's co-ordinates for K and Mn (TABLE 3.1) structure factors, F_c^{KMn}, were calculated from the appropriate tables of atomic scattering factors [316] (K^+, Mn^{+2}, O^{-2}), and of $\sin 2\bar{1}\bar{1}hx$ and $\cos 2\bar{1}\bar{1}hx$ [317].

The observed structure amplitudes, $|F_o|$, calculated from the corrected densities, were normalised to $|F_c^{KMn}|$ using the values from the high-angle spots only ($\sin\theta > 0.6$), where the contribution of the oxygen atoms to the structure

factor/...

factor should be small. Signs for the remaining F_o's were determined by adding the oxygen contributions, based on Mooney's co-ordinates, to F_c^{KMn}.

The first Fourier synthesis gave strong peaks for the K and Mn atoms at

K : x = 0.183 ; z = 0.162

Mn: x = 0.440 ; z = 0.177

The structure factors F_c^{KMn} were recalculated using these values.

The double oxygen peak $O_{3,4}$ was well resolved at

$O_{3,4}$: x = 0.427 ; z = 0.307

A second, less well-defined peak, enabled the position of the O_2 atom to be estimated at

O_2 : x = 0.083 ; z = 0.393

As there was no definite peak corresponding to the O_1 atom - possibly because of the 'swamping' effect of the Mn atom or the inaccuracy of Mooney's co-ordinates - its position was estimated at

O_1 : x = 0.318 ; z = 0.072

The regular tetra-hedral arrangement for the MnO_4^- ion and the coplanarity, parallel to the projection, of the O_1 and O_2 atoms were assumed and the Mn to O_2 distance was taken as the bond length.

Using these oxygen co-ordinates, the contribution F_c^O was determined and together with F_c^{KMn} gave the calculated structure factors F_c.

At this stage the temperature correction (TABLE 3.5) was applied to F_o and F_u was re-normalised to F_c using the same range of reflections. ($\sin\theta > 0.6$).

The first Difference synthesis was carried out using coefficients ($F_u - F_c^{KMn}$). The oxygen contributions were

omitted/...

omitted in an attempt to sharpen the oxygen peaks. Slight adjustments were made to all but the Mn positions. The co-ordinates at this stage are given in TABLE 3.6.

TABLE 3.6.

AFTER FIRST DIFFERENCE SYNTHESIS		
ATOM	x	z
K	0.175	0.158
Mn	0.440	0.177
O_1	0.333	0.073
O_2	0.100	0.417
O_3	0.417	0.300
O_4	0.417	0.300

F_c was re-calculated using these positions and renormalised with F_u.

A second Difference synthesis was performed with coefficients, $(F_u - F_c)$, including all contributions. No changes were suggested and a second Fourier synthesis was calculated using these values of F_u as coefficients. This synthesis showed slight corrections for K, O_2 and $O_{3,4}$ and gave no definite peak for O_1. The position of O_2 was also not completely unambiguous.

A new structure factor was calculated, $(F_c^{KMnO_{3,4}})$. The third Difference synthesis using $(F_u - F_c^{KMnO_{3,4}})$ as coefficients gave a more clearly defined peak for O_2 at

$$O_2 : x = 0.097 \; ; \; z = 0.408.$$

The position of O_1 was still not completely established, and further calculations based on a regular tetrahedron and Mn-O bond-length of 1.58Å, showed that a peak approximating to O_1 on the third Difference map lay at a distance of 1.27Å. The angle, peak-Mn-O_2, was approximately the tetrahedral angle (109°). An estimated position for O_1 was taken along this direction but at

distance/...

distance corresponding to 1.6Å.

The two possibilities were then

O_1 (peak) : x = 0.345 ; z = 0.062

O_2 (estimated) : x = 0.318 ; z = 0.027

The contributions to the structure factor for both positions and the corresponding residuals (R) were calculated.

The residual factor $R = \frac{\sum \left| |F_u| - |F_c| \right|}{\sum |F_u|}$

R (peak) = 0.274

R (estimated) = 0.296

Because the "peak" position gave the lower residual, it was taken as the O_1 position.

A fourth Difference synthesis, after careful scaling of observed and calculated structure factors, using $\sum |F_c| / \sum |F_u|$, suggested no further changes.

The residual factor R = 0.230 or 23%

The co-ordinates at this stage are given in TABLE 3.7.

TABLE 3.7

AFTER FOURTH DIFFERENCE SYNTHESIS		
ATOM	x	z
K	0.175	0.150
Mn	0.437	0.188
O_1	0.345	0.062
O_2	0.097	0.408
O_3	0.408	0.300
O_4	0.408	0.300

A final (third) unirradiated Fourier synthesis was performed and the electron-density projection $\rho(x,z)$ is shown in FIGURE 3.2. The coefficients for this synthesis were the structure factors, F_u, based on the co-ordinates in TABLE 3.7, after normalisation with the calculated and

irradiated/...

irradiated structure factors, F_c and F_i, respectively. (TABLE 3.9).

In FIGURE 3.2, the unbroken lines represent contours at intervals of 200 units, while for greater detail in the oxygen peaks, the intermediate 100 unit contours have been drawn in with broken lines. THE BROKEN LINES DO NOT REPRESENT NEGATIVE CONTOURS.

3.3.4.3. Recalculation of Sin θ.

The values of the lattice parameters (Section 3.3)

$$a = 9.132\text{Å} \; ; \quad c = 7.405\text{Å}$$

for unirradiated $KMnO_4$, compared to Mooney's values

$$a = 9.09\text{Å} \; ; \quad c = 7.41\text{Å} \; ,$$

were used to recalculate sin θ_{h0l}. The changes were small and the effect on the correction factors and atomic scattering factors used, based on Mooney's values, was insignificant in comparison to other uncertainties e.g. absorption and temperature corrections.

The same applied to the small increase in lattice parameters on irradiation:

$$a = 9.151\text{Å} \; ; \; c = 7.438\text{Å}$$

3.3.4.4. Irradiated $KMnO_4$ (500 Mrad).

Measurements on the integrated Weissenberg photograph of the irradiated crystal gave a set of densities, D_m (TABLE 3.3). These were corrected in the same way as in the unirradiated determination. Values of A* and $|F_o|$ are listed in TABLE 3.3. The same temperature correction (B=2.2) was applied giving values of the irradiated structure amplitude, $|F_i|$ (TABLE 3.5).

3.3.4.5. Normalisation.

Prout and Woods [279,280] reported no change in the positions of the Ag and Mn atoms in $AgMnO_4$ on irradiation. It was thus assumed that there would be no change in the K

and/...

and Mn positions in irradiated $KMnO_4$. Any change was sought in the positions of the oxygen atoms. The unirradiated and irradiated structure factors were therefore normalised using values where the oxygen contributions to the total structure factor were small.

Signs for the irradiated structure factors were taken to be the same as the unirradiated. Where low values caused doubt, trial and error was used or these factors were omitted in preliminary calculations.

There were thus three sets of structure factors:-

$$F_u \ , \ F_i \ , \ F_c .$$

TABLE 3.8 shows the reflections with low oxygen contributions to F_c, and the details of the normalisation process. The scaling factors were: unirradiated x 1.686
irradiated x 1.073

TABLE 3.9 gives the normalised values of F_u and F_i compared to F_c.

The values of F_i were used as coefficients in the calculation of the first irradiated Fourier synthesis. The electron-density projection $\rho(x,z)$ is shown in FIGURE 3.3.

In FIGURE 3.3 as in FIGURE 3.2, the contours are at 200 unit intervals (unbroken lines) with intermediate 100 unit contours filled in for the oxygen peaks (broken lines).

TABLE 3.8./...

TABLE 3.8

hol	Sin θ	$\|F_u\|$	$\|F_i\|$	$\|F_c\|$	$\|F_u\|/\|F_i\|$	$\|F_c\|/\|F_u\|$	$\|F_c\|/\|F_i\|$
208	0.8489	4.11	6.71	8.90	0.6125	2.165	1.326
303	0.4204	11.9	17.9	19.7	0.6648	1.655	1.101
405	0.6206	10.2	16.6	15.5	0.6145	1.520	0.934
508	0.9328	3.99	6.06	4.32	0.6584	1.083	0.713
800	0.6781	10.3	15.6	18.8	0.6603	1.825	1.205
802	0.7092	6.38	9.97	10.9	0.6399	1.708	1.083
806	0.9213	7.64	12.7	11.5	0.6016	1.505	0.906
1003	0.9028	2.04	3.31	5.73	0.6163	2.809	1.731
		Σ_u= 56.56	Σ_i=88.85	Σ_c=95.35	Σ_u/Σ_i=0.6366	Σ_c/Σ_u=1.686	Σ_c/Σ_i=1.073

TABLE 3.9.

h01	F_c	F_u	F_i	$F_i - F_u$
002	23.6	19.2	17.2	2.0
004	9.30	9.14	8.06	1.08
006	13.5	14.9	14.6	0.3
008	13.0	12.9	12.4	0.5
101	9.04	8.23	5.82	2.41
102	14.8	14.1	14.1	0
104	6.61	9.26	8.18	1.08
105	3.94	6.59	5.91	0.68
107	6.92	8.06	7.44	0.62
108	8.63	6.73	6.43	0.30
200	11.7	14.4	13.2	1.20
201	15.1	14.0	12.8	1.20
202	12.1	16.1	15.1	1.00
203	13.9	13.1	13.7	0.60
204	5.44	5.48	4.91	0.57
205	6.11	5.60	4.59	1.01
207	9.94	8.04	9.07	1.03
208	8.90	6.93	7.20	0.27
209	12.1	9.86	8.85	1.01
301	5.33	6.14	5.56	0.58
302	0.45	8.26	7.68	0.58
303	19.7	20.1	19.2	0.90
304	8.43	9.93	10.5	0.57
305	7.42	8.67	9.20	0.53
306	5.42	8.70	8.76	0.06
308	2.62	3.59	3.98	0.39
309	3.69	5.93	5.13	0.80
400	18.7	12.6	12.0	0.50
401	30.6	22.6	20.1	2.50
403	11.0	14.4	14.8	0.40
404	2.73	3.62	4.22	0.60
405	15.5	17.2	17.8	0.60
407	14.0	14.4	16.5	2.10
501	7.54	6.29	5.16	1.13
503	7.71	13.00	13.1	0.10
504	10.0	8.62	9.40	0.78
506	8.07	8.18	9.24	1.06
507	5.55	3.81	3.53	0.28
508	4.32	6.73	6.50	0.23

TABLE 3.9/...

TABLE 3.9 contd.

h01	F_c	F_u	F_i	$F_i - F_u$
600	$\overline{7.28}$	$\overline{8.68}$	$\overline{7.89}$	0.79
601	5.32	8.53	7.65	$\overline{0.88}$
602	9.98	8.85	7.88	$\overline{0.97}$
603	$\overline{3.17}$	$\overline{4.86}$	$\overline{3.42}$	1.44
604	$\overline{6.77}$	$\overline{3.59}$	$\overline{3.25}$	0.34
607	3.63	3.89	3.26	$\overline{0.63}$
608	9.53	6.98	6.03	$\overline{0.95}$
701	3.27	3.84	3.28	$\overline{0.56}$
702	$\overline{17.2}$	$\overline{14.6}$	$\overline{14.4}$	0.20
703	$\overline{10.2}$	$\overline{5.36}$	$\overline{5.32}$	0.04
704	9.57	10.7	11.9	1.20
705	6.40	5.65	6.33	0.68
707	0.29	6.46	5.93	$\overline{0.53}$
800	$\overline{18.8}$	$\overline{17.4}$	$\overline{16.7}$	0.70
802	10.9	10.8	10.7	$\overline{0.10}$
806	$\overline{11.5}$	$\overline{12.9}$	$\overline{13.6}$	$\overline{0.70}$
902	$\overline{4.66}$	$\overline{4.01}$	$\overline{4.47}$	$\overline{0.46}$
904	$\overline{4.94}$	$\overline{4.00}$	$\overline{4.38}$	$\overline{0.38}$
905	10.1	9.24	9.22	$\overline{0.02}$
1002	2.08	4.06	3.86	$\overline{0.20}$
1003	5.73	3.44	3.55	0.11
1004	$\overline{0.31}$	$\overline{4.59}$	$\overline{3.19}$	1.40
1101	5.08	2.71	3.78	1.07
1102	10.8	5.61	5.03	$\overline{0.58}$
1103	$\overline{10.9}$	$\overline{9.22}$	$\overline{10.0}$	$\overline{0.78}$

3.3.4.6. Electron Density Profiles.

The unirradiated (FIGURE 3.2) and irradiated (FIGURE 3.3) electron-density syntheses were compared directly.

Comparative electron-density profiles drawn through various sections are shown in FIGURES 3.4 to 3.10.

3.3.4.7./...

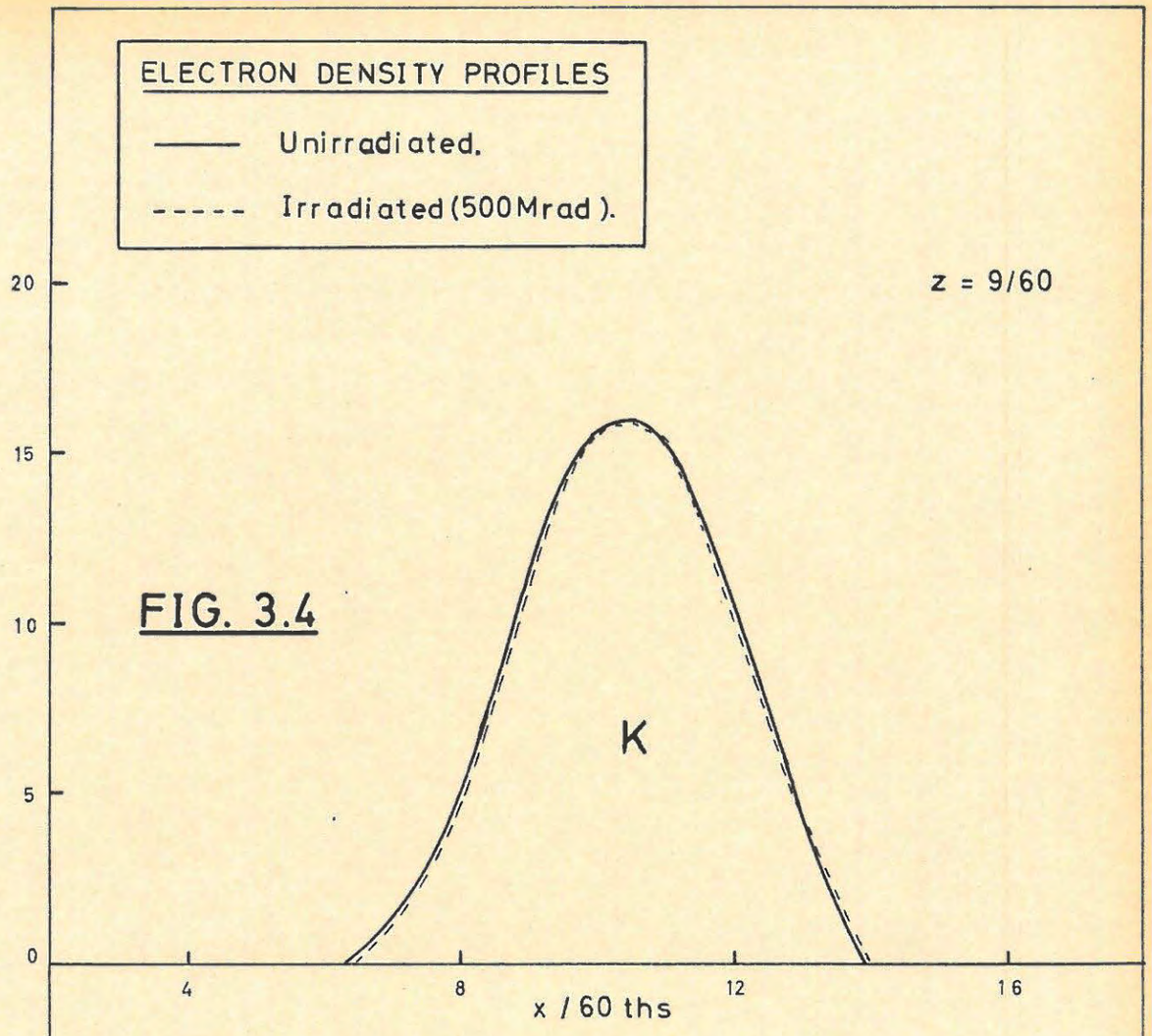
ELECTRON DENSITY PROFILES
Unirradiated.
Irradiated (500 Mrad).
z = 9/60
K
20
15
10
5
0
4
8
12
16
x / 60 ths

FIG. 3.4

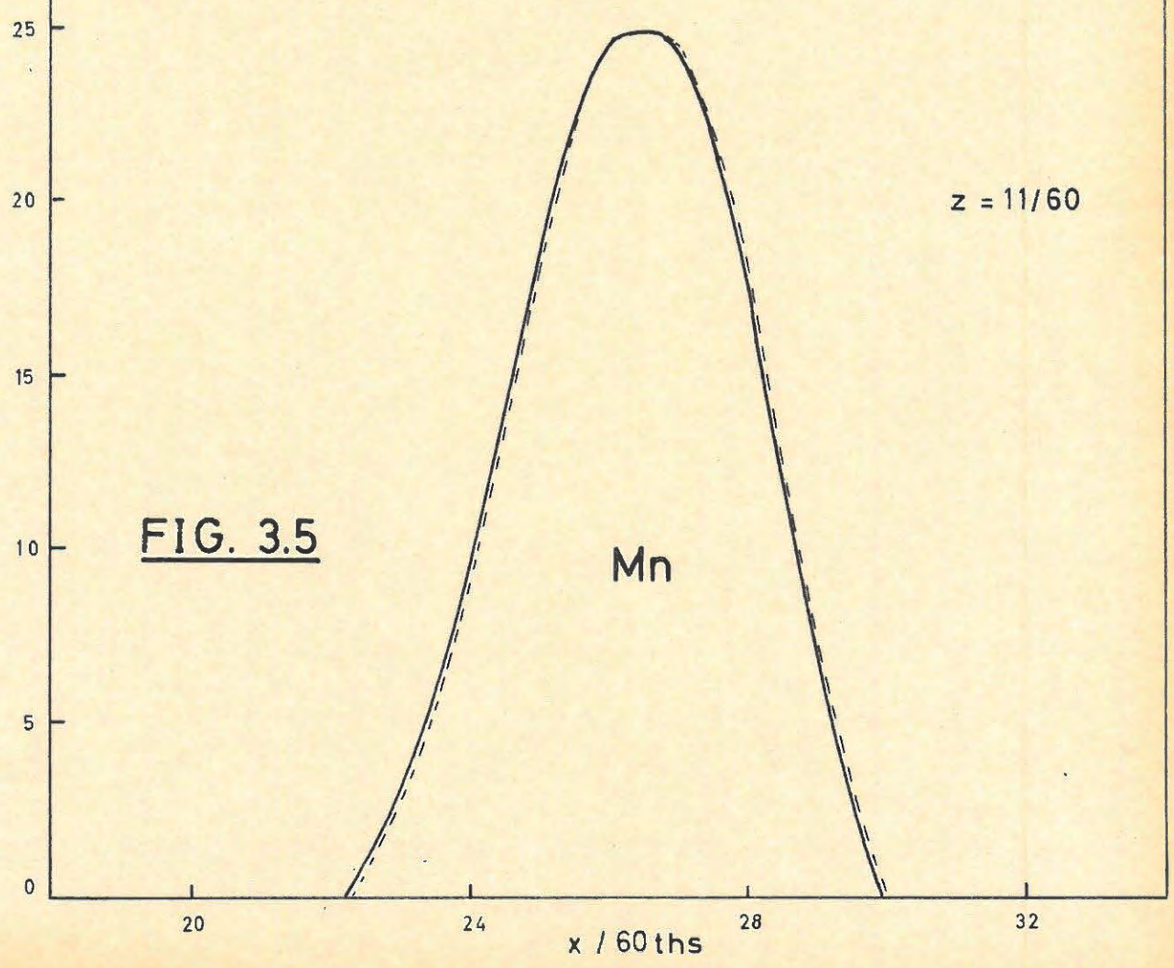
z = 11/60
Mn
25
20
15
10
5
0
20
24
28
32
x / 60 ths

FIG. 3.5

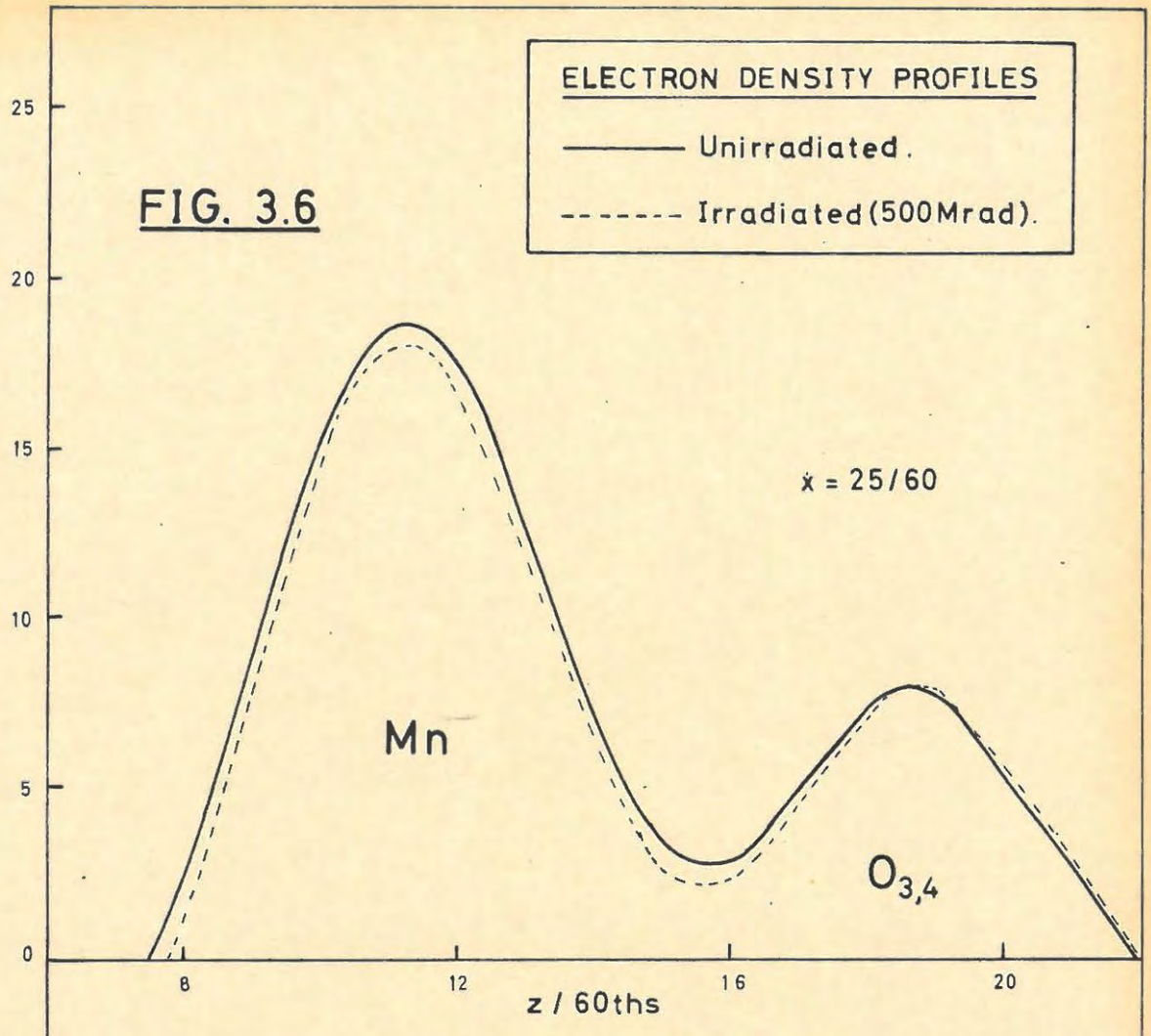
ELECTRON DENSITY PROFILES
Unirradiated.
Irradiated (500Mrad).
x = 25/60
Mn
O3,4
25
20
15
10
5
0
8
12
16
20
z / 60ths

FIG. 3.6

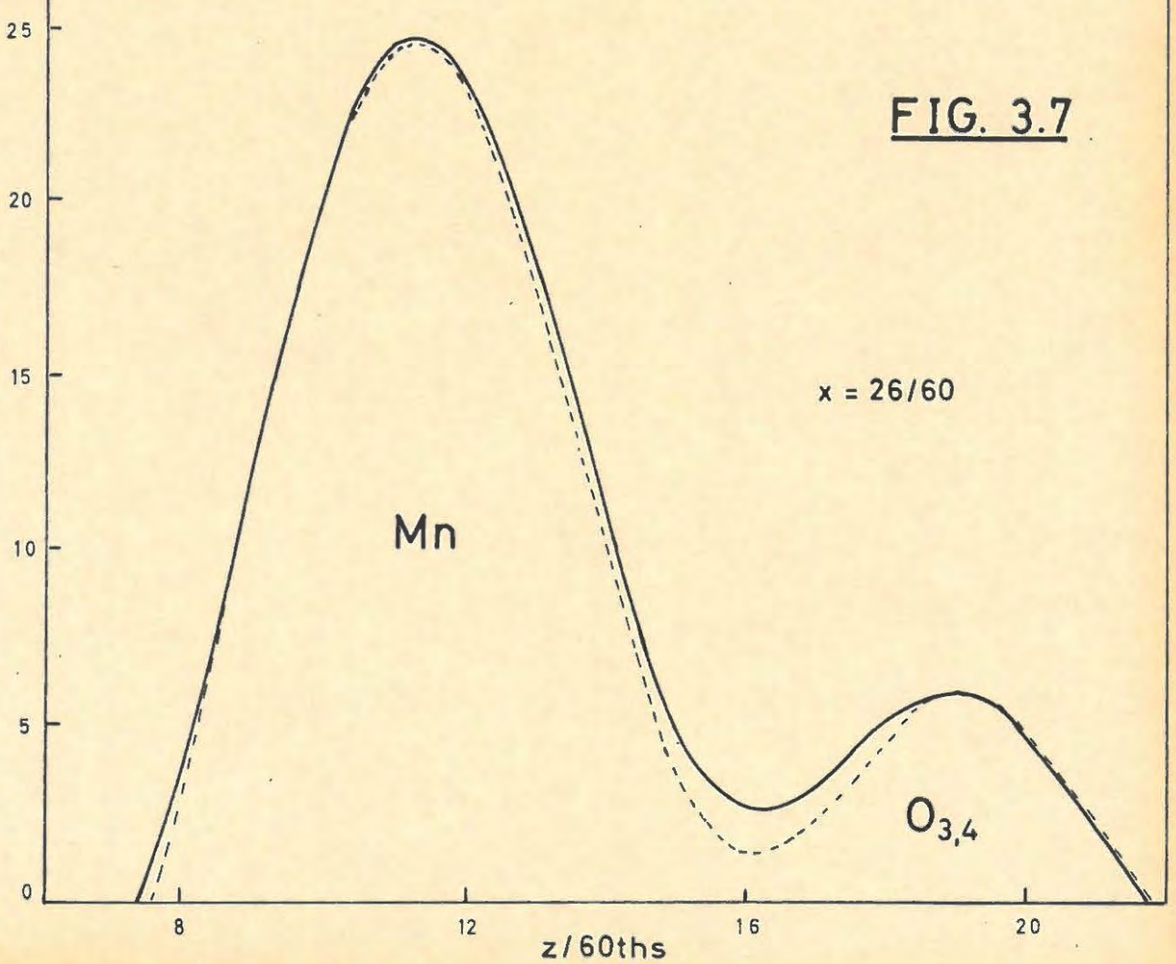
x = 26/60
Mn
O3,4
25
20
15
10
5
0
8
12
16
20
z/60ths

FIG. 3.7

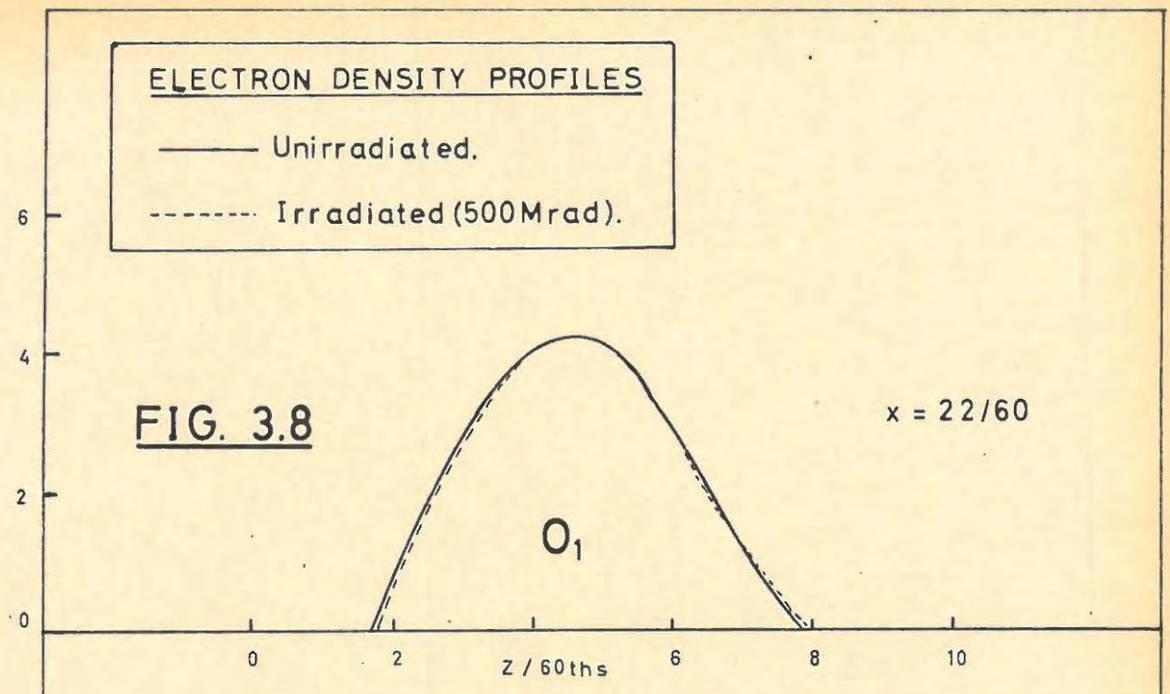

FIG. 3.8

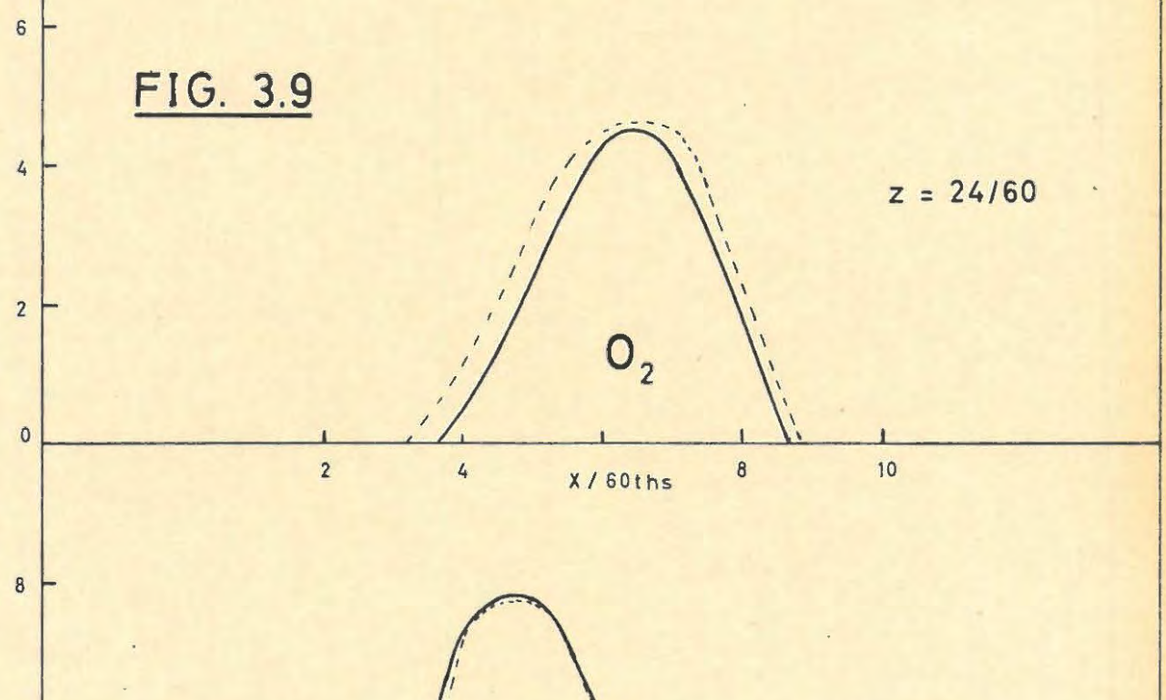

FIG. 3.9

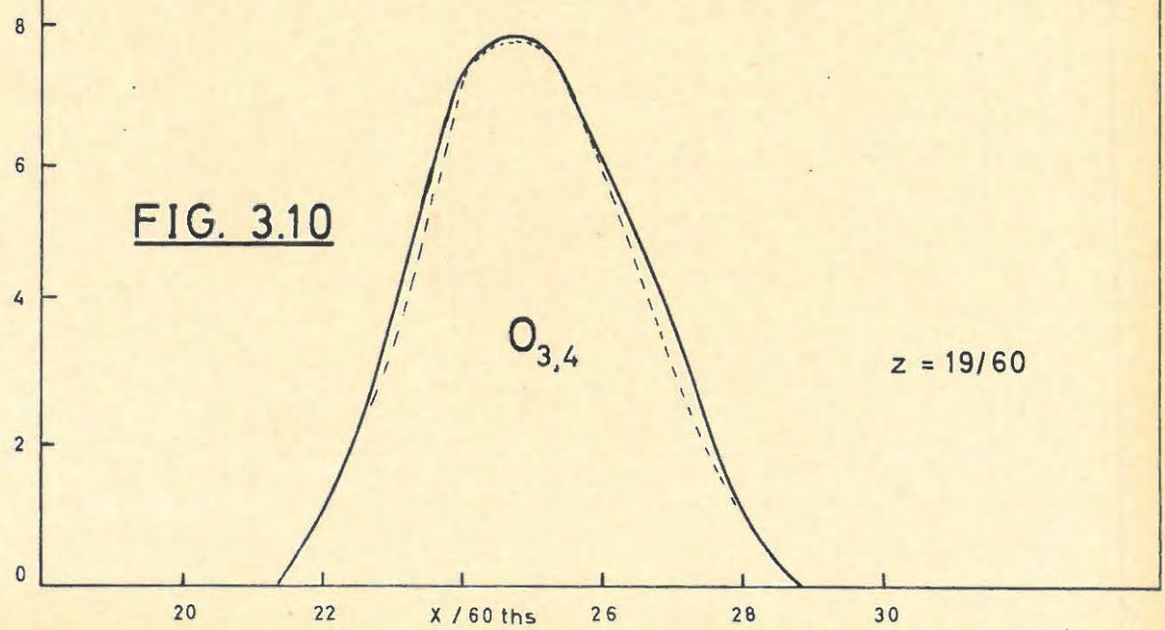

FIG. 3.10

3.3.4.7. The Irradiated - Unirradiated Difference Synthesis.

Finally a Difference synthesis was performed using the normalised values of $(F_i - F_u)$ as coefficients. These values are listed in TABLE 3.9. The synthesis is illustrated in FIGURE 3.11. In contrast to FIGURES 3.2 and 3.3, the contours are at 40 unit intervals (not 200 units), and the unbroken lines represent POSITIVE contours and the broken lines, NEGATIVE contours.

3.3.4.8. The $KMnO_4$ Unit Cell.

A scale projection, parallel to [010], of the $KMnO_4$ structure is shown in FIGURE 3.12. The ionic radii[318] used were:-

K^+ 1.33Å
Mn^{+7} 0.46Å
O^{-2} 1.40Å

3.4. LATTICE PARAMETERS AND LATTICE EXPANSION ON IRRADIATION.

3.4.1. Precession Photographs [319].

Measurements from zero-layer precession photographs (magnification factor: 6) of both unirradiated and irradiated crystals, revealed no changes greater than 1 in 10^4 in the parameters. The values from the photographs, which were processed together, were:-

$$b = 5.701\text{Å} \; ; \quad c = 7.384\text{Å}$$

3.4.2. Extrapolation Method [320-322].

For an orthorhombic crystal oscillated about its b-axis, the Bragg angles of spots lying on the zero-layer line of the resulting photograph are given by:-

$$\sin^2\theta_{h0l} = \frac{\lambda^2}{4}\left(\frac{h^2}{a^2} + \frac{l^2}{c^2}\right)$$

$$\text{i.e.} \quad a = \frac{\lambda}{2}\sqrt{\left(h^2 + \frac{a^2}{c^2}l^2\right)}\ \text{cosec}\ \theta$$

If/...

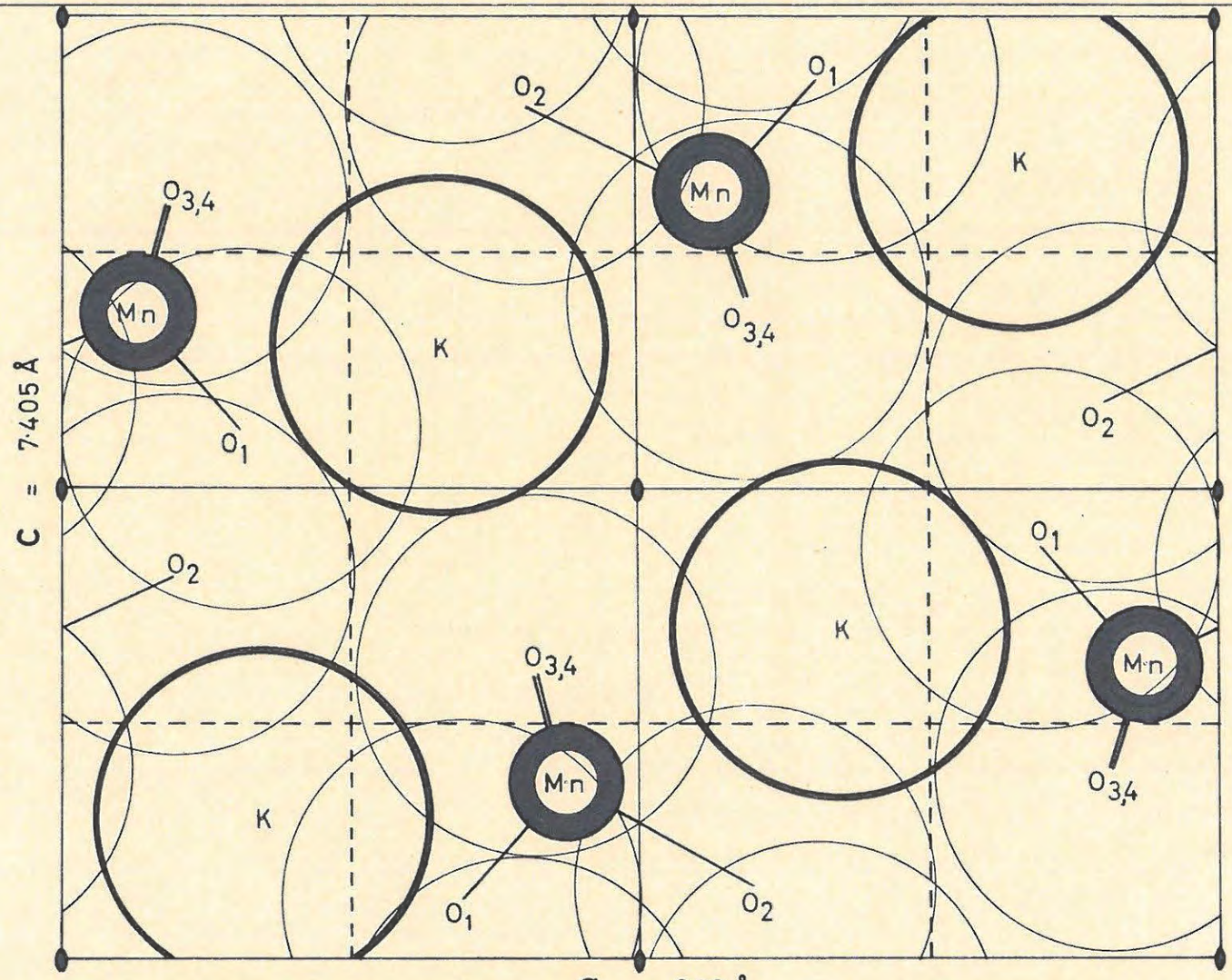
O2
O1
Mn
K
O3,4
O3,4
Mn
O1
K
O2
O2
O1
K
Mn
O3,4
O3,4
Mn
K
O1
O2
c = 7·405 Å
a = 9·13 Å

FIG. 3.12

If h is large compared to l, a small error in a/c will not greatly affect the derived value of a.

Starting with approximate values of a and c (Mooney's values of a = 9.09Å ; c = 7.41Å), several values of a can be derived from reflections having $\theta > 60^{\circ}$. The 'true' value of a is obtained by extrapolation to $\theta = 90^{\circ}$. From a , c can be determined. A second photograph about the a- or c-axis is required to determine b in the same way.

Measurements were made on normal-beam, zero-layer Weissenberg photographs of unirradiated and irradiated crystals. The crystals were approximately the same size and the photographs were taken under the same conditions and processed together. Emphasis was on similar conditions for comparison and detection of expansion, rather than on absolute measurement.

Systematic errors that may arise in the accurate determination of lattice parameters include eccentricity of the specimen, lack of knowledge of the exact film radius, absorption by the specimen and film shrinkage. Nassimbeni[322] reported no film shrinkage under standard processing conditions. Various functions have been used for extrapolation in an attempt to minimise the other errors e.g.

(1) $\cos^2\theta/\theta$ and (2) $\cos^2\theta/\sin^2\theta$ [323]

(3) $\cot\theta . \cos^2\theta$ [324]

(4) $(\cos^2\theta/\sin\theta) + (\cos^2\theta/\theta)$ [325]

The eccentricity error is proportional to $\cos^2\theta$, but the absorption error is covered best by function (3) above.

Function (4) can give a plot which will be accurately linear down to $\theta = 30^{\circ}$, a much lower angle than for $\cos^2\theta$.

Although/...

Although a plot of cot θ may have a greater range of linearity, it has the disadvantage that the high-angle points are not brought very close to the extrapolation limit. It also accentuates random errors.

Function (4) was used as recommended by Parrish [326]. Tables of the function are given by Nelson and Riley [327].

The weighted mean wavelength for Cu K_α was taken as 1.5418Å after Lonsdale [328].

3.4.3. Results.

FIGURES 3.13 and 3.14 show the plots for unirradiated and irradiated crystals respectively.

To measure the parameter b, comparative unirradiated and irradiated rotation photographs, about the b-axes, were taken using a large radius (5.73 cm) semi-circular camera. The films were processed together.

The values of the unirradiated and irradiated parameters as well as the percentage expansion on irradiation. are given in TABLE 3.10.

TABLE 3.10.

	UNIRRADIATED	IRRADIATED (500 Mrad)	EXPANSION %
a	9.132 Å	9.151 Å	0.21
b	5.679 Å	5.696 Å	0.30
c	7.405 Å	7.438 Å	0.45
Vol.	384.028	387.699	0.96

Although the change in b can be questioned on account of the inaccuracy of the rotation method for determining parameters, the change is in the right direction and of the same order as in a and c. That

these/...

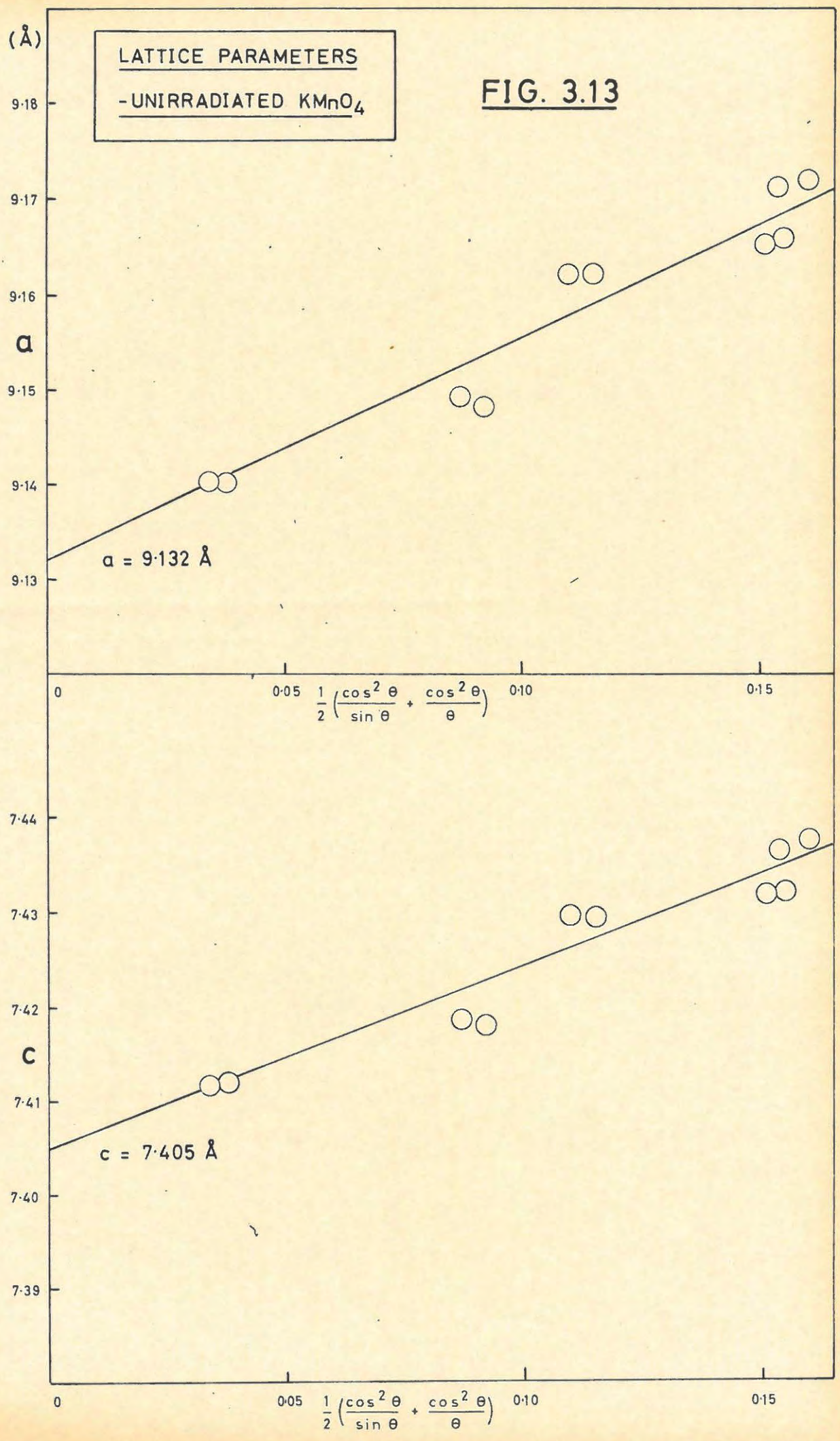
(Å)
LATTICE PARAMETERS
-UNIRRADIATED KMnO4
FIG. 3.13
9·18
9·17
9·16
a
9·15
9·14
9·13
a = 9·132 Å
0
0·05
1/2 (cos² θ/sin θ + cos² θ/θ)
0·10
0·15
7·44
7·43
7·42
c
7·41
7·40
7·39
c = 7·405 Å
0
0·05
1/2 (cos² θ/sin θ + cos² θ/θ)
0·10
0·15

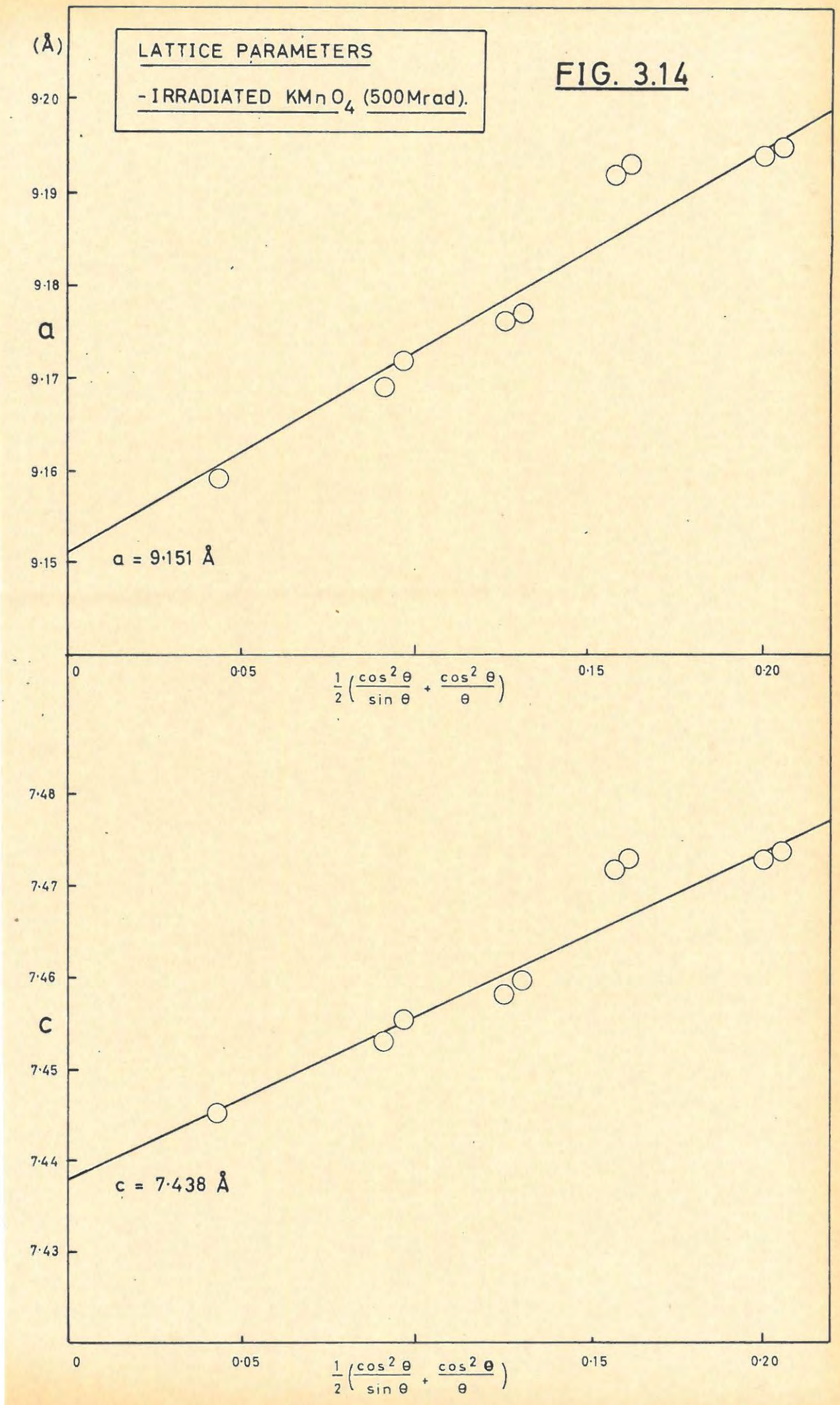
LATTICE PARAMETERS
- IRRADIATED KMnO4 (500Mrad).
FIG. 3.14
(Å)
9·20
9·19
9·18
a
9·17
9·16
9·15
a = 9·151 Å
0
0·05
0·15
0·20
$\frac{1}{2}\left(\frac{\cos^2\theta}{\sin\theta} + \frac{\cos^2\theta}{\theta}\right)$
7·48
7·47
7·46
c
7·45
7·44
7·43
c = 7·438 Å
0
0·05
0·15
0·20
$\frac{1}{2}\left(\frac{\cos^2\theta}{\sin\theta} + \frac{\cos^2\theta}{\theta}\right)$

these changes (a and c) are less ambiguous can be seen from FIGURES 3.13 and 3.14. The magnitudes of the changes lie outside the limits of the possible choice of extrapolation slope.

3.5. DIFFUSE X-RAY REFLECTIONS FROM IRRADIATED SINGLE CRYSTALS OF POTASSIUM PERMANGANATE.

The damage produced in a crystal on irradiation can have the following effects which may be detected by X-ray diffraction investigations (see Introduction):-

(1) Lattice expansions.

(2) An artificial temperature factor.

(3) Pronounced diffuse scattering.

Lattice expansions were found for irradiated (500 Mrad) $KMnO_4$ (see section 3.4), but no artificial temperature factor was apparent.

To investigate the presence of diffuse scattering a number of series of Laue photographs were taken.

3.5.1. "Standard" Conditions for Laue Photographs.

The Philips generator was operated at 40 kV and 20 mA and the copper radiation was not filtered, except where specified.

A flat-plate camera loaded with a two-film pack was used. The first film was Crystallex to cut down the heavy background at long exposures, and the second film was Industrex D. The exposure was 8 hours at a crystal-to-film distance of 4 cms. Processing was standard.

3.5.2. The Axes of the Crystal.

A section through a $KMnO_4$ crystal, perpendicular to the needle (b-)axis is shown in FIGURE 3.16. The axes and interfacial angles are as shown.

The/...

The "standard" AXIAL position used in referring to the Laue photographs, was taken as the setting with the b-axis vertical and the a-axis parallel to the X-ray beam.

3.5.3. Initial Laue Series.

With the b-axis vertical and starting from the standard AXIAL position, a series of Laue photographs was taken at 5° intervals, through 90°. These photographs showed a large number of diffuse maxima, as well as asterism and radial streaking. Very intense diffuse reflections, encountered at a setting of AXIAL + 75°, were chosen for closer study.

A sub-series was taken at settings
AXIAL + 70°, 72°, 73°, 74°, $74\frac{1}{2}^{\circ}$, 75°, $75\frac{1}{2}^{\circ}$, 76° and 77°.

Plate I shows the settings
(a) 70° (b) 72° (c) 74° (d) 76° (e) 78°.

The indices of the reciprocal lattice point (relp), associated with these diffuse maxima, were determined, by comparison with rotation photographs, to be 210.

The diffuse spots are considered to arise from 'domains' of diffuse intensity surrounding the reciprocal lattice point. The shape of these domains varies.

3.5.4. The Relation between the Bragg (characteristic), Laue and Diffuse Reflections [329].

FIGURE 3.15 represents the zero-layer of the reciprocal lattice for $KMnO_4$ with the c* axis perpendicular to the paper. SS is the sphere of reflection, centre P, with unit radius OP.

The initial position of the relp 210 corresponding to Cu K_{α}, λ = 1.5418 Å, is A. L is the point of intersection of OA produced, with the sphere of reflection.

PL/...

RECIPROCAL LATTICE DIAGRAM FOR THE DIFFUSE REFLECTIONS ASSOCIATED WITH 210

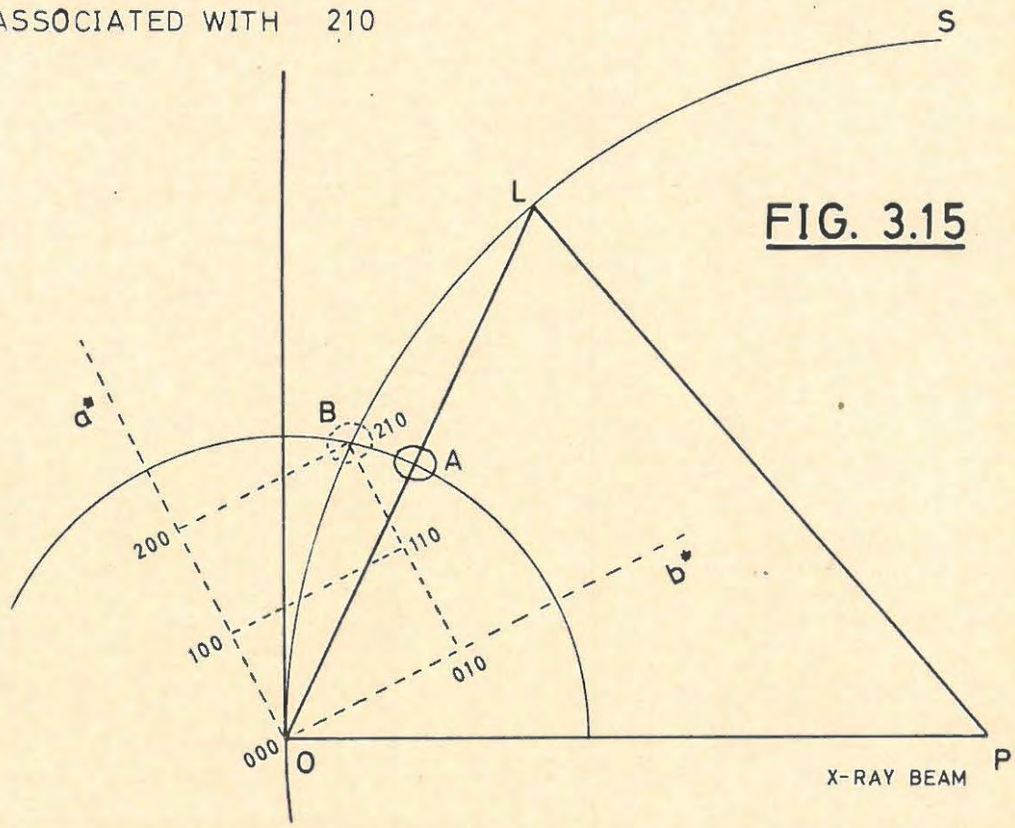

FIG. 3.15

$KMnO_4$ AXES AND INTERFACIAL ANGLES

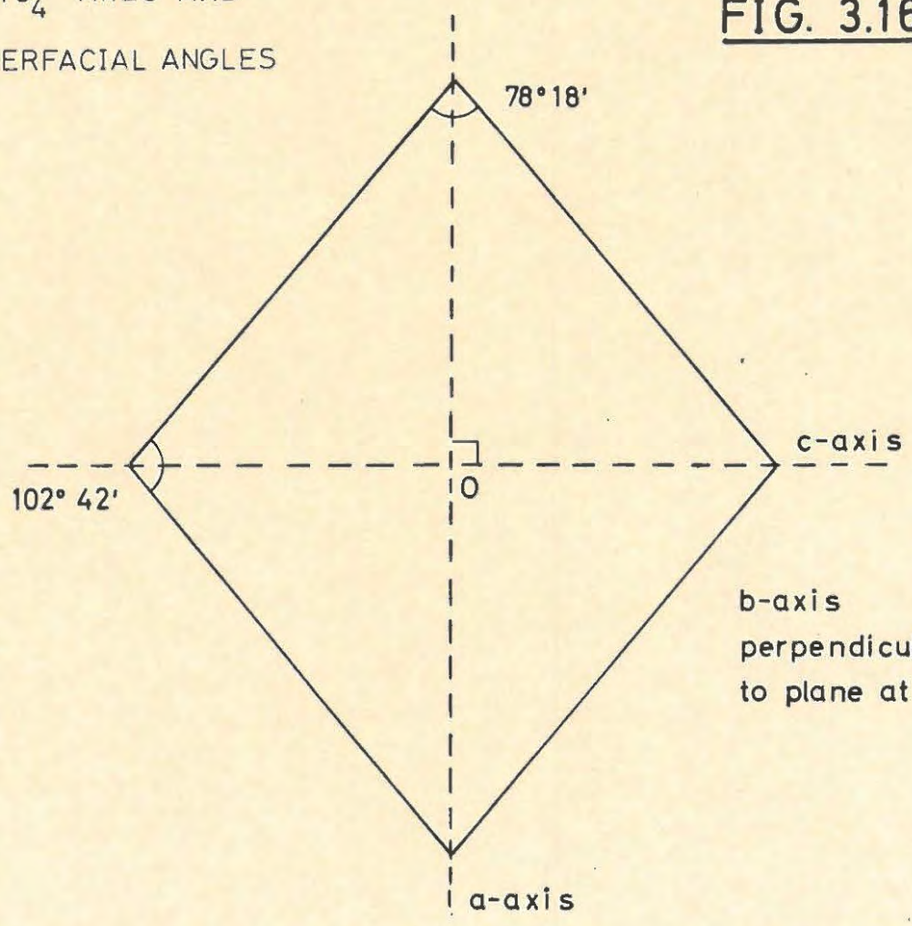

FIG. 3.16

PL thus defines the direction of the Laue reflection 210.

Suppose now that the reciprocal lattice rotates about the c* axis at O, in an anti-clockwise direction:-

L moves along the circle SS and the Laue spot approaches the position of the characteristic (Bragg) reflection at B, where the relp 210 intersects the sphere of reflection. Before the co-incidence setting is reached however, the diffuse domain about A intersects SS, in a region between B and L. A faint diffuse reflection then appears slightly displaced from the position of the 210 Bragg reflection, towards that of the Laue spot. As A moves towards B, the diffuse reflection grows stronger and its displacement from the Bragg position decreases. Finally Laue, Bragg and diffuse reflections coincide when A reaches B. Further rotation displaces the Laue spot on the other side of the Bragg position and the diffuse domain moves slowly out of the sphere of reflection while the Laue spot moves away rapidly.

The series of Laue photographs shown in PLATE I was taken with the b-axis perpendicular to the X-ray beam. The angles between the a-axis and the X-ray beam were:-

(a) 70° (b) 72° (c) 74° (d) 76° (e) 78°.

The diffuse reflections corresponding to both the K_{α} and K_{β} components of the unfiltered copper radiation can be seen.

PLATE I (a) shows the appearance of the 210α diffuse spot.

PLATE I (b) shows the 210β diffuse reflection, and the Laue reflection (L) approaching the 210α diffuse spot.

Coincidence of the Laue and 210α diffuse spots occurs in PLATE I (c), and of the 210β diffuse and Laue spots in PLATE I (d).

Insertion/...

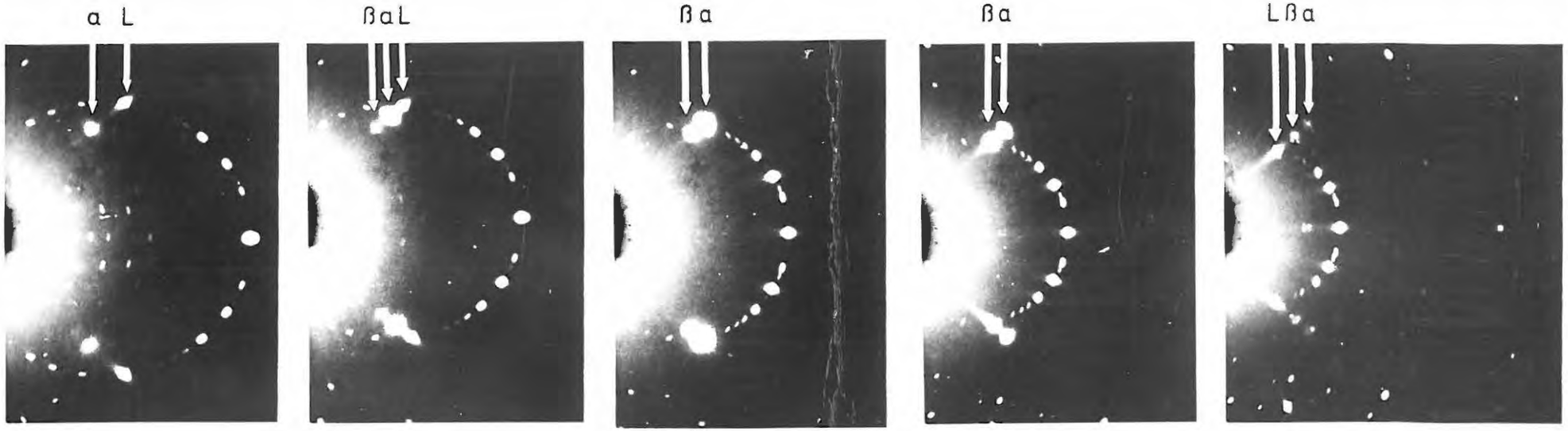

(a) 70° (b) 72° (c) 74° (d) 76° (e) 78°

PLATE I

GAMMA-IRRADIATED $KMnO_4$ (Dose:500Mrad), b-axis vertical.

(angles between a-axis and X-ray beam.)

Insertion of a Ni filter in the beam suppressed the K_β component. Only the diffuse reflection corresponding to the K_α radiation was apparent under these conditions.

According to Bunn [330] for Cu radiation the K_β component has about 1/6th the intensity of the K_α component. It would be expected that the one diffuse spot would be fainter than the other. This, however, depends upon the setting of the crystal. Lonsdale and Smith [331] state that often the K_β diffuse spot is more intense than the K_α, because its angle of mis-setting is less.

3.5.5. Unirradiated $KMnO_4$.

Comparative Laue photographs of an irradiated (500 Mrad) crystal and an unirradiated crystal, taken under the same conditions and processed together, are shown in PLATE II. (f) and (g) respectively. Faint diffuse reflections associated with (210) are visible for the unirradiated crystal, but these are larger and far more intense for the irradiated crystal.

3.5.6. Increased Irradiation Doses.

Laue photographs taken in the same setting (AXIAL + 75°), using a number of 500 Mrad crystals as well as crystals that had received total doses of 700 Mrad and 900 Mrad, all showed strong diffuse reflections. This confirmed that the diffuse scattering was not caused by the peculiar irregularities of a single crystal. There was no apparent increase in size or intensity of these diffuse reflections with increased irradiation dose, within this range of doses.

3.5.7. Laue Photographs at Liquid-air Temperature.

To determine whether the diffuse reflections were caused or enhanced by the thermal motion of the atoms, Laue

photographs/...

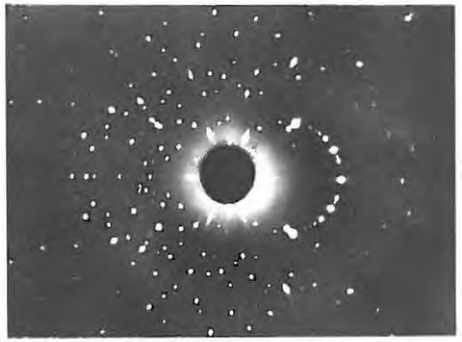

(f)

(h)

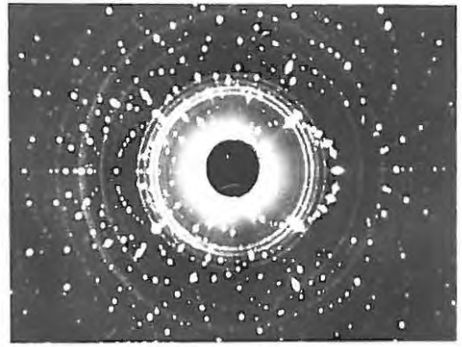

PLATE II

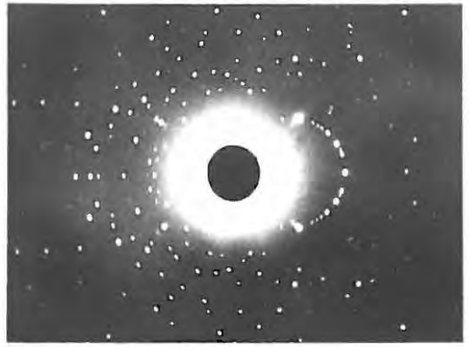

(g)

(i)

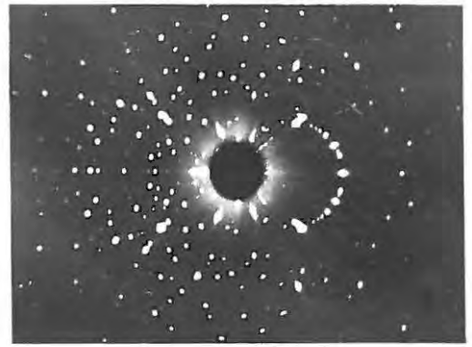

photographs were taken with the irradiated (500 Mrad) crystal at the temperature of liquid air. A Stoë low-temperature attachment was modified for use with the Unicam single-crystal goniometer.

Although icing-up and the attendant ice-pattern of rings and spots were unavoidable during the long exposures involved (5 hrs), the diffuse reflections associated with 210 were clearly visible and showed no marked decrease in intensity compared to Laues taken with the crystal at room temperature.

PLATE II (h) and (i) show the Laues at liquid-air, and room temperatures respectively.

3.5.8. The Three-Dimensional Form of the Diffuse Maxima.

Laue photographs with the b-axis vertical have shown that the two-dimensional shape of the diffuse maxima is approximately elliptical. This was confirmed by a 5° oscillation photograph using a Ni filter.

To ascertain whether the three-dimensional form was that of an ellipsoid or of a flat disc, series of Laue photographs were taken:-

(i) with the a-axis vertical.

(ii) with the c-axis vertical.

The required crystal settings and the positions of the 210 reflection on a flat film at a distance of 4 cms, for these settings are given in TABLE 3.11.

X is the horizontal distance of the 210 reflection from the centre of the film and Y the vertical distance.

TABLE 3.11./...

TABLE 3.11.

VERTICAL AXIS	SETTING	X cm	Y cm
b	a-Axial + 73° 54'	1.43	1.19
a	c-Axial + 20° 12'	1.13	1.46
c	b-Axial - 26° 52'	1.84	0

Laue photographs about all three axes showed elliptical diffuse maxima associated in particular with the relp 210, but also with many other relps. The three-dimensional form can thus be assumed to be that of an ellipsoid. This shape was predicted by Kanazaki[3328] for cubic crystals with pairs of defects.

3.6. LAUE STUDIES ALONG THE INDUCTION PERIOD IN THE THERMAL DECOMPOSITION OF UNIRRADIATED AND IRRADIATED POTASSIUM PERMANGANATE CRYSTALS.

Assuming that the diffuse scattering found in Laue photographs of irradiated (500 Mrad) $KMnO_4$, and studied in particular about the reflection 210, was due to structural defects, it was of interest to follow these diffuse reflections as the thermal decomposition of the irradiated material proceeded. The irradiation dose (500 Mrad) is higher than that of Prout and Herley [277] (10 Mrad) and any differences between irradiated and unirradiated Laues under the same conditions, should be more marked.

3.6.1. The Thermal Decompositions.

Runs were done to determine the curves for unirradiated $KMnO_4$ at 215°C, and irradiated (500 Mrad) $KMnO_4$ at 185°C. These temperatures were chosen to give induction periods of approximately 100 mins. The results are listed in TABLE 3.12 and the curves are shown in FIGURE 3.17 (Unirradiated) and FIGURE 3.18 (Irradiated).

TABLE 3.12./...

TABLE 3.12

UNIRRADIATED $KMnO_4$			215°C		18.8 mg.
t	p	t	p	t	p
20	0.53	110	4.72	165	49.92
40	1.02	116	5.62	172	58.33
55	1.53	122	6.98	177	62.45
63	1.83	129	9.87	185	69.32
69	2.07	135	15.12	196	76.31
78	2.47	143	23.10	205	79.72
87	2.93	149	29.90	215	79.97
95	3.37	154	35.98	p_f	80.00
102	3.87	160	44.06	p_a	91.8

IRRADIATED $KMnO_4$	500 Mrad		185°C		17.2 mg.
t	p	t	p	t	p
33	0.25	143	30.65	220	70.23
40	0.38	146	36.55	233	72.05
81	1.54	150	40.94	245	73.44
90	1.83	155	44.34	260	75.30
105	2.45	160	47.35	280	77.13
115	3.00	165	49.84	300	78.25
120	3.44	170	52.14	320	79.38
125	4.20	175	54.69	340	80.00
130	5.56	180	57.36		
134	9.19	190	62.20	p_f	80.00
137	15.65	200	66.03	p_a	64.0
140	22.96	210	68.69		

Two runs each, on unirradiated and irradiated (500 Mrad) $KMnO_4$ were done at 230°C, to check the final pressure, p_f, against the sample weight, w.

The results are given in TABLE 3.13.

TABLE 3.13./...

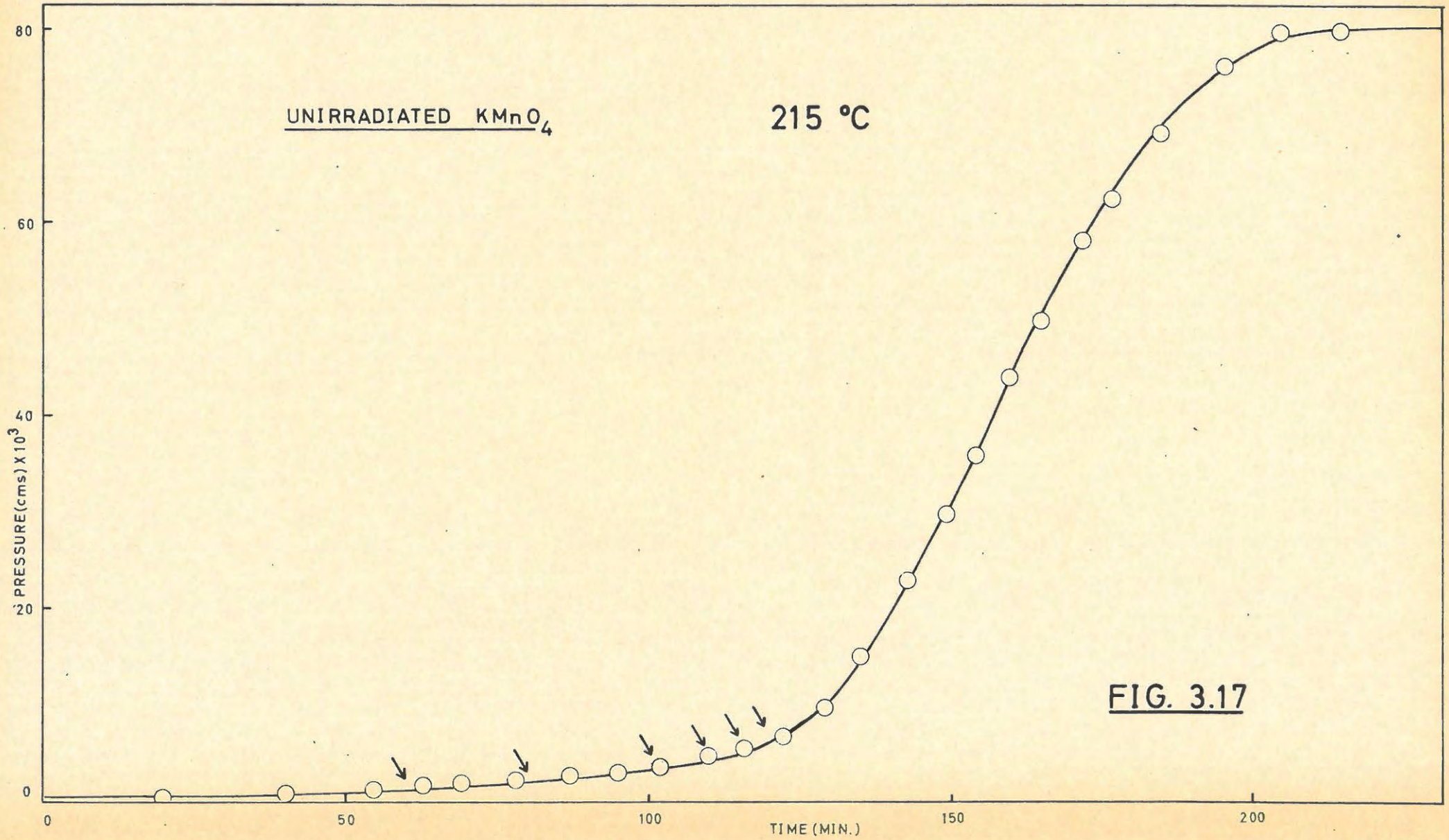
UNIRRADIATED $KMnO_4$
215 °C
PRESSURE(cms) X 10^3
0
20
40
60
80
0
50
100
150
200
TIME (MIN.)

FIG. 3.17

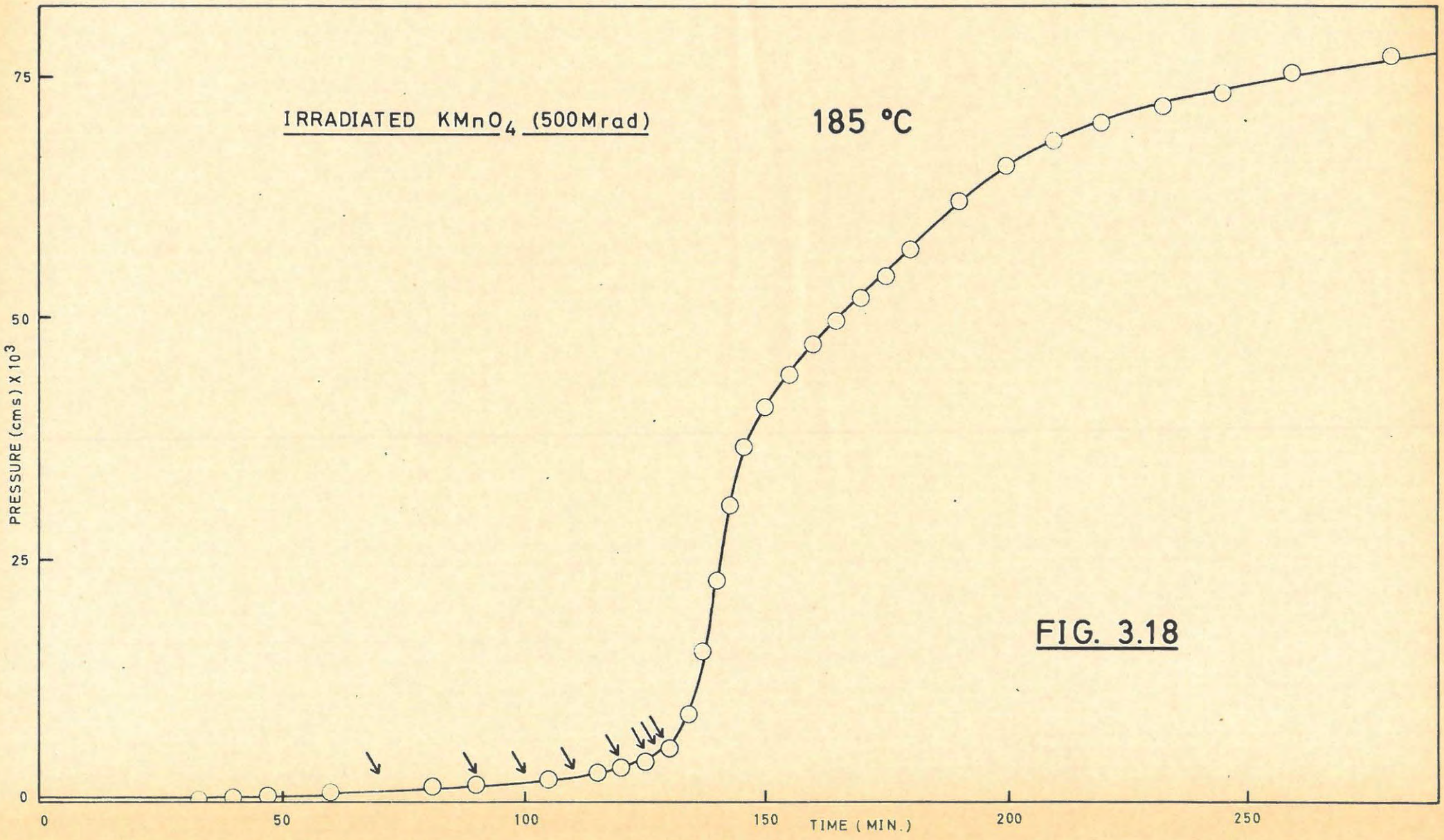
IRRADIATED KMnO4 (500Mrad)
185 °C
PRESSURE (cms) X 10^3
75
50
25
0
0
50
100
150
200
250
TIME (MIN.)

FIG. 3.18

TABLE 3.13

UNIRRADIATED			IRRADIATED		
p_f	w	p_f/w	p_f	w	p_f/w
73.0	17.0	4.294	72.1	17.1	4.216
73.9	17.2	4.297	72.1	17.1	4.216

These values are close enough to be within the limits of the errors involved in weighing. There is thus no detectable loss of gas during irradiation.

3.6.2. The Laue Photographs.

Fresh batches of crystals were used for each run to avoid uncertainties caused by heating lags. The decompositions were interrupted at the points marked on the curves, FIGURES 3.17 and 3.18.

The crystals were mounted with the b-axis vertical and in the reflecting position for the relp 210 (a-AXIAL + 76°), and Laue photographs using unfiltered copper radiation and standard conditions (Section 3.5.1) were taken.

3.6.2.1. Unirradiated $KMnO_4$ (215°C)

0 mins: Slight diffuse reflections. Spots sharp and well defined. PLATE II.(g).

60 mins: No significant change.

80 mins: Slight asterism. PLATE III.(j).

110 mins: More marked asterism and the diffuse reflections are increased in intensity. PLATE III.(k).

115 mins: High-angle reflections are disappearing. PLATE III.(l).

120 mins: Most of the reflections have vanished, although the 210 reflection and accompanying diffuse reflections, remain. Rings from amorphous fragments have appeared. PLATE III.(m).

3.6.2.2./...

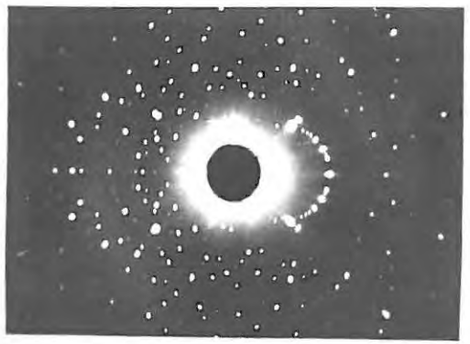

(j)

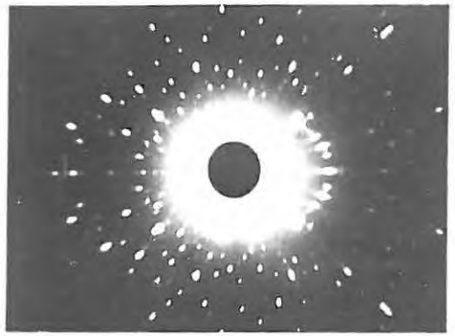

(k)

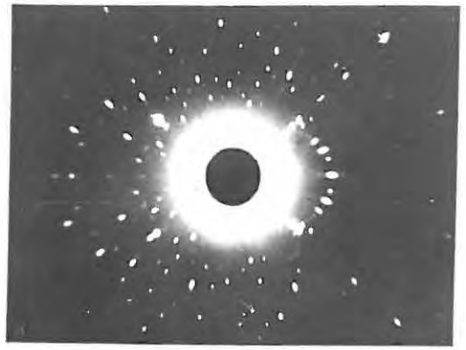

(l)

PLATE III

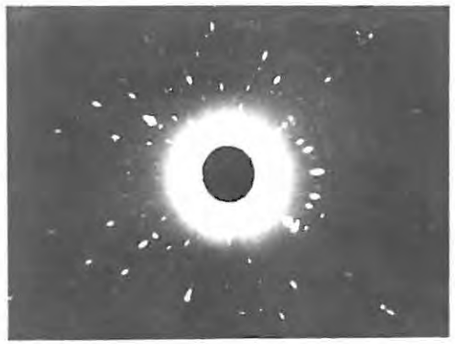

(m)

3.6.2.2. Irradiated (500 Mrad) $KMnO_4$ (185°C).

0 mins: Spots well defined. Strong diffuse reflections are associated with the 210 reflection. PLATE II.(i).

70 mins: Asterism evident. PLATE IV.(n).

90 mins: Asterism and the intensity of the diffuse reflections increasing. PLATE IV.(o).

100 mins: Effects more marked.

110 mins: High-angle spots begin to disappear; diffuse reflections become larger and more intense. PLATE IV.(p).

120 mins: The majority of reflections have vanished. A notable exception is 210 and its accompanying diffuse reflections. PLATE IV.(q).

127 mins: Signs of circular streaking, otherwise similar to 120 mins. PLATE IV.(r).

At this stage the crystal fragments. One such fragment, randomly oriented, gave the Laue photograph shown in PLATE IV.(s).

3.7. DISCUSSION.

3.7.1. Irradiation Effects in Permanganates.

The thermal decompositions of crystals of the permanganates of Na, K, Rb, Cs, Ag and to a lesser degree, Ba are affected by pre-irradiation with γ-rays (1.1 Mev)[196]. The "induction periods" are shortened and the maximum velocities are increased. The effects have been explained by assuming that interstitial cations are produced during irradiation. On heating, these defects migrate and return to vacant lattice sites. The release of energy associated with the combination of an interstitial and a vacancy, creates a centre of decomposed material that grows during the induction period and creates strain in the crystal.

This/...

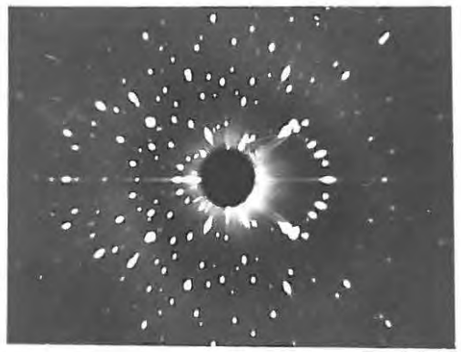

(n)

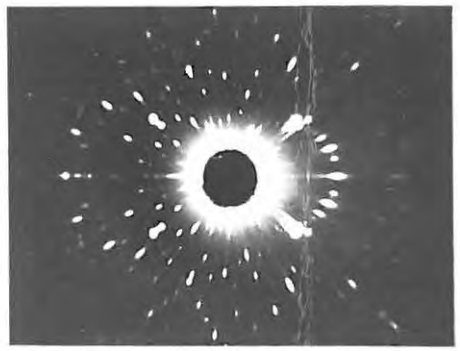

(o)

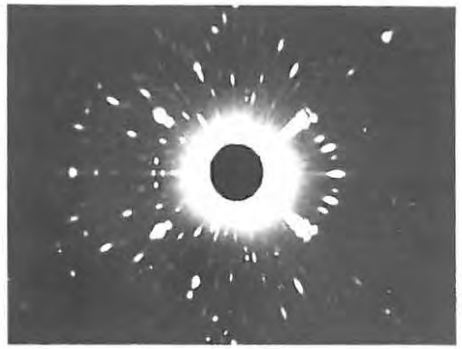

(p)

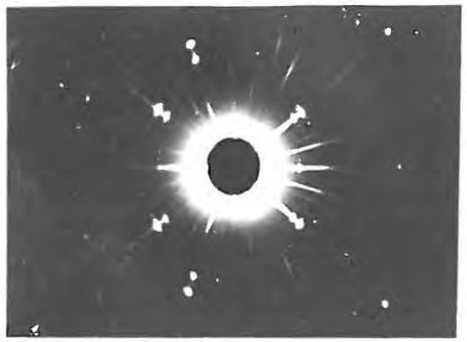

(q)

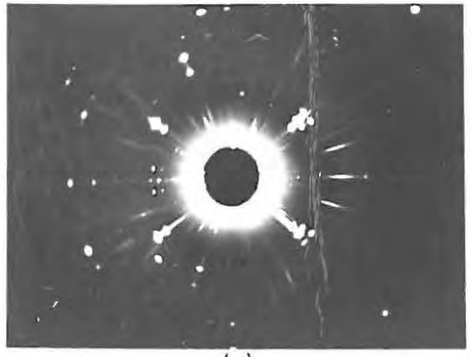

(r)

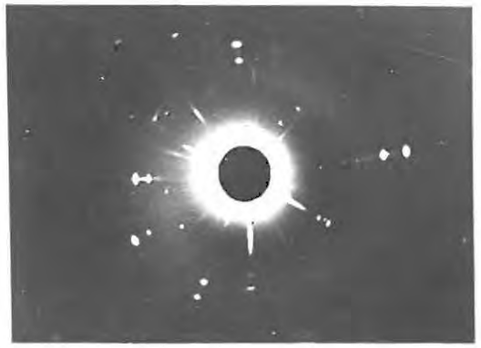

(s)

PLATE IV

This increasing strain finally fractures the crystal at the end of the induction period. The decomposition then accelerates by the Prout-Tompkins mechanism [275].

The production of a reasonable concentration of interstitial atoms should produce distortion within the lattice. Predictions have been made of the effects of distortion of the lattice on the diffraction of X-rays. (See Introduction 1.4.8). These are:-

(i) A reduction in intensity of the Bragg reflections by an "artificial temperature factor",

(ii) Slowly varying background scattering.

(iii) Changes in lattice parameters.

(iv) Characteristic diffuse scattering in the neighbourhood of the Bragg directions.

Several investigators have met with success in attempts to detect distortion. (Introduction 1.4.8).

3.7.2. The Crystal Structure of Unirradiated $KMnO_4$.

An electron-density projection (h0l), FIGURE 3.2, for the unirradiated salt showed that the structure assigned to $KMnO_4$ by Mooney [283], who used qualitative visual estimates of the diffraction spot densities, was innacurate. The atomic positions, obtained from the projection, compared with those of Mooney and those of Ramaseshan [289] are given in TABLES 3.7, 3.1 and 3.2 respectively. The agreement with Ramaseshan's values is good, and incidentally confirms the accuracy if not the usefulness of the anomalous scattering method. There is some disagreement on the position of the oxygen atom, O_1. This atom was, however, never completely resolved, and the only manner of estimating the correctness of its position was to calculate the position, from several alternatives, which would give a minimum value

to/...

to the residual factor, R.

Orthogonal projections were not calculated as the main interest in the study lay in the detection of radiation-induced changes in the structure, rather than in an absolute determination of the structure itself.

The structure of $KMnO_4$ is very similar to that of $CsMnO_4$ [293].

3.7.3. Comparison of the X-ray Diffraction results obtained with Unirradiated and Irradiated $KMnO_4$ crystals.

Comparison of the electron-density projections of unirradiated $KMnO_4$ (FIGURE 3.2) and irradiated (500 Mrad) $KMnO_4$ (FIGURE 3.3) shows a remarkable degree of similarity. There is no detectable shift in the peak positions of the K and Mn atoms on irradiation. Comparison of the electron-density profiles drawn through these peak positions (FIGURES 3.4 to 3.10), confirms this and also shows that no decrease in the peak-height or broadening of the peak occurs on irradiation. These results support those obtained by Woods [279,280] for $AgMnO_4$, where it was concluded that the Ag and Mn atoms were not detectably affected by irradiation. Some doubt had remained because of his measurement of intensities using the positive-print method.

The oxygen atoms give relatively low peaks which are rather diffuse in comparison to the strong sharp peaks of the K and Mn atoms. This prevents accurate comparison, but from the results obtained no change could be detected in the height, width or position of the peaks on irradiation.

The (Irradiated - Unirradiated) Difference Synthesis (FIGURE 3.11), is virtually flat. The ripples shown are small in comparison to the peaks in the electron-density syntheses. (40 unit contours to 200 unit contours).

No conclusions can be drawn from these ripples because of the errors involved in intensity measurement and correction.

Of the effects predicted by Huang [130] et al, no artificial temperature factor and no increased background were observed, but expansion of the lattice in all three crystallographic directions was detected. The values of the parameters are given in TABLE 3.10. The percentage increases were:-

a: 0.21% b: 0.30% c: 0.45%.

This corresponds to a volume increase of 0.96%.

This expansion is of the order of expansion previously detected in irradiated materials. (Introduction 1.4.8).

Unirradiated $KMnO_4$ shows faint diffuse reflections associated with some relps, but this diffuse scattering is far more marked in Laue photographs of the irradiated material. In contrast to similar reflections with unirradiated material, these reflections do not disappear on reducing the temperature of the crystal to that of liquid air, showing that the scattering here, is not caused by the thermal motion of atoms, but rather by the formation of crystal defects.

The three-dimensional shape of the diffuse reflection associated with the 210 relp, is that of an ellipsoid, rather than that of a lemniscate as predicted by Huang [130]. Ellipsoidal diffuse reflections were predicted by Kanazaki[137] for pairs of point defects in cubic crystals.

The failure to observe any decrease in the peak heights of the electron-density profiles, suggests that there is either no displacement of atoms or that the concentration of displaced atoms is very low and they can only be detected by using more precise methods. The fact that diffuse

reflections/...

reflections are obtained, however, supports the latter view but gives no indication of the nature of the displaced atoms. Consequently, if the radiation damage is to be more exactly defined, the accuracy of intensity measurement required, would be beyond that obtainable with a photographic, multiple-film technique. Furthermore accurate correction factors should be applied, especially for absorption [303], and some allowance should be made for possible changes in extinction on irradiation [342].

This means that the most accurate structure analysis possible must be performed on the unirradiated material, and then a comparison must be made with the structure of the irradiated crystal, determined under the same precise conditions. Recording of intensities with diffractometer apparatus is recommended by Azaroff [186], and computing facilities are required for full structure refinement.

As can be seen from the two structure analyses, a reasonable approximation to the structure of a crystal can be obtained even allowing for some variations in the magnitudes of the intensities and possible errors in the application of corrections. As Guinier has stated [118], X-rays exaggerate the perfection of crystals, thus permitting structure determination using imperfect crystals, but handicapping the study of defects in the solid state.

The development of strain along the induction periods in the thermal decompositions of both unirradiated and irradiated $KMnO_4$, as shown by the Laue photographs in PLATES III and IV, is similar to that shown by Herley [277,278] and for $AgMnO_4$ by Woods [279,280]. Bragg [343] has shown that radial asterism of Laue spots is expected if there is a random deviation of the normal to the crystal plane all round its mean direction, owing to distortion.

The point of interest is the way in which the diffuse reflections persist along the induction period and, if anything, become more intense. This indicates that the imperfections produced on irradiation do not anneal along the induction period. This weighs against the mechanism proposed by Prout [193], that interstitial K^+ ions formed on irradiation, migrate to vacancies and recombine with the accompanying release of Wigner energy, when the crystal is heated. The persistence of the diffuse reflections rather favours the disruption of the MnO_4^- group by the breaking of Mn-O bonds. This is supported, too, by the increased intensity of these reflections at the end of the induction period in the decomposition of the unirradiated salt, by which stage such disruption of many of the MnO_4^- groups should have occurred. Thus the unirradiated salt, on heating, reaches a stage where it shows the characteristics of the irradiated salt before decomposition. This indicates that the damage produced on irradiation is similar to that occurring during normal decomposition.

No change in the final pressure of gas obtained from a fixed weight of $KMnO_4$ was detected after a dose of 500 Mrad (see TABLE 3.13), in contrast to a decrease of about 13% for irradiated $AgMnO_4$ [280]. This indicates that even if some decomposition occurs on irradiation, the products are trapped within the crystal.

4. APPARATUS AND EXPERIMENTAL PROCEDURES FOR THE THERMAL DECOMPOSITION STUDIES.

4.1. Description of the Apparatus.

The apparatus is similar to that described in detail by Herley [333]. It is shown diagrammatically in FIGURE 4.1.

The pumping system consists of an Edwards "Speedivac" three-stage oil-diffusion pump, model 203B, backed by an Edwards "Speedivac" gas ballast rotary high vacuum pump, model 25C20A.

The constant-temperature decomposition vessel has been described by Prout and Herley [334], and has a temperature control of approximately $\pm$ 0.03°C at 220°C. A larger, electrically heated furnace was used for dehydration of batches of nickel oxalate. The temperature control was only about $\pm$ 2°C.

Pressures were measured with a McLeod gauge. The volume of the McLeod bulb was 135.2 ml at 25°C.

For studies on ammonium dichromate and nickel oxalate, traps containing P_2O_5 were used to absorb water vapour (and ammonia from the ammonium dichromate), as no liquid air was available. In the study of the thermal decomposition of calcium azide, cold traps surrounded by liquid air were used as shown in the diagram. One protected the decomposition vessel from mercury vapour from the McLeod gauge, one was in the back line and the third protected the backing pump.

The volumes of the sections of the line used, are dealt with under the calculation of percentage decompositions for the specific substances.

4.2./...

FIG. 4.1

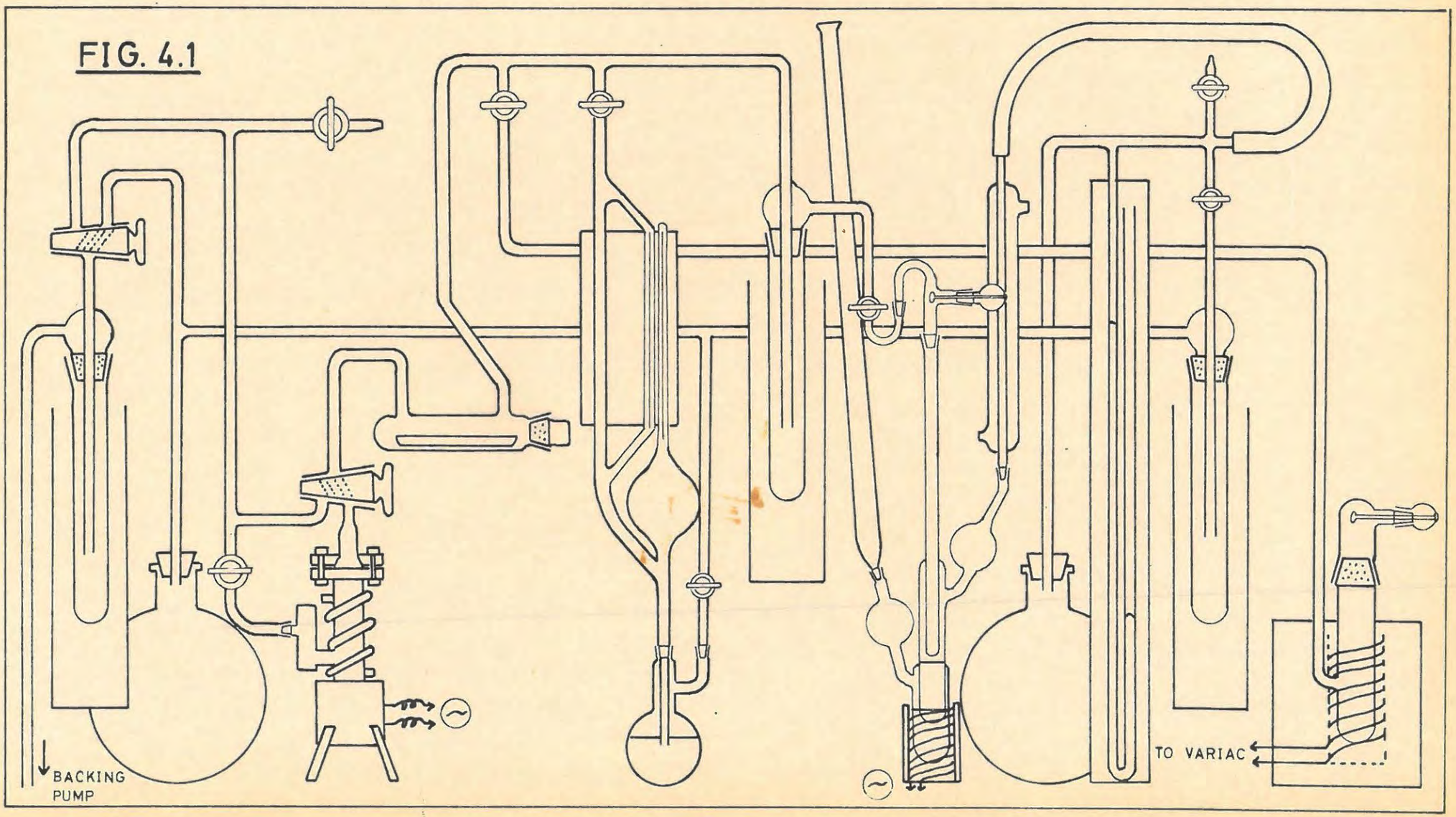

4.2. Experimental Procedure.

Samples were decomposed either in a small platinum bucket or in a small glass bucket. The buckets were carefully cleaned and dried in a flame before each run. The line was pumped hard for several hours before commencing a decomposition. The bucket was then lowered into the vessel at the decomposition temperature and the decomposition system was immediately isolated from the pumping system. There was a heating lag of about 5 mins., after introduction of the bucket, before the thermometer in the vessel registered the decomposition temperature.

When a cold trap was used in the decomposition system, the level of the surrounding liquid air was maintained to within 1 cm. to minimise errors in pressure measurements.

Pressures were normalised to final pressures (p_f) of 75×10^{-3} cms Hg (nickel oxalate and ammonium dichromate) and 80×10^{-3} cms Hg (calcium azide). The actual final pressures (p_a) corresponding to the sample weight (w mg.) used, are recorded for each run. For runs involving interruptions, the expected final pressure (p_{exp}) was calculated from the sample weight (w) and the ratio p_a/w for uninterrupted runs.

Further experimental procedures are described under the relevant sections.

5. THE THERMAL DECOMPOSITION OF NICKEL OXALATE.

5.1 Previous Work on Nickel Oxalate.

Jacobs and Kureishy [335] studied the thermal decomposition of dehydrated nickel oxalate in the temperature range 240 - 280°C. The main section of the decomposition curve was analysed using the AVRAMI-EROFEYEV equation [336,337]:-

$$\left[- \log(1-\alpha'') \right]^{\frac{1}{n}} = k''t \qquad \ldots\ldots \qquad (5.1)$$

with n = 2. $\alpha'' = (\alpha-\alpha_o)/(1-\alpha_o)$ and α_o is the fraction decomposed at the end of the initial reaction. They concluded that this was the two-dimensional growth of nuclei after an initial acceleratory surface reaction. The final decay stages obeyed the unimolecular law:-

$$- \log (1-\alpha'') = k''' t \qquad \ldots\ldots \qquad (5.2)$$

The initial process followed the contracting area formula:-

$$1 - (1 - \alpha')^{\frac{1}{2}} = k't \qquad \ldots\ldots \qquad (5.3)$$

where $\alpha' = \alpha/\alpha_o$. This corresponds to initiation of reaction at a number of sites followed by spreading over the surface at constant rate.

The activation energies of all three stages were approximately 32 kcals/mole.

Allen and Scaife [338] in a study of the initial reaction only, had proposed the equation:-

$$V = k (t-t_o)^{\frac{1}{2}} \qquad \ldots\ldots \qquad (5.4)$$

where V = volume of CO_2 per 0.1 gm of anhydrous oxalate, and t_o allows for the heating lag. They interpreted this in terms of a surface reaction with rate-determining step the diffusion of anion vacancies from the surface into the interior.

Jacobs/...

Jacobs rejected this mechanism on the grounds that the observed conductivity of oxalates was too small and that the values of the activation energies indicated the same rate-determining step throughout.

Danes and Ponec [339] studied the thermal decomposition under high pressures of carbon dioxide (100-800 mm). They found that the acceleratory period was fitted by the Prout-Tompkins equation [340]:-

$$\log (p/(p_f-p) = kt + \text{const.} \ldots\ldots\ldots \quad (5.5)$$

The Avrami-Erofeyev (5.1) fitted from $\alpha = 0.04$ to $\alpha = 0.40$. The higher temperatures (270-300°C) required are in agreement with the inhibiting effect of CO_2 reported by Jacobs.

Because of the lack of agreement on the analyses to be applied, it was necessary to re-examine the kinetics of decomposition of the unirradiated salt, before commencing a study of the pre-irradiated material.

5.2 EXPERIMENTAL.

5.2.1 Preparation.

Nickel oxalate dihydrate was prepared by mixing equal volumes of hot aqueous solutions, 0.2 molar, of "Analytical Reagent" nickel sulphate and "Analytical Reagent" potassium oxalate. The mixture was allowed to stand overnight and was then filtered. The precipitate was washed twenty times with distilled water and dried in an air oven at 120°C.

Dehydration was carried out in a vacuum at 150°C for 8 hrs. The pale yellow powder was stored over P_2O_5 and precautions were taken in subsequent handling to prevent hydration of the salt.

5.2.2/...

5.2.2 Apparatus: as described in SECTION 4.

5.3 RESULTS.

5.3.1 Reproducibility.

Three consecutive runs were done at 260°C. The results are given in TABLE 5.1.

The reproducibility was satisfactory. The rate constants k_2, in :-

$$\log \left[(p-p_o)/(p_f-p)\right] = k_2 t + C \qquad \ldots\ldots\ldots \quad (5.6)$$

were 0.0573, 0.0563 and 0.0570 per min.; and of k_3, in:-

$$1 - (1-p/p_f)^{\frac{1}{3}} = k_3 t \qquad \ldots\ldots\ldots \quad (5.7)$$

were 0.0213, 0.0221 and 0.0204 per min.

TABLE 5.1

NICKEL OXALATE Run 1. 260°C 8.8 mg.					
t	p	t	p	t	p
4	0.70	34	17.77	58	61.89
7	1.34	36	21.03	60	65.30
10	1.88	38	24.37	62	68.11
13	2.28	40	27.75	64	69.89
16	2.75	42	31.46	66	71.30
19	3.35	44	35.28	68	72.56
22	4.63	46	39.15	70	73.83
24	5.93	48	43.27	72	74.56
26	7.63	50	47.21	74	74.89
28	9.71	52	51.05		
30	12.13	54	54.73	p_f	75.00
32	14.74	56	58.42	p_a	121.0

TABLE 5.1 contd.

RUN 2.		260°C			8.6 mg.
t	p	t	p	t	p
5	0.46	40	18.24	64	60.75
10	1.20	41	19.94	66	63.21
15	1.70	42	21.88	68	65.50
20	2.19	44	25.80	70	67.53
25	3.72	46	30.08	72	69.17
27	4.74	48	34.06	74	71.00
30	6.73	50	38.23	76	72.44
32	8.33	52	41.99	78	73.82
34	10.07	54	45.70	80	74.28
35	11.11	56	49.09	83	74.67
36	12.24	58	52.37	86	74.90
37	13.60	60	55.52	p_f	75.00
39	16.65	62	58.28	p_a	114.5

RUN 3.		260°C			7.7 mg.
t	p	t	p	t	p
4	0.60	35	14.32	65	66.32
10	1.12	38	19.00	68	69.54
14	1.64	41	24.16	71	71.83
17	2.01	44	29.42	74	73.51
19	2.43	47	35.51	77	74.40
22	3.57	50	40.60	80	74.82
25	4.98	53	48.10	85	74.98
28	7.40	56	52.63		
30	8.02	59	57.50	p_f	75.00
33	11.96	62	61.97	p_a	104.1

5.3.2 The Effect of Temperature.

5.3.2 (a) The Main reaction.

8 to 9 mg. of nickel oxalate were decomposed at various temperatures to obtain the critical increment of the chemical process(es) occurring. These are discussed later. These runs are listed in TABLE 5.2 as well as the runs at 260°C in TABLE 5.1.

TABLE 5.2/...

TABLE 5.2

NICKEL OXALATE		240°C			8.6 mg.
t	p	t	p	t	p
5	0.30	136	18.55	220	60.30
10	0.68	142	21.54	228	62.58
20	1.11	148	25.06	236	64.99
30	1.42	154	28.37	244	67.16
40	1.64	160	31.60	252	68.50
50	1.93	166	34.84	260	69.57
60	2.22	172	37.41	270	70.87
70	2.73	178	41.45	280	72.17
80	3.53	184	44.87	290	73.21
90	4.64	190	47.78	300	73.98
100	6.22	196	50.82	310	74.47
110	8.39	202	53.63	320	74.69
120	11.63	208	56.27	p_f	75.00
130	15.71	214	58.37	p_a	105.8

		245°C			8.6 mg.
t	p	t	p	t	p
5	0.33	80	7.19	160	56.21
10	0.88	90	10.48	166	59.69
15	1.21	95	12.80	170	61.32
20	1.45	100	15.44	175	63.58
25	1.68	105	18.42	180	65.89
30	1.83	110	21.86	186	68.24
35	2.01	115	25.56	192	69.50
40	2.18	120	29.17	198	70.42
45	2.34	126	33.96	204	71.49
50	2.63	130	37.23	210	72.06
55	3.05	135	40.65	220	73.1[illegible]
60	3.57	140	44.11	230	74.00
65	4.26	145	47.36	240	74.8[illegible]
70	5.11	150	50.72	p_f	75.00
75	6.08	155	53.72	p_a	98.0

Table 5.2 contd./...

TABLE 5.2 contd.

248°C					8.5 mg.
t	p	t	p	t	p
1	0.15	68	14.60	120	59.43
5	0.44	72	18.18	125	62.66
10	1.02	75	21.10	130	64.86
15	1.40	78	24.11	135	66.41
20	1.66	81	27.13	140	67.83
25	1.95	84	30.32	145	69.14
30	2.15	87	33.18	150	70.35
35	2.40	90	35.82	155	71.67
40	2.86	94	39.71	160	72.76
45	3.59	98	43.24	165	73.86
50	4.91	102	46.37	170	75.05
56	7.11	106	49.68	175	75.30
60	9.01	110	52.77	p_f	75.00
64	11.53	115	56.01	p_a	84.2

250°C					8.7 mg.
t	p	t	p	t	p
1	0.06	54	10.40	92	54.22
5	0.32	56	12.33	95	56.86
10	0.81	59	15.49	98	59.28
15	1.13	61	17.79	102	62.29
20	1.37	63	20.17	106	64.93
25	1.60	65	22.60	110	67.18
30	1.87	68	26.45	115	70.19
35	2.31	71	30.62	120	72.43
40	3.21	74	34.50	125	74.10
43	4.06	77	38.22	130	74.68
46	5.17	80	41.84	135	75.06
48	6.15	83	45.09		
50	7.29	86	48.47	p_f	75.00
52	8.69	89	51.47	p_a	117.1

TABLE 5.2./...

TABLE 5.2 contd.

255°C					8.6 mg.
t	p	t	p	t	p
1	0.12	45	17.23	71	59.89
5	0.43	47	20.77	74	63.24
10	1.03	49	24.35	77	66.10
15	1.40	51	28.12	80	68.36
20	1.74	53	31.79	83	70.19
25	2.20	55	35.37	86	71.53
30	3.41	57	39.09	89	72.75
33	4.58	59	42.65	92	73.97
36	6.40	61	46.16	95	74.64
39	9.15	63	49.60	98	74.82
41	11.34	65	52.89	p_f	75.00
43	14.22	67	55.55	p_a	122.7

263°C					8.3 mg.
t	p	t	p	t	p
1	0.11	34	15.18	50	51.77
4	0.35	35	17.08	52	55.45
7	0.76	36	19.33	54	59.26
10	1.06	37	21.51	56	62.50
14	1.35	38	23.83	58	65.38
18	1.70	39	26.11	60	67.63
22	2.42	40	28.71	62	69.53
24	3.17	42	33.99	64	71.05
26	4.21	44	39.39	66	72.31
28	5.86	45	41.63	68	72.94
30	8.31	46	43.87	72	75.00
31	9.66	47	45.86	74	75.00
32	11.34	48	48.11	p_f	75.00
33	13.13	49	50.24	p_a	120.2

TABLE 5.2./...

TABLE 5.2 contd.

265°C					8.8 mg.
t	p	t	p	t	p
1	0.17	32	25.67	46	61.42
4	0.51	33	28.33	48	65.32
7	0.98	34	30.95	50	67.92
10	1.39	36	36.86	52	70.34
13	1.72	37	39.52	54	72.29
16	2.17	38	42.32	56	73.83
19	3.34	39	45.16	58	74.59
22	5.68	40	47.73	60	74.83
24	8.03	41	50.22		
26	11.36	42	52.45	p_f	75.00
28	15.50	43	54.78	p_a	126.7
30	20.35	44	57.16		

270°C					11.1 mg.
t	p	t	p	t	p
1	0.16	24	14.92	38	56.02
4	0.53	25	17.54	40	61.07
7	1.05	27	23.72	42	64.63
10	1.53	28	26.61	44	68.62
12	1.77	29	29.85	46	71.21
14	2.20	30	33.02	48	73.57
16	3.13	31	36.18	50	74.54
18	4.83	32	39.37	52	75.05
19	5.93	33	42.35	54	75.00
20	7.21	34	45.03		
22	10.47	35	47.87	p_f	75.00
23	12.50	36	50.47	p_a	162.0

TABLE 5.2./...

TABLE 5.2 contd.

275°C					8.6 mg.
t	p	t	p	t	p
1	0.19	13	25.86	21	71.85
3	0.53	14	33.81	22	73.37
5	1.00	15	41.76	23	74.38
7	1.63	16	49.26	24	74.83
9	3.96	17	55.81	25	75.00
10	7.03	18	61.67	26	74.90
11	12.01	19	66.11	p_f	75.00
12	18.55	20	69.49	p_a	133.4

5.3.2 (b) The Initial Reaction.

The initial reaction was examined by decomposing 60 mg. of the salt at various temperatures.

The results are given in TABLE 5.3.

TABLE 5.3

INITIAL REACTION.	240°C				61.6 mg.
t	p	t	p	t	p
1	0.150	20	8.33	54	15.92
2	0.312	22	8.98	58	16.82
4	0.688	24	9.65	62	17.65
6	1.37	27	10.41	66	18.51
8	2.36	30	11.17	70	19.28
10	3.42	34	12.16	75	20.26
12	4.57	38	12.99	80	21.54
14	5.73	42	13.76	85	23.04
16	6.68	46	14.55	90	25.07
18	7.56	50	15.23	p'_f	13.76

TABLE 5.3./...

TABLE 5.3 contd.

245°C					61.3 mg.
t	p	t	p	t	p
1	0.174	17	8.21	40	16.26
3	0.519	19	9.33	43	16.97
5	1.11	22	10.69	46	17.73
7	2.17	25	11.90	49	18.43
9	3.36	28	12.85	52	19.11
11	4.63	31	13.80	55	20.08
13	5.81	34	14.75	58	21.04
15	7.04	37	15.61	p_f'	14.75

250°C					76.5 mg.
t	p	t	p	t	p
1	0.199	16	10.89	34	21.99
2	0.398	18	12.54	36	22.99
4	1.01	20	14.23	38	24.07
6	2.12	22	15.53	40	25.36
8	3.69	24	16.72	42	26.79
10	5.50	26	17.73	44	28.36
12	7.26	28	18.85	46	30.67
14	9.09	31	20.39	p_f'	17.73

255°C					72.1 mg.
t	p	t	p	t	p
1	0.457	11	9.36	25	20.39
2	0.816	12	10.57	27	21.94
3	1.25	13	11.47	29	23.73
4	1.75	14	12.43	31	26.04
5	2.47	16	14.12	33	29.40
6	3.36	18	15.52		
8	5.71	20	16.97	p_f'	15.52
10	8.18	22	18.35		

TABLE 5.3./...

TABLE 5.3 contd.

260°C					67.9 mg.
t	p	t	p	t	p
1	0.186	11	8.18	20	17.49
2	0.386	12	9.40	21	18.60
4	1.07	13	10.63	22	19.53
5	1.65	14	11.80	23	20.61
6	2.47	15	12.91	24	22.30
7	3.44	16	13.80	25	24.49
8	4.56	17	14.75	26	28.26
9	5.51	18	15.80	27	34.74
10	6.91	19	16.74	p_f'	14.75

5.3.3 Mathematical Analysis of the Unirradiated p-t plots.

A typical pressure-time plot for the thermal decomposition of unirradiated nickel oxalate powder is given in FIGURE 5.1, curve B.

The plot is sigmoid and shows an initial burst of gas up to $\alpha = 0.01$, followed by a period of acceleration that changes at about $\alpha = 0.5$ into a period of decay. There is no apparent induction period between the first evolution of gas and the main acceleration of the reaction.

The Avrami-Erofeyev equation:-

$$\left[-\log (1-\alpha')\right]^{\frac{1}{n}} = kt \qquad \ldots\ldots\ldots \qquad (5.8)$$

where $\alpha' = (\alpha-\alpha_o)/(1-\alpha_o)$, and α_o is the fractional decomposition at the end of the initial reaction, gave only a fair fit in the range $0.17 < \alpha < 0.80$.

The unimolecular law:-

$$\log (p_f-p) = k't + C \qquad \ldots\ldots\ldots \qquad (5.9)$$

fitted reasonably well from $0.75 < \alpha < 0.97$.

A satisfactory analysis, however, was obtained using the Prout-Tompkins equation:-

log/...

$$\log\left[\frac{p-p_o}{p_f-p}\right] = k_2 t + C \qquad \ldots\ldots \qquad (5.6)$$

where p_o is the pressure at the end of the initial reaction. FIGURE 5.1, curve A.

The extent of fit was $0.013 < \alpha < 0.5$.

The decay process conformed best to the contracting sphere formula:-

$$1 - (1-p/p_f)^{\frac{1}{3}} = k_3 t \qquad \ldots\ldots \qquad (5.7)$$

The equation fitted over $0.5 < \alpha < 0.98$, FIGURE 5.1, curve C.

The plots for the initial reaction conformed to the "contracting area" formula:-

$$1 - (1-p/p_f')^{\frac{1}{2}} = k_1 t \qquad \ldots\ldots \qquad (5.10)$$

where p_f' is the pressure at the end of the initial reaction. The p-t curve and analysis are shown in FIGURE 5.2.

The values of k_1, k_2 and k_3 are tabulated in TABLE 5.4.

The critical increment was then determined using the equation:-

$$2.303 \log_{10} k = E/RT + K_1 \qquad \ldots\ldots \qquad (5.11)$$

where E = the activation energy (kcal/mole)

K_1 = a constant

T = the decomposition temperature in degrees Kelvin

and R = 1.98 calories,

by plotting the values of $\log k_1$, $\log k_2$ and $\log k_3$ against $1/T^{o}K$, FIGURE 5.3.

The values of the activation energies obtained from these plots are

Initial reaction	33.0	kcals/mole
Acceleratory period	33.6	kcals/mole
Decay period	35.4	kcals/mole

TABLE 5.4./...

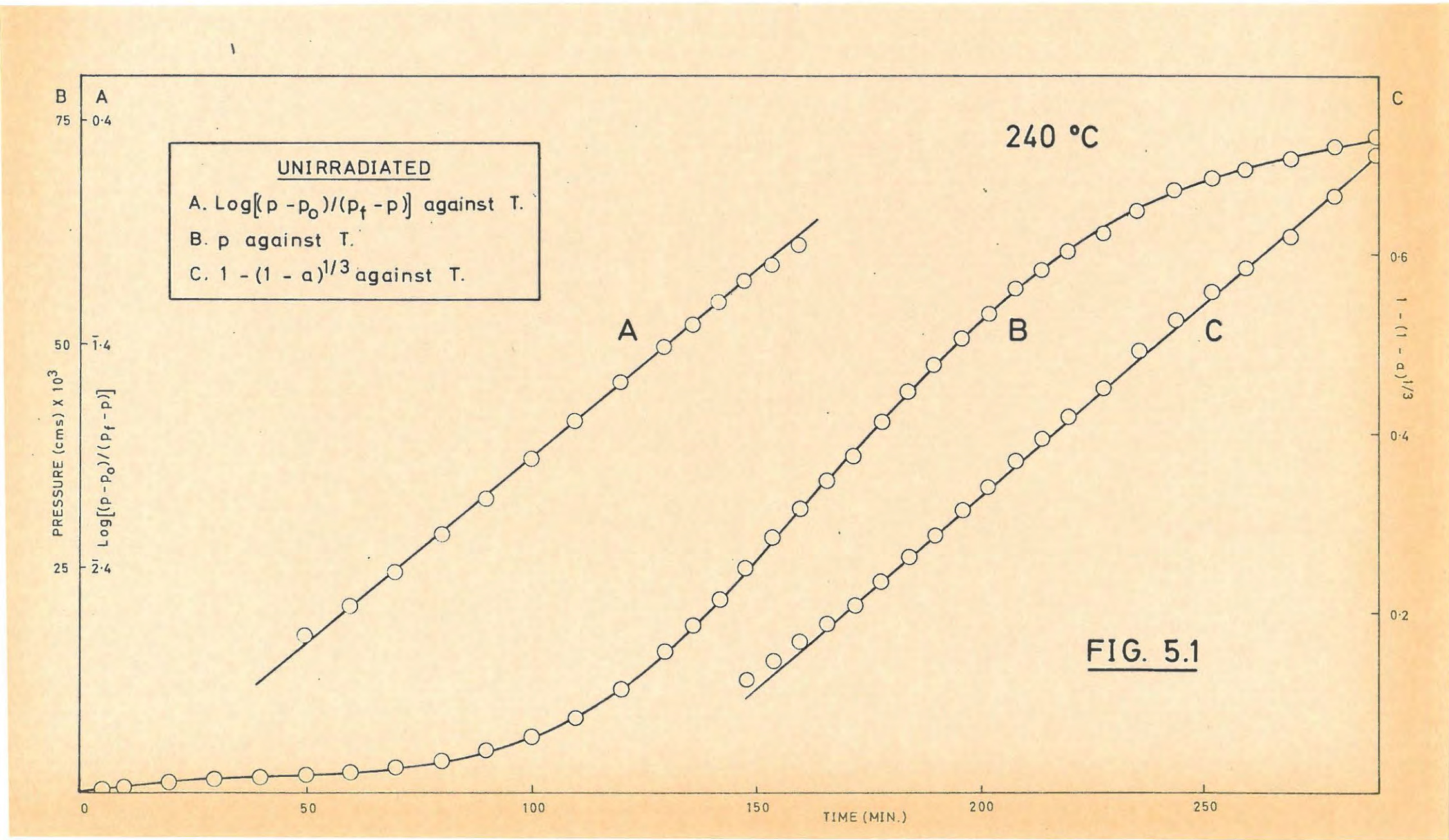
UNIRRADIATED
A. Log[(p - p0)/(pf - p)] against T.
B. p against T.
C. 1 - (1 - a)^1/3 against T.
240 °C
A
B
C
B
A
C
75
50
25
0·4
1·4
2·4
0·6
0·4
0·2
PRESSURE (cms) X 10^3
Log[(p - p0)/(pf - p)]
1 - (1 - a)^1/3
0
50
100
150
200
250
TIME (MIN.)

FIG. 5.1

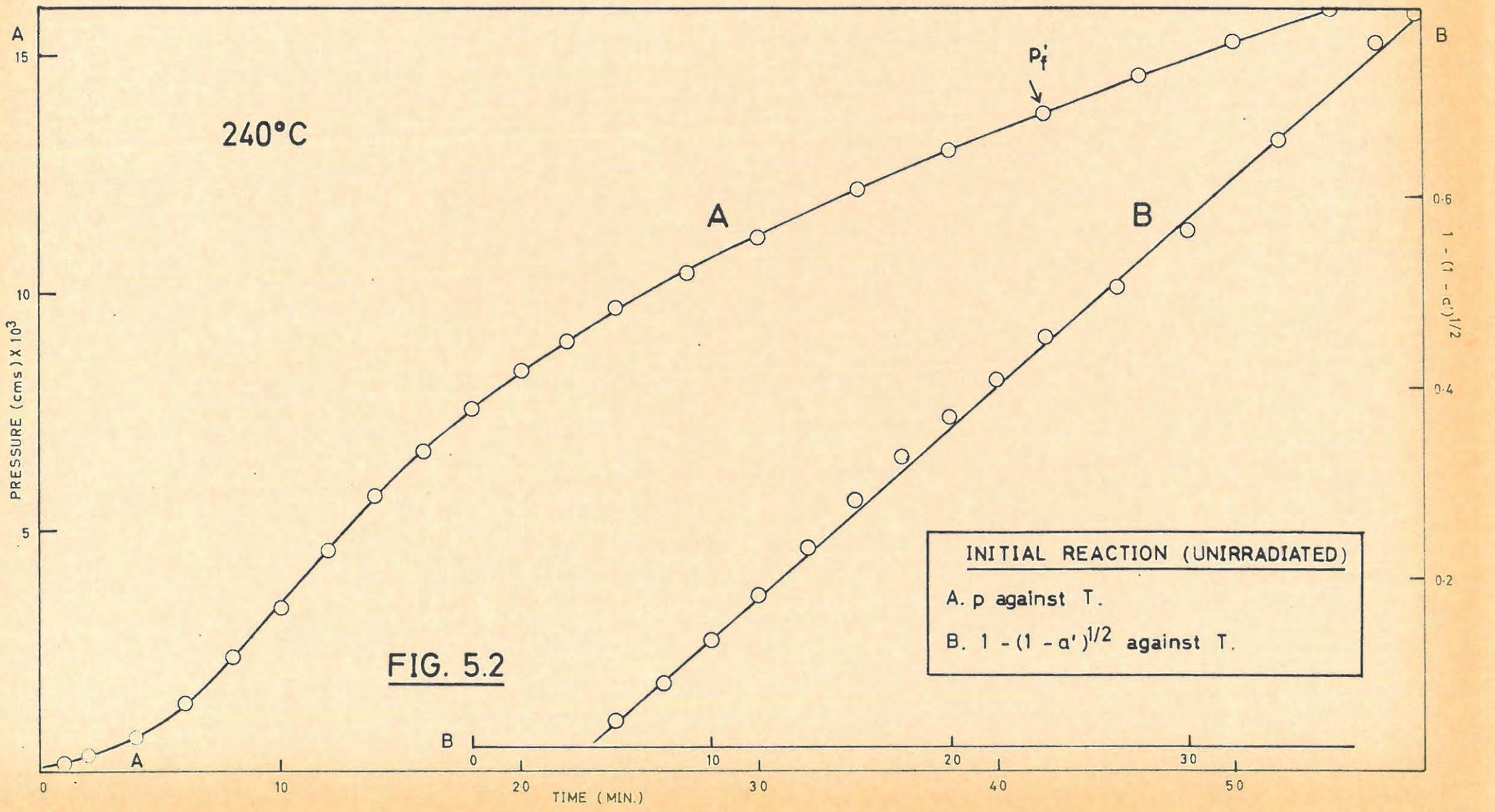
240°C
A
B
P_f'
PRESSURE (cms) X 10^3
TIME (MIN.)
$1-(1-\alpha')^{1/2}$
INITIAL REACTION (UNIRRADIATED)
A. p against T.
B. $1-(1-\alpha')^{1/2}$ against T.

FIG. 5.2

TABLE 5.4.

NICKEL OXALATE			
Temp. °C	Initial k_1 x 100 min^{-1}	Acceleratory k_2 x 100 min^{-1}	Decay k_3 x 100 min^{-1}
240	2.183	1.71	0.422
245	2.790	2.125	0.578
248		3.36	
250	4.164		0.988
255	6.00	5.97	1.503
260	7.143	5.73	2.04
260		5.63	2.13
260		5.70	2.21
265		10.07	2.585
270		11.53	

5.3.4 Visual observations.

The decomposing powder was a uniform light brown colour at the end of the initial reaction. During the subsequent acceleration the salt became darker, and at $\alpha = 0.5$ it was black. No change in colour was evident during the decay.

5.3.5 The Effect of Mixing with Solid Product.

8 mg. of nickel oxalate powder was weighed into the bucket and heated in a burner flame, giving approximately 2 mg. of product. 7.5 mg. of the powder was weighed into the bucket and intimately mixed with the residue. The mixture was then decomposed at 250°C. The results are given in TABLE 5.5. No marked effect was observed on comparison with TABLE 5.2 (250°C).

TABLE 5.5./...

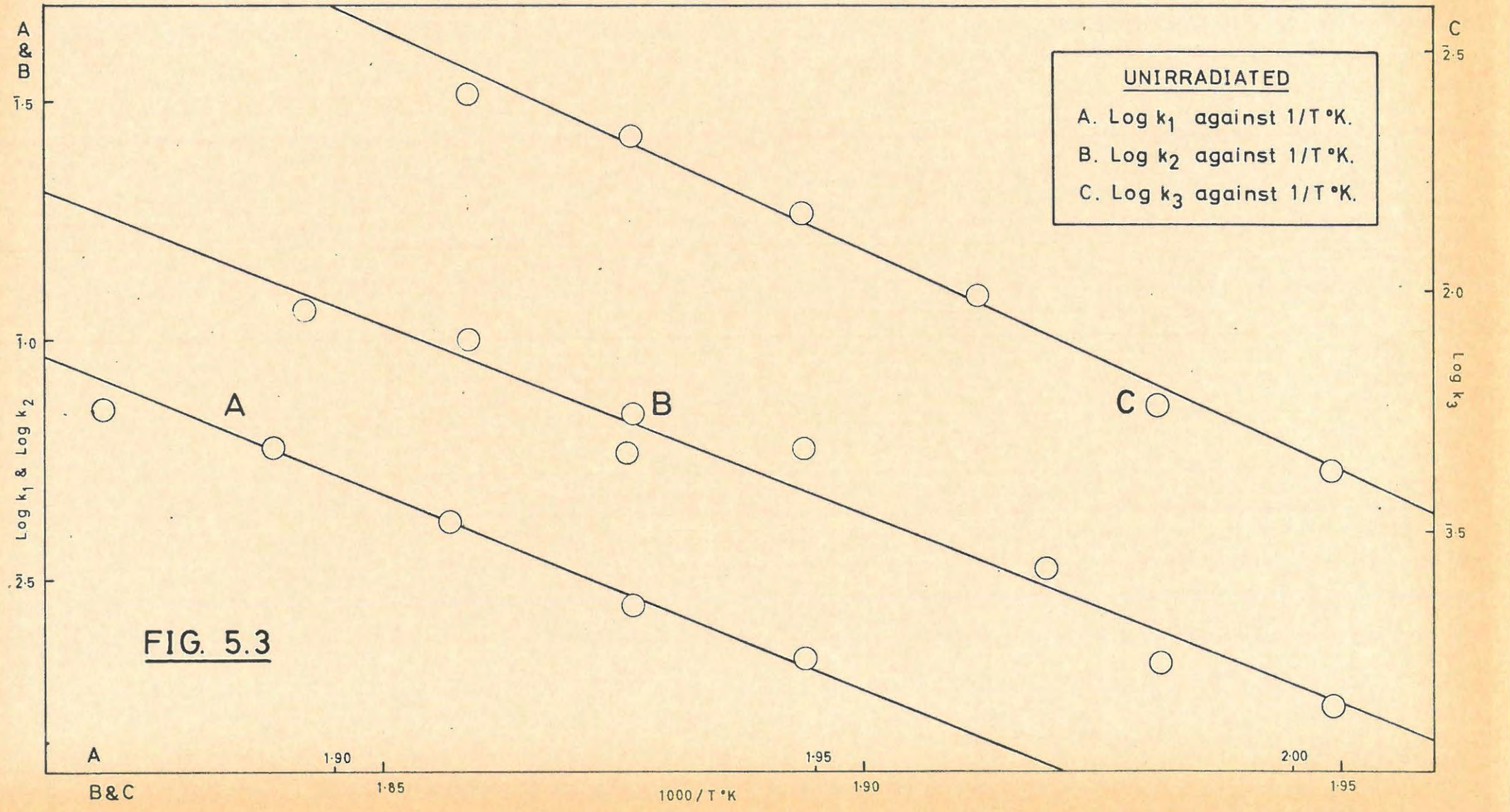
UNIRRADIATED
A. Log k_1 against 1/T °K.
B. Log k_2 against 1/T °K.
C. Log k_3 against 1/T °K.
A
B
C
A & B
C
Log k_1 & Log k_2
Log k_3
$\bar{1}\cdot5$
$\bar{1}\cdot0$
$\bar{2}\cdot5$
$\bar{2}\cdot5$
$\bar{2}\cdot0$
$\bar{3}\cdot5$
A
B&C
1·90
1·85
1·95
1·90
2·00
1·95
1000 / T °K

FIG. 5.3

TABLE 5.5.

EFFECT OF PRODUCT		250°C	7.5 mg. + 2 mg. product		
t	p	t	p	t	p
1	0.06	51	24.84	89	63.81
6	0.48	54	29.05	95	66.87
12	0.99	58	34.43	100	68.90
20	1.37	61	38.23	106	70.81
27	1.93	64	41.88	120	73.79
33	3.64	67	45.49	130	74.68
39	8.41	70	48.86	140	74.94
42	12.31	74	52.48		
45	16.43	78	56.10	p_f	75.00
48	20.63	83	59.85	p_a	117.95

5.3.6 The Effect of Interrupting a Decomposition.

The decomposition was interrupted at different times by raising the sample to a part of the apparatus at room temperature, where it was allowed to remain for 1 hour in the gas evolved up to that time. The sample was then lowered and the decomposition continued.

The composite run is tabulated in TABLE 5.6 and shown in FIGURE 5.4.

Interruption at $\alpha < 0.5$ causes a new acceleration of reaction when heating is continued, while at $\alpha > 0.5$ the reaction continues normally.

TABLE 5.6./...

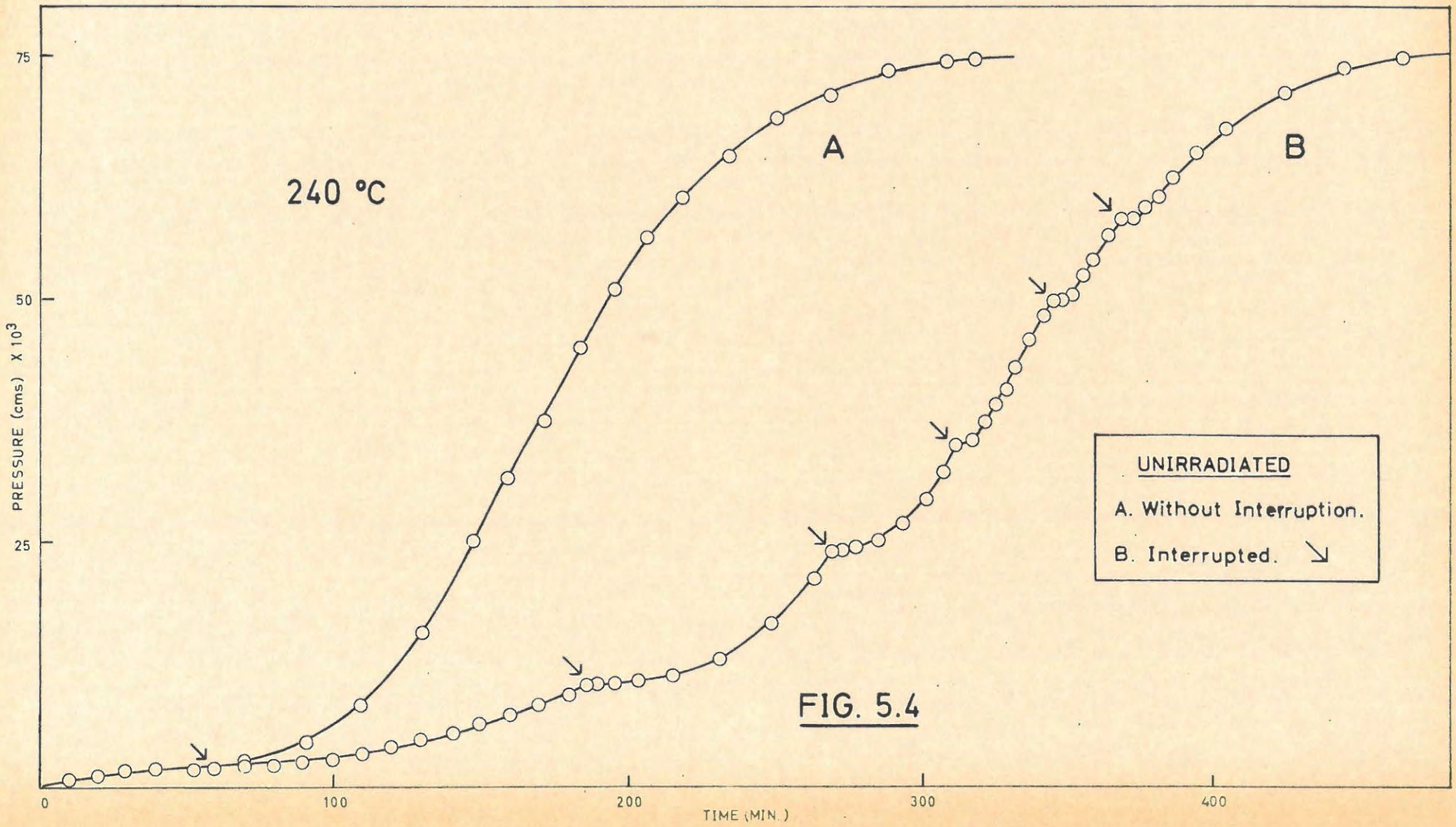
240 °C
A
B
UNIRRADIATED
A. Without Interruption.
B. Interrupted.
PRESSURE (cms) X 10³
TIME (MIN.)
75
50
25
0
100
200
300
400

FIG. 5.4

TABLE 5.6.

UNIRRADIATED AND INTERRUPTED 240°C					9.0 mg.
t	p	t	p	t	p
10	0.58	210	11.06	338	44.45
20	1.04	216	11.45	343	48.31
30	1.35	222	11.84	346*	49.39
40	1.59	232	13.03	348	49.58
52	1.84	240	14.36	352	50.55
60*	1.98	250	16.80	356	52.15
64	2.07	264	21.45	366*	56.63
70	2.15	270*	24.02	370	58.26
80	2.27	274	24.12	374	58.32
90	2.50	278	24.45	378	59.45
100	2.81	286	25.20	382	60.69
110	3.38	290	25.74	388	62.66
120	4.04	294	26.85	396	64.86
130	4.72	298	27.90	406	67.45
140	5.39	302	29.43	416	69.35
150	6.26	306	31.30	426	71.29
161	7.27	308	32.12	436	72.64
170	8.25	312*	34.82	446	73.66
180	9.48	318	35.57	456	74.24
186*	10.38	322	37.49	466	74.62
190	10.50	326	39.09		
196	10.52	330	40.89	p_f	75.00
204	10.78	334	42.57	p_a	133.0

*Interruption.

5.3.7 The Effect of Pre-irradiation with Gamma-rays.

5.3.7.1 Irradiation.

Pre-irradiation was carried out at about 25°C in the spent-fuel facility at Harwell (mean γ-ray energy 1.1 Mev, flux 4.0 Mrad per hr) on specimens sealed in evacuated Pyrex ampoules that had previously been baked out. The doses given varied from 40 Mrad to 600 Mrad.

5.3.7.2./...

5.3.7.2 Reproducibility.

Three consecutive runs were done on pre-irradiated (200 Mrad) samples at 250°C. The results are tabulated in TABLE 5.7.

Reproducibility was satisfactory. For the accelerat-ory period, the values of the rate constant, k_5, in the equation:-

$$\log \left[\frac{p-p_o}{p_f-p}\right] = n \log (t-t_o) + n \log k_5 \quad \ldots \quad (5.12)$$

were 0.0290, 0.0308, 0.0296 per min;

and for the decay, k_3 in

$$1 - (1-p/p_f)^{\frac{1}{3}} = k_3 t \quad \ldots\ldots\ldots \quad (5.7)$$

gave 0.0216, 0.0220, 0.0219 per min.

TABLE 5.7.

IRRADIATED 200 Mrad Run 1. 250°C 8.5 mg.					
t	p	t	p	t	p
1	0.49	23	10.43	46	44.26
2	1.31	24	11.58	48	47.76
3	1.78	25	12.75	50	50.97
4	1.99	26	14.01	52	54.02
5	2.12	27	15.29	54	56.88
6	2.24	28	16.67	56	59.63
8	2.40	30	19.50	58	62.29
10	2.64	32	22.29	60	64.65
12	2.94	34	25.22	64	68.68
14	3.39	36	28.22	66	70.40
16	4.21	37	29.69	68	72.02
18	5.55	38	31.06	71	74.10
19	6.39	39	32.54	73	74.49
20	7.22	40	34.11	75	74.74
21	8.20	42	37.46	p_f	75.00
22	9.30	44	40.98	p_a	127.6

TABLE 5.7 contd./..

TABLE 5.7 contd.

200 Mrad	Run 2	250°C			8.5 mg.
t	p	t	p	t	p
1	0.50	22	12.01	49	67.54
2	1.40	24	15.83	51	69.77
3	1.86	26	19.68	53	71.33
4	2.06	28	23.70	55	72.64
5	2.17	30	27.71	57	73.25
6	2.24	32	32.09	59	73.67
8	2.46	34	36.70	61	74.10
10	2.66	36	41.76	63	74.48
12	2.89	38	46.55	65	74.59
14	3.41	40	51.21	67	74.53
16	4.34	42	55.45		
18	6.10	44	59.36	p_f	75.00
20	8.77	47	64.73	p_a	138.7

200 Mrad	Run 3	250°C			8.6 mg.
t	p	t	p	t	p
1	0.45	26	17.12	54	66.12
3	2.08	28	20.49	56	68.37
4	2.29	30	23.80	58	70.28
5	2.34	32	27.29	60	71.72
6	2.41	34	30.72	62	72.67
8	2.64	36	34.44	64	73.55
10	2.79	38	38.25	66	74.07
12	2.99	40	42.30	68	74.43
14	3.42	42	46.30	70	74.76
16	4.30	44	50.31	72	75.02
18	5.85	46	54.07	74	75.02
20	8.08	48	57.27		
22	10.96	50	60.45	p_f	75.00
24	13.93	52	63.44	p_a	126.8

5.3.7.3./...

5.3.7.3 The Effect of Various Doses of γ-rays.

5.3.7.3 (a) The Main Reaction.

A series of runs was done at constant temperature (245°C) on samples that had received doses ranging from 40 to 600 Mrad. The results are listed in TABLE 5.8 and TABLE 5.11 (200 Mrad at 245°C), and shown in FIGURE 5.5.

TABLE 5.8

IRRADIATED		40 Mrad	245°C		8.4 mg.
t	p	t	p	t	p
2	0.56	60	5.81	135	55.99
4	1.06	65	7.00	140	59.33
6	1.24	70	8.63	145	62.61
8	1.27	75	10.74	150	65.50
10	1.32	80	13.21	155	67.80
14	1.50	85	16.31	160	69.56
17	1.63	90	19.48	165	71.12
21	1.75	95	22.58	170	72.11
26	2.02	100	26.01	175	73.30
30	2.28	105	29.49	180	73.98
33	2.49	110	33.60	185	74.42
39	3.03	116	38.54	190	74.65
45	3.50	121	43.42	195	74.82
50	4.02	125	47.22	p_f	75.00
55	4.98	130	51.87	p_a	123.1

		100 Mrad	245°C		8.9 mg.
t	p	t	p	t	p
2	0.67	43	9.12	86	52.24
4	1.11	46	10.80	89	55.50
6	1.30	49	12.53	92	58.69
8	1.43	52	14.87	96	62.31
10	1.53	55	17.30	100	65.28
13	1.69	58	20.16	104	67.48
16	1.83	62	24.57	108	69.16
20	2.10	65	28.07	113	70.80
24	2.66	68	31.49	118	72.03
28	3.50	71	35.02	124	73.21

31/...

TABLE 5.8 contd.

t	p	t	p	t	p
31	4.39	74	38.55	130	73.90
34	5.42	77	42.11	140	74.77
37	6.56	80	45.47	p_f	75.00
40	7.80	83	48.83	p_a	131.5

		400 Mrad	245°C		8.1 mg.
t	p	t	p	t	p
1	1.00	22	9.74	46	54.62
2	2.14	24	12.06	48	58.83
3	2.58	26	14.63	50	62.67
4	2.75	27	16.08	52	65.77
5	2.86	29	19.22	54	68.42
7	3.05	31	22.69	56	70.39
9	3.26	32	24.36	58	71.98
11	3.51	34	28.18	60	73.18
13	3.95	36	31.95	62	74.08
15	4.59	38	36.21	64	74.72
17	5.64	40	40.41	66	74.97
19	7.03	42	44.93	p_f	75.00
20	7.84	44	49.86	p_a	125.2

		600 Mrad	245°C		8.6 mg.
t	p	t	p	t	p
1	0.84	20	12.20	47	64.06
2	1.96	22	16.11	49	66.31
3	2.58	24	20.40	51	68.46
4	2.85	26	24.59	53	69.92
5	3.00	28	28.66	55	71.22
6	3.11	30	32.87	57	72.40
8	3.35	33	39.26	59	73.48
10	3.60	35	43.64	61	73.98
11	3.80	37	47.60	63	74.49
13	4.39	39	51.47	65	74.82
14	4.84	41	55.06		
16	6.47	43	58.48	p_f	75.00
18	8.95	45	61.41	p_a	132.7

5.3.7.3.(b)/...

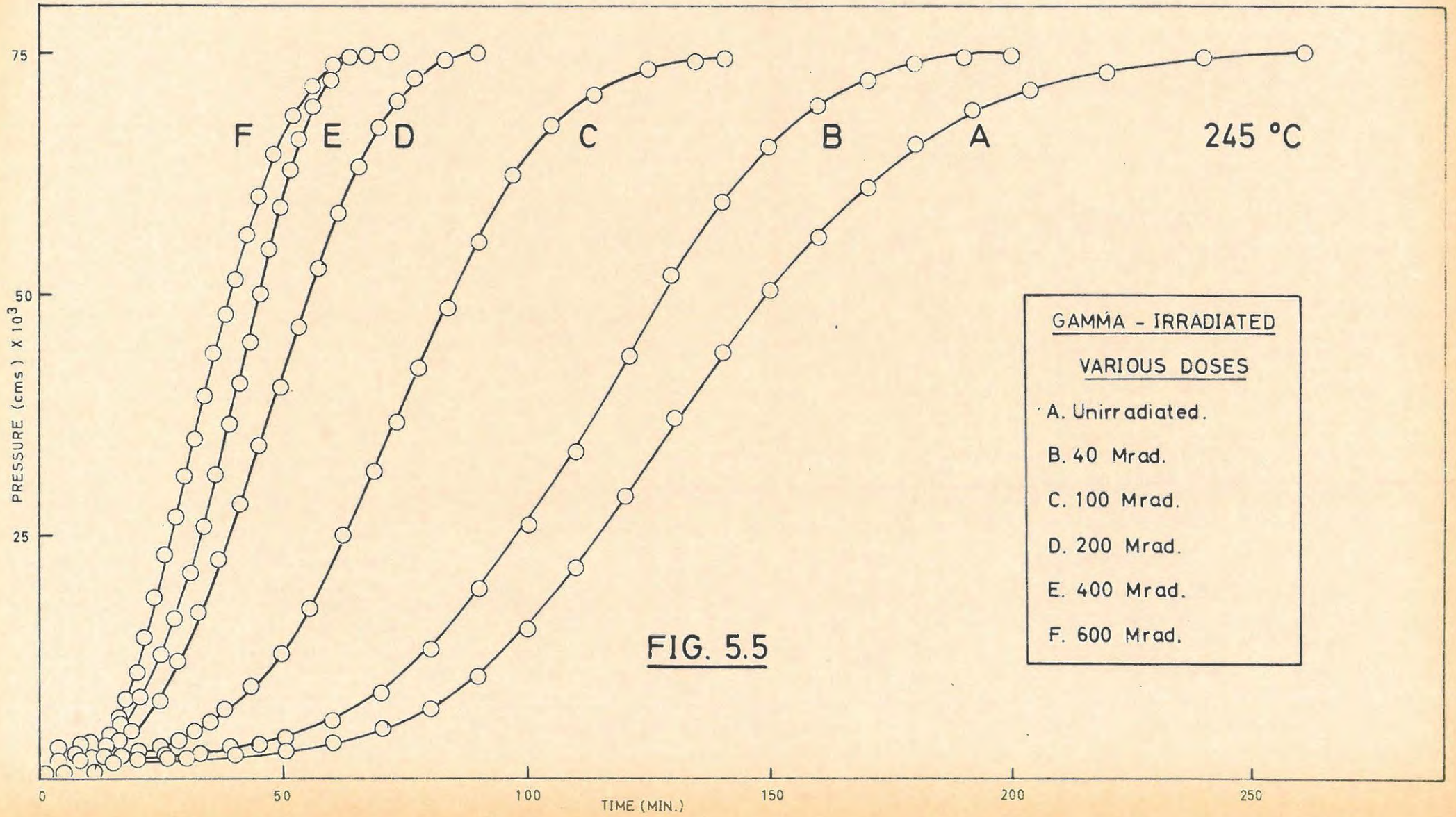
75
50
25
PRESSURE (cms) X 10^3
F
E
D
C
B
A
245 °C
GAMMA - IRRADIATED
VARIOUS DOSES
A. Unirradiated.
B. 40 Mrad.
C. 100 Mrad.
D. 200 Mrad.
E. 400 Mrad.
F. 600 Mrad.
0
50
100
150
200
250
TIME (MIN.)

FIG. 5.5

5.3.7.3 (b) The Initial Reaction.

The effect of various doses of γ-rays on the initial reaction was studied by decomposing samples, with doses ranging from 40 Mrad to 600 Mrad, at constant temperature (105°C). Sample weights of about 60 mg. were used and the pressures normalised to correspond to a fixed sample weight of 61.9 mg. The results are listed in TABLE 5.9 as well as TABLE 5.12 (200 Mrad 105°C).

The effect is illustrated in FIGURE 5.6 and p_f', the pressure at the end of the initial reaction, is plotted against the γ-dose in FIGURE 5.8, curve C.

The values of k_4 from:-

$$\log (p_f' - p) = k_4 t + C \qquad \ldots\ldots \qquad (5.13)$$

and the values of p_f', for the different γ-doses are given in TABLE 5.10.

TABLE 5.9.

INITIAL REACTION	600 Mrad	105°C		61.9 mg.	
t	p	t	p	t	p
1	0.37	34	29.45	95	40.32
3	1.19	37	30.71	100	40.75
5	2.98	40	31.89	111	41.79
7	5.41	44	33.04	120	42.10
9	8.13	48	33.97	130	42.73
11	11.05	52	34.93	140	42.97
13	13.47	56	35.55	150	43.41
15	15.82	60	36.19	160	43.80
17	18.02	65	37.11	170	44.17
19	19.93	70	37.63	180	44.49
22	22.58	75	38.28	190	44.69
25	24.68	80	38.98	210	45.33
28	26.41	85	39.60		
31	28.02	90	39.83	p_f'	42.0

TABLE 5.9./...

TABLE 5.9 contd.

400 Mrad			105°C		61.9 mg.
t	p	t	p	t	p
1	0.06	32	14.70	90	23.51
4	0.60	35	15.58	100	24.17
7	2.17	39	16.62	110	24.80
9	3.52	44	17.82	120	25.41
11	4.92	48	18.60	130	25.85
13	6.17	52	19.49	140	26.32
16	8.08	56	20.13	150	26.79
18	9.15	60	20.82	160	27.18
20	10.13	65	21.36	170	27.48
23	11.51	70	21.95	180	27.75
26	12.65	75	22.35	210	28.50
29	13.80	80	22.77	p_f'	26.8

100 Mrad			105°C		61.9 mg.
t	p	t	p	t	p
1	0.06	45	4.23	130	7.02
3	0.14	50	4.44	140	7.27
6	0.47	55	4.75	150	7.41
10	0.99	60	4.99	160	7.57
15	1.67	70	5.43	170	7.77
20	2.19	80	5.78	180	7.93
25	2.72	90	6.09	210	8.20
30	3.16	100	6.34		
35	3.53	110	6.55	p_f'	7.40
40	3.90	120	6.81		

40 Mrad			105°C		61.9 mg.
t	p	t	p	t	p
1	0.065	50	2.51	120	3.98
5	0.278	56	2.75	130	4.13
10	0.613	62	2.89	141	4.24
15	0.923	68	3.07	150	4.35
20	1.21	75	3.22	160	4.48
25	1.48	82	3.35	180	4.50
31	1.76	90	3.51	210	4.55
38	2.08	100	3.67		
45	2.36	112	3.87	p_f'	4.30

TABLE 5.10./...

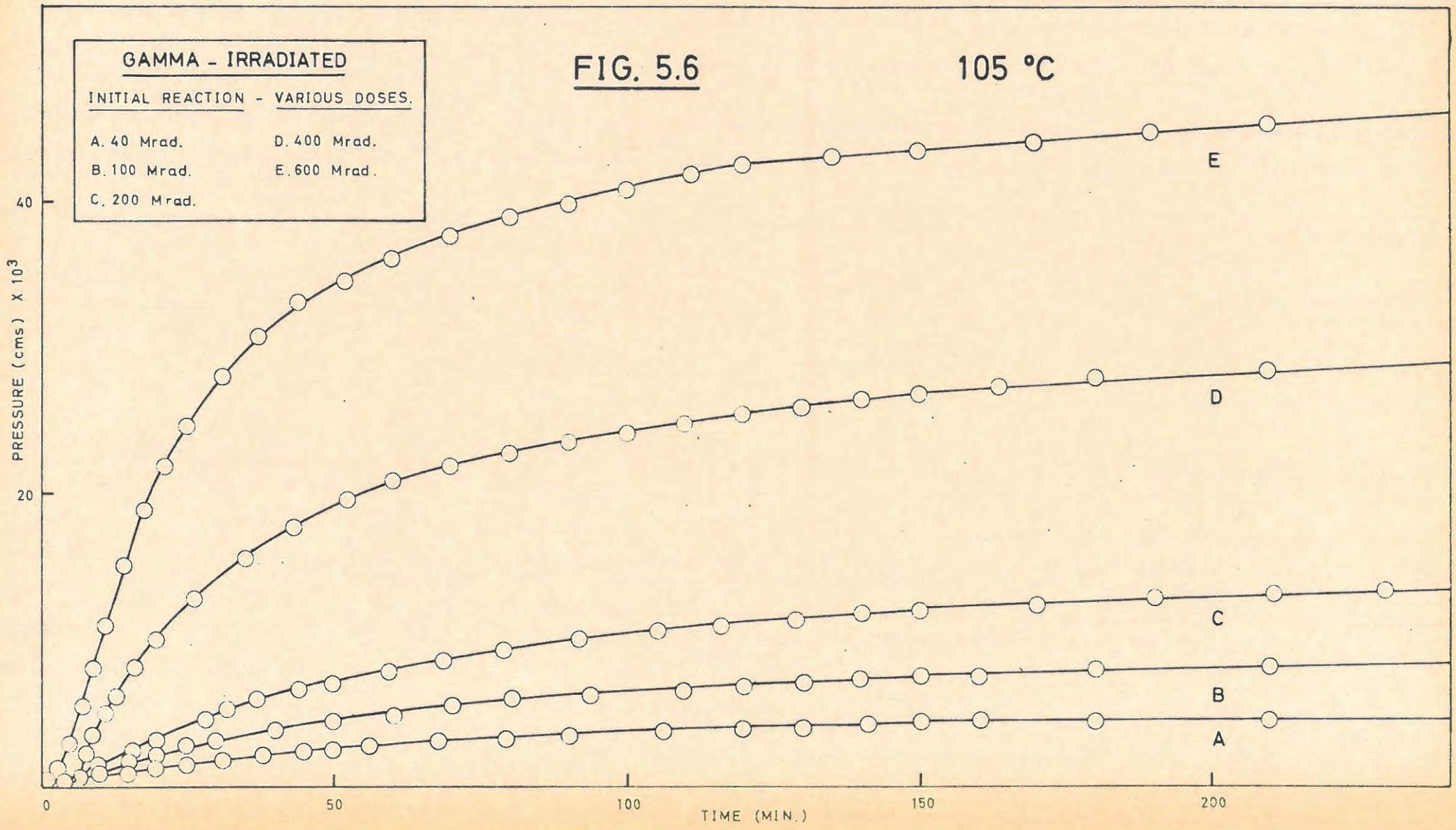
GAMMA - IRRADIATED
INITIAL REACTION - VARIOUS DOSES.
A. 40 Mrad.
B. 100 Mrad.
C. 200 Mrad.
D. 400 Mrad.
E. 600 Mrad.
FIG. 5.6
105 °C
PRESSURE (cms) X 10³
40
20
0
50
100
150
200
TIME (MIN.)
E
D
C
B
A

TABLE 5.10.

INITIAL REACTION. 105°C		61.9 mg.
Dose (Mrad)	k_4 cm per min	p_f cm Hg x 10^3
40	0.0081	4.30
100	0.0086	7.40
200	0.0090	11.90
400	0.0102	28.5
400	0.0108	26.8
600	0.0150	42.00

5.3.7.4 The Effect of Temperature.

5.3.7.4 (a) The Main Reaction.

Samples of pre-irradiated (200 Mrad) nickel oxalate were decomposed at various temperatures in the range 240°C to 260°C, to determine the critical increment of the process(es) occurring during the main acceleratory and decay periods. The results are listed in TABLE 5.11 as well as TABLE 5.7.

TABLE 5.11.

IRRADIATED	200 Mrad	240°C			8.5 mg.
t	p	t	p	t	p
1	0.36	36	12.16	78	56.90
2	1.22	40	16.36	80	59.11
3	1.87	44	20.38	84	62.51
4	2.12	48	24.47	86	64.05
5	2.24	52	28.54	90	66.75
6	2.29	54	30.61	92	67.95
8	2.45	56	32.59	94	69.02
10	2.58	60	36.89	98	70.66
13	2.82	62	38.86	102	71.85
16	3.00	64	41.04	106	72.86
19	3.25	66	43.26	110	73.62
22	3.70	68	45.61	114	74.44
25	4.47	72	49.68	116	74.88
28	5.75	74	52.31	p_f	75.00
31	7.67	76	54.38	p_a	118.8

TABLE 5.11 contd.

200 Mrad		245°C			8.6 mg.
t	p	t	p	t	p
1	0.31	28	11.54	60	58.19
2	1.29	32	16.61	62	60.60
3	1.96	34	19.37	64	62.88
4	2.23	36	22.16	66	65.04
5	2.30	38	25.18	68	67.38
6	2.35	40	28.15	70	68.76
8	2.54	42	30.86	72	69.90
10	2.72	44	33.92	74	71.10
13	2.97	46	37.04	78	72.84
16	3.46	48	40.24	82	74.04
19	4.16	50	43.28	86	74.88
22	5.81	52	46.33	88	75.24
24	7.35	54	49.59	p_f	75.00
26	9.23	56	52.57	p_a	125.0

200 Mrad		255°C			8.5 mg.
t	p	t	p	t	p
1	0.52	20	15.74	37	56.33
2	1.77	21	17.78	38	58.14
3	2.35	22	19.86	39	60.09
4	2.53	23	21.99	41	63.93
5	2.65	24	24.33	42	65.50
6	2.74	25	26.72	44	68.28
8	3.03	26	29.18	46	70.34
10	3.45	27	31.48	48	71.91
12	4.32	29	36.74	50	73.00
14	6.13	30	39.10	52	73.85
15	7.42	31	41.62	54	74.81
16	8.67	32	43.90	56	75.06
17	10.29	34	49.30	58	75.06
18	12.02	35	51.64	p_f	75.00
19	13.80	36	53.88	p_a	124.1

TABLE 5.11./...

TABLE 5.11 contd.

200 Mrad		265°C			8.4 mg.
t	p	t	p	t	p
1	0.55	14	15.86	26	66.98
2	1.30	15	19.63	27	69.57
3	1.85	16	23.76	28	71.53
4	2.25	17	28.03	29	72.92
5	2.44	18	32.77	30	73.71
6	2.59	19	37.70	31	74.33
7	2.72	20	42.61	32	74.82
9	3.72	21	47.67	33	74.76
10	4.80	22	52.24		
11	6.92	23	56.60	p_f	75.00
12	9.31	24	61.01	p_a	137.7
13	12.34	25	64.10		

200 Mrad		260°C			8.5 mg.
t	p	t	p	t	p
1	0.61	19	18.02	38	56.71
2	1.68	20	19.72	39	58.61
3	2.19	21	21.16	40	60.23
4	2.36	22	22.84	41	61.85
5	2.48	23	24.38	42	63.71
6	2.63	24	26.23	43	64.91
7	2.81	26	30.08	45	67.91
8	3.03	28	34.30	47	70.26
10	4.22	29	36.53	48	71.04
11	5.33	30	38.68	50	72.03
12	6.83	31	40.94	52	73.23
13	8.47	32	43.32	55	74.38
14	10.04	33	45.73	57	74.66
15	11.69	34	47.96	59	74.75
16	13.49	35	50.30		
17	14.87	36	52.40	p_f	75.00
18	16.52	37	54.34	p_a	99.66

5.3.7.4./...

5.3.7.4 (b) The Initial Reaction.

The effect of temperature on the initial reaction was studied by decomposing 60 mg. samples of the pre-irradiated (200 Mrad) salt at various temperatures in the range 105°C to 125°C.

The results are given in TABLE 5.12.

TABLE 5.12.

INITIAL REACTION	200 Mrad	105°C		61.9 mg.	
t	p	t	p	t	p
1	0.107	50	7.18	129	11.31
4	0.384	56	7.83	140	11.73
7	0.803	61	8.19	150	11.86
10	1.37	66	8.47	160	12.13
13	1.94	72	8.92	170	12.30
16	2.50	78	9.30	180	12.57
20	3.21	84	9.65	190	12.82
24	3.92	91	10.02	200	13.10
28	4.58	98	10.45	210	13.19
32	5.21	105	10.63	220	13.30
37	5.85	112	10.96	230	13.41
44	6.69	120	11.15	p'_f	11.90

	200 Mrad	115°C		65.0 mg.	
t	p	t	p	t	p
1	0.043	47	9.44	120	13.24
3	0.242	50	9.74	125	13.32
5	0.584	54	10.02	130	13.32
7	1.15	58	10.52	135	13.49
9	1.78	62	10.73	140	13.54
11	2.48	66	11.17	150	13.88
13	3.10	70	11.31	156	13.85
15	3.69	74	11.55	162	14.00
17	4.29	78	11.89	170	14.11
19	4.82	82	11.94	180	14.23
23	5.85	86	12.09	190	14.39
27	6.66	91	12.27	200	14.59
32	7.51	95	12.35	210	14.82
35	8.01	100	12.67	220	14.91
38	8.39	105	12.86	229	14.88
41	8.84	110	12.97	247	15.11
44	9.16	115	13.12	p'_f	12.5

TABLE 5.12 contd.

		200 Mrad	135°C		64.1 mg.
t	p	t	p	t	p
1	0.098	15	8.66	38	13.66
2	0.240	16	9.15	40	13.83
3	0.519	17	9.47	42	13.97
4	1.03	18	9.87	44	14.13
5	1.75	19	10.16	47	14.52
6	2.55	20	10.51	50	14.75
7	3.41	22	11.05	54	15.20
8	4.30	24	11.57	57	15.24
9	5.09	26	11.97	60	15.42
10	5.84	28	12.35	64	15.54
11	6.49	30	12.75	69	15.84
12	7.08	32	12.95	73	16.04
13	7.67	34	13.19	77	16.18
14	8.21	36	13.44	p_f'	14.1

		200 Mrad	160°C		52.2 mg.
t	p	t	p	t	p
1	0.264	8	11.86	15	15.65
2	0.525	9	12.95	16	15.77
3	1.04	10	13.73	17	15.84
4	3.02	11	14.30		
5	6.19	12	14.78	p_f'	15.2
6	8.61	13	15.08		
7	10.48	14	15.25		

		200 Mrad	120°C		55.1 mg.
t	p	t	p	t	p
1	0.082	24	6.29	62	10.67
2	0.170	27	6.92	66	10.93
4	0.474	29	7.25	70	11.15
6	0.992	31	7.59	75	11.37
8	1.65	33	7.88	80	11.54
10	2.37	36	8.21	85	11.84

10/....

TABLE 5.12 contd.

t	p	t	p	t	p
12	3.03	39	8.52	90	11.87
14	3.71	42	8.86	95	12.14
16	4.29	46	9.30	100	12.38
18	4.88	50	9.71	105	12.54
20	5.39	54	10.11		
22	5.82	58	10.33	p'_f	11.7

		200 Mrad		125°C	62.4 mg.
t	p	t	p	t	p
1	0.123	26	9.68	61	13.34
2	0.259	28	10.10	64	13.44
4	0.810	30	10.36	67	13.55
6	1.74	32	10.67	70	13.62
8	2.88	34	10.93	74	13.84
10	4.01	37	11.34	78	14.06
12	5.05	40	11.80	82	14.30
14	5.98	43	12.06	86	14.53
16	6.81	46	12.41	90	14.67
18	7.59	49	12.71	94	14.67
20	8.18	52	12.88	98	14.67
22	8.77	55	13.02		
24	9.29	58	13.15	p'_f	12.9

5.3.7.5 Mathematical Analysis.

A typical pressure-time plot for the thermal decomposition of pre-irradiated salt is shown in FIGURE 5.7, Curve B.

Over the acceleratory period a poor fit is obtained with the Prout-Tompkins equation:-

$$\log\left[\frac{p-p_o}{p_f-p}\right] = k_2 t + C \qquad \ldots\ldots \qquad (5.6)$$

However the modified Prout-Tompkins equation is applicable:-

$$\log\left[\frac{p-p_o}{p_f-p}\right] = k \log (t-t_o) + \text{const.} \quad \ldots \qquad (5.14)$$

where/...

where p_o and t_o are the pressure and time at the end of the initial reaction.

To derive rate constants this may be written as:-

$$\log \left[\frac{p-p_o}{p_f-p}\right] = n \log (t-t_o) + n \log k_5 \quad \ldots\ldots \quad (5.12)$$

For all temperatures of decomposition, n = 3.

A plot of $\left[\frac{p-p_o}{p_f-p}\right]^{\frac{1}{3}}$ against t

is shown in FIGURE 5.7, curve A. The extent of fit is $\alpha = p_o/p_f$ to $\alpha = 0.5$.

The contracting sphere formula:-

$$1 - (1-p/p_f)^{\frac{1}{3}} = k_3 t \quad \ldots\ldots \quad (5.7)$$

again describes the decay region, see FIGURE 5.7, curve C. The range over which it applies is $0.53 < \alpha < 0.97$.

The Avrami-Erofeyev and unimolecular equations do not hold.

The p-t plots for the initial reaction, an example of which is shown in FIGURE 5.8, curve A, do not reach a definite final pressure, but pass into a slow, almost linear region representing the main reaction. On estimating p_f' for the initial reaction, the unimolecular law:-

$$\log (p_f' - p) = k_4 t + C \quad \ldots\ldots \quad (5.15)$$

is valid. FIGURE 5.8, curve B.

The values of k_4, k_5 and k_3 at various temperatures are tabulated in TABLE 5.13.

The values of log k_4, log k_5 and log k_3 are plotted against $1/T^oK$ in FIGURE 5.9.

The values of the activation energies obtained from these plots are, with unirradiated values in brackets for comparison:-

Initial reaction : 15.4 kcal/mole (33.C kcal/mole)
Acceleratory reaction: 30.1 kcal/mole (33.6 kcal/mole)
Decay reaction : 31.5 kcal/mole (35.4 kcal/mole)

TABLE 5.13./...

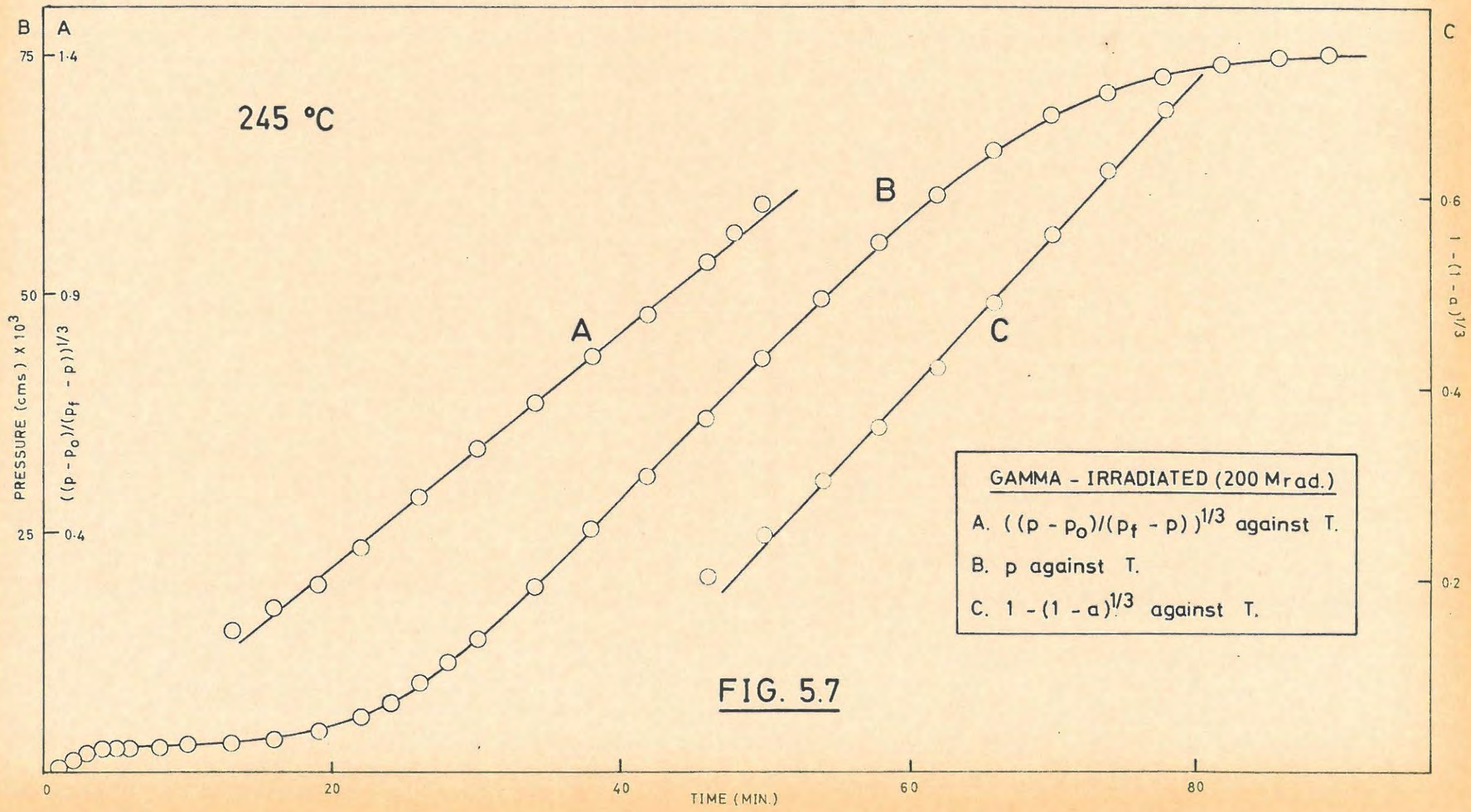
B
A
C
75
50
25
1·4
0·9
0·4
0·6
0·4
0·2
245 °C
A
B
C
PRESSURE (cms) X 10^3
$((p - p_o)/(p_f - p))^{1/3}$
$1 - (1 - a)^{1/3}$
GAMMA - IRRADIATED (200 Mrad.)
A. $((p - p_o)/(p_f - p))^{1/3}$ against T.
B. p against T.
C. $1 - (1 - a)^{1/3}$ against T.
0
20
40
60
80
TIME (MIN.)

FIG. 5.7

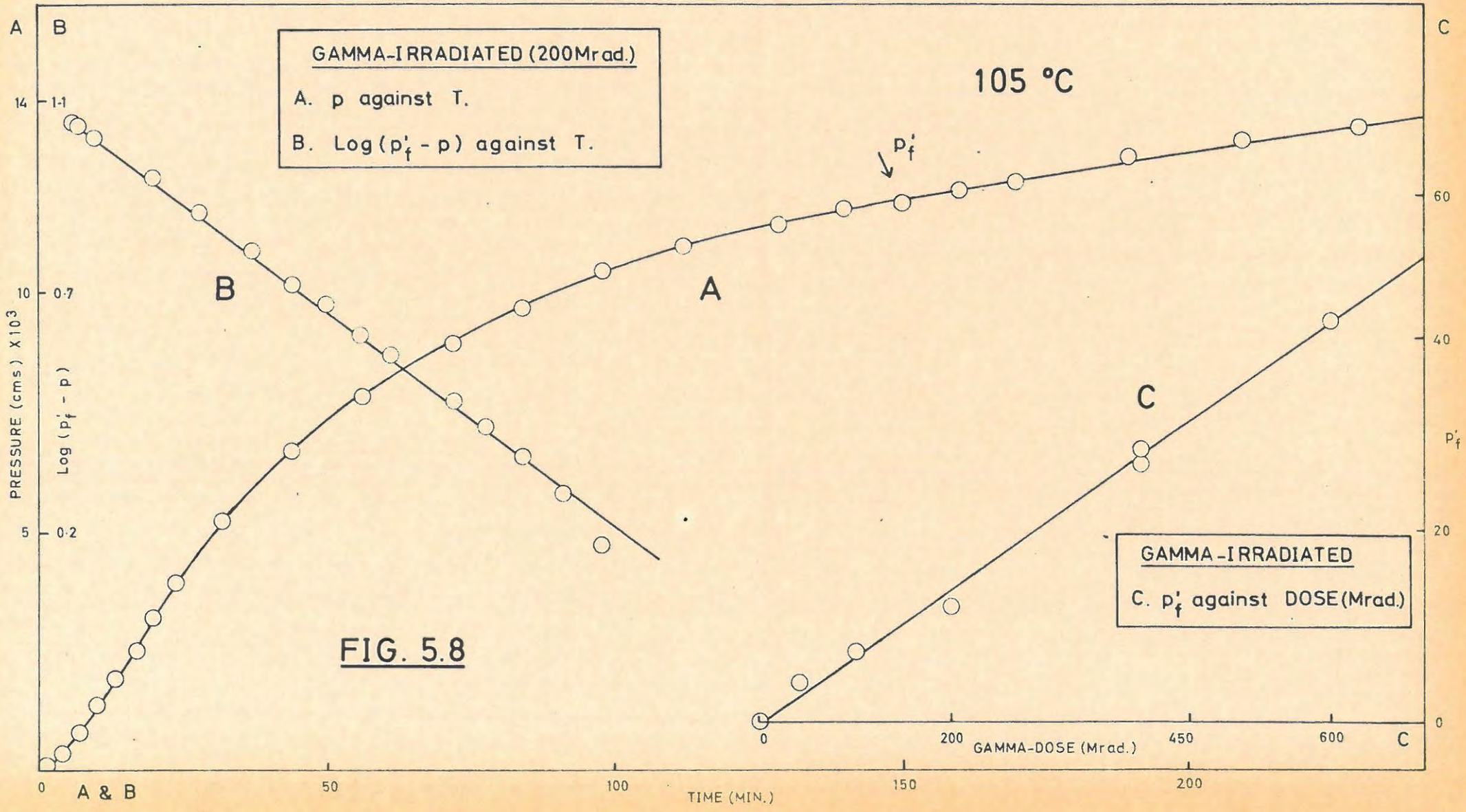
A
B
C
GAMMA-IRRADIATED (200Mrad.)
A. p against T.
B. Log (p'f - p) against T.
105 °C
p'f
B
A
C
GAMMA-IRRADIATED
C. p'f against DOSE (Mrad.)
PRESSURE (cms) X10³
Log (p'f - p)
p'f
TIME (MIN.)
A & B
GAMMA-DOSE (Mrad.)
14
10
5
1·1
0·7
0·2
60
40
20
0
50
100
150
200
450
600

FIG. 5.8

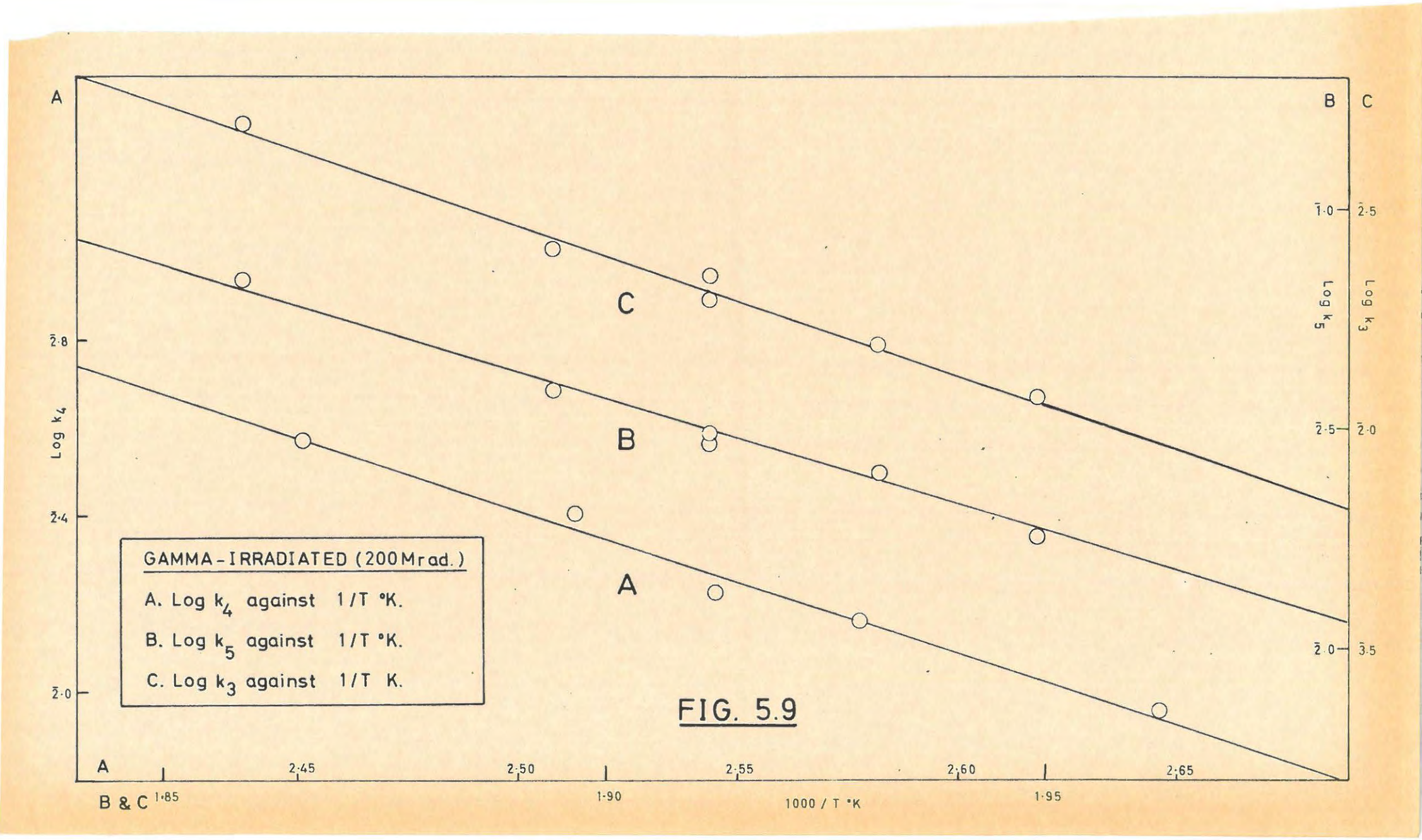
A
B
C
Log k_4
Log k_5
Log k_3
$\bar{2}\cdot8$
$\bar{2}\cdot4$
$\bar{2}\cdot0$
$\bar{1}\cdot0$
$\bar{2}\cdot5$
$\bar{2}\cdot0$
$\bar{2}\cdot5$
$\bar{3}\cdot5$
GAMMA-IRRADIATED (200 Mrad.)
A. Log k_4 against 1/T °K.
B. Log k_5 against 1/T °K.
C. Log k_3 against 1/T K.
A
B & C
2·45
2·50
2·55
2·60
2·65
1·85
1·90
1·95
1000 / T °K

FIG. 5.9

TABLE 5.13.

NICKEL OXALATE 200 Mrad				
INITIAL REACTION			ACCEL.	DECAY
Temp. °C	k_4 x 100 cm/min.	Temp. °C	k_5 x 100 per min.	k_3 x 100 per min.
105	0.904	240	1.78	1.18
115	1.453	245	2.48	1.56
120	1.683	250	2.90	2.16
125	2.545	250	3.08	2.20
135	3.713	250	2.96	2.19
160	13.44	255	3.86	2.55
		265	6.89	4.90

5.3.7.6 The Effect of Annealing.

Annealing the irradiated powder (200 Mrad) in vacuum at 150°C for 8 hr. prior to decomposition at 250°C, eliminated the initial reaction completely but had no effect on the remainder of the reaction.

The run is tabulated in TABLE 5.14.

TABLE 5.14.

IRRADIATED AND ANNEALED 200 Mrad 250°C 8.6 mg.					
t	p	t	p	t	p
1	0.09	30	18.77	52	61.47
2	0.16	31	21.17	54	63.68
3	0.24	32	23.61	56	65.66
4	0.32	33	25.92	58	67.30
5	0.43	34	28.26	60	68.60
7	0.59	35	30.42	62	69.50
10	0.81	36	32.66	64	70.69
14	1.12	37	34.89	66	71.71
18	1.73	38	36.90	68	72.56
20	2.55	39	39.04	70	73.47
22	4.01	41	43.23	72	74.20
24	6.61	42	45.16	74	74.54
26	10.13	44	48.79	76	74.94
27	12.16	46	52.34	78	74.96
28	14.30	48	55.43	p_f	75.00
29	16.49	50	58.64	p_a	132.5

5.3.7.7 The Effect of Hydrating and De-hydrating.

The irradiated (200 Mrad) salt was "hydrated" by standing it in a closed vessel containing a beaker of water. The salt assumed the green colour of nickel oxalate dihydrate. This was decomposed at 260°C in the usual manner.

The hydrated salt was dehydrated in vacuum at 150°C for 8 hr. and then decomposed at 260°C.

The runs are listed in TABLE 5.15 and illustrated in FIGURE 5.10 where they are compared with the p-t plot for the irradiated anhydrous salt.

After addition to, and removal of, water from the salt the irradiation effect was destroyed and the decomposition approximated to that of the unirradiated salt.

TABLE 5.15.

IRRADIATED AND HYDRATED		200 Mrad		260°C	8.4 mg.
t	p	t	p	t	p
1	0.33	28	24.73	56	65.69
2	0.98	30	30.76	58	66.89
3	1.10	32	36.36	60	67.91
4	1.07	34	41.04	62	68.79
5	1.07	36	45.18	65	70.09
8	1.22	38	48.43	68	71.94
12	1.56	40	51.62	71	72.70
16	2.39	42	54.05	74	73.35
20	5.27	44	56.30	77	73.85
23	10.48	46	58.29	80	74.43
25	15.60	48	60.11	83	74.79
26	18.51	50	61.84	p_f	75.00
27	21.59	54	64.45	p_a	103.7

TABLE 5.15./...

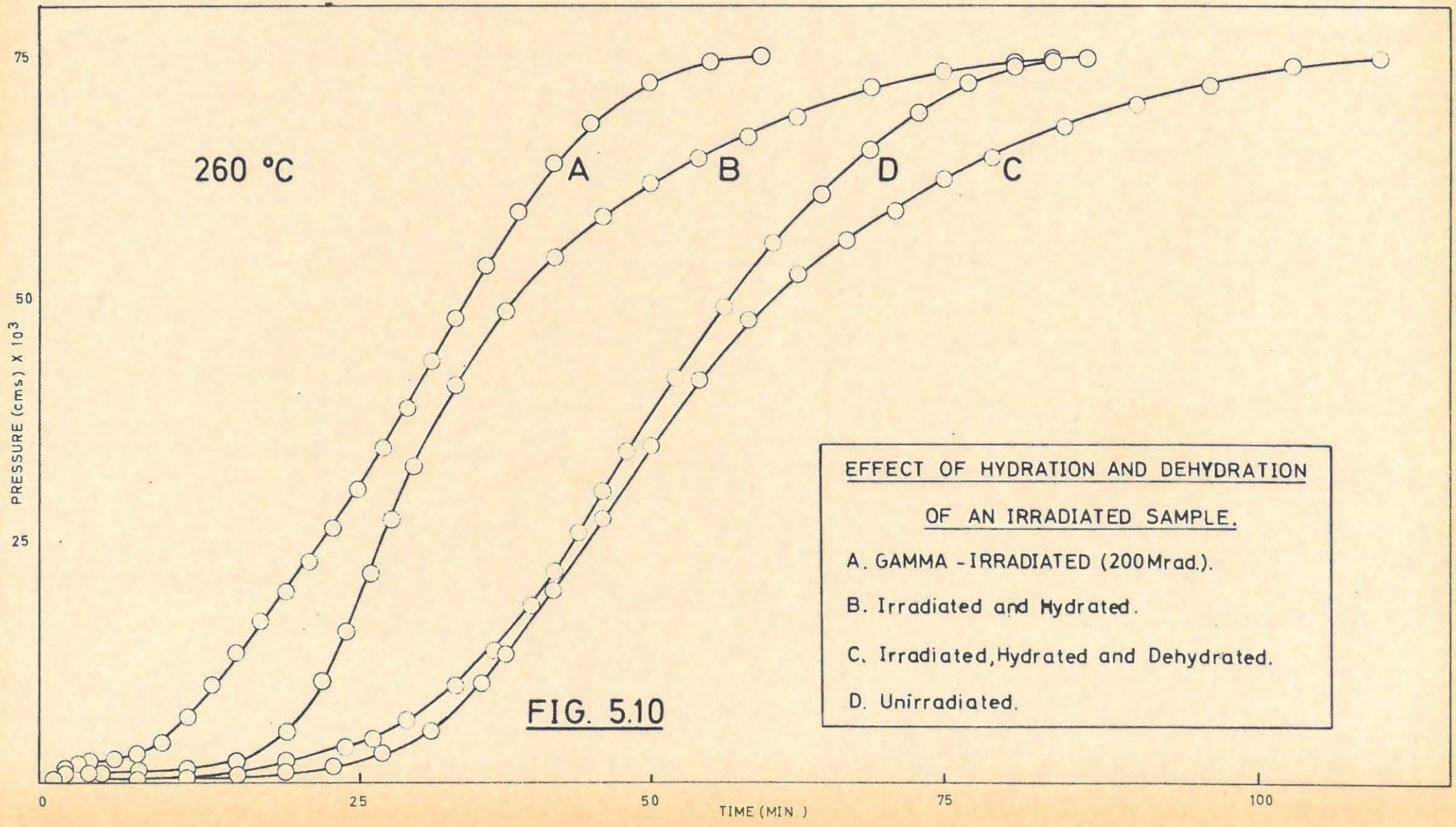
260 °C
A
B
D
C
75
50
25
PRESSURE (cms) X 10³
0
25
50
75
100
TIME (MIN.)
EFFECT OF HYDRATION AND DEHYDRATION
OF AN IRRADIATED SAMPLE.
A. GAMMA - IRRADIATED (200 Mrad.).
B. Irradiated and Hydrated.
C. Irradiated, Hydrated and Dehydrated.
D. Unirradiated.

FIG. 5.10

TABLE 5.15 contd.

IRRADIATED, HYDRATED & DEHYDRATED 200 Mrad 260°C 8.3 mg.					
t	p	t	p	t	p
1	0.10	40	16.43	72	60.79
2	0.13	42	19.86	74	62.32
3	0.18	44	23.50	76	63.79
4	0.23	46	27.26	78	64.58
5	0.27	48	30.86	81	66.45
8	0.41	50	34.55	84	67.69
12	0.59	52	38.14	87	68.77
16	0.80	54	41.57	90	69.90
20	1.15	56	44.91	93	70.92
24	1.84	58	47.63	96	71.94
28	3.19	60	50.22	99	73.24
30	4.28	62	52.45	103	73.98
32	5.40	64	54.14	106	74.37
34	7.85	66	55.97	110	74.88
36	10.34	68	57.34	p_f	75.00
38	13.22	70	59.09	p_a	132.3

5.3.7.8 The Effect of Interrupting a Decomposition.

The decomposition of the irradiated (400 Mrad) salt was interrupted at different stages by raising the sample into the evolved gas, where it cooled and stood for an hour before the decomposition was continued.

The run is given in TABLE 5.16 and shown in FIGURE 5.11.

The effect is similar to that for unirradiated material, (Section 5.3.6).

TABLE 5.16./...

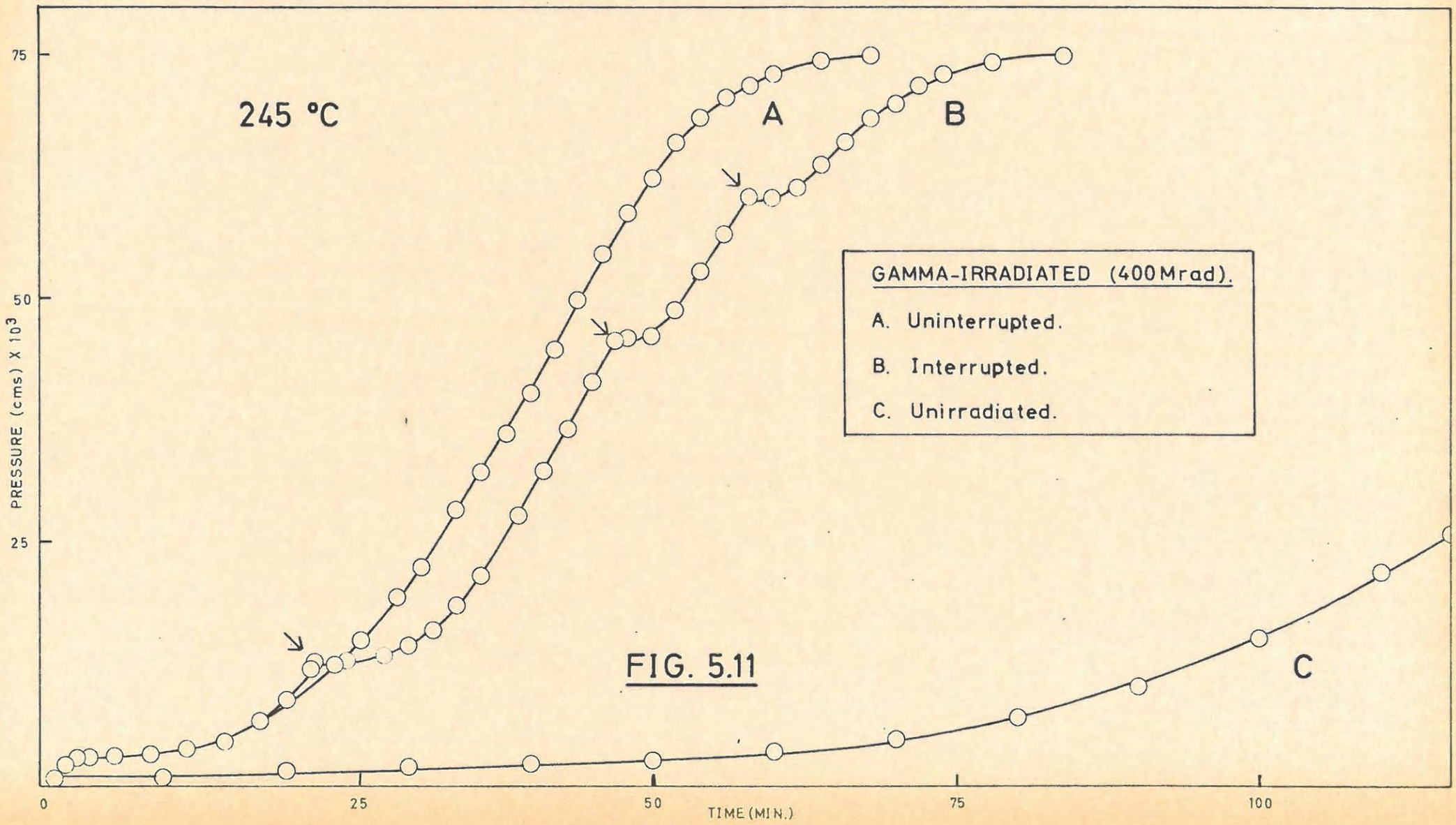
245 °C
A
B
C
GAMMA-IRRADIATED (400 Mrad).
A. Uninterrupted.
B. Interrupted.
C. Unirradiated.
PRESSURE (cms) X 10³
TIME (MIN.)
0
25
50
75
100

FIG. 5.11

TABLE 5.16.

IRRADIATED & INTERRUPTED		400 Mrad	245°C		8.6 mg.
t	p	t	p	t	p
1	0.53	32	15.72	58*	60.33
4	2.72	34	18.16	60	60.33
7	3.08	36	21.61	62	61.44
10	3.38	39	27.67	64	63.92
13	3.84	41	31.94	66	66.15
16	4.97	43	36.56	68	68.57
18	6.55	45	41.14	70	70.12
20	8.82	47*	45.55	72	71.98
22*	12.56	48	45.59	74	73.22
23	12.97	50	46.21	76	73.90
25	12.91	52	48.83	78	74.40
28	13.35	54	52.72	p_f	75.00
30	14.22	56	56.64	p_a	121.0

* Interruption.

5.3.7.9 The Effect of Interrupting a Decomposition and Irradiating with Gamma-rays.

The decomposition at 240°C of weighed samples in Pyrex ampoules was interrupted at various stages and the samples sealed under vacuum and irradiated (200 Mrad). The decomposition was then continued at the same temperature.

The results are listed in TABLE 5.17 and illustrated in FIGURE 5.12.

TABLE 5.17.

INTERRUPTED & IRRADIATED		200 Mrad	240°C		8.5 mg.
t	p	t	p	t	p
1	0.10	70	5.38	160	58.52
4	0.21	76	6.71	170	63.13
10	0.69	82	8.11	180	66.94
20	1.23	88	11.53	190	69.24
30	1.57	92	13.39	200	71.13
36	1.71	98	16.41	210	72.82
40*	1.75	104	19.20	220	73.79

TABLE 5.17 contd.

t	p	t	p	t	p
42	2.35	111	22.87	230	74.48
44	3.11	120	28.95	240	74.68
46	3.51	126	33.44		
50	3.88	132	37.96	p_f	75.00
54	4.11	140	44.48	p_a	106.0
60	4.38	150	52.08		

		200 Mrad	240°C		8.4 mg.
t	p	t	p	t	p
1	0.07	95	6.02	158	38.74
5	0.18	96	6.14	162	43.77
10	0.39	98	6.31	166	48.54
20	0.81	100	6.42	170	52.65
30	1.07	104	6.57	174	56.23
40	1.27	108	6.70	178	59.37
50	1.45	114	6.95	182	62.29
60	1.66	120	7.42	186	64.72
70	2.03	126	8.55	190	66.76
80	2.93	130	9.91	195	68.89
85	3.78	134	11.87	200	70.66
90*	4.95	138	14.83	206	72.10
91	5.11	142	18.74	214	73.85
92	5.38	146	23.21	224	74.86
93	5.66	150	28.10	p_f	75.00
94	5.85	154	33.34	p_a	139.2

		200 Mrad	240°C		8.4 mg.
t	p	t	p	t	p
1	0.10	123	16.99	180	35.48
5	0.22	124	17.20	185	40.87
10	0.50	125	17.35	190	46.67
20	0.91	126	17.46	195	52.30
30	1.15	127	17.57	200	57.03
40	1.36	129	17.71	206	61.95
50	1.55	131	17.82	212	65.76
60	1.72	134	17.93	220	69.33

TABLE 5.17 contd.

t	p	t	p	t	p
70	2.06	137	18.06	230	72.15
80	2.86	140	18.17	240	73.32
90	4.40	145	18.44	250	74.32
100	7.16	150	19.04	260	74.83
110	11.57	155	20.14	270	74.98
115	13.96	160	21.66		
120*	16.40	165	23.64		
121	16.55	170	26.37	p_f	75.00
122	16.75	175	30.22	p_a	128.8

		200 Mrad	240°C		8.4 mg.
t	p	t	p	t	p
1	0.10	165	24.51	230	38.12
5	0.24	170*	26.90	236	41.35
10	0.54	171	27.13	242	44.95
20	0.97	172	27.35	250	50.26
38	1.45	173	27.56	260	57.06
50	1.69	174	27.79	270	62.68
60	1.88	175	27.92	280	66.44
70	2.10	176	28.00	290	69.19
82	2.65	180	28.35	300	71.00
90	3.26	184	28.54	310	72.10
100	4.26	188	28.66	320	73.00
110	5.50	194	28.95	345	74.83
120	7.39	200	29.54	355	75.00
130	10.20	206	30.54		
140	13.78	212	31.95		
150	17.59	218	33.57	p_f	75.00
160	22.12	224	35.56	p_a	113.4

TABLE 5.17./...

TABLE 5.17 contd.

		200 Mrad	240°C		8.5 mg.
t	p	t	p	t	p
1	0.11	150	20.89	222	58.68
10	0.70	156	25.94	228	59.74
20	1.37	162	31.82	236	61.27
30	1.78	168	38.61	244	62.78
40	2.08	174	45.85	252	64.44
50	2.37	178	50.45	260	66.35
60	2.68	180*	52.42	270	68.29
70	3.20	182	53.13	284	70.71
82	4.16	184	53.88	300	72.89
90	5.00	188	54.61	320	74.10
100	6.15	192	54.93	340	74.64
110	7.62	197	55.21		
120	9.32	202	55.65	p_f	75.00
130	11.54	206	56.09	p_a	89.0
140	15.01	214	57.30		

		200 Mrad	240°C		8.6 mg.
t	p	t	p	t	p
1	0.06	170	10.22	278	52.61
10	0.59	180	11.65	284	53.20
20	1.01	190	13.83	290	54.01
30	1.27	200	17.36	296	55.16
40	1.46	212	23.79	304	57.29
50	1.65	220	29.03	310	59.12
60	1.88	230	36.48	320	62.38
70	2.23	240	43.91	330	65.17
80	2.83	250*	50.44	340	67.52
90	3.44	252	50.82	350	69.40
100	4.08	254	51.23	360	70.66
110	4.82	256	51.45	370	71.33
120	5.55	258	51.60	380	72.60
130	6.33	260	51.69	400	74.20
140	7.17	264	51.88		
150	8.07	268	52.05	p_f	75.00
160	9.10	272	52.25	p_a	131.3

* Interruption.

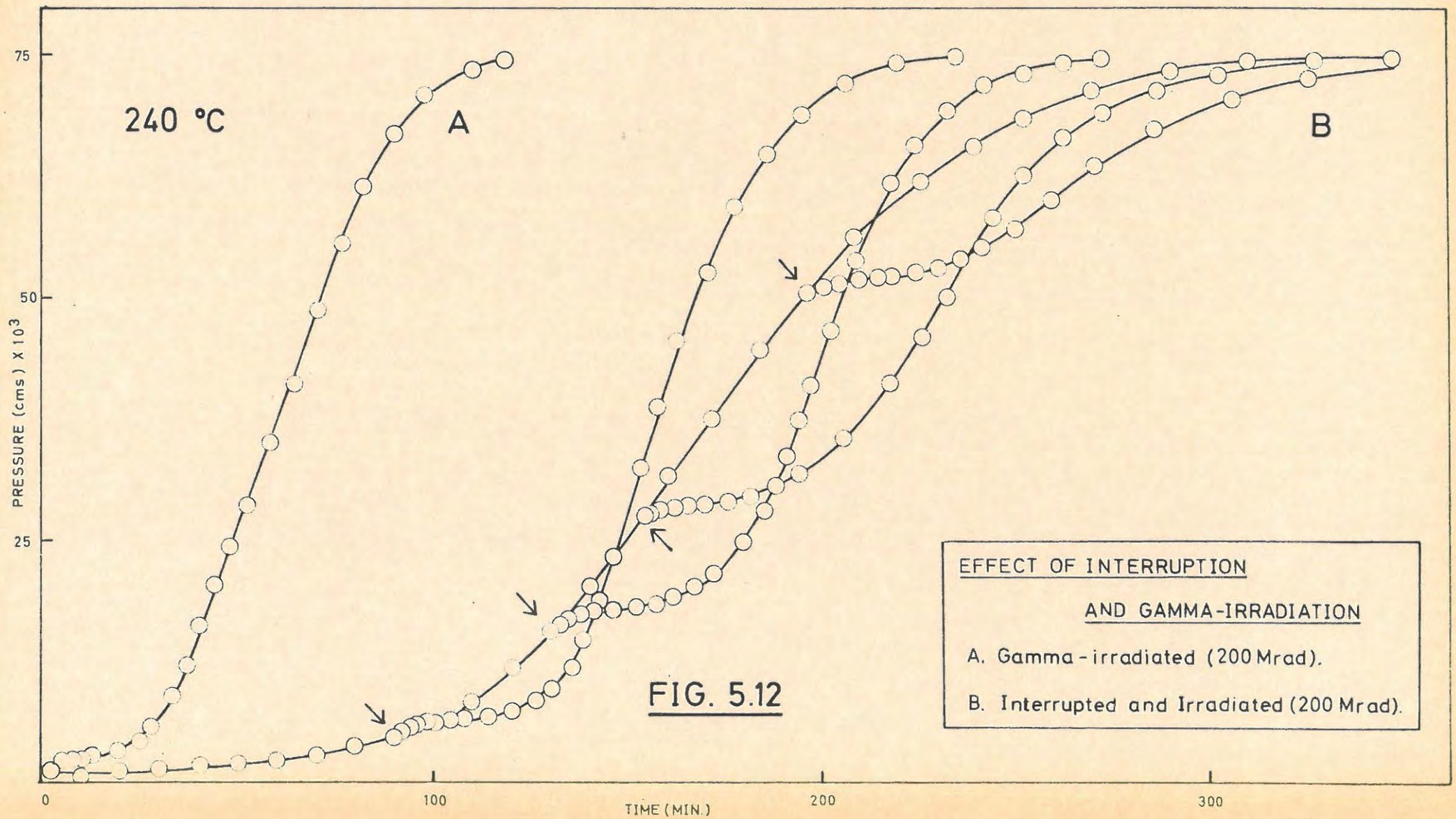
240 °C
A
B
75
50
25
PRESSURE (cms) X 10^3
0
100
200
300
TIME (MIN.)
EFFECT OF INTERRUPTION
AND GAMMA-IRRADIATION
A. Gamma-irradiated (200 Mrad).
B. Interrupted and Irradiated (200 Mrad).

FIG. 5.12

5.4 DISCUSSION.

5.4.1 Unirradiated Nickel Oxalate.

The results obtained for the decomposition of unirradiated nickel oxalate are in agreement with those obtained by Jacobs [335]. The analysis of the acceleratory and decay parts of the p-t plots is different however. The Prout-Tompkins equation covers the entire acceleratory region as against Jacobs' α = 6 to 97 per cent when using the Avrami-Erofeyev equation. Danes and Ponec [339] also applied the Prout-Tomkins equation to the acceleratory period. The Avrami-Erofeyev equation fitted from α = 4 to 40%.

The contracting sphere equation gives a better fit over the decay period than the unimolecular law used by Jacobs, while the analysis of the initial reaction is in agreement with that of Jacobs.

The decomposition may be interpreted as the formation of a layer of nickel over the surface of the particles during the intial reaction as Jacobs suggested. Decomposition will commence at imperfections such as surface steps. At the end of the initial reaction, this layer of product creates strain at the interface of the product and reactant and initiates a branching reaction as postulated in the Prout-Tompkins mechanism. The strain effect has been described by applying dislocation theory[341].

The product layer obstructs an emerging dislocation, causing a pile up of dislocations such that the stress at the head of a group of n dislocations is n times the stress of the leading dislocation. When this stress exceeds the cohesive strength of the crystal, cracks develop, probably by transformation to cleavage dislocations on linear steps along which parts of the crystal are separated. The

cleavage/...

cleavage dislocation climbs along the fissure, thereby lengthening it, while the other piled-up dislocations glide near the barrier and produce further cleavage. After α = 0.5, the number of dislocations is greatly reduced, the strain effect is diminished, and the reaction continues by the inward progression of the reaction interface on approximately spherical particles.

The agreement of the activation energies for the initial, acceleratory and decay regions indicates that the same chemical reaction occurs at all stages. Jacobs suggested that the rate-determining step is the electron transfer from oxalate to nickel ions. This is followed by the rapid break-up of unstable oxalate radicals to CO_2. An alternative is that the reaction during the acceleratory and decay stages proceeds by electron transfer from oxalate ions to anion vacancies, followed by the decomposition of the radical. The rate-determining step is again the electron transfer process.

Interruption of the reaction over the acceleratory period may cause amorphous nickel formed at the interface during decomposition, to crystallise as the temperature is dropped. Coherence with the parent lattice will be destroyed and the product will no longer create strain at the interface. Before the reaction can regain its normal rate a new coherent layer of amorphous product must be formed at the interface and approximately the same system of branching planes of reaction must be established. This causes a new acceleration of reaction when heating is resumed.

The collapse of the interface following interruption in the decay period is of little significance, since the reaction is not propagated by the strain mechanism.

5.4.2./...

5.4.2 Irradiated Nickel Oxalate.

Pretreatment with γ-rays is responsible for a higher initial rate in the subsequent thermal decomposition; after the initial short deceleratory reaction the usual acceleratory reaction begins, but the acceleration is greater than in the corresponding decomposition of unirradiated oxalate. The plots in FIGURE 5.6 show that the duration of the initial gas evolution in the thermal decomposition is independent of the γ-ray dose, but that p'_f increases with dose.

The explanation of the effects of pre-irradiation is to be sought in this initial decay reaction. The value of 15.7 kcal/mole for the activation energy is significantly different from the average activation energy for the main reaction, which is 32.7 kcal/mole. Therefore, it is concluded that the reaction occurring during the first stage is different from the main reaction. The colour of the irradiated salt suggests the production of nickel by the γ-rays.

The primary act of pre-irradiation is assumed to be the freeing of electrons from oxalate ions and the subsequent trapping of these electrons by Ni^{++} to produce nickel. On heating, the initial reaction is the decomposition of the intermediate, arising from the oxalate ions. The nature of this intermediate is uncertain, but the amount produced is proportional to the γ-ray dose in the range 0 to 600 Mrad. (FIGURE 5.8). The decomposition plots of this product of irradiation obey a unimolecular decay law. The calculated velocity constants at a fixed temperature are independent of the γ-ray dose. (TABLE 5.10).

The formation of nickel and the unstable intermediate during irradiation is assumed to occur mainly in subgrain boundaries, at dislocations, and at surface imperfections.

Further/...

Further, changes in thermal decomposition after irradiation are assumed to be due to additional anion vacancies formed by the decomposition of the unstable intermediate during the initial reaction. Reaction spreads through the subgrain boundary network and over the free surfaces, forming a nickel/nickel oxalate interface. Strain in the reactant at this interface causes the usual accelerating reaction by the Prout-Tompkins mechanism. The acceleration differs from that for unirradiated material in that the probability of branching decreases with time.

The results of hydration and redehydration of irradiated material indicate that the formation and collapse of the hydrate results in a redistribution of subgrain boundaries, so that a large number of intermediate groups and their resulting vacancies are no longer favourably situated for propagation of the reaction. The decomposition of the redehydrated irradiated material is approximately the same as that of the unirradiated material.

The results obtained by interrupting a decomposition, irradiating, and then continuing the decomposition, show that the irradiation effect occurs up to α = C.5, but not beyond. Evidently sites in subgrain boundaries and dislocations which are affected by irradiation are still available during the acceleration of the reaction with the unirradiated material. The plots in FIGURE 5.12 show that the greater the time of interruption, the smaller the acceleration. This is to be anticipated, since the normal decomposition will progressively destroy regions such as subgrain boundaries, which are likely to be affected by irradiation. At α = 0.5 this destruction is evidently complete.

6. THE THERMAL DECOMPOSITION OF AMMONIUM DICHROMATE.

6.1. PREVIOUS WORK.

Early work on ammonium dichromate [344-346] was concerned mainly with the nature of the final products of the thermal decomposition.

Fischbeck and Spingler [347] made a kinetic study of the thermal decomposition of ammonium dichromate (188-218°C) in vacuum, as well as of the chromate and trichromate. They found that the pressure increased with the fourth power of the time over the acceleratory period, and that the contracting sphere equation [348]:-

$$1 - (1 - p/p_f)^{\frac{1}{3}} = kt \qquad \ldots\ldots \qquad (6.1)$$

held for the decay. The activation energy for the decay was given as 49 kcals/mole, and the mechanism suggested was the growth and coalescence of hemispheres of product.

Simpson and Taylor[349,350] studied the decomposition over a similar temperature range. They reported that the curves obtained for the combined evolution of nitrogen and nitrous oxide, were sigmoid followed by a process of constant rate (45 to 70% decomposition). The autocatalytic period was analysed in terms of the Prout-Tompkins equation[351]:-

$$\log \left[p/(p_f - p)\right] = kt + \text{const} \ldots \qquad (6.2)$$

where p_f is the pressure at the end of the sigmoid. A single value of k was required and the reproducibility of k was only about 20%. The activation energy for this section of the curve was 33 kcal/mole, while the 'constant rate process' had an activation energy of 38 to 41 kcal/mole depending on the crystal size. Prolonged grinding was reported to remove the induction period.

Pre-irradiation for four months at a low dose-rate, with γ-rays from a Co^{60} source of low intensity, reduced the induction period slightly and altered the fit of the

Prout-/...

Prout-Tompkins equation so that two values of k were obtained.

Water and ammonia both inhibited the reaction, while ageing of the material over P_2O_5 for two years, changed the decomposition kinetics. The induction period was reduced and the acceleration of the autocatalytic period increased. The power law:-

$$p^{1/n} = k't + \text{const.} \qquad \ldots\ldots\ldots \qquad (6.3)$$

with n = 3, applied up to $\alpha = 0.35$.

Analysis in terms of the Prout-Tompkins equation implied a mechanism of interfering branching chains. According to Simpson and Taylor this was followed by reaction at an interface of constant area.

The change in kinetics on ageing was compared to that for mercury fulminate[352,353]. Ageing was considered to change the grain structure of the crystals as a result of loss of traces of water and ammonia during storage over P_2O_5. A large number of non-contiguous blocks prevent the propagation of chains of reaction.

Erofeyev[354] studied the dependence of the rate of thermal decomposition of ammonium dichromate on the initial surface area of the substance. Rate/time curves showed two maxima. The first increased with specific surface and the gases evolved were mainly the condensable gases NH_3 and N_2O. The second maximum, which is that reported by previous investigators for samples of small surface, decreased with an increase in specific surface, and contained a considerably smaller fraction of condensable gases.

Two kinds of reaction centres were proposed: surface centres and volume centres. As the specific surface increases the reaction taking place as a result of the growth of surface centres acquires greater importance.

The/...

The samples with different surfaces were obtained by grinding, however. The defects thus produced could play a more important part in the decomposition than the creation of a larger surface.

Because of the lack of agreement on the analyses to be applied to the unirradiated decomposition, it was decided to study the decomposition further before proceeding to an examination of the effects of pre-irradiation.

6.2. EXPERIMENTAL.

6.2.1. Preparation.

Single crystals were obtained by slow evaporation in air at room temperature of solutions, initially saturated at 30°C (50 gm/100 ml) with B.D.H. "Analar" ammonium dichromate. The first crop of large imperfect crystals was filtered off and the filtrate yielded small (5 - 20 mg.) crystals which were hand selected, dried on filter paper and then stored over silica-gel.

A batch of very small crystals was obtained by rapid cooling, with stirring, of a similar saturated solution.

Some of the recrystallised salt was ground in an agate mortar.

6.2.2. Apparatus.

This was as described (Section 4). A P_2O_5 trap was used to remove water vapour and ammonia from the evolved gases, as no liquid air was available.

6.3./...

6.3. RESULTS.

6.3.1. Reproducibility.

Three consecutive runs were performed on the whole large crystals at 225°C. The results are given in TABLE 6.1. The reproducibility was satisfactory. For the acceleratory period the rate constants k_1, from:

$$p^{\frac{1}{3}} = k_1 t + C \qquad \ldots\ldots\ldots \qquad (6.4)$$

were 0.1950, 0.2057, 0.1971 cm $Hg^{\frac{1}{3}}$/min., while for the decay period, k_2, from:

$$1 - (1 - p/p_f)^{\frac{1}{3}} = k_2 t \qquad \ldots\ldots\ldots \qquad (6.5)$$

gave 0.01113, 0.01058, 0.01020 per min., respectively.

TABLE 6.1.

WHOLE CRYSTALS		225°C		Run 1	8.3 mg
t	p	t	p	t	p
2	0.07	31	38.74	65	70.22
5	0.09	33	41.92	70	72.07
10	0.16	36	45.90	75	72.51
15	0.55	39	49.72	80	75.26
18	1.80	42	53.28	85	74.29
20	4.12	45	55.55	90	75.03
22	8.22	48	58.75	95	75.63
24	14.29	51	61.21	100	75.57
27	26.21	55	65.30	p_f	75.00
29	33.14	60	69.06	p_a	42.5

TABLE 6.1 contd.

TABLE 6.1 contd.

225°C Run 2					4.0 mg.
t	p	t	p	t	p
2	0.18	27	34.69	60	68.18
5	0.18	29	38.51	65	70.21
10	0.30	31	42.10	70	69.31
15	1.43	33	45.13	75	71.76
17	3.20	36	47.84	80	73.53
19	6.67	40	52.31	90	74.52
21	12.14	45	57.87	100	75.33
23	19.98	50	62.96	p_f	75.00
25	27.79	55	64.70	p_a	19.41

225°C Run 3					13.5 mg.
t	p	t	p	t	p
2	0.03	25	31.83	60	67.86
5	0.06	27	37.78	65	69.92
8	0.11	30	43.24	70	71.33
11	0.47	33	46.44	75	72.71
14	1.47	36	49.36	80	73.18
17	4.37	40	53.20	85	73.96
20	12.27	44	56.80	90	74.24
21	15.95	48	59.92	100	75.04
22	20.22	52	62.90	p_f	75.00
23	24.22	56	65.89	p_a	65.03

6.3.2. Crystal Size and the Effect of Grinding.

Runs at 225°C were done on samples from the batch of small crystals and on the ground material. The results are tabulated in TABLE 6.2 and a comparison of 'whole' crystals, small crystals and ground crystals is made in FIGURE 6.1.

TABLE 6.2./...

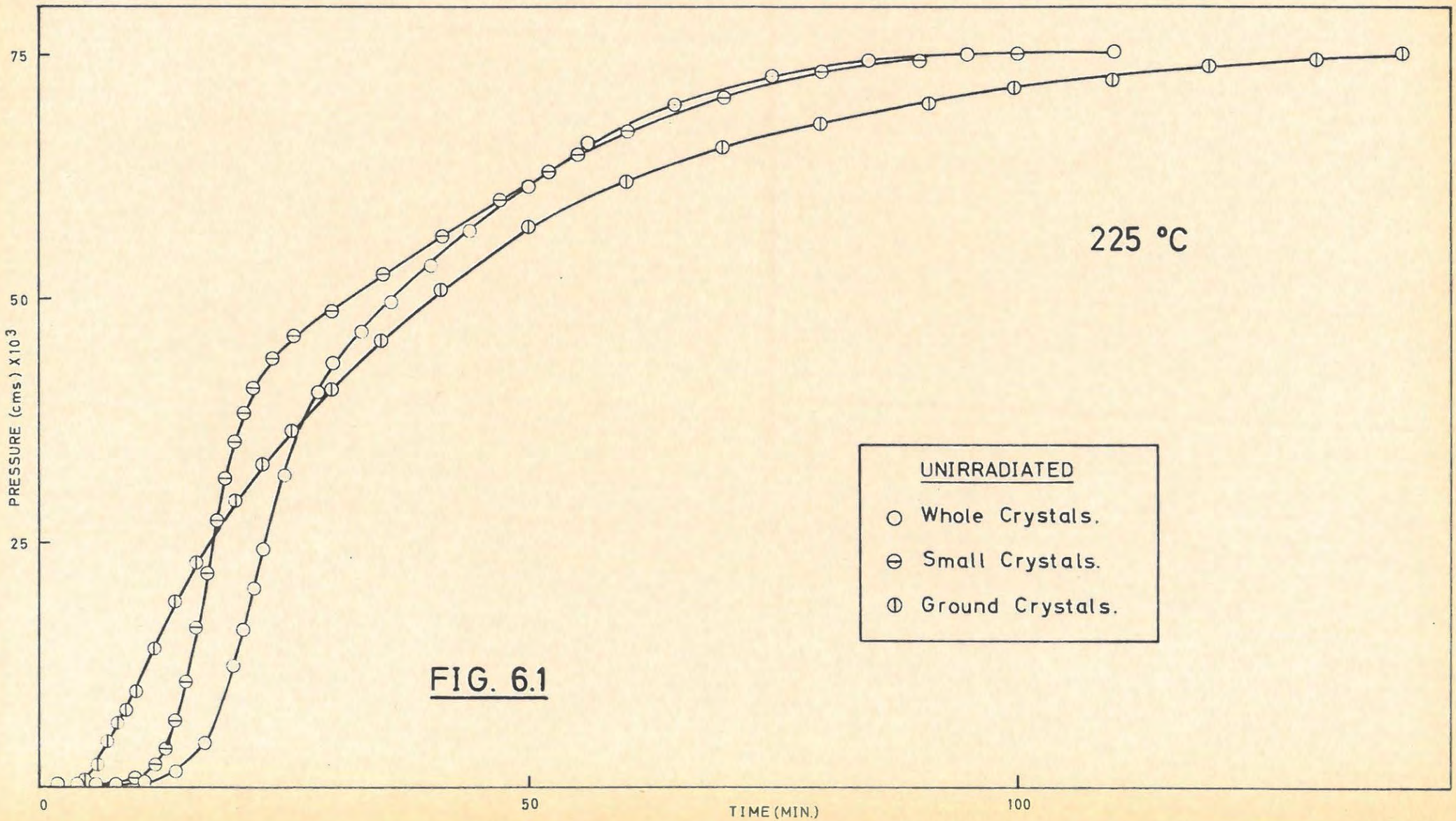
75
50
25
PRESSURE (cms) X10³
0
50
100
TIME (MIN.)
225 °C
UNIRRADIATED
Whole Crystals.
Small Crystals.
Ground Crystals.

FIG. 6.1

TABLE 6.2.

GROUND CRYSTALS		225°C			14.3 mg.
t	p	t	p	t	p
2	0.04	19	28.10	65	64.12
3	0.04	20	29.35	70	65.55
4	0.12	23	33.06	75	66.91
5	0.50	26	36.28	80	67.96
6	2.11	30	40.75	85	69.26
7	4.74	35	45.62	91	70.03
8	6.61	38	48.92	100	71.58
9	7.98	41	50.98	110	72.53
10	9.89	43	52.79	120	73.90
12	14.38	46	55.03	131	74.89
14	19.05	50	57.39	140	75.10
16	23.17	55	60.06	p_f	75.00
18	26.32	60	61.92	p_a	62.93

SMALL CRYSTALS		225°C			17.0 mg.
t	p	t	p	t	p
2	0.02	21	38.23	60	67.12
4	0.05	22	40.61	65	69.05
6	0.20	24	43.71	70	70.74
8	0.46	26	45.81	75	72.50
10	0.80	28	47.41	80	73.51
12	2.19	30	48.63	85	74.33
13	3.88	32	50.01	90	74.48
14	6.81	35	52.59	95	74.95
15	10.90	38	54.45	100	75.04
16	16.25	41	56.11	105	75.44
17	21.72	44	57.72	110	75.21
18	26.95	47	60.00		
19	31.58	50	61.60	p_f	75.00
20	35.29	55	64.85	p_a	80.54

6.3.3. The Effect of Temperature.

15 to 20 mg. samples of large whole crystals were decomposed at various temperatures in the range 195°C to 225°C, to determine the critical increment of the process(es) occurring. The results are listed in TABLE 6.3.

TABLE 6.3./..

TABLE 6.3.

WHOLE CRYSTALS		195°C			19.3 mg.
t	p	t	p	t	p
4	0.03	160	35.91	520	62.40
20	0.20	170	38.00	560	64.30
32	0.36	180	39.80	600	66.06
40	0.61	190	41.09	640	67.43
52	1.50	200	42.07	680	68.44
60	2.50	210	43.31	700	68.81
68	4.09	220	44.24	720	69.22
76	6.01	240	45.72	760	69.94
84	8.61	260	47.22	800	70.66
92	11.69	280	48.55	840	71.48
100	14.92	300	49.84	880	72.20
108	18.43	320	50.79	940	73.02
116	21.98	340	51.86	1000	73.74
124	25.21	360	52.94	1220	74.66
132	28.12	400	55.46	p_f	75.00
140	30.46	440	58.04	p_a	72.7
150	33.53	480	60.20		

		200°C			14.3 mg.
t	p	t	p	t	p
3	0.04	130	38.86	360	64.17
10	0.15	145	42.17	390	66.17
20	0.24	160	44.68	410	67.33
30	0.43	180	46.97	440	69.03
40	1.03	196	48.44	470	69.96
50	2.49	210	49.95	500	70.99
60	5.07	228	52.08	532	71.77
70	8.79	240	53.27	560	72.37
80	13.60	260	55.15	600	72.99
90	19.09	280	57.00	644	73.96
100	24.99	300	59.57	700	74.65
110	30.33	320	61.02	p_f	75.00
120	34.89	340	62.69	p_a	72.20

TABLE 6.3./...

TABLE 6.3. contd.

205°C					17.9 mg.
t	p	t	p	t	p
12	0.17	90	39.07	240	63.88
16	0.22	95	41.05	260	66.25
20	0.41	101	43.29	280	67.38
25	0.60	105	44.02	300	69.04
30	1.00	110	45.06	320	70.57
35	1.82	115	45.86	340	71.33
40	3.20	120	46.57	360	71.81
45	5.45	125	47.57	380	72.82
50	8.41	135	49.16	410	73.77
55	12.34	145	50.58		
60	16.34	155	51.97	p_f	75.00
65	20.95	170	54.11	p_a	83.0
70	25.21	180	55.93		
75	29.24	190	57.25		
80	32.87	200	59.06		
85	36.38	220	61.62		

215°C					13.1 mg.
t	p	t	p	t	p
2	0.04	42	30.05	111	64.53
5	0.08	45	34.41	116	65.63
7	0.09	47	37.41	120	66.25
9	0.13	49	39.00	125	67.63
12	0.18	51	41.40	130	68.75
15	0.30	54	43.47	135	69.01
18	0.44	57	45.08	140	69.54
20	0.87	60	46.20	145	70.52
22	1.48	65	48.00	155	70.78
24	2.46	70	50.06	175	71.67
26	3.88	75	52.25	190	73.38
28	6.08	80	54.42	205	73.82
30	8.67	85	55.74	220	74.87
32	11.87	90	57.94	240	75.53
35	17.23	95	59.98		
38	22.56	100	60.94	p_f	75.00
40	25.83	105	64.28	p_a	63.47

TABLE 6.3. contd.

TABLE 6.3. contd.

220°C					16.4 mg.
t	p	t	p	t	p
3	0.02	29	21.04	73	63.23
5	0.04	30	23.91	80	66.59
8	0.08	32	29.17	85	68.41
11	0.14	34	33.89	90	69.83
13	0.30	37	39.53	95	70.47
15	0.46	39	41.95	100	71.59
17	0.82	41	43.77	110	72.73
20	2.64	44	46.08	120	73.64
22	4.81	47	47.78	130	74.39
24	8.13	50	49.31	140	74.87
25	10.37	55	52.36		
27	15.31	60	55.59	p_f	75.00
28	18.24	65	58.75	p_a	72.90

6.3.4. Mathematical Analysis.

6.3.4.(a) Whole Crystals.

A typical p/t plot for the thermal decomposition of unirradiated whole crystals is given in FIGURE 6.2, curve A. The curve consists of an acceleratory period, followed by a transition period and a subsequent decay.

The Prout-Tompkins equation (6.2) fitted only over the first part of the acceleratory period. Beyond $\alpha = 0.3$, the equation did not hold. The acceleratory period was best analysed in terms of the power law:-

$$p^{1/n} = k_1 t + C \qquad \ldots\ldots \qquad (6.6)$$

with $n = 3$. A plot of $p^{\frac{1}{3}}$ against t and an enlarged plot of p against t for this period, are shown in FIGURE 6.2, curves C and D respectively. The range over which the power law applied was $0.01 < \alpha < 0.33$.

The decay period conformed to the contracting sphere equation:-

$$1 - (1 - p/p_f)^{\frac{1}{3}} = k_2 t \qquad \ldots\ldots \qquad (6.7)$$

The/...

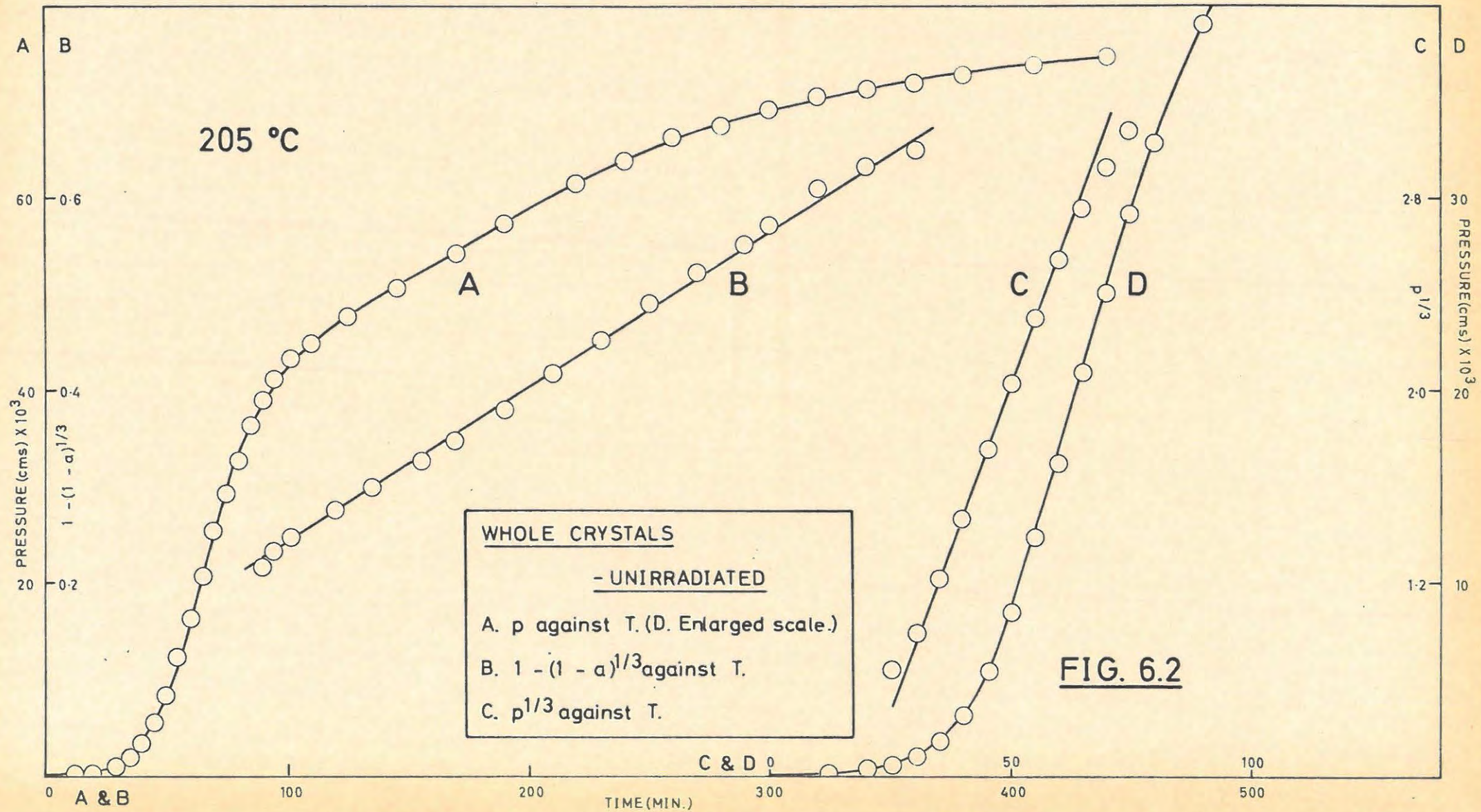
A
B
C
D
205 °C
A
B
C
D
60
40
20
0·6
0·4
0·2
2·8
2·0
1·2
30
20
10
PRESSURE (cms) X 10³
1 - (1 - a)^1/3
p^1/3
PRESSURE (cms) X 10³
WHOLE CRYSTALS
- UNIRRADIATED
A. p against T. (D. Enlarged scale.)
B. 1 - (1 - a)^1/3 against T.
C. p^1/3 against T.
0
A & B
100
200
300
C & D
0
50
100
400
500
TIME (MIN.)

FIG. 6.2

The plot is shown in FIGURE 6.2, curve B. The extent of fit was $0.55 < \alpha < 0.97$.

6.3.4.(b) Ground Crystals.

For the ground crystals, FIGURE 6.3, the acceleratory reaction was replaced by a linear reaction passing smoothly into the decay where the contracting sphere equation applied (curve B).

The values of k_1 and k_2 for the whole crystals are tabulated in TABLE 6.4. The critical increment was then determined using the equation:-

$$2.303 \log_{10} k = \frac{E}{RT} + K_1 \quad \ldots\ldots \quad (6.8)$$

where E = the activation energy (kcal/mole)

K_1 = a constant.

T = the decomposition temperature in degrees Kelvin.

and R = 1.98 calories.

The values of $\log k_1$ and $\log k_2$ for whole crystals, are plotted against $1/T^{o}K$ in FIGURE 6.4. The values of the activation energies obtained from these plots are:-

Acceleratory reaction : 31.7 kcals/mole

Decay reaction : 38.7 kcals/mole

TABLE 6.4.

UNIRRADIATED WHOLE CRYSTALS.		
Temp. ^{o}C	$k_1 \times 100$ $(cm\ Hg)^{\frac{1}{3}} min^{-1}$	$k_2 \times 1000$ min^{-1}
195	2.738	0.627
200	3.483	1.055
205	5.280	1.585
215	11.45	3.980
220	15.57	6.250
225	19.71	10.20
225	19.50	11.13
225	20.57	10.58

6.3.5./...

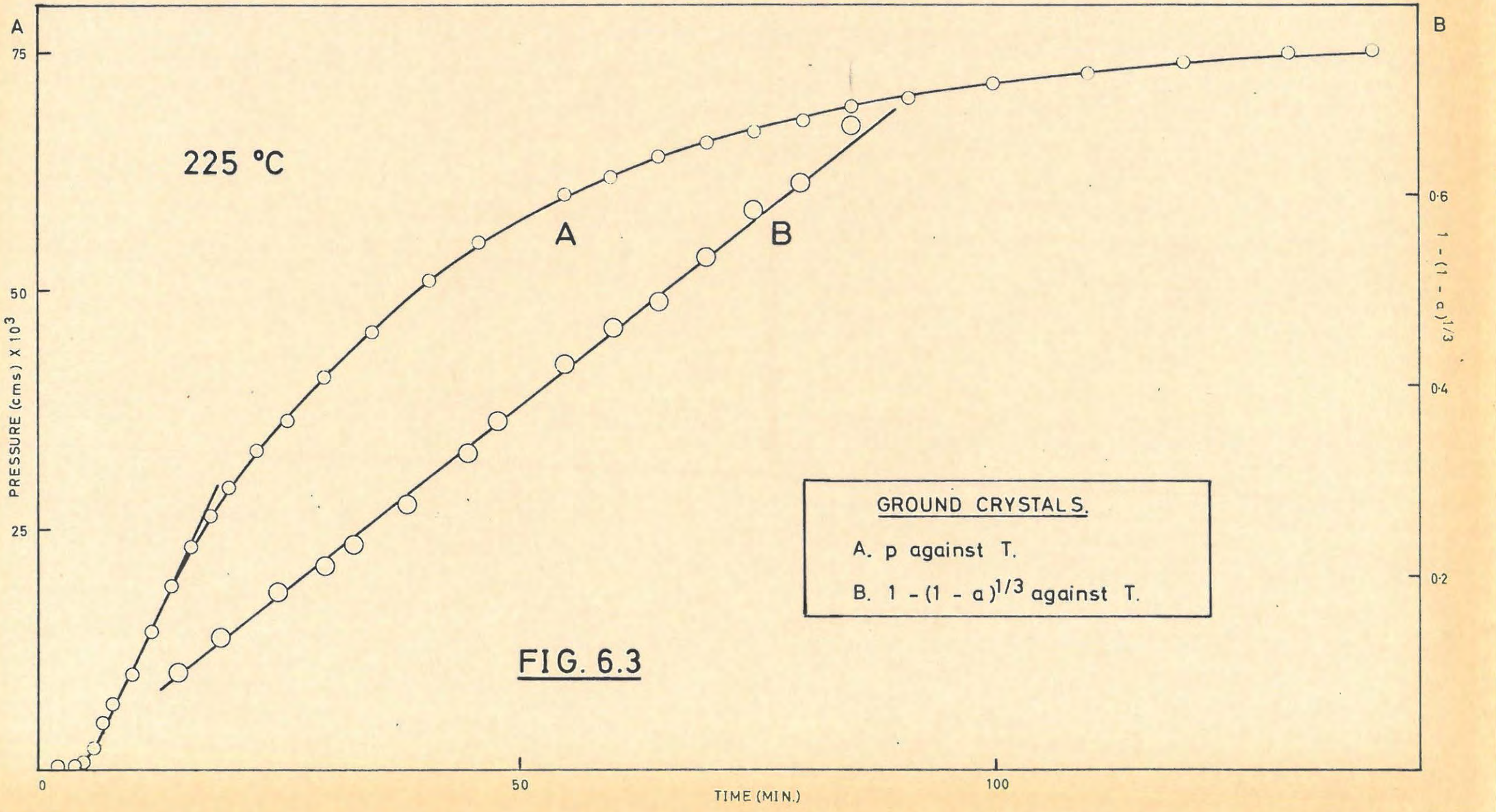
A
75
50
25
PRESSURE (cms) X 10³
225 °C
A
B
B
0·6
0·4
0·2
1 - (1 - α)^1/3
GROUND CRYSTALS.
A. p against T.
B. 1 - (1 - α)^1/3 against T.
0
50
100
TIME (MIN.)

FIG. 6.3

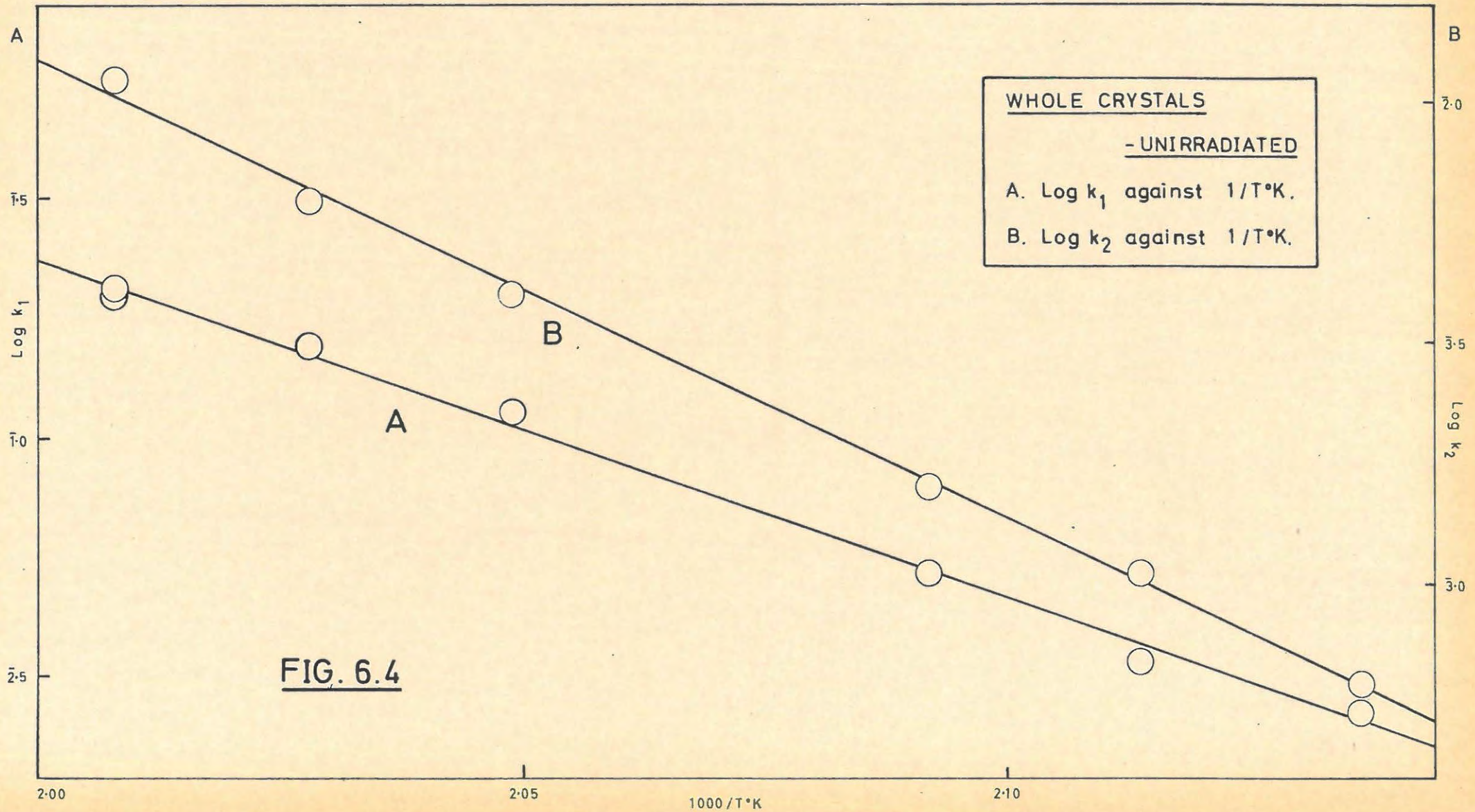
WHOLE CRYSTALS
- UNIRRADIATED
A. Log k_1 against 1/T°K.
B. Log k_2 against 1/T°K.
A
B
$\bar{1}\cdot5$
$\bar{1}\cdot0$
$\bar{2}\cdot5$
Log k_1
$\bar{2}\cdot0$
$\bar{3}\cdot5$
$\bar{3}\cdot0$
Log k_2
2·00
2·05
2·10
1000/T°K

FIG. 6.4

6.3.5. Visual observations.

On heating, the crystal changed from its original orange colour to a deep wine-red. Microscopic examination showed that over the acceleratory period the surface became covered with three-dimensional nuclei, and by the end of the acceleratory period the surface was covered with black product.

At low temperatures (205 to 220°C) the large crystals retained their shape through the decomposition, but at 225°C fracture occurred and at 245°C shattering was complete.

6.3.6. The Effect of Pre-irradiation with γ-rays.

6.3.6.1. Irradiation.

Pre-irradiation of batches of whole crystals, small crystals and ground material, was carried out at about 25°C in the spent fuel facility at Harwell (mean γ-ray energy 1.1 Mev, flux 4.0 Mrad per hour). The specimens were sealed in evacuated Pyrex ampoules that had previously been baked out. The γ-dose given was 100 Mrad. The colour of the crystals was darkened to an orange-brown after irradiation.

6.3.6.2. Irradiation Effects on Whole, Small and Ground Crystals.

The effects of pre-irradiation on the thermal decomposition of whole and small crystals at 225°C, are shown in FIGURES 6.5 and 6.6 respectively. The curve for pre-irradiated ground crystals was superimposable on that given in FIGURE 6.3 for the unirradiated ground crystals.

The results for the three runs are given in TABLE 6.5 and TABLE 6.6 (whole crystal 100 Mrad 225°C).

TABLE 6.5./...

TABLE 6.5.

GROUND CRYSTALS		225°C	100 Mrad		11.5 mg.
t	p	t	p	t	p
1	0.21	19	26.79	55	60.63
2	0.22	21	29.70	60	63.20
3	0.32	23	31.93	65	64.97
4	1.04	25	34.28	70	67.52
5	3.01	27	35.85	75	69.61
6	6.25	30	38.50	80	70.66
7	8.81	33	41.12	85	72.35
8	10.04	36	43.80	90	73.82
9	12.00	39	46.39	95	74.59
11	14.39	42	49.53	100	74.60
13	17.43	45	52.38	105	74.84
15	20.43	48	55.60	p_f	75.00
17	23.82	51	57.47	p_a	65.88

SMALL CRYSTALS		225°C	100 Mrad		14.3 mg.
t	p	t	p	t	p
4	0.05	22	26.48	54	64.85
6	0.11	23	29.88	58	66.64
8	0.38	24	33.05	62	68.04
10	0.57	26	38.50	66	69.45
11	0.71	27	40.97	70	70.63
12	0.95	28	43.04	75	71.39
13	1.44	30	45.79	80	72.41
14	2.44	32	47.65	85	73.01
15	4.00	34	49.61	90	73.78
17	8.19	37	51.76	95	74.47
18	11.28	40	54.24	100	74.90
19	14.62	43	56.63	105	75.44
20	18.76	46	59.08	p_f	75.00
21	22.66	50	62.28	p_a	75.5

6.3.6.3./...

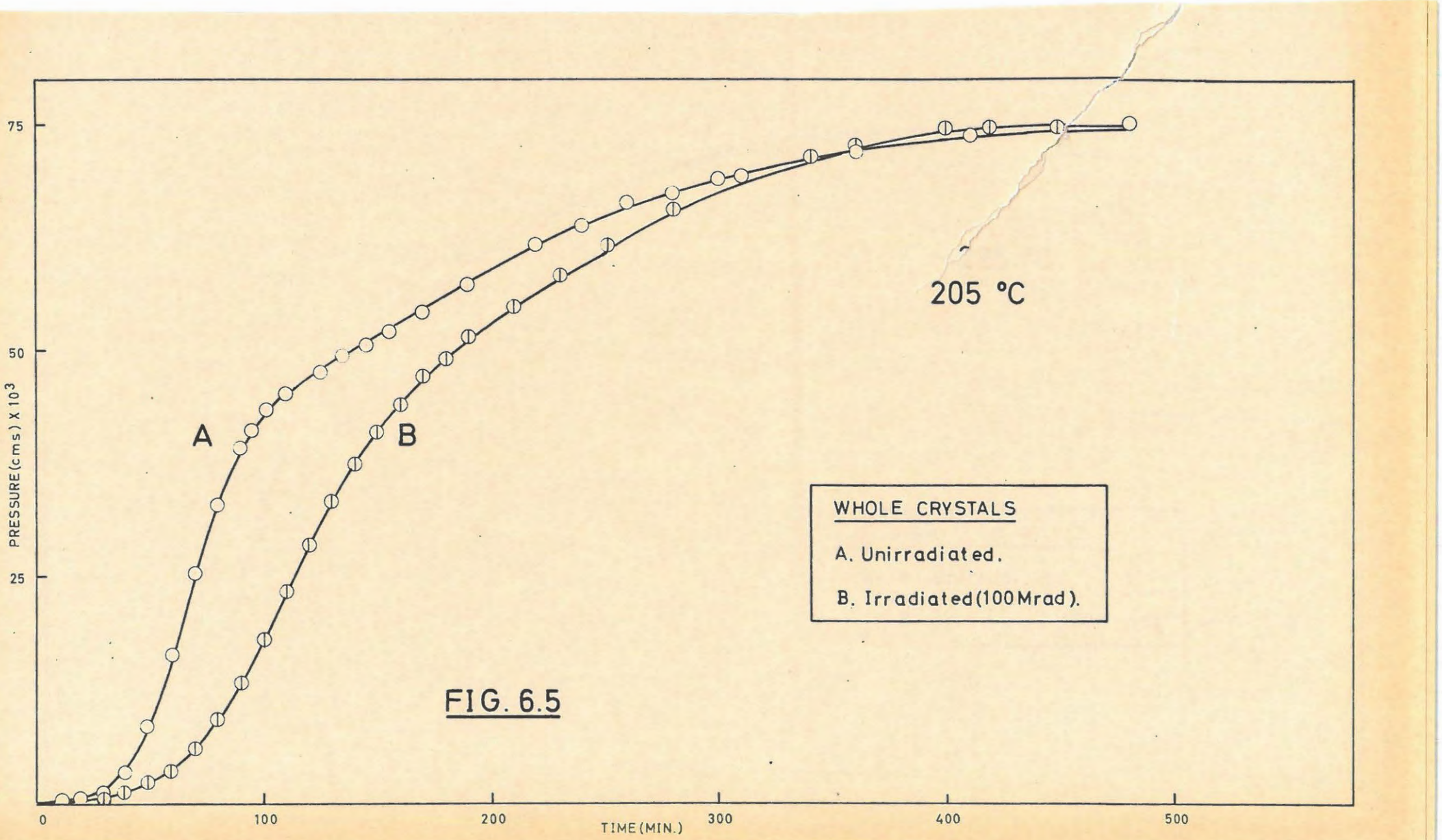
75
50
25
PRESSURE (cms) X 10³
A
B
205 °C
WHOLE CRYSTALS
A. Unirradiated.
B. Irradiated (100 Mrad).
0
100
200
300
400
500
TIME (MIN.)

FIG. 6.5

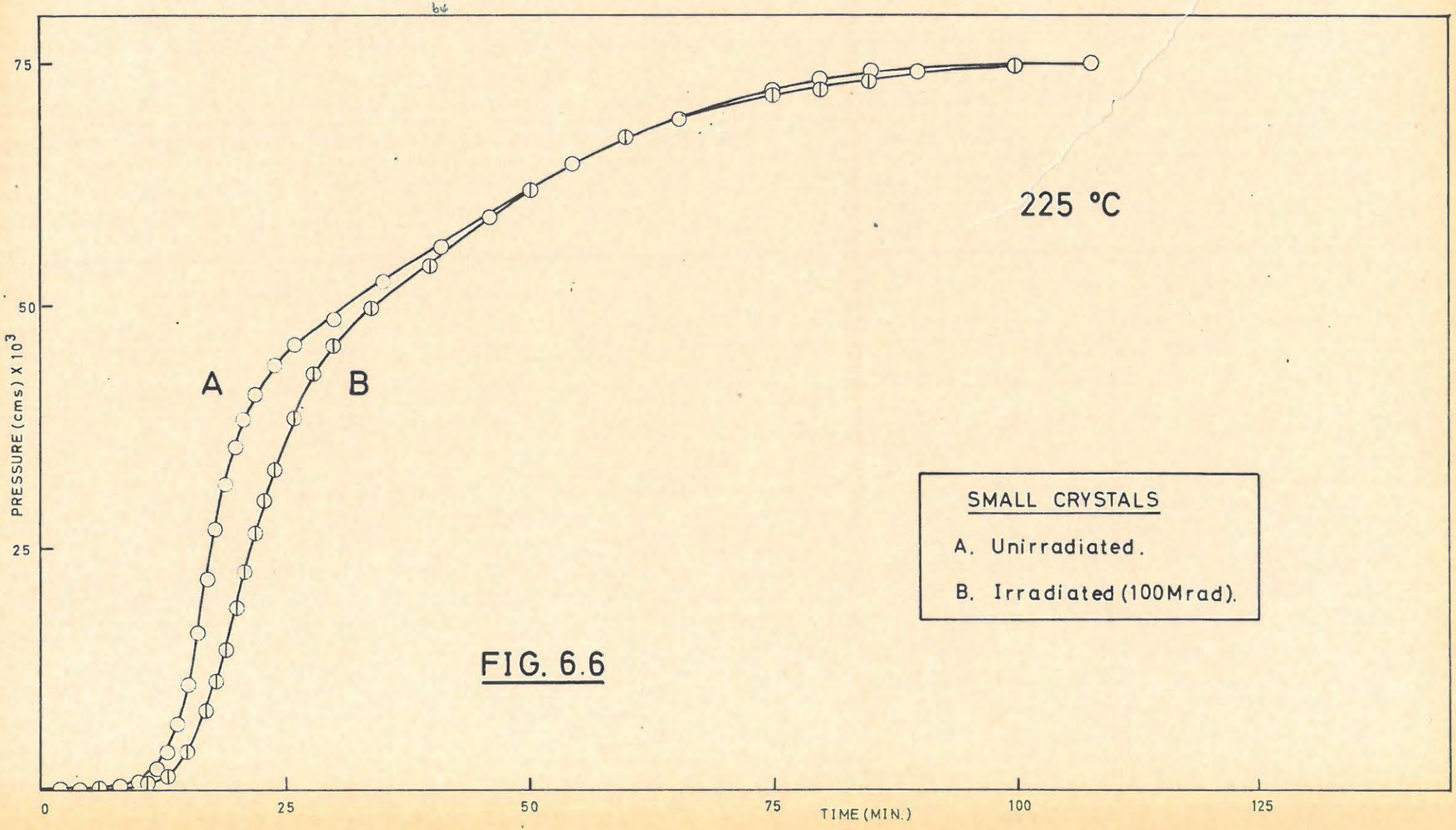
75
50
25
PRESSURE (cms) X 10^3
A
B
225 °C
SMALL CRYSTALS
A. Unirradiated.
B. Irradiated (100Mrad).
0
25
50
75
100
125
TIME (MIN.)

FIG. 6.6

6.3.6.3. The Effect of Temperature.

8 to 14 mg. samples of pre-irradiated (100 Mrad) whole crystals were decomposed at temperatures in the range 195°C to 225°C, to determine the critical increment of the process(es) occurring. The results are listed in TABLE 6.6.

TABLE 6.6.

WHOLE CRYSTALS		195°C	100 Mrad		11.7 mg.
t	p	t	p	t	p
10	0.06	210	22.71	580	62.26
20	0.12	222	25.52	600	63.27
30	0.16	240	29.81	640	65.71
40	0.22	250	31.89	680	67.74
50	0.37	262	34.21	720	68.95
60	0.54	275	36.47	760	70.47
70	0.82	292	39.80	820	72.10
80	1.26	315	42.10	880	73.21
90	1.83	335	44.61	920	73.62
100	2.59	360	47.01	980	73.82
105	2.97	380	48.43	1060	74.73
115	4.02	400	50.63	1100	75.44
120	4.63	421	51.76	1145	74.93
130	6.07	440	53.13		
140	7.52	460	54.78	p_f	75.00
160	11.10	480	56.31	p_a	73.90
170	13.21	500	57.65		
180	15.37	520	59.12		
190	17.64	540	60.50		
200	20.19	560	61.16		

		200°C	100 Mrad		11.1 mg.
t	p	t	p	t	p
2	0.04	150	30.05	370	63.49
15	0.13	160	33.42	390	64.98
30	0.27	170	36.23	420	67.59
40	0.57	180	38.73	440	68.89
50	1.11	190	41.08	460	69.85
60	2.00	200	43.08	480	70.61

TABLE 6.6 contd.

TABLE 6.6 contd.

t	p	t	p	t	p
70	3.43	210	44.65	520	71.97
80	5.39	225	47.30	540	73.04
90	7.86	240	49.51	580	73.81
100	10.99	260	52.04	620	75.09
110	14.65	280	54.22	680	75.29
120	18.28	301	56.35		
130	22.20	330	59.48	p_f	75.00
140	26.18	350	61.50	p_a	75.29

			205°C 100 Mrad		16.6 mg.
t	p	t	p	t	p
1	0.06	85	10.77	210	54.87
5	0.10	90	13.13	220	56.99
9	0.25	95	15.58	230	58.32
14	0.35	100	18.10	240	60.05
20	0.42	105	20.90	251	61.67
25	0.52	110	23.30	265	63.17
30	0.65	120	28.43	280	65.55
35	0.86	125	30.79	295	67.25
39	1.06	130	33.10	310	69.34
42	1.29	135	35.29	325	70.48
44	1.42	140	37.33	340	71.34
46	1.61	145	39.25	360	73.09
50	2.06	150	40.86	380	74.13
58	3.35	155	42.26	400	74.89
60	3.64	160	43.94	420	74.87
65	4.70	170	47.05		
70	5.98	180	48.99	p_f	75.00
75	7.37	190	51.52	p_a	85.85
80	9.05	200	53.48		

TABLE 6.6 contd.

TABLE 6.6 contd.

			215°C 100 Mrad 13.4 mg.		
t	p	t	p	t	p
2	0.04	49	18.08	125	63.29
5	0.05	52	20.96	130	64.95
10	0.12	55	23.87	135	66.46
15	0.25	58	26.52	140	67.40
18	0.39	62	29.71	150	69.64
22	1.05	66	32.59	160	71.20
24	1.44	70	35.69	170	72.61
26	1.96	75	39.13	180	73.56
28	2.66	80	42.22	190	74.21
30	3.39	85	45.58	200	75.00
32	4.43	90	48.23	210	75.37
35	6.22	95	51.22		
37	7.58	100	53.70	p_f	75.00
40	9.99	105	55.93	p_a	75.87
43	12.50	110	57.72		
45	14.30	115	59.71		
47	16.40	120	61.73		

			220°C 100 Mrad 8.1 mg.		
t	p	t	p	t	p
2	0.07	34	14.99	80	62.50
5	0.09	36	17.77	85	65.25
8	0.15	38	20.46	90	67.57
11	0.21	40	22.91	95	69.66
13	0.26	42	25.47	100	71.24
15	0.52	44	28.26	105	72.81
17	0.82	47	32.00	110	73.85
20	1.64	50	35.81	115	74.43
22	2.51	53	39.75	120	74.89
24	3.75	56	42.95	125	75.25
26	5.36	60	47.17		
28	7.32	65	51.88	p_f	75.00
30	9.69	70	55.88	p_a	75.25
32	12.29	75	59.37		

TABLE 6.6 contd.

TABLE 6.6 contd.

225°C 100 Mrad 12.4 mg.					
t	p	t	p	t	p
1	0.05	24	15.81	54	62.10
3	0.09	25	18.16	57	64.63
5	0.13	26	20.47	60	66.57
7	0.21	28	25.12	63	67.88
9	0.28	30	30.04	66	69.27
11	0.39	32	34.58	70	70.76
13	0.66	34	38.77	75	72.01
15	0.86	36	41.92	80	73.26
17	2.86	38	45.17	85	74.16
19	5.36	40	47.81	90	74.61
20	7.12	42	50.25	95	74.99
21	9.12	45	53.73		
22	11.12	48	56.69	p_f	75.00
23	13.48	51	59.16	p_a	79.50

6.3.6.4. Mathematical Analysis.

A typical p/t plot for the thermal decomposition of pre-irradiated (100 Mrad) whole large crystals is given in FIGURE 6.7, curve A.

As in the unirradiated decomposition, the acceleratory period is fitted by the power law:-

$$p^{1/n} = k_1 t + C \qquad \ldots\ldots\ldots \qquad (6.6)$$

with n = 3. This plot is also shown in FIGURE 6.7, curve C, together with an enlarged section of the acceleratory curve, curve D.

The decay period is once again fitted by the contracting sphere equation:-

$$1 - (1 - p/p_f)^{\frac{1}{3}} = k_2 t \qquad \ldots\ldots\ldots \qquad (6.7)$$

FIGURE 6.7, curve B.

The transition period is, however, less marked in the pre-irradiated decomposition, and the extent of fit of

both/...

both analyses is increased. For the acceleratory period, the power law holds for $0.013 < \alpha < 0.43$ (compared to $0.013 < \alpha < 0.33$ for the unirradiated salt), while in the decay period, the contracting sphere equation holds from $\alpha = 0.44$ onwards (compared to $\alpha = 0.55$ onwards for the unirradiated salt).

The values of k_1 and k_2 for the irradiated (100 Mrad) whole crystals are given in TABLE 6.7, and plotted against $1/T^{o}K$ in FIGURE 6.8.

The values of the activation energies obtained from these plots are, with the unirradiated values in brackets for comparison:-

Acceleratory reaction: 35.4 kcals/mole (31.7 kcals/mole)
Decay reaction : 39.8 kcals/mole (38.7 kcals/mole)

TABLE 6.7.

WHOLE CRYSTALS 100 Mrad.		
Temp. ^{o}C	$k_1 \times 10^2$ $(cm\ Hg)^{\frac{1}{3}} min^{-1}$	$k_2 \times 10^3$ min^{-1}
195	1.470	0.822
200	2.330	1.298
205	2.700	2.075
215	6.325	4.86
220	9.250	8.58
225	15.20	10.74

6.4. DISCUSSION/...

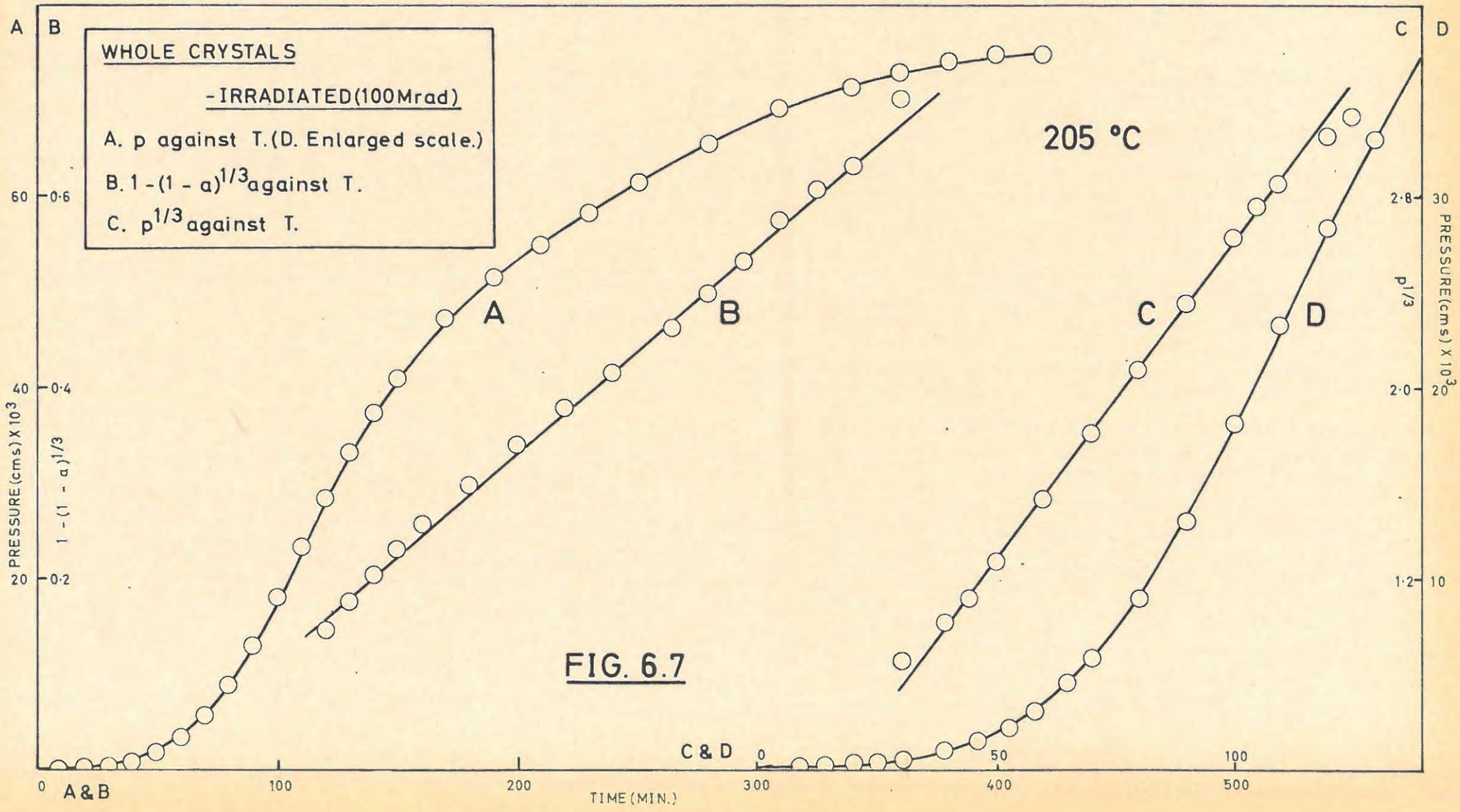
WHOLE CRYSTALS
-IRRADIATED(100Mrad)
A. p against T.(D. Enlarged scale.)
B. 1 - (1 - a)^1/3 against T.
C. p^1/3 against T.
205 °C
A
B
C
D
A&B
C&D
PRESSURE(cms) X 10^3
1 - (1 - a)^1/3
p^1/3
TIME(MIN.)
0
100
200
300
400
500
50
60
40
20
0·6
0·4
0·2
2·8
2·0
1·2
30
20
10

FIG. 6.7

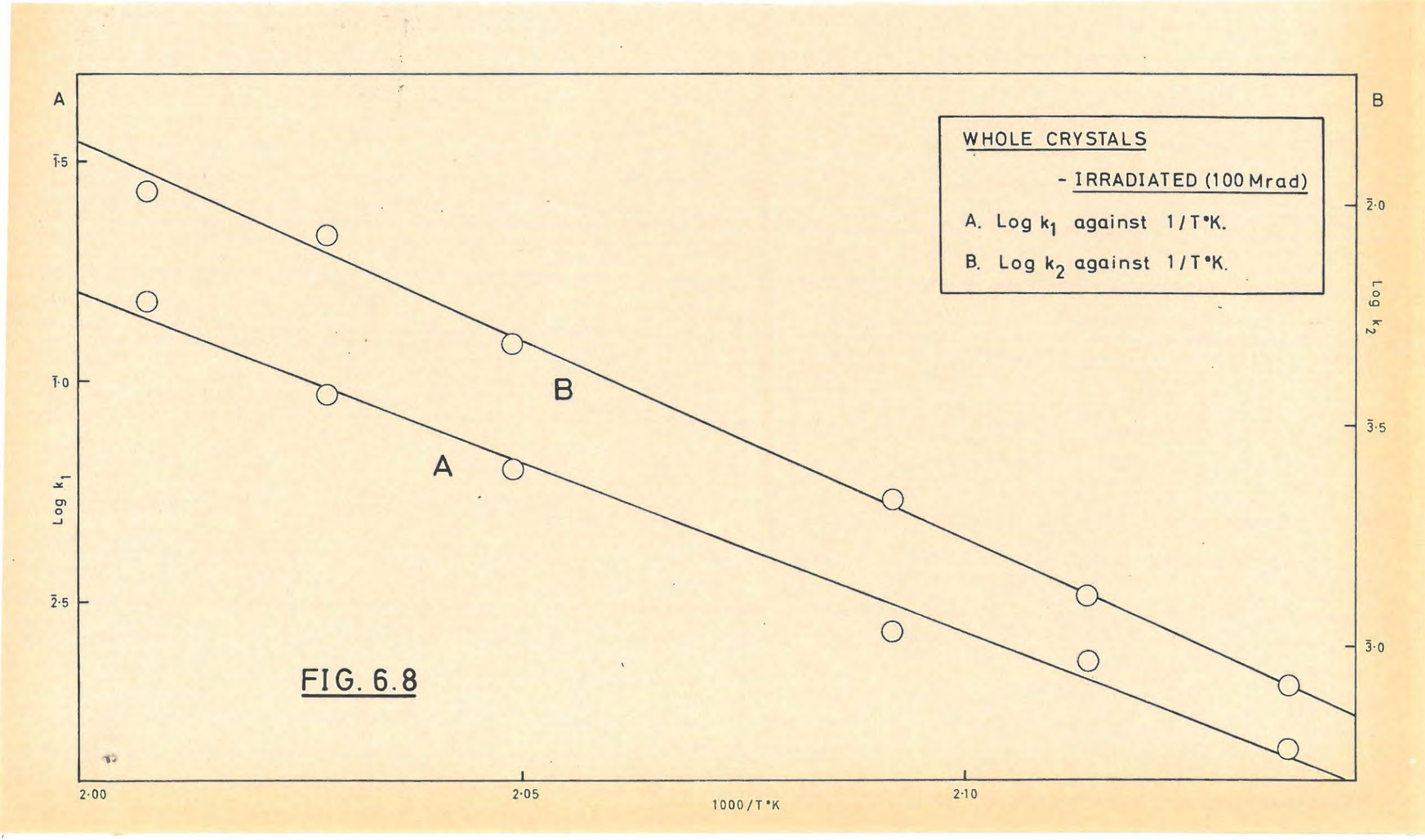
WHOLE CRYSTALS
- IRRADIATED (100 Mrad)
A. Log k_1 against 1/T°K.
B. Log k_2 against 1/T°K.
A
B
$\bar{1}\cdot5$
$\bar{1}\cdot0$
$\bar{2}\cdot5$
$\bar{2}\cdot0$
$\bar{3}\cdot5$
$\bar{3}\cdot0$
Log k_1
Log k_2
2·00
2·05
2·10
1000/T°K

FIG. 6.8

6.4. DISCUSSION.

6.4.1. Unirradiated Whole and Ground Crystals.

The obvious feature of the p/t plots for the decomposition of unirradiated large crystals is the change from a rapid acceleration of the reaction to a fast decay reaction, which then changes into a slower decay reaction. With small crystals the difference between the times taken for acceleration and the final decay is even more marked. With ground crystals the acceleratory reaction is replaced by a linear one passing smoothly into a decay stage. The fast decay reaction in whole crystals, where neither of the mathematical expressions fit, is eliminated with ground crystals.

Simpson and Taylor [350] did not follow the reaction to completion and mistook the decay region for a period during which reaction occurred at an interface of constant area. The rate of evolution of gas was thus taken to be constant; this, it has been shown, is not correct.

The crystals that were used were grown slowly from an initially dilute solution in pure, dust-free water. Consequently they were well formed with smooth faces. It is assumed that on heating, vacancies of opposite effective charge migrate to the surface and aggregate at the relatively few surface imperfections. Aggregation results in a changed topography at which initial decomposition is favoured, and thus nuclei for further reaction are formed. Nuclei grow at the reaction interface because of the strain exerted on the reactant material, adjacent to the recrystallising product phase. The surface nuclei (constant in number) grow three-dimensionally over the acceleratory period. The decay period occurs when the surface nuclei touch. At this point, bearing in mind that the nuclei have

been/...

been growing inward as well as along the surface, there will be a marked reduction in the area of the reactant/product interface, and thus a distinct change in the rate of gas evolution at the now diminishing interface.

With small crystals, the crystals are less perfect and the number of vacancies present will be higher and consequently the rate faster than with large crystals. In addition to more nuclei, the total surface area will be larger. Because of this high rate the change to the decay reaction will be more abrupt. The period of reaction when neither of the equations fits the p/t plots, is a decay reaction which is faster than the normal decay, and represents the time when some nuclei have touched and the decay is commencing but the acceleratory period is not completely over.

When the crystals are ground to a fine powder, a very large number of vacancies is created and thus, when reaction begins, the whole surface of a crystal becomes a type of "diffuse" nucleus, in that reaction takes place all over the surface in a thin layer of surface material, and no nucleus of any definite geometric form appears. Reaction in the ground particle could be analysed as a rapid one along an emergent grain boundary, which then sweeps forward to meet up with other reaction interfaces of the same type i.e. one-dimensional nuclei. This would give an approximately linear rise in pressure. Thereafter the reaction is of the contracting envelope type. The lower rate of gas evolution over the first period makes the change to the decay reaction less abrupt. In addition the intermediate stage found with whole crystals will vanish and a clear cut transition from initial reaction to decay reaction will occur.

The/...

The observations of ageing, made by Simpson and Taylor, support a mechanism of nucleation through vacancy aggregation, in that this process would occur over a long period. The change from the Prout-Tompkins equation "fitting" the acceleratory region to the power law expression (n = 3) applying with ageing, is in accord with the results reported here, although it is assumed here that the ageing process occurs very rapidly when the crystal is suddenly raised to the decomposition temperature.

The analysis applied by Simpson and Taylor may be criticised with respect to two points. From the p/t plots for $N_2 + N_2O$ evolution, no induction period is apparent, so that their report of this would appear to be erroneous. The Prout-Tompkins equation has been completely misapplied. This equation, from a consideration of the theoretical derivation, is applicable only to decompositions where the sigmoid p/t plot has an inflexion point at $\alpha = 0.50$. The section of the p/t plot to which this was applied by Simpson and Taylor does not fulfil this requirement and includes a small portion of the fast decay region. The value of p_f chosen is obviously incorrect.

6.4.2. Pre-irradiated crystals.

Rather surprisingly the rate constant in the acceleratory period for the decomposition of large crystals is reduced on pre-irradiation with γ-rays. The change from acceleratory period to the decay period is less marked although there is still a portion of the p/t plot which is not described by either the power law or the contracting envelope formula. Pre-irradiation has no real effect on the subsequent thermal decomposition of ground crystals.

The crystals are coloured brown after irradiation which is indicative of F-centre formation. These F-centres

would/...

would be formed by the capture of electrons by anion vacancies. Thus the number of vacancies of this type will be reduced. Consequently, on heating the crystal, there will be a decrease in the number of vacancies of opposite charge that will aggregate. The number of nuclei will be reduced and consequently the rate of gas evolution. Thus the change from the acceleratory period to the decay will be less abrupt and a "smoother" p/t plot will be obtained.

It is reasonable to assume that aggregation of vacancies and the allied crystal topography changes will occur during grinding and thus γ-rays will have little effect on the thermal decomposition of ground material.

The increase in the activation energy in the decay period is probably due to the difficulty of escape of evolved gases through the product matrix.

7. THE THERMAL DECOMPOSITION OF CALCIUM AZIDE.

7.1. PREVIOUS WORK.

The investigations of Andreev [355] and Marke [356] of the iso-thermal decomposition of calcium azide showed that the decomposition comprised a marked induction period followed by a period of acceleration where the exponential relationship:

$$\log p = k_1 t + c_1 \quad \ldots\ldots \quad (7.1)$$

fitted to a limited extent. The decay period of the decomposition was considered to follow the unimolecular decay law:

$$\log (p_f - p) = k_2 t + c_2 \quad \ldots\ldots \quad (7.2)$$

where p_f is the final pressure.

The degree of reproducibility of the pressure-time plots for the whole and ground crystals was poor. Marke found no pronounced change in k_1 on grinding the crystals and determined approximate activation energies of 18 kcal/mole and 19 kcal/mole for the acceleratory and decay periods, respectively. Andreev's value for the activation energy of the acceleratory reaction varied from 20.8 kcal/mole (81 - 61°C) to 27 kcal/mole (106 - 93°C), using a split-run technique.

In contradiction, Garner and Reeves [357] concluded that the acceleratory period followed the power law:-

$$p^{\frac{1}{3}} = k_3 t + c_3 \quad \ldots\ldots \quad (7.3)$$

Reproducibility of results again was not good. A four-fold increase in k_3 was found on grinding the crystals, and exposure to ultra-violet light in air accelerated the reaction and shortened the induction period. The third-power law still fitted the pressure-time plots for the irradiated material. The average activation energy for the decomposition of the unirradiated salt during the

acceleratory/...

acceleratory period was 18.5 kcal/mole. and for the decay reaction, 17.8 kcal/mole.

Tompkins and Young [358] studied the changes in conductivity that take place on heating a pellet of calcium azide. The conductance was ascribed wholly to the motion of vacancies as no photoconductance was displayed on irradiation. A fairly abrupt irreversible decrease in conductivity at 97°C was considered to result from the formation of neutral vacancy pairs.

Anomalous rates of decomposition were found for fresh material below 97°C, with an apparent activation energy of 35 kcal/mole compared to 18 kcal/mole above 97°C. Aged or well-annealed material did not show this effect. The third-power law applied to the acceleratory reaction.

7.2. EXPERIMENTAL.

7.2.1. Preparation.

(a) Hydrazoic acid: prepared as in "Inorganic Syntheses"[359].

(b) Calcium oxide : prepared from Merck A.R. calcium carbonate, heated in a platinum dish at 1200°C in a muffle for 12 hrs., stored over P_2O_5 while cooling and used immediately[360].

(c) Calcium azide : An aqueous suspension of calcium oxide (3.2 gms/100 ml) was titrated at 50°C with the ca 3% aqueous solution of hydrazoic acid, using phenolphthalein as an external indicator. At the end-point the suspension was dissolved. A slight excess (5 ml) of acid was added and the solution was evaporated in a vacuum oven at 50°C with a slow air bleed. The final stages to dryness were carried out at 25°C, using a liquid-air trap in the pumping system. The solution was kept acid at all stages.

The/...

The product was dried under vacuum over P_2O_5 and then ground for 15 mins in a Wig-L-Bug, using nylon ampoules and nylon grinding balls.

Storage was under vacuum over P_2O_5 in a blackened desiccator.

7.2.2. Apparatus.

This was as described in Section 4. No marked differences were noted if the Pt decomposition bucket was replaced by a Pyrex one.

Normalisation for comparative purposes was to a final pressure of 80×10^{-3} cms Hg.

7.3. RESULTS.

7.3.1. Reproducibility.

Three consecutive runs were carried out on the unirradiated salt, at 120°C. The results are given in TABLE 7.1. The reproducibility was satisfactory.

For the acceleratory period, the rate constants, k_1, from the equation:

$$p^{\frac{1}{3}} = k_1 t + C_1 \qquad \ldots\ldots \qquad (7.4)$$

were 0.0790, 0.0713, 0.0766 cm $Hg^{\frac{1}{3}}$ per min., while for the decay period, k_2, from:

$$1 - (1 - p/p_f)^{\frac{1}{3}} = k_2 t \qquad \ldots\ldots \qquad (7.5)$$

gave values of 0.0121, 0.0101, 0.0114 per min., respectively.

TABLE 7.1.

UNIRRADIATED		120°C Run 1			3.4 mg.
t	p	t	p	t	p
6	0.03	80	15.47	120	68.95
12	0.08	83	19.92	125	71.77
20	0.14	86	24.86	131	74.34
31	0.20	89	30.04	137	76.02
40	0.28	92	35.24	143	77.03

TABLE 7.1 contd.

TABLE 7.1 contd.

t	p	t	p	t	p
50	0.55	96	42.35	150	78.28
61	1.84	99	47.13	160	79.30
65	2.96	102	51.55	170	79.77
68	4.27	105	55.49	180	80.02
71	6.07	108	58.98		
74	8.47	112	63.06	p_f	80.00
77	11.55	116	66.48	p_a	95.02

			120°C Run 2		3.6 mg.
t	p	t	p	t	p
10	0.07	76	6.25	118	70.27
21	0.16	82	12.55	125	74.02
30	0.22	86	18.69	132	76.64
40	0.29	90	26.46	142	78.36
51	0.47	95	36.94	152	79.03
57	0.73	101	47.52	162	80.00
62	1.20	104	54.25		
66	1.85	108	59.92	p_f	80.00
72	3.81	112	64.80	p_a	107.0

			120°C Run 3		3.3 mg.
t	p	t	p	t	p
5	0.03	70	4.07	120	67.50
10	0.06	75	7.30	125	70.30
15	0.10	80	12.62	135	73.62
20	0.15	85	19.71	145	76.14
30	0.21	90	29.03	155	77.98
40	0.30	95	37.46	170	78.80
50	0.49	100	45.23	180	79.45
55	0.64	104	51.97	190	80.02
60	1.01	109	58.02	p_f	80.00
65	1.98	115	63.97	p_a	92.07

7.3.2./...

7.3.2. The Effect of Ageing.

Two runs were carried out at 130°C on the unirradiated salt. The first run was done on the freshly prepared salt and the second after an interval of 4 months, during which the salt had been stored in the dark, under vacuum over P_2O_5 drying agent. The results are given in TABLE 7.2.

No change with ageing was found, within the limits of reproducibility of a high-temperature run.

TABLE 7.2

FRESH		130°C			4.6 mg.
t	p	t	p	t	p
10	0.22	46	18.19	62	71.13
20	0.38	48	25.34	64	74.06
30	0.80	50	33.16	66	75.64
35	1.61	52	41.34	70	78.31
38	2.83	54	49.39	75	79.53
40	4.36	56	56.66	80	80.01
42	6.99	58	62.84	p_f	80.00
44	11.48	60	67.64	p_a	128.02

AGED (4 months)		130°C			2.4 mg.
t	p	t	p	t	p
12	0.55	41	11.05	55	69.81
24	0.99	43	19.60	60	76.42
32	2.25	45	40.68	65	79.58
35	3.51	47	51.42	70	79.87
37	5.03	49	57.59	p_f	80.00
39	7.35	52	65.18	p_a	62.89

7.3.3./...

7.3.3. The Effect of Temperature.

Samples of the unirradiated salt were decomposed at various temperatures in the range 105°C to 130°C, to determine the critical increment of the process(es) occurring. The results are listed in TABLE 7.3.

TABLE 7.3

UNIRRADIATED		105°C			3.4 mg.
t	p	t	p	t	p
20	0.02	216	5.52	340	66.58
60	0.07	228	8.38	354	71.81
80	0.08	240	12.30	370	75.15
100	0.15	254	18.45	384	76.53
120	0.23	264	23.59	400	78.95
140	0.37	274	29.65	421	79.26
160	0.70	286	37.27	440	79.50
180	1.44	298	44.63		
194	2.43	310	51.89	p_f	80.00
206	3.85	326	61.06	p_a	94.3

		110°C			2.9 mg.
t	p	t	p	t	p
15	0.03	145	5.29	238	64.54
30	0.09	150	6.66	248	69.62
40	0.14	156	8.76	262	74.98
50	0.18	163	11.79	284	78.54
60	0.22	168	14.27	303	79.75
71	0.27	174	17.86	310	80.54
80	0.33	180	22.04	320	80.01
91	0.47	186	26.55	330	80.01
100	0.63	192	30.87	340	79.93
110	0.99	200	37.54	350	80.01
121	1.67	208	43.89		
130	2.53	218	52.00	p_f	80.00
137	3.52	226	57.39	p_a	76.6

TABLE 7.3 contd.

TABLE 7.3 contd.

115°C					3.6 mg.
t	p	t	p	t	p
25	0.10	116	10.94	168	65.78
31	0.14	121	14.98	174	69.43
65	0.39	126	19.91	180	72.58
71	0.50	130	24.55	186	74.53
78	0.72	134	29.24	194	77.02
84	1.09	139	35.57	202	78.17
90	1.65	143	40.62	210	79.41
97	2.71	147	45.36	221	79.96
102	3.96	152	51.29	230	79.96
107	5.71	157	56.20	p_f	80.00
112	8.28	162	61.27	p_a	98.1

125°C					3.7 mg.
t	p	t	p	t	p
10	0.01	63	22.77	87	71.69
20	0.03	65	28.32	91	74.53
30	0.08	67	34.32	95	76.42
40	0.28	69	40.23	100	78.11
44	0.56	71	45.48	105	79.04
48	1.19	73	50.50	110	79.50
52	2.62	75	55.06	115	79.82
55	4.68	77	59.21	120	79.89
57	7.15	79	62.61		
59	10.87	81	65.41	p_f	80.00
61	16.99	84	68.98	p_a	97.57

130°C					3.1 mg.
t	p	t	p	t	p
7	0.25	43	3.86	61	77.14
12	0.40	46	9.97	64	78.63
17	0.53	48	41.54	67	79.47
23	0.72	50	55.09	70	79.71
28	0.93	52	64.63	75	79.88
33	1.23	54	69.30		
37	1.63	56	72.53	p_f	80.00
40	2.33	58	74.78	p_a	84.87

7.3.4./...

7.3.4. Mathematical Analysis.

A typical p/t plot for the thermal decomposition of the unirradiated salt is shown in FIGURE 7.1, curve B. The curve consists of an "induction period" (IP), followed by an acceleratory period and subsequent decay period, with the point of inflexion at $\alpha \approx 0.5$. An enlarged plot of the unirradiated "induction period" shows that this is in fact a slow reaction and not a true induction period with no evolution of gas. (FIGURE 7.1, curve D). The end of the "induction period" was arbitrarily taken as the point at which p = 1.0 (cm x 10^3).

The power law:

$$p^{1/n} = k_1 t + C_1 \qquad \ldots\ldots \qquad (7.6)$$

was applied to the acceleratory period, with n = 3. The extent of fit was improved by plotting $(p - p_o)^{\frac{1}{3}}$ against t, where p_o = 1.0, is the pressure at the end of the IP. The power law then held over the range $0.015 < \alpha < 0.5$. This plot is shown in FIGURE 7.1, curve A.

The Avrami-Erofeyev equation:

$$\left[- \log (1 - \alpha)\right]^{1/n} = k't + C' \ldots. \qquad (7.7)$$

with n = 3, also applied over the acceleratory period ($0.05 < \alpha < 0.55$), while the equation:-

$$\log (p - p_o) = k''t + \text{const.} \ldots\ldots \qquad (7.8)$$

gave a fair fit for the early stages of the acceleratory period up to about α = 0.3.

The decay period conformed to the contracting sphere equation:-

$$1 - (1 - p/p_f)^{\frac{1}{3}} = k_2 t \qquad \ldots\ldots \qquad (7.5)$$

This plot is shown in FIGURE 7.1, curve C. The extent of fit was $0.5 < \alpha < 0.98$.

The values of k_1 and k_2, as well as the lengths of the "induction periods" (IP), at various temperatures, are

tabulated/...

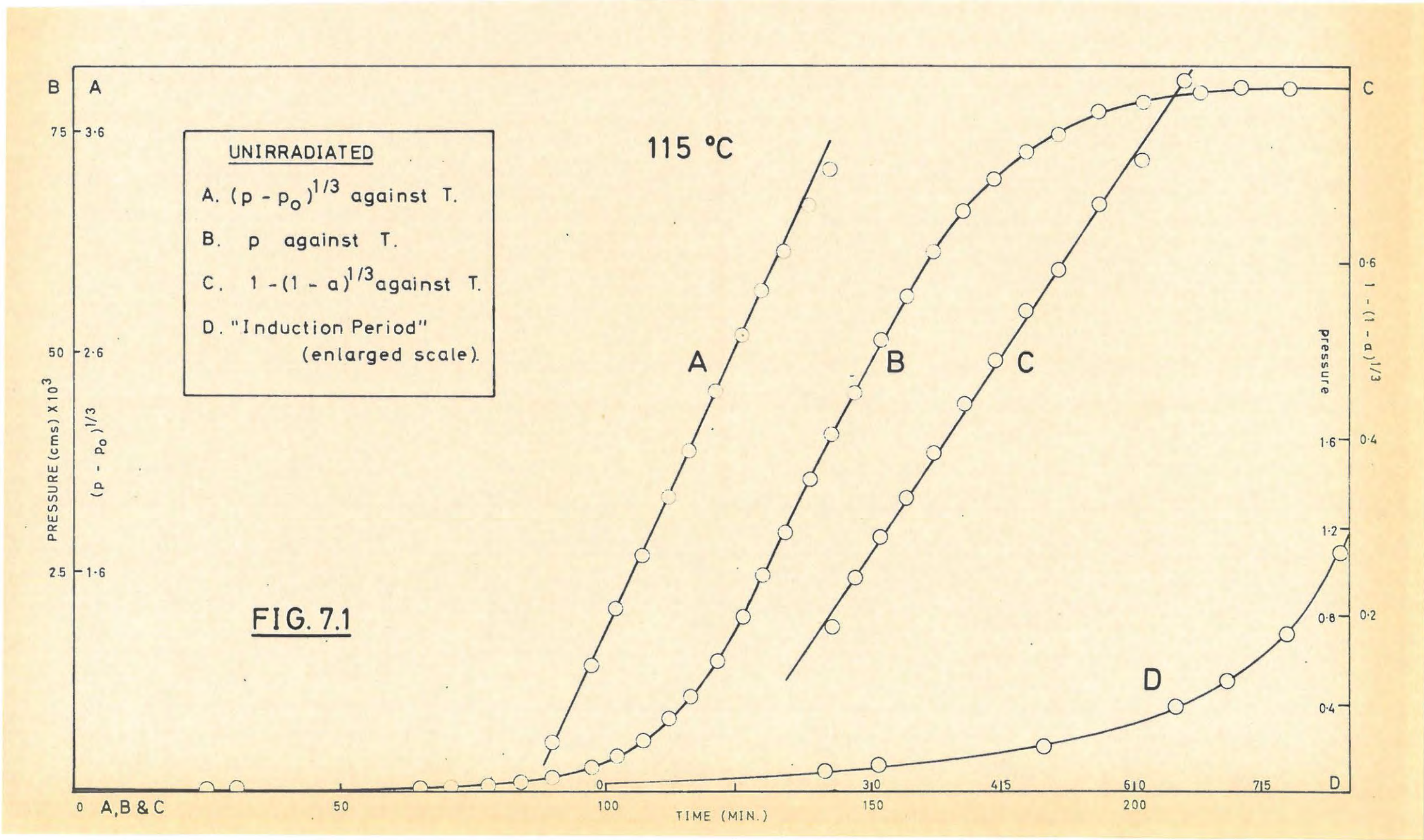
UNIRRADIATED
A. $(p - p_o)^{1/3}$ against T.
B. p against T.
C. $1 - (1 - a)^{1/3}$ against T.
D. "Induction Period" (enlarged scale).
115 °C
A
B
C
D
B
A
C
D
75
50
2.5
3·6
2·6
1·6
PRESSURE (cms) X 10^3
$(p - p_o)^{1/3}$
pressure
$1 - (1 - a)^{1/3}$
1·6
1·2
0·8
0·4
0·6
0·4
0·2
0
50
100
150
200
310
415
610
715
A,B & C
TIME (MIN.)

FIG. 7.1

tabulated in TABLE 7.4.

The values of log IP, log k_1 and log k_2 are plotted against $1/T^{o}K$ in FIGURE 7.2. The values of the activation energies obtained from these plots are:-

Induction period : 18.2 kcal/mole.

Acceleratory reaction: 27.1 kcal/mole.

Decay reaction : 18.8 kcal/mole.

The value of 27 kcal/mole for the acceleratory reaction was confirmed by plotting the rate constants obtained from equations (7.7) and (7.8) against $1/T^{o}K$ and calculating the activation energies. A second preparation (also ground) gave activation energies, using the same analyses as above, of:-

Induction period : 18.0 kcal/mole.

Acceleratory reaction: 26.9 kcal/mole.

Decay reaction : 21.4 kcal/mole.

TABLE 7.4

UNIRRADIATED CaN_6			
Temp. ^{o}C	IP (Induction Period) (mins)	Acceleratory $k_{1\frac{1}{3}} \times 100$ (cm $Hg^{\frac{1}{3}}$ per min)	Decay $k_2 \times 1000$ (per min)
105	160	2.170	5.02
110	105	2.788	6.60
115	78	4.540	8.929
120	57	7.900	12.14
		7.133	10.10
		7.661	11.41
125	44	12.90	17.88
130	37	18.47	26.96

7.3.5./...

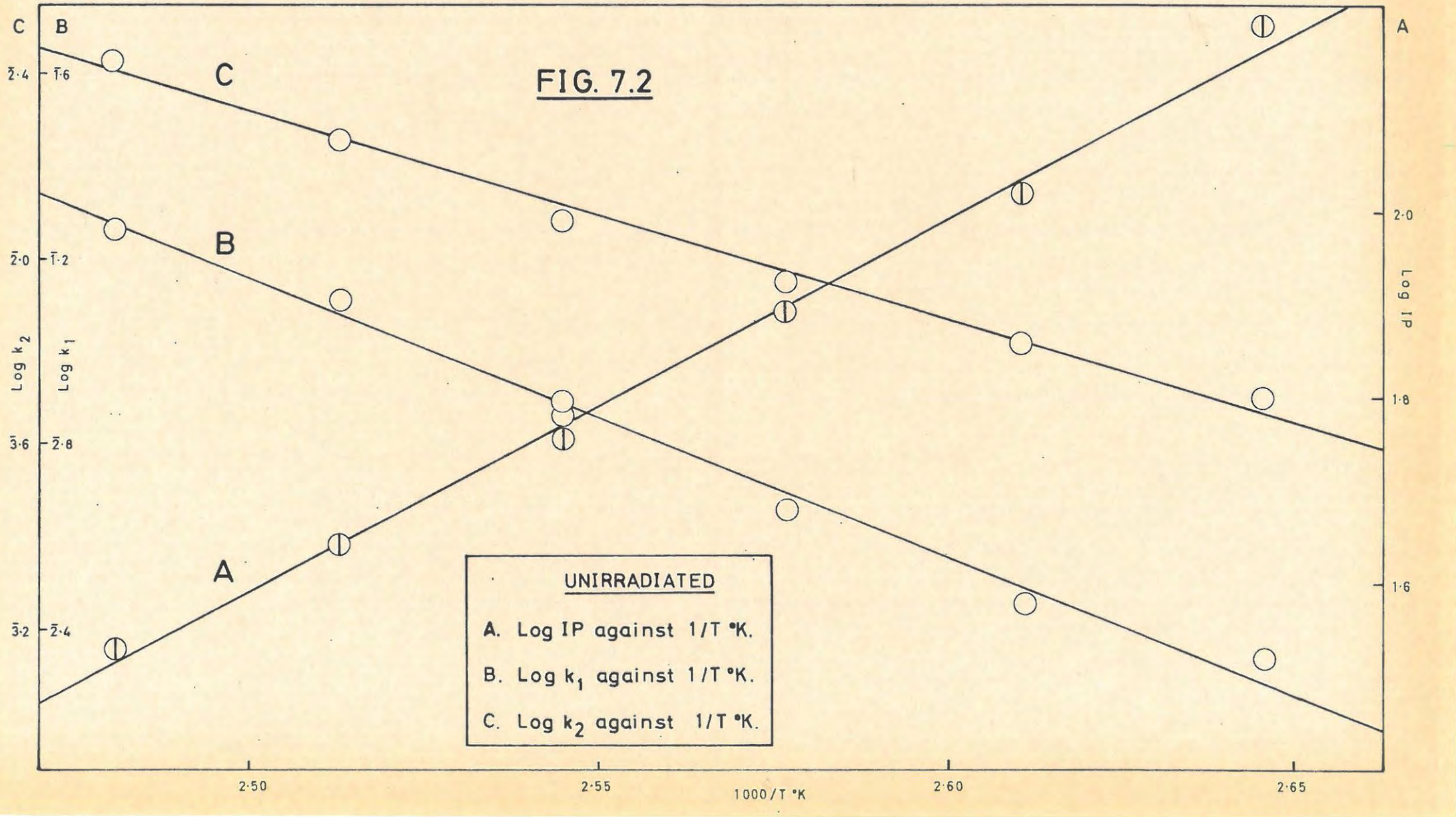
FIG. 7.2
C
B
A
C
B
A
$\bar{2}\cdot4$
$\bar{1}\cdot6$
$\bar{2}\cdot0$
$\bar{1}\cdot2$
$\bar{3}\cdot6$
$\bar{2}\cdot8$
$\bar{3}\cdot2$
$\bar{2}\cdot4$
Log k_2
Log k_1
2·0
1·8
1·6
Log IP
UNIRRADIATED
A. Log IP against 1/T °K.
B. Log k_1 against 1/T °K.
C. Log k_2 against 1/T °K.
2·50
2·55
2·60
2·65
1000/T °K

7.3.5. The Effect of Interrupting a Decomposition.

a) Raising the sample into the evolved gas.

A decomposition at 120°C was interrupted at various stages by raising the sample into evolved gas, allowing it to cool for 15 mins. and replacing it at the same temperature (See TABLE 7.5). Interruptions were at the stages marked. Except for very short heating lags (2-3 mins), the run continued normally.

b) Raising into vacuum.

A second run where the sample was raised into vacuum instead of the evolved gas is tabulated in TABLE 7.6. The lag is similar to that above (a) (3-4 mins) and the run continued normally.

TABLE 7.5

PRODUCT GAS		120°C			2.6 mg.
t	p	t	p	t	p
10	0.01	83	4.10	122	66.55
21	0.05	86	5.70	125	69.95
30*	0.08	90	8.95	129	74.04
43	0.21	95	16.04	132	76.22
51	0.32	100	28.60	135*	77.71
57	0.49	103	37.28	135	77.45
60	0.63	106*	44.82	138	77.27
63	0.82	106	44.14	143	78.79
66	1.12	109	47.56	148	80.31
69	1.54	111	51.73	153	80.04
70*	1.75	113	55.48	160	79.76
70	1.99	115	58.68		
73	1.95	116*	59.36	p_f	80.00
76	2.09	116	58.83	p_a	73.38
80	2.93	119	62.26		

* Interruption.

TABLE 7.6/...

TABLE 7.6

VACUUM		120°C			3.7 mg.
t	p	t	p	t	p
8	0.01	98	15.73	146	73.57
40	0.13	101	16.59	149	73.63
50	0.32	104	19.74	152	74.02
55	0.50	107	26.59	155	75.25
60*	0.81	113	40.86	160	77.43
66	0.92	118*	50.59	163	78.14
71	1.26	121	50.81	166	78.74
74	1.69	124	51.83	171	79.34
77	2.30	127	55.94	176	79.74
80	3.16	130	61.19	184	80.02
84	4.88	133	64.21		
88	7.61	136	68.14	p_f	80.00
91	10.54	139	70.73	p_a	106.55
95*	15.53	143*	73.60		

*Interruption.

7.3.6. The Effect of Interruption and Admission of Water Vapour.

(a) At the end of the Induction Period.

A decomposition at 120°C was interrupted at the end of the induction period (p = 1.0, t = 45 mins), by raising the sample into vacuum. After cooling for 15 mins, water vapour, from water that had been frozen under vacuum in the liquid-air trap, was admitted to the sample. After 10 mins contact, the trap was once more surrounded by liquid-air and after a further 10 mins the sample was lowered back into the decomposition vessel.

The reaction did not continue unaffected. A second "induction period" followed (35 mins), at the end of which the procedure above was repeated. Again an induction period (40 mins) followed. A further interruption and admission of water vapour at this point was followed by an induction period (40 mins) and the reaction was then allowed to go to completion. The final pressure obtained was lower than

expected/...

expected from the sample weight used. (51.5 instead of 80). The results are given in TABLE 7.7 Run 2, and illustrated in FIGURE 7.3, curve B.

An uninterrupted run, TABLE 7.7 Run 1, is shown in FIGURE 7.3, curve A, while curve C is the acceleratory period of the final section of the interrupted run, with pressures normalised to $p_f = 80$.

Rate constants, k_1, for the uninterrupted and interrupted runs were obtained from the plots of $p^{\frac{1}{3}}$ against t shown in FIGURE 7.3, curves E and D respectively. The values were:

uninterrupted $k_1 = 0.102$ $cm^{\frac{1}{3}}$ per min.,

interrupted (normalised) $k_1 = 0.077$ $cm^{\frac{1}{3}}$ per min.,

while calculation of k_1 for curve B, interrupted (not normalised), gave a value of $k_1 = 0.054$ $cm^{\frac{1}{3}}$ per min.

TABLE 7.7

UNINTERRUPTED		120°C			3.9 mg.
t	p	t	p	t	p
20	0.08	67	17.90	110	78.02
32	0.22	72	29.73	120	80.03
40	0.48	77	40.73	130	79.43
45	0.86	82	51.34		
50	1.66	88	61.87	p_f	80.00
55	3.26	95	72.32	p_a	106.23
60	6.79	104	75.54		

INTERRUPTED		120°C			4.0 mg.
t	p	t	p	t	p
10	0.03	95	1.58	181	11.19
20	0.04	100	1.59	186	14.93
30	0.11	105	1.62	192	19.94
36	0.24	110	1.72	200	26.47
40	0.40	115	1.88	210	33.60

TABLE 7.7 contd.

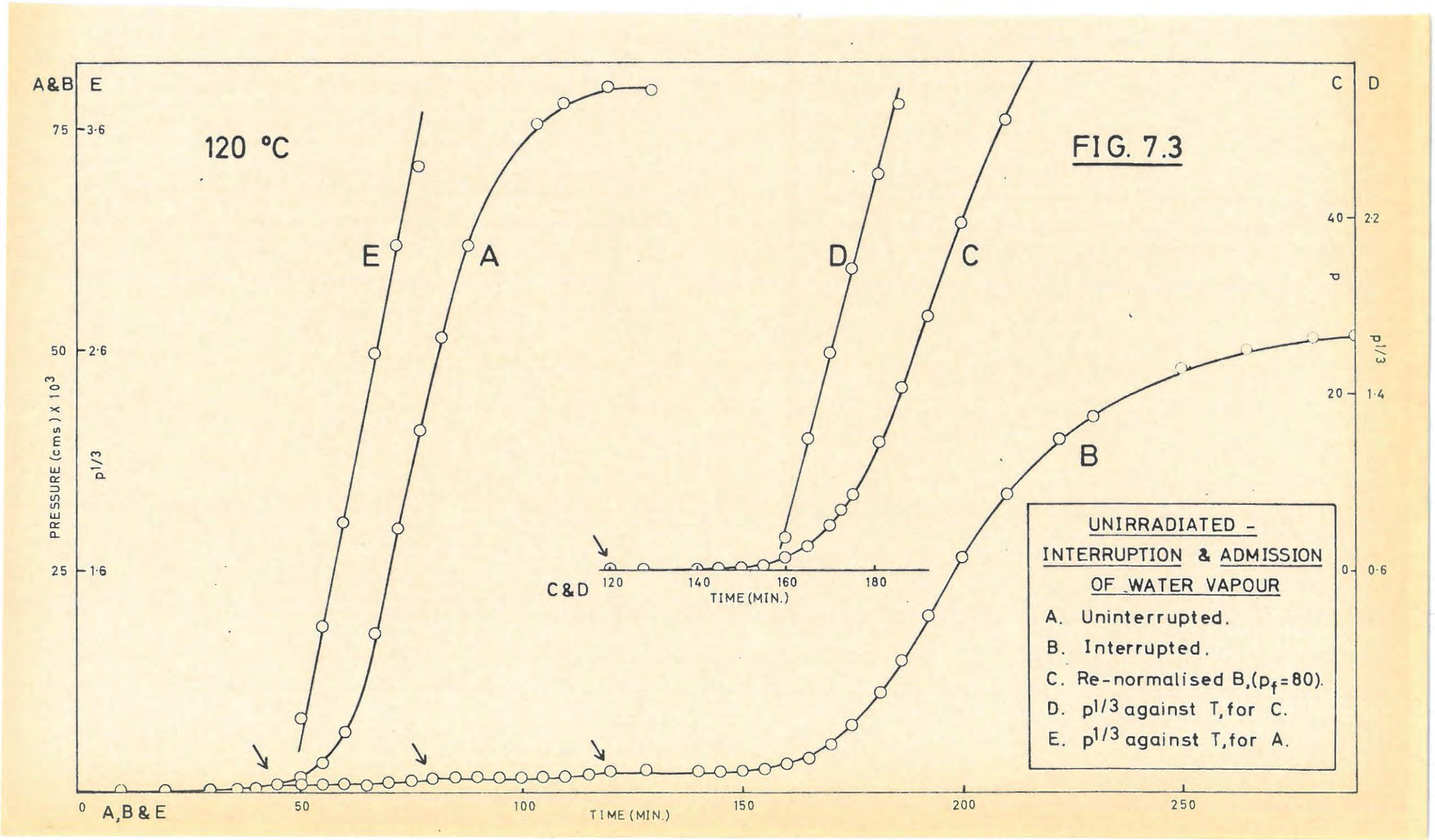
A&B
E
C
D
120 °C
FIG. 7.3
75
3·6
50
2·6
25
1·6
40
2·2
20
1·4
0
0·6
PRESSURE (cms) X 10³
p1/3
p
E
A
D
C
B
C&D
120
140
160
180
TIME (MIN.)
UNIRRADIATED -
INTERRUPTION & ADMISSION
OF WATER VAPOUR
A. Uninterrupted.
B. Interrupted.
C. Re-normalised B, (p_f=80).
D. $p^{1/3}$ against T, for C.
E. $p^{1/3}$ against T, for A.
0
A,B&E
50
100
150
200
250
TIME (MIN.)

TABLE 7.7 contd.

t	p	t	p	t	p
45*	0.84	120*	2.26	222	39.72
50	0.84	128	2.26	230	42.33
55	0.84	140	2.28	250	47.77
60	0.85	145	2.33	265	49.91
65	0.89	150	2.46	280	51.44
70	1.00	155	2.68	310	51.48
75	1.21	160	3.13	p_f	51.45
80*	1.58	165	3.93	$p_f$exp.	80.00
85	1.58	170	5.31	p_a	70.80
90	1.58	175	7.52		

*Interruption and admission of water vapour.

(b) At other stages in the decomposition.

Further interruptions of the decomposition with the admission of water vapour were carried out. The results are illustrated in a composite curve in FIGURE 7.4. The interruptions were at the points marked and the procedure was the same as in (a). The results are listed in TABLE 7.8.

Admission of water vapour at t = o, had no effect on the subsequent decomposition.

TABLE 7.8

INTERRUPTED		120°C			4.3 mg.
t	p	t	p	t	p
30*	0.01	60	0.32	82	3.73
40	0.02	70	0.99		
50	0.10	77	2.15		

TABLE 7.8 contd.

TABLE 7.8 contd.

120°C					4.3 mg.
t	p	t	p	t	p
38	0.35	64	5.50	95	5.73
43	0.57	67	5.50	100	5.91
48	1.03	71	5.51	105	6.26
52	1.74	75	5.52	111	6.91
55	2.68	80	5.53	117	7.90
57	3.73	85	5.56	123	9.43
60*	5.48	90	5.62		

120°C					4.2 mg.
t	p	t	p	t	p
20	0.06	62*	17.00	105	18.01
30	0.17	66	17.00	110	18.49
40	0.54	70	17.01	116	19.35
45	1.21	73	17.05	125	21.00
48	1.93	77	17.06	131	22.90
51	3.16	82	17.08	137	26.02
54	4.99	88	17.16		
58	7.98	94	17.32		
60	12.61	100	17.60		

120°C					4.1 mg.
t	p	t	p	t	p
10	0.07	76	6.25	113	48.74
21	0.16	82	12.55	117	50.86
30	0.22	86	18.69	121	52.14
40	0.29	90	26.46	128	53.44
51	0.47	95	36.94	135	53.98
57	0.73	98*	44.42	p_f	54.00
62	1.20	102	44.44	$p_f$exp	80.00
66	1.85	107	45.00	p_a	77.59
72	3.81	110	46.74		

*Interruption and admission of water vapour.

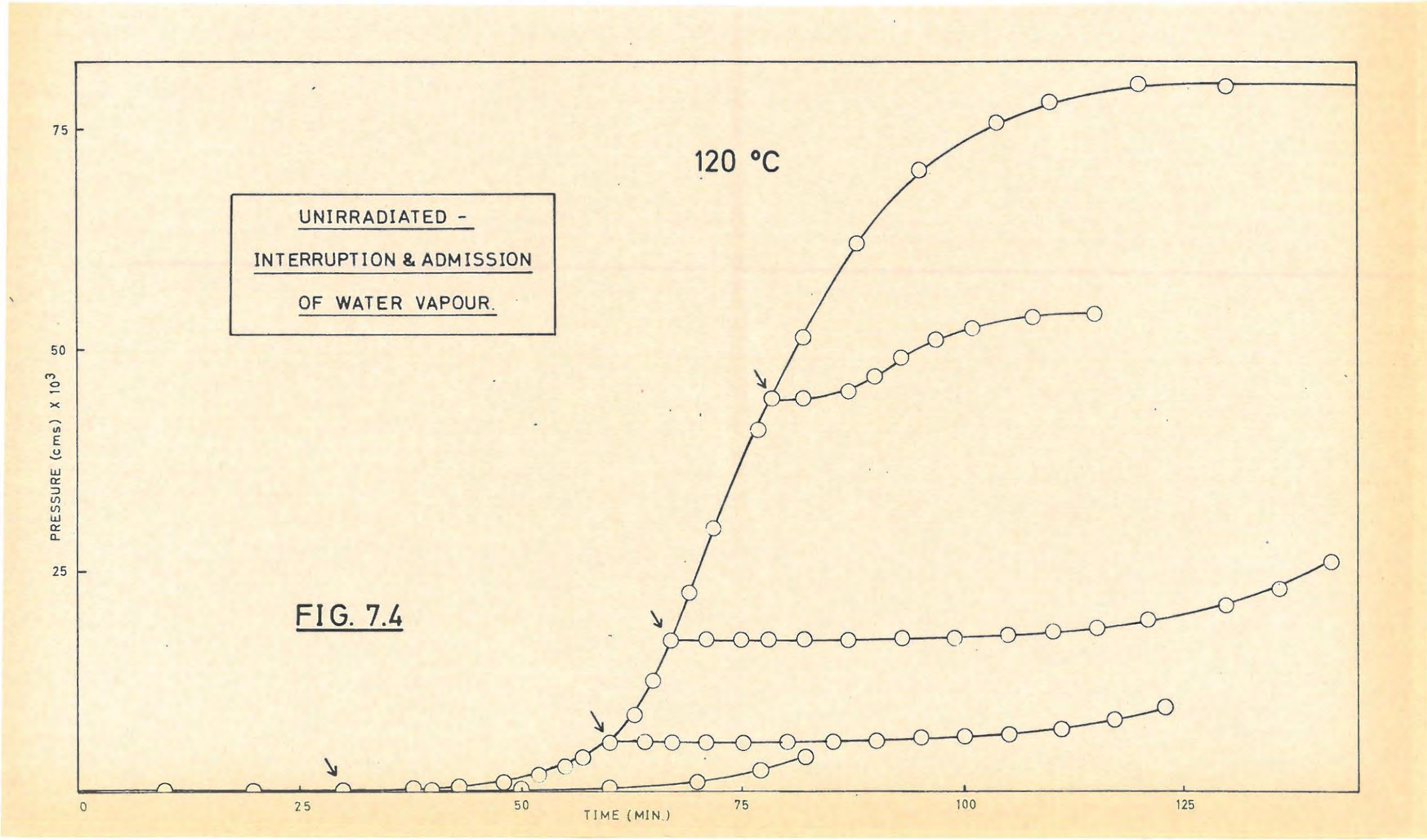
120 °C
UNIRRADIATED -
INTERRUPTION & ADMISSION
OF WATER VAPOUR.
PRESSURE (cms.) X 10³
75
50
25
0
25
50
75
100
125
TIME (MIN.)

FIG. 7.4

7.3.7. Visual Observations.

On heating, the white salt darkens slightly and is pale grey by α = 0.06. By α = 0.5 the salt is dark grey and at the end of the reaction is black. Admission of water vapour to the grey or black salt destroys the colour immediately and the salt turns white. No change in colour was observed on irradiation with γ-rays, X-rays or UV-light.

7.3.8. THE EFFECT OF PRE-IRRADIATION WITH GAMMA-RAYS.

7.3.8.1. Irradiation.

Pre-irradiation of samples sealed under vacuum in Pyrex ampoules, which had been baked out and painted black beforehand, was carried out at about 25°C at:

(a) Harwell, in the spent-fuel facility (mean γ-ray energy 1.1 Mev, flux 4.0 Mrad/hr) for doses of 0.25 to 8 Mrad, and

(b) Wantage, Co^{60} source (dose rate 3,400 rad/min) for doses from 1000 to 100,000 rad.

7.3.8.2. Reproducibility and Handling Conditions.

Because of the possibility of the radiolytic formation of nuclei of, say, calcium or calcium nitride, all handling of irradiated material was done in an atmosphere of dry nitrogen and, to cut down on the handling time, in all but a few runs the sample weights were estimated.

An ampoule containing calcium azide that had received a dose of 4 Mrad, was opened under argon and two samples were decomposed at 110°C. These runs are tabulated in TABLE 7.9, Runs 1 and 2. A third sample from the ampoule was exposed to dry nitrogen and then decomposed, TABLE 7.9, Run 3.

A second ampoule, which had received the same dose (4 Mrad) at the same time, was opened under nitrogen and

two/...

two samples decomposed at 110°C, TABLE 7.9, Runs 4 and 5.

All five runs are closely reproducible. This shows that the pre-irradiation effect is consistent from one sample to another with the same dose, and that the handling conditions under nitrogen and under argon are equivalent.

TABLE 7.9

ARGON Run 1		4 Mrad		110°C	
t	p	t	p	t	p
5	0.43	22	9.90	45	69.45
10	0.72	27	29.79	50	73.27
13	0.91	29	34.79	55	76.20
16	1.16	32	45.00	60	78.00
18	1.54	35	54.17	65	79.40
20	4.51	38	60.41	p_f	80.00
21	8.23	41	65.17	p_a	57.58

ARGON Run 2		4 Mrad		110°C	
t	p	t	p	t	p
6	0.24	27	44.81	44	75.66
12	0.42	29	53.17	47	77.64
15	0.54	31	58.79	50	78.22
17	0.67	33	63.28	55	79.32
19	1.03	35	66.69	62	79.77
21	7.29	37	69.33		
23	13.02	39	71.53	p_f	80.00
25	32.65	41	73.46	p_a	139.61

NITROGEN Run 3				110°C	
t	p	t	p	t	p
5	0.40	25	23.77	45	75.46
11	0.77	27	38.70	50	77.06
14	0.96	29	49.23	64	79.95
17	1.30	31	56.40		
19	1.88	33	61.73	p_f	80.00
21	6.65	36	66.20	p_a	71.58
23	17.88	40	71.62		

TABLE 7.9 contd.

TABLE 7.9 contd.

NITROGEN Run 4	4 Mrad			110°C	
t	p	t	p	t	p
15	0.44	31	43.55	43	74.24
20	0.58	33	56.36	44	76.70
25	1.35	34	60.02	51	78.03
27	5.77	35	63.08	58	80.06
28	12.19	37	67.39		
29	24.49	39	70.54	p_f	80.00
30	34.94	41	72.66	p_a	63.04

NITROGEN Run 5	4 Mrad			110°C	
t	p	t	p	t	p
10	0.42	28	55.06	45	76.84
22	7.98	29	58.16	52	79.02
23	16.16	30	61.04	60	79.81
24	28.27	32	65.18		
25	37.36	34	68.15	p_f	80.00
26	45.12	37	71.60	p_a	76.81
27	50.77	40	73.78		

Two samples of the irradiated (0.25 Mrad) salt were handled in dry nitrogen and two samples in air. The samples were then decomposed at 100°C. The four runs are tabulated in TABLE 7.10.

TABLE 7.10

NITROGEN Run 1	0.25 Mrad			100°C	
t	p	t	p	t	p
10	0.03	39	18.32	52	70.28
20	0.10	40	22.59	54	73.39
26	0.24	42	32.75	57	76.91
32	1.18	43	37.12	60	78.75
34	2.61	44	41.89	63	79.51
36	8.26	46	51.37	70	79.95
37	10.79	48	59.50	p_f	80.00
38	14.12	50	66.12	p_a	49.26

TABLE 7.10 contd.

TABLE 7.10 contd.

NITROGEN Run 2		0.25 Mrad		100°C	
t	p	t	p	t	p
10	0.06	40	27.76	55	77.39
22	0.21	42	38.96	58	78.75
30	0.60	44	49.63	62	79.38
32	1.23	46	58.20	70	80.00
34	3.54	48	65.34		
36	9.45	50	70.29	p_f	80.00
38	16.57	52	73.79	p_a	53.41

AIR Run 1		0.25 Mrad		100°C 2.0 mg.	
t	p	t	p	t	p
10	0.09	43	7.33	61	75.30
20	0.21	45	11.71	63	77.00
25	0.29	47	19.94	65	77.42
28	0.34	49	33.33	70	78.74
31	0.40	51	46.07	76	79.66
33	0.43	53	56.36		
35	0.51	55	64.33	p_f	80.00
38	0.84	57	69.50	p_a	55.76
41	2.17	59	73.32		

AIR Run 2		0.25 Mrad		100°C	
t	p	t	p	t	p
10	0.09	45	9.25	62	70.96
20	0.15	47	15.43	64	73.77
30	0.27	49	24.05	68	77.40
33	0.33	52	39.22	72	78.93
36	0.43	54	48.21	76	79.56
39	0.81	56	56.28	80	79.91
41	2.61	58	62.60	p_f	80.00
43	5.25	60	67.36	p_a	119.86

The/...

The induction period was lengthened slightly and the constant k_1, from

$$p^{\frac{1}{3}} = k_1 t + C_1 \qquad \ldots\ldots \qquad (7.4)$$

for the acceleratory period, decreased as shown in TABLE 7.11.

TABLE 7.11

		0.25 Mrad	100°C
HANDLED IN	RUN	IP (mins)	k_1 $cm^{\frac{1}{3}}$ per min
NITROGEN	1	30	0.234
	2	29	0.241
AIR	3	38	0.188
	4	38	0.184

7.3.8.3. The Effect of Annealing.

An irradiated (4 Mrad) sample was annealed in a vacuum for 1 hour at 50°C. The temperature was then raised to 90°C and the sample was decomposed in the normal way. The results of this run and those on a 'blank' sample are given in TABLE 7.12, Runs 2 and 1 respectively. The p/t curves are superimposable, showing that the irradiation effect is not annealed under these conditions.

7.3.8.4. The Effect of Ageing.

The irradiated (4 Mrad) material was stored in the dark, under vacuum over P_2O_5, for 5 months. A sample was then decomposed at 90°C. The results are given in TABLE 7.12, Run 3, which was then compared with Run 1. The values of the rate constants, k_1, (7.4) for the acceleratory period were:

Run 1, $k_1 = 0.117$ $cm^{\frac{1}{3}}$ per min.,

Run 3, $k_1 = 0.123$ $cm^{\frac{1}{3}}$ per min.,

showing that there was no marked ageing effect over 5 months.

TABLE 7.12/...

TABLE 7.12.

GAMMA-IRRADIATED. Run 1 4 Mrad 90°C					
t	p	t	p	t	p
15	0.06	59	20.02	84	72.72
30	0.18	62	27.81	88	75.46
40	0.45	65	35.98	94	77.95
47	1.54	68	44.61	106	80.00
51	4.47	71	52.15	120	79.71
53	9.08	74	58.57		
55	12.19	77	64.02	p_f	80.00
57	15.92	80	68.40	p_a	118.18

"ANNEALED" (1 hr. at 50°C) Run 2 4 Mrad 90°C					
t	p	t	p	t	p
5	0.01	48	2.09	67	38.92
10	0.11	52	4.79	71	48.56
20	0.19	54	7.46	75	57.21
26	0.28	56	11.08	98	79.98
32	0.41	58	15.84	103	80.01
37	0.63	60	21.18		
41	0.80	62	26.57	p_f	80.00
45	1.32	64	31.73	p_a	60.09

"AGED" (5 months) Run 3 4 Mrad 90°C					
t	p	t	p	t	p
21	0.08	56	3.21	85	57.55
28	0.23	60	5.76	90	63.88
35	0.40	63	9.58	95	69.06
40	0.61	66	17.60	101	72.88
43	0.80	69	26.42	106	75.80
46	1.03	72	33.68	114	79.20
50	1.53	76	42.24	p_f	80.00
53	2.22	80	49.84	p_a	57.43

7.3.8.5./...

7.3.8.5. The Effect of Various Doses of γ-rays.

Two series of runs were done, both at 100°C.

(a) The first series was on samples irradiated in the spent-fuel facility at Harwell, with doses from 0.25 Mrad to 8 Mrad. The results are given in TABLE 7.13.

TABLE 7.13.

GAMMA-IRRADIATED			8 Mrad	100°C	
t	p	t	p	t	p
10	0.17	33	20.83	42	71.23
15	0.24	34	28.34	43	73.35
20	0.33	35	35.86	44	74.91
23	0.46	36	43.43	46	77.33
26	0.81	37	50.23	48	78.43
29	6.85	38	56.36	52	79.44
30	8.52	39	61.28	56	80.00
31	11.48	40	65.39	p_f	80.00
32	14.84	41	68.43	p_a	81.4

			4 Mrad	100°C	
t	p	t	p	t	p
5	0.02	34	17.88	46	75.37
10	0.08	35	25.44	48	77.34
15	0.13	36	34.43	50	78.27
20	0.25	37	42.65	54	79.34
25	0.40	38	49.59	60	79.94
30	1.82	39	55.45		
31	3.28	40	59.79	p_f	80.00
32	8.28	42	67.52	p_a	42.2
33	12.13	44	72.17		

TABLE 7.13 contd.

TABLE 7.13 contd.

			0.25 Mrad 100°C		
t	p	t	p	t	p
10	0.03	39	18.32	52	70.28
20	0.10	40	22.59	54	73.39
26	0.24	42	32.75	57	76.91
32	1.18	43	37.12	60	78.75
34	2.61	44	41.89	63	79.51
36	8.26	46	51.37	70	79.95
37	10.79	48	59.50	p_f	80.00
38	14.12	50	66.12	p_a	49.3

(b) The second series was on samples irradiated at the Vantage Co^{60} source, with doses from 1000 rad to 100,000 rad. The results are given in TABLE 7.14 and illustrated in FIGURE 7.5.

TABLE 7.14

GAMMA-IRRADIATED			100,000 rad		100°C
t	p	t	p	t	p
33	0.24	65	23.75	88	71.94
41	0.61	67	29.66	92	74.62
46	1.28	69	35.68	97	76.64
50	2.46	71	41.51	102	78.13
53	3.92	73	47.22	107	78.85
56	6.34	76	55.22	126	80.76
59	10.24	79	61.50		
61	13.87	82	66.14	p_f	80.00
63	18.54	85	69.45	p_a	93.2

			50,000 rad		100°C
t	p	t	p	t	p
25	0.10	72	21.49	97	70.06
35	0.23	74	26.81	102	73.54
49	0.76	77	34.69	108	76.23
55	1.85	80	42.26	114	77.99
60	3.61	83	49.10	120	79.59
64	6.53	86	55.17	130	79.86
67	10.19	89	59.81	p_f	80.00
70	16.49	93	65.69	p_a	73.88

TABLE 7.14 contd.

TABLE 7.14 contd.

			25,000 rad		100°C
t	p	t	p	t	p
40	0.28	81	25.58	108	70.52
50	0.41	84	33.39	114	73.90
58	1.09	87	40.88	121	76.68
64	1.58	90	47.90	130	78.58
68	3.32	93	53.94	140	79.65
72	8.49	96	58.73	150	80.06
75	12.77	100	64.30	p_f	80.00
78	18.44	104	67.73	p_a	135.1

			10,000 rad		100°C
t	p	t	p	t	p
45	0.21	86	24.07	118	71.81
52	0.36	89	31.18	128	76.32
61	0.95	92	37.59	140	78.54
66	1.78	95	44.48	158	79.71
70	3.04	98	50.01		
75	6.07	103	58.40	p_f	80.00
80	12.34	108	64.63	p_a	84.69
83	17.44	113	68.91		

			1000 rad		100°C
t	p	t	p	t	p
50	0.16	100	13.22	151	72.70
60	0.40	106	20.08	160	75.68
71	1.07	112	28.96	170	77.35
77	1.87	118	38.37	191	79.28
82	2.93	129	55.76	205	79.68
88	4.84	135	63.63	p_f	80.00
94	8.20	142	68.13	p_a	89.64

The/...

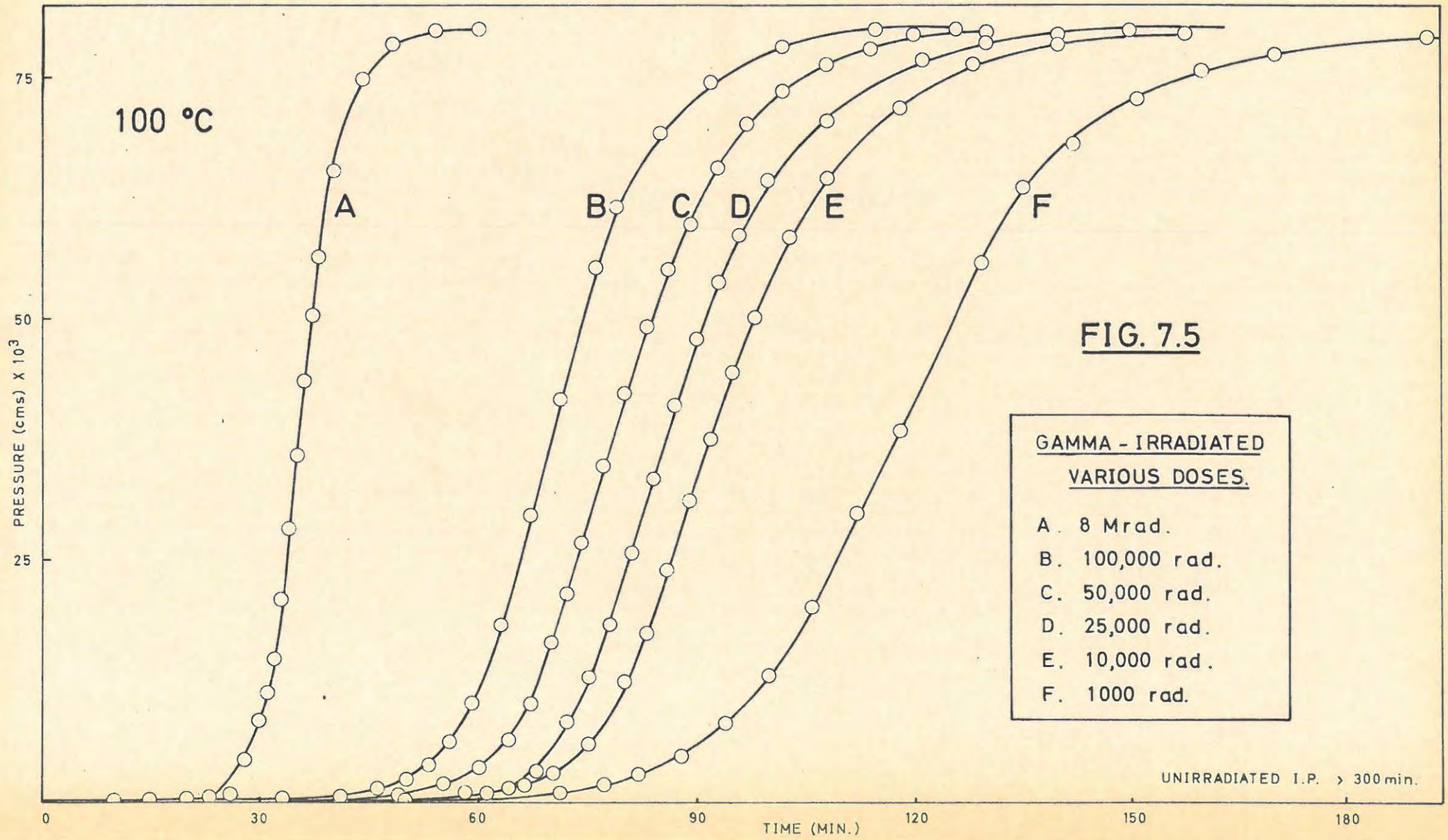
100 °C
A
B
C
D
E
F
75
50
25
PRESSURE (cms) X 10^3
0
30
60
90
120
150
180
TIME (MIN.)
GAMMA - IRRADIATED
VARIOUS DOSES.
A. 8 Mrad.
B. 100,000 rad.
C. 50,000 rad.
D. 25,000 rad.
E. 10,000 rad.
F. 1000 rad.
UNIRRADIATED I.P. > 300 min.

FIG. 7.5

The values of the rate constants, k_1, from:

$$p^{\frac{1}{3}} = k_1 t + C_1 \qquad \ldots\ldots \qquad (7.4)$$

for the acceleratory period, are tabulated against the corresponding γ-doses in TABLE 7.15 and the dose and log (dose) are plotted against k_1 in FIGURE 7.6. The value of k_1 reaches a "saturation" value of 0.113 $cm^{\frac{1}{3}}$ per min., at a dose of approximately 40,000 rad, for this radiation.

The lengths of the induction period (IP) and log (IP) are also tabulated in TABLE 7.15. No simple relationship between these values and the irradiation dose or log (dose), was found.

The extent of fit of the $p^{\frac{1}{3}}$ analysis over the acceleratory period remained unchanged, viz. up to $\alpha \simeq 0.5$, for doses from 1000 rad to 8 Mrad.

TABLE 7.15

GAMMA-IRRADIATED CaN_6				100°C
DOSE(d) (rad)	log d	k_1 x 100 ($cm^{\frac{1}{3}}$ per min)	IP (mins)	log IP
1000	3.000	5.63	71	1.851
10,000	4.000	9.10	63	1.799
25,000	4.398	10.7	58	1.763
50,000	4.699	11.3	51	1.708
100,000	5.000	11.3	43	1.634

The values of IP (mins), k_1 (cm $Hg^{\frac{1}{3}}$ per min), and k_2 (per min), at 110°C for unirradiated and irradiated (0.25 Mrad) samples are compared in TABLE 7.16 and the percentage change in these values is also listed.

TABLE 7.16/...

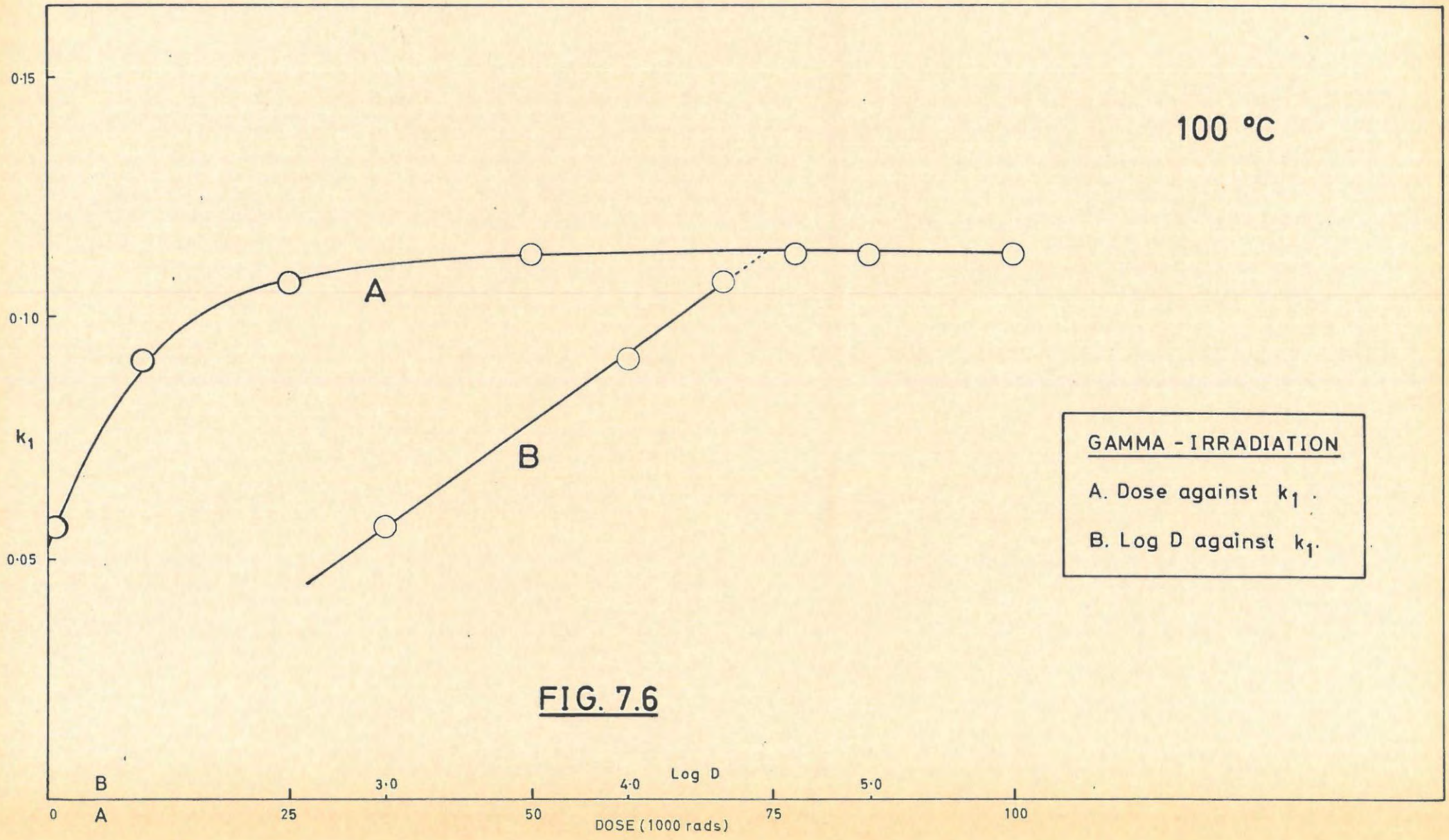
100 °C
0·15
0·10
0·05
k_1
A
B
GAMMA - IRRADIATION
A. Dose against k_1 .
B. Log D against k_1.
B
A
0
25
50
75
100
3·0
4·0
5·0
Log D
DOSE (1000 rads)

FIG. 7.6

TABLE 7.16.

CaN_6	0 - 0.25 Mrad		110°C
	Unirradiated	Irradiated	Change
IP	105	16	15%
k_1	0.0279	0.498	1750%
k_2	0.0066	0.0250	380%

7.3.8.6. The Effect of Temperature.

Samples of the irradiated (8 Mrad) salt were decomposed at various temperatures in the range 80°C to 100°C. The results are listed in TABLE 7.17.

TABLE 7.17.

GAMMA-IRRADIATED CaN_6		8 Mrad		80°C	
t	p	t	p	t	p
30	0.23	156	6.32	217	64.15
50	0.38	162	8.92	224	69.13
70	0.57	168	12.45	230	72.17
85	0.80	174	17.18	240	77.00
95	0.97	180	22.97	250	79.10
110	1.33	186	29.12	260	79.53
120	1.68	192	36.45		
130	2.17	197	42.30	p_f	80.00
140	3.00	204	50.87	p_a	47.72
150	4.63	210	57.47		

		8 Mrad		85°C	
t	p	t	p	t	p
61	1.12	105	24.62	150	76.63
71	1.71	110	33.03	157	78.55
80	2.86	116	43.25	165	79.29
85	4.25	120	49.21	180	80.03
89	6.29	126	57.56		
93	9.39	132	64.41	p_f	80.00
97	13.46	138	69.43	p_a	27.11
101	17.98	144	73.21		

TABLE 7.17 contd.

TABLE 7.17 contd.

8 Mrad 90°C					
t	p	t	p	t	p
10	0.14	66	12.99	88	69.72
20	0.26	68	17.57	91	72.65
30	0.36	70	22.75	95	75.66
40	0.52	72	28.91	100	78.02
50	0.93	74	35.76	105	79.34
55	1.40	76	42.41	112	81.12
58	1.93	79	52.12	120	80.0
61	3.34	82	59.63	p_f	80.00
64	9.41	85	65.13	p_a	75.04

8 Mrad 95°C					
t	p	t	p	t	p
11	0.01	42	22.23	56	74.01
22	0.07	44	31.93	58	76.45
30	0.34	46	41.78	60	78.53
34	1.02	48	50.97	63	79.99
36	2.33	50	58.80	66	80.08
38	7.90	52	65.20	p_f	80.00
40	13.61	54	70.12	p_a	72.07

8 Mrad 100°C					
t	p	t	p	t	p
10	0.17	34	28.34	44	74.91
15	0.24	35	35.86	46	77.33
20	0.33	36	43.43	48	78.43
23	0.46	37	50.23	52	79.44
26	0.81	38	56.36	56	80.0
29	6.85	39	61.28	60	79.78
30	8.52	40	65.39		
31	11.48	41	68.43	p_f	80.00
32	14.84	42	71.23	p_a	81.18
33	20.83	43	73.35		

TABLE 7.17 contd.

TABLE 7.17 contd.

8 Mrad 100°C					
t	p	t	p	t	p
17	0.16	27	20.24	37	73.05
20	0.41	28	27.83	39	75.93
21	0.58	29	36.05	42	78.53
22	0.92	30	43.86	45	79.37
23	1.60	31	50.60	50	79.71
24	3.50	32	56.03		
25	7.57	33	60.83	p_f	80.00
26	13.09	35	68.25	p_a	81.70

7.3.8.7. Mathematical Analysis.

A typical p/t plot for the gamma-irradiated salt is shown in FIGURE 7.7, curve B. The analysis used for the unirradiated material, was applied and holds unchanged. For the acceleratory period:-

$$(p - p_o)^{\frac{1}{3}} = k_1 t + C_1 \qquad \ldots\ldots\ldots \qquad (7.4)$$

applies over the range $0.013 < \alpha < 0.5$, FIGURE 7.7, curve A. The Avrami-Erofeyev equation (7.7) fitted over $0.05 < \alpha < 0.5$ and log p against t (7.8) also gave a partial fit up to $\alpha \approx 0.3$.

For the decay period, the contracting sphere equation:-

$$1 - (1 - p/p_f)^{\frac{1}{3}} = k_2 t \qquad \ldots\ldots\ldots \qquad (7.5)$$

holds from $0.5 < \alpha < 0.98$, FIGURE 7.7, curve C.

The values of k_1 and k_2, as well as the lengths of the induction period (IP), at various temperatures, are listed in TABLE 7.18.

The values of log IP, log k_1 and log k_2 are plotted against $1/T^{\circ}K$ in FIGURE 7.8. The values of the activation energies obtained from these plots, with unirradiated values in brackets for comparison, are:-

Induction/...

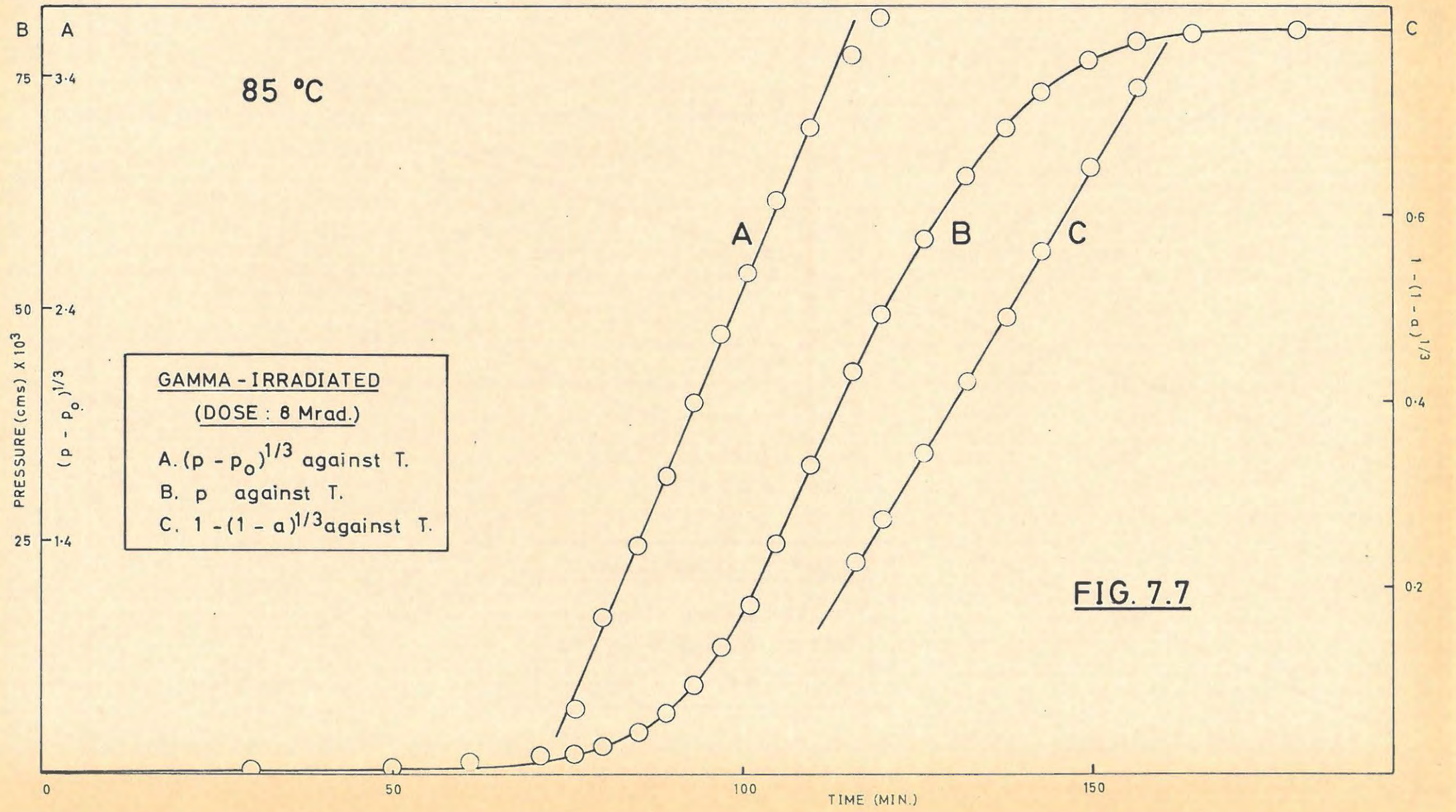
B
A
C
85 °C
75
50
25
3·4
2·4
1·4
0·6
0·4
0·2
PRESSURE (cms) X 10³
(p - p₀)^1/3
1 - (1 - a)^1/3
A
B
C
GAMMA - IRRADIATED
(DOSE : 8 Mrad.)
A. (p - p₀)^1/3 against T.
B. p against T.
C. 1 - (1 - a)^1/3 against T.
0
50
100
150
TIME (MIN.)

FIG. 7.7

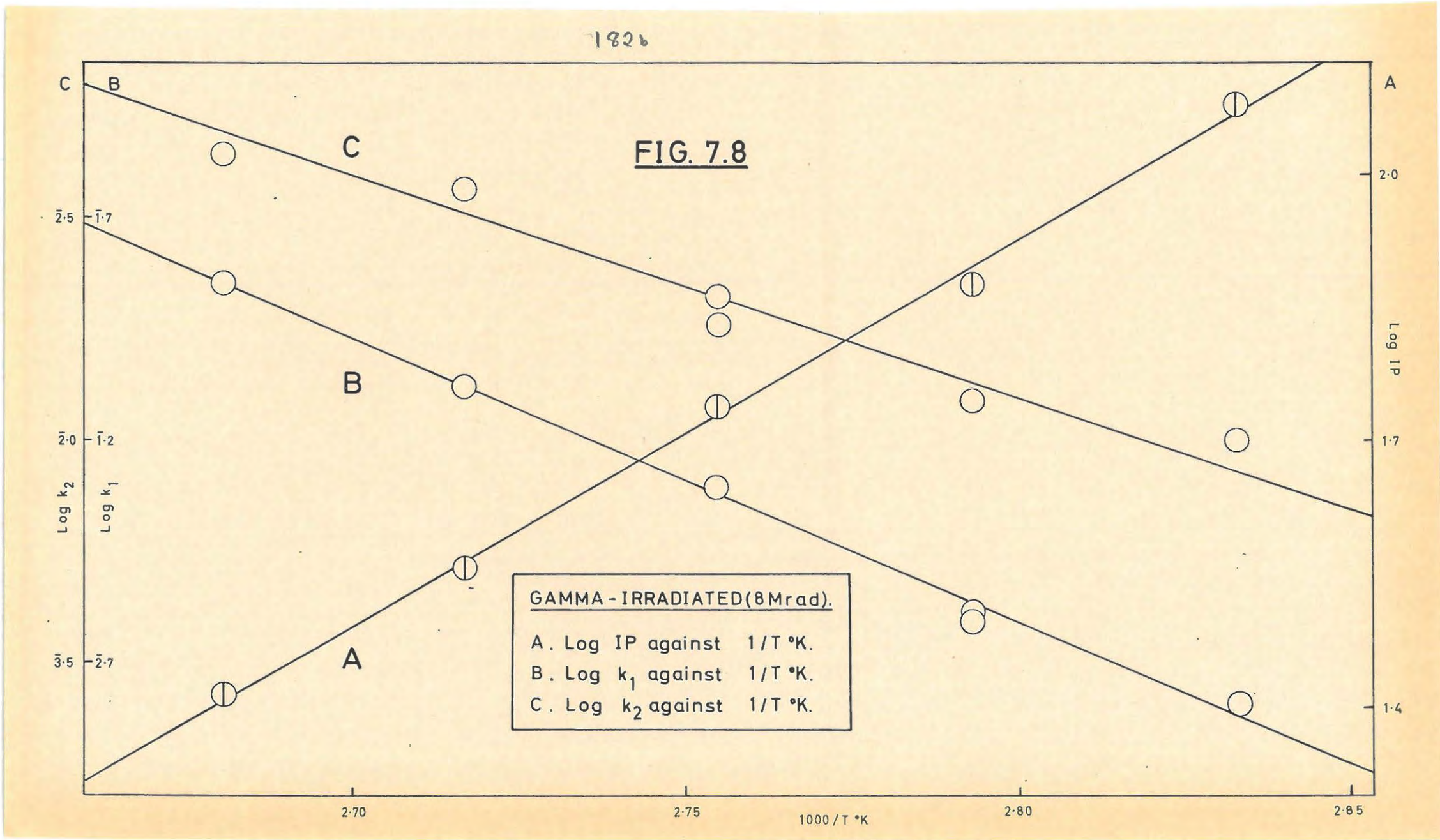
C
B
A
C
B
A
FIG. 7.8
2·5
1·7
2·0
1·2
3·5
2·7
2·0
1·7
1·4
Log k2
Log k1
Log IP
GAMMA-IRRADIATED(8Mrad).
A. Log IP against 1/T °K.
B. Log k1 against 1/T °K.
C. Log k2 against 1/T °K.
2·70
2·75
2·80
2·85
1000/T °K

Induction period : 19.8 kcal/mole (18.2 kcal/mole)

Acceleratory reaction: 28.1 kcal/mole (27.1 kcal/mole)

Decay reaction : 22.5 kcal/mole (18.8 kcal/mole)

TABLE 7.18

GAMMA-IRRADIATED CaN_6 8 Mrad			
Temp. °C	IP (Induction Period) (mins)	Acceleratory k_1 x 100 (cm $Hg^{\frac{1}{3}}$ per min)	Decay k_2 x 100 (per min)
80	120	4.05	1.000
85	75	6.25	1.238
90	55	12.55	2.107
95	36	21.10	3.707
100	26	26.45	4.431
100	22	36.13	4.427

7.3.8.8. The Effect of Interrupting an Irradiated Decomposition.

An irradiated (8 Mrad) decomposition at 90°C was interrupted at various stages by raising the sample into vacuum, allowing it to cool for 15 mins. and replacing it at the same temperature, see TABLE 7.19. Interruptions were at the stages marked. Except for short heating lags (2-3 mins), the run continued normally.

TABLE 7.19

VACUUM 8 Mrad 90°C					
t	p	t	p	t	p
10	0.01	70	13.33	101	61.19
20	0.02	72	13.92	104	65.86
30	0.11	74	15.36	107	70.52
40	0.51	77	22.51	110	73.64
46*	1.32	79	29.89	113	75.80
48	1.32	81*	36.04	116	77.12
51	1.37	83	36.19	120	78.40
54	1.44	85	36.66	125	79.42
57	1.59	87	38.09	130	80.03

TABLE 7.19 contd.

TABLE 7.19 contd.

t	p	t	p	t	p
60	2.01	89	42.42	135	79.99
63	3.45	91	49.82		
65	6.27	94*	58.40	p_f	80.00
67	10.89	97	58.81	p_a	84.20
68*	13.06	99	59.55		

*Interruption.

7.3.8.9. The Effect of Interrupting an Unirradiated Decomposition and Irradiating with Gamma-rays.

Unirradiated samples were weighed into small Pyrex ampoules. These samples were then decomposed at 110°C and interrupted at various stages of the decomposition by raising the ampoule from the decomposition vessel. The ampoules were removed from the line under dry nitrogen, sealed under vacuum and irradiated at Harwell, receiving a dose of 0.25 Mrad. On return the samples were opened under dry nitrogen, replaced in the line and decomposition continued at the same temperature (110°C). The results of these runs are tabulated in TABLE 7.20, together with an unirradiated blank run and two irradiated (0.25 Mrad) blank runs.

A composite decomposition curve is given in FIGURE 7.9.

TABLE 7.20

UNIRRADIATED BLANK				110°C	2.9 mg.
t	p	t	p	t	p
40	0.09	156	7.04	250	74.85
70	0.26	166	11.29	266	78.14
90	0.52	176	17.45	282	79.14
100	0.75	194	34.09	301	79.91
110	1.07	202	42.28		
124	1.77	214	54.14	p_f	80.00
136	2.90	226	63.81	p_a	83.90
146	4.46	236	69.34		

TABLE 7.20 contd.

TABLE 7.20 contd.

IRRADIATED BLANK			0.25 Mrad 110°C		3.1 mg.
t	p	t	p	t	p
4	0	24	31.87	36	75.58
8	0.02	25	42.58	38	76.82
13	0.11	26	51.00	40	77.98
16	0.41	27	57.09	42	78.98
18	0.97	28	61.58	44	78.90
20	2.55	29	64.34	50	80.41
21	4.60	30	66.86		
22	9.99	32	71.08	p_f	80.00
23	21.34	34	73.55	p_a	84.43

IRRADIATED BLANK			0.25 Mrad 110°C		3.0 mg.
t	p	t	p	t	p
5	0.03	25	11.23	37	70.73
10	0.07	26	20.30	40	74.36
13	0.13	27	30.09	44	77.33
15	0.17	28	39.56	48	78.84
17	0.27	29	46.64	52	79.60
19	0.45	30	51.68		
21	1.07	31	55.92	p_f	80.00
23	3.11	33	62.77	p_a	82.58
24	5.55	35	67.43		

			0.25 Mrad 110°C		3.6 mg.
t	p	t	p	t	p
30*	0.02	53	13.44	62	74.28
34	0.05	54	53.77	64	75.68
40	0.17	55	56.83	68	78.11
43	0.28	56	61.05	73	79.29
46	0.48	57	64.07		
49	1.17	58	67.15	p_f	80.00
51	2.66	60	71.28	p_a	81.27

TABLE 7.20 contd.

TABLE 7.20 contd.

			0.25 Mrad 110°C		3.1 mg.
t	p	t	p	t	p
20	0.02	89	2.80	100	70.66
50	0.34	90	5.08	102	73.36
60	0.42	91	10.70	106	76.65
70*	0.51	93	37.64	110	78.37
76	0.51	94	45.86	114	79.39
80	0.55	95	53.30	120	80.02
84	0.68	96	58.75	p_f	80.00
87	1.28	98	66.06	p_a	79.52

			0.25 Mrad 110°C		3.6 mg.
t	p	t	p	t	p
60	0.13	142	3.10	154	73.81
104	0.68	144	9.43	156	76.60
114	1.04	145	21.86	158	78.29
120	1.46	146	33.51	160	78.91
124*	1.73	147	44.06	162	79.76
128	1.71	148	52.54	164	79.69
132	1.75	149	59.15	166	80.00
134	1.81	150	64.06		
136	1.88	151	67.30	p_f	80.00
140	2.24	152	69.89	p_a	78.30

			0.25 Mrad 110°C		2.9 mg.
t	p	t	p	t	p
100	1.02	182	8.61	194	64.54
110	1.14	183	9.16	195	68.37
120	1.30	184	9.80	196	70.44
134	1.74	185	10.54	198	74.20
144	2.27	187	13.30	200	76.05
154	3.27	189	21.57	202	77.43
166	5.53	190	31.00	207	79.22
172*	7.26	191	42.69	212	79.98
176	7.32	192	53.43	p_f	80.00
180	7.76	193	59.92	p_a	72.68

TABLE 7.20 contd.

TABLE 7.20 contd.

0.25 Mrad 110°C 3.6 mg.					
t	p	t	p	t	p
30	0.02	182	16.50	193	59.59
60	0.05	183	17.59	194	64.24
90	0.24	184	18.60	195	67.79
110	0.59	185	19.76	196	70.93
128	1.51	186	20.98	198	75.63
140	2.80	187	22.62	200	78.06
158	7.04	188	25.50	202	79.00
164	9.47	189	29.27	204	79.72
170	12.52	190	35.92	206	80.01
174*	14.80	191	44.16	p_f	80.00
178	14.85	192	52.40	p_a	93.41

0.25 Mrad 110°C 3.3 mg.					
t	p	t	p	t	p
40	0.08	174	31.46	186	58.29
94	1.38	176	33.00	187	62.19
108	2.97	177	34.04	188	65.88
120	5.56	178	35.13	190	71.85
130	8.73	179	36.18	192	75.88
140	12.87	180	37.39	194	78.11
150	18.07	181	38.69	196	79.40
158	23.21	182	41.26	198	79.59
164	28.04	183	44.61	200	79.83
168*	30.52	184	48.90	p_f	80.00
172	31.05	185	53.54	p_a	93.80

0.25 Mrad 110°C 3.9 mg.					
t	p	t	p	t	p
20	0	190*	40.30	207	63.48
50	0.01	194	40.46	208	66.59
80	0.14	196	40.87	209	68.94
100	0.44	198	42.34	210	70.91
116	1.10	199	43.53	211	73.14
130	2.53	200	44.80	212	74.71
144	5.86	201	46.22	214	77.39

TABLE 7.20 contd.

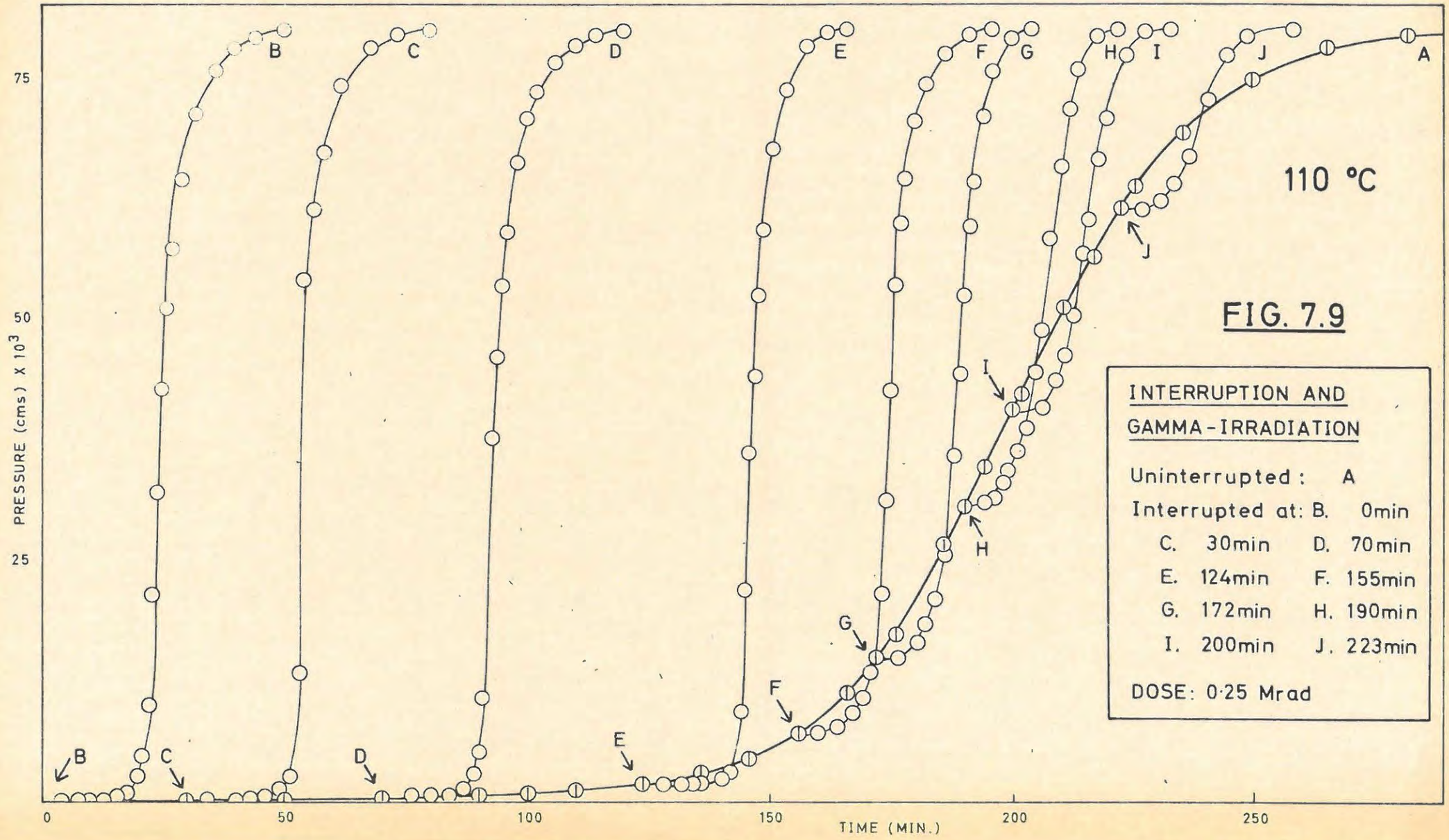
PRESSURE (cms) X 10^3
75
50
25
0
50
100
150
200
250
TIME (MIN.)
B
C
D
E
F
G
H
I
J
A
110 °C
INTERRUPTION AND
GAMMA-IRRADIATION
Uninterrupted : A
Interrupted at: B. 0min
C. 30min D. 70min
E. 124min F. 155min
G. 172min H. 190min
I. 200min J. 223min
DOSE: 0·25 Mrad

FIG. 7.9

TABLE 7.20 contd.

t	p	t	p	t	p
156	11.50	202	48.09	216	78.95
168	20.31	203	50.67	218	79.74
176	27.55	204	53.52	220	79.93
182	33.32	205	56.84	p_f	80.00
184	37.86	206	60.17	p_a	95.47

				0.25 Mrad 110°C 3.8 mg.	
t	p	t	p	t	p
40	0.04	196	52.10	226	70.04
60	0.07	204	57.83	227	71.37
78	0.20	210*	61.32	228	72.82
96	0.55	214	61.35	230	75.34
108	1.09	216	61.57	232	77.11
118	1.98	217	61.84	234	78.34
132	4.69	218	62.27	236	79.11
148	11.06	219	62.80	240	79.83
160	19.31	221	64.10	246	80.01
176	33.54	222	64.74	p_f	80.00
186	43.79	224	66.84	p_a	111.35

*Interruption and Irradiation.

7.3.8.10. The Effect of Interruption and Admission of Water Vapour.

a) At the end of the Induction Period.

Interruption and admission of water vapour at the end of the induction period (p = 1.0, t = 45 mins) of an irradiated (4 Mrad) decomposition at 90°C was carried out in the same way as for unirradiated material (7.3.6).

The successive induction periods for the irradiated run were 45 mins., 41 mins., 34 mins., 29 mins., 26 mins. and 29 mins. The reaction was then allowed to go to completion. The final pressure (p_f) was much lower than expected from the sample weight used. (22.2 instead of 80).

The/...

The residue was strongly heated using a bunsen flame and further evolution of gas occurred, bringing the final pressure up to 35.2 (p_f').

The results are given in TABLE 7.21, Run 2. Run 1 is an irradiated (4 Mrad) blank. The runs are shown in FIGURE 7.10, curves B and A respectively. Curve C is the acceleratory period of the final section of the interrupted run, with pressures normalised to $p_f = 80$.

Rate constants, k_1, for the uninterrupted and interrupted runs were obtained from the plots of $p^{\frac{1}{3}}$ against t, shown in FIGURE 7.10 curves E and D respectively.

The values were: uninterrupted: $k_1 = 0.130$ $cm^{\frac{1}{3}}$ per min
interrupted : $k_1 = 0.18$ $cm^{\frac{1}{3}}$ per min.,

while for curve B, not normalised, $k_1 = 0.113$ $cm^{\frac{1}{3}}$ per min.

TABLE 7.21.

GAMMA-IRRADIATED CaN_6 Run 1 4 Mrad 90°C					
t	p	t	p	t	p
21	0.08	56	3.21	85	57.55
28	0.23	60	5.76	90	63.88
35	0.40	63	9.58	95	69.06
40	0.61	66	17.60	101	72.88
43	0.80	69	26.42	106	75.80
46	1.03	72	33.68	114	79.20
50	1.53	76	42.24	p_f	80.00
53	2.22	80	49.84	p_a	57.43

Run 2 4 Mrad 90°C 4.1 mg.					
t	p	t	p	t	p
10	0.08	120*	2.84	209	5.36
22	0.19	126	2.86	219	5.39
30	0.31	130	2.86	226	5.56

TABLE 7.21 contd.

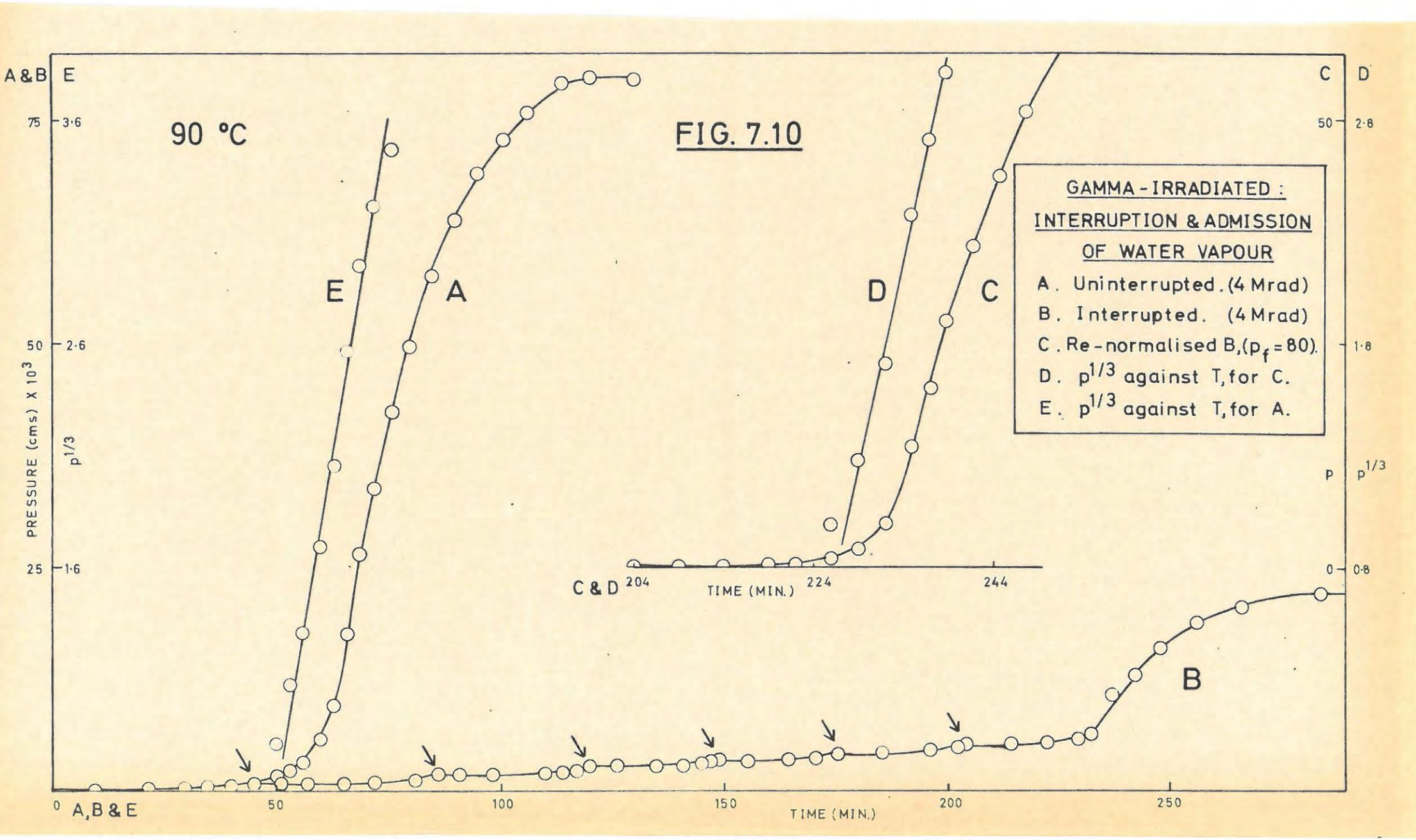
A&B
E
C
D
90 °C
FIG. 7.10
GAMMA - IRRADIATED :
INTERRUPTION & ADMISSION
OF WATER VAPOUR
A . Uninterrupted . (4 Mrad)
B . Interrupted . (4 Mrad)
C . Re-normalised B, (p_f = 80).
D . $p^{1/3}$ against T, for C.
E . $p^{1/3}$ against T, for A.
PRESSURE (cms) X 10^3
$p^{1/3}$
P
$p^{1/3}$
TIME (MIN.)
A,B & E
C & D
B
E
A
D
C
75
50
25
3·6
2·6
1·6
2·8
1·8
0·8
0
50
100
150
200
250
204
224
244

TABLE 7.21 contd.

t	p	t	p	t	p
35	0.40	135	2.88	229	5.80
40	0.55	141	2.96	232	6.42
45*	0.71	145	3.10	235	10.22
51	0.73	147	3.23	237	10.75
57	0.73	149*	3.42	239	11.49
65	0.74	155	3.45	242	12.97
72	0.80	164	3.50	245	14.60
75	0.85	167	3.58	248	16.08
78	0.96	170	3.71	252	17.77
81	1.14	172	3.85	256	18.93
84	1.54	175*	4.25	260	19.95
86*	1.91	180	4.29	266	20.59
91	1.91	185	4.36	272	21.48
98	1.91	190	4.43	284	22.11
104	1.92	196	4.54	p_f	22.2
110	2.00	199	4.68	p'_f	35.2
114	2.14	202	4.96	p_a	48.0
117	2.36	204*	5.34	p_{exp}	109

*Interruption and Admission of Water Vapour.

b) At other stages in the decomposition.

Further interruptions of the irradiated (4 Mrad) decomposition, with the admission of water vapour as in (a), were carried out. The results are illustrated in a composite curve in FIGURE 7.11. The interruptions were at the points marked. All pressures are normalised on the basis of the sample weight used, to give an expected $p_f = 80$. The results of the runs are given in TABLE 7.22.

Analysis of the acceleratory periods of curves A and B, gave values of k_1 of 0.177 and 0.102 (cm $Hg^{\frac{1}{3}}$ per min) respectively. If curve B was normalised to $p_f = 80$, $k_1 =$ 0.121 $cm^{\frac{1}{3}}$ per min.

TABLE 7.22/...

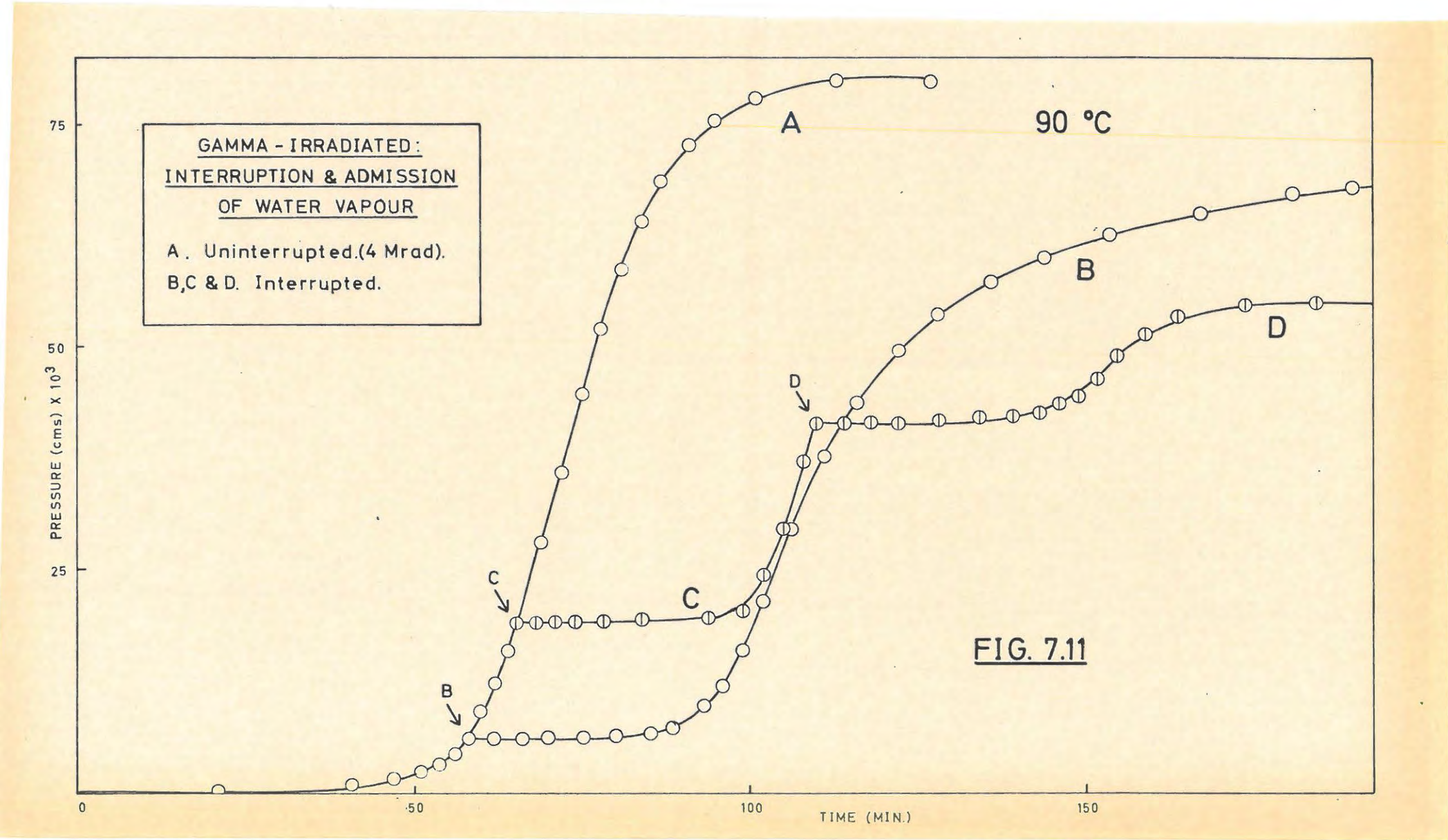
GAMMA - IRRADIATED:
INTERRUPTION & ADMISSION
OF WATER VAPOUR
A. Uninterrupted.(4 Mrad).
B,C & D. Interrupted.
90 °C
A
B
C
D
PRESSURE (cms) X 10³
TIME (MIN.)
0
50
100
150
25
50
75

FIG. 7.11

TABLE 7.22

4 Mrad				90°C	4.4 mg.
t	p	t	p	t	p
21	0.18	70	6.18	116	43.95
28	0.32	75	6.21	122	49.54
35	0.57	80	6.32	128	53.56
41	0.92	85	6.62	136	57.26
47	1.59	88	7.39	144	60.03
51	2.35	93	9.80	154	62.70
54	3.38	96	11.92	167	65.00
56	4.38	99	15.88	181	67.29
58*	6.16	102	21.48	$p_f$exp	80.00
62	6.16	106	29.43	p_f	68.0
66	6.16	111	37.63	p_a	100.0

4 Mrad				90°C	2.8 mg.
t	p	t	p	t	p
39	0.72	80	19.22	135	42.11
43	1.00	90	19.55	139	42.50
47	1.36	95	20.35	142	43.13
51	2.04	98	24.26	145	44.45
55	5.53	101	29.49	148	46.55
57	9.82	104	36.96	151	48.86
59	14.54	106*	41.55	155	51.34
61*	19.03	110	41.56	160	53.23
64	19.02	114	41.58	170	54.86
67	19.06	118	41.63	$p_f$exp	80.0
70	19.10	124	41.72	p_f	55.0
74	19.14	130	41.87	p_a	55.0

*Interruption and Admission of Water Vapour.

7.3.9. THE EFFECT OF PRE-IRRADIATION WITH X-RAYS.

7.3.9.1. Irradiation.

Samples were spread thinly on celluloid sheet and covered with cellophane, under dry nitrogen. Irradiation was carried out in the beam from a Philips PW 1009 X-ray generator, using either the unfiltered copper radiation, or

a/...

a nickel filter, and the beam intensities, sample distances and exposures specified below.

7.3.9.2. The Effect of Various Doses of X-rays.

Two series of runs were carried out.

(a) The generator was operated at 40kV and 20mA; unfiltered Cu radiation was used with a window to sample distance of 13 cms. Exposures ranged from 8 hrs. to 90 secs. A further sample was irradiated for 90 secs., at 13 cms and 20kV and 5mA. Samples of each exposure were decomposed at 100°C. The runs are listed in TABLE 7.23 and illustrated in FIGURE 7.12.

(b) The generator was operated at 9kV and 2mA; a nickel filter was used and the sample distance was increased to 29 cms. Exposures ranged from 10 hrs. to 15 secs. Samples were decomposed at 120°C. The results are listed in TABLE 7.24, and illustrated in FIGURE 7.13, where they are compared with the decomposition curve of the unirradiated material.

TABLE 7.23

40kV 20mA 13 cms 8 hr. 100°C					
t	p	t	p	t	p
5	0.14	28	15.03	36	79.42
10	0.26	29	26.60	40	80.00
15	0.37	30	41.76		
20	0.47	31	57.01	p_f	80.00
23	0.59	32	67.33	p_a	83.81
26	1.20	34	77.42		

TABLE 7.23 contd.

TABLE 7.23 contd.

1 hr. 100°C					
t	p	t	p	t	p
10	0.62	32	5.65	40	74.63
16	0.81	33	9.97	42	78.63
21	0.94	34	19.08	44	79.53
25	1.06	35	32.32	48	79.95
27	1.20	36	45.82	p_f	80.00
29	1.50	38	65.91	p_a	85.85

30 min. 100°C					
t	p	t	p	t	p
10	0.81	33	3.02	42	58.07
18	1.39	35	7.70	43	65.53
22	1.57	36	11.85	45	75.59
25	1.75	37	16.29	47	79.20
27	1.88	38	21.92	49	79.94
29	2.03	40	38.31	p_f	80.00
31	2.35	41	48.41	p_a	53.98

10 min. 100°C					
t	p	t	p	t	p
10	0.15	39	10.90	48	69.86
20	0.30	40	17.68	50	74.23
25	0.37	41	26.15	53	78.50
30	0.51	42	35.06	56	79.43
33	0.73	43	43.13	60	79.97
35	0.99	45	57.07	p_f	80.00
37	2.06	46	61.91	p_a	97.47

90 sec. 100°C					
t	p	t	p	t	p
16	0.02	49	34.86	66	80.05
25	0.03	51	48.83	70	80.05
34	0.12	53	59.45		
41	1.34	55	66.97	p_f	80.00
45	10.02	58	74.32	p_a	53.13
47	20.79	62	78.57		

TABLE 7.23 contd.

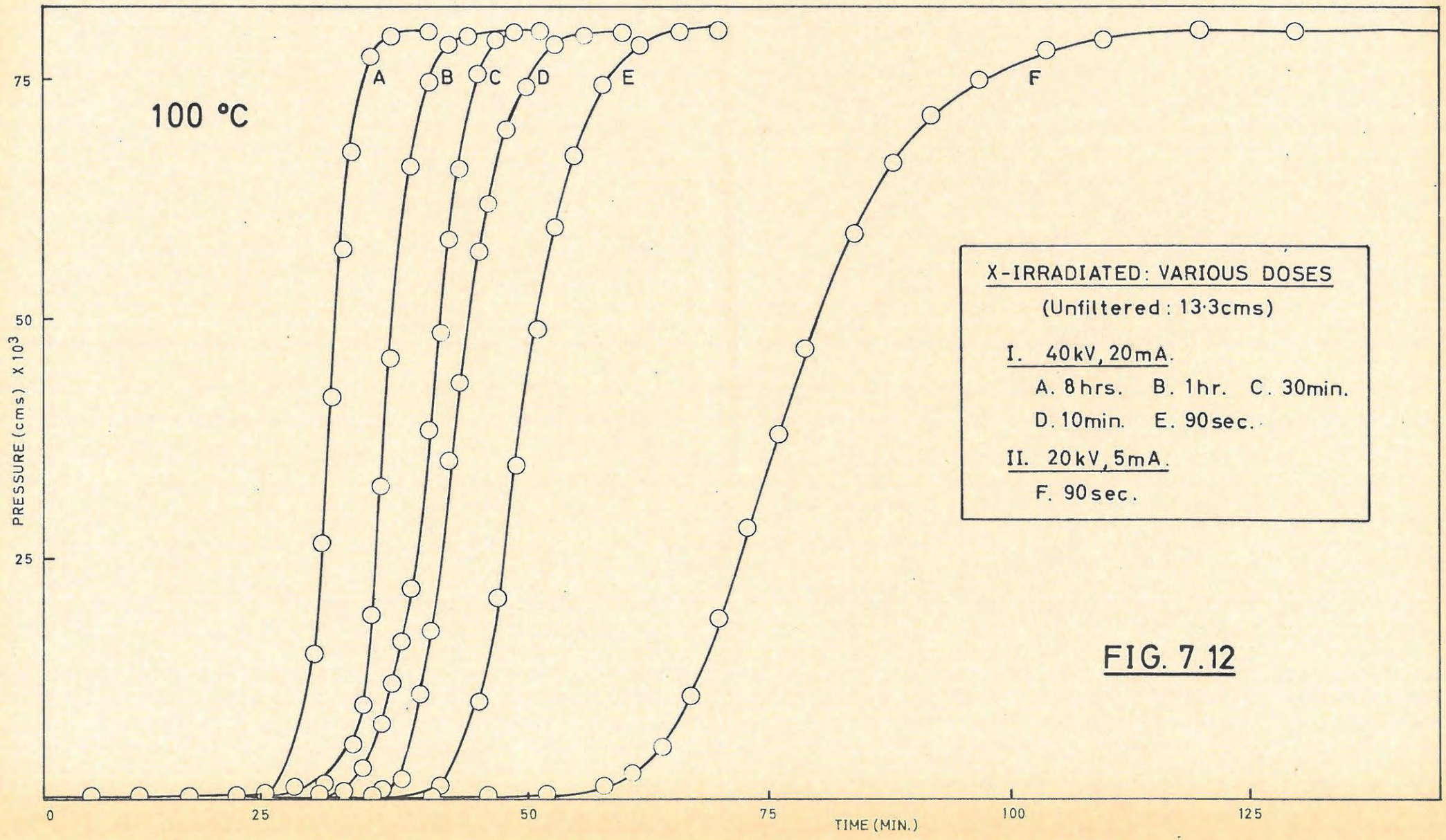
100 °C
A
B
C
D
E
F
X-IRRADIATED: VARIOUS DOSES
(Unfiltered : 13·3cms)
I. 40kV, 20mA.
A. 8hrs. B. 1hr. C. 30min.
D. 10min. E. 90sec.
II. 20kV, 5mA.
F. 90sec.
PRESSURE (cms) X 10³
TIME (MIN.)
0
25
50
75
100
125

FIG. 7.12

TABLE 7.23 contd.

20kV 5mA 13 cms 90 sec. 100°C					
t	p	t	p	t	p
20	0.02	67	10.54	92	71.03
40	0.09	70	18.62	97	74.72
46	0.18	73	28.13	104	77.87
52	0.39	76	37.77	110	78.92
58	1.38	79	46.87	120	80.15
61	2.61	84	58.97	p_f	80.00
64	5.25	88	66.09	p_a	77.66

TABLE 7.24.

9kV 2mA 29 cms Ni filter 10 hrs. 120°C					
t	p	t	p	t	p
6	0.18	26	44.45	34	72.89
12	0.32	27	52.01	36	74.46
16	0.37	28	57.80	40	77.49
20	0.67	29	62.05	45	79.02
23	8.09	30	65.12	51	79.97
24	21.42	31	67.88	p_f	80.00
25	34.25	32	69.63	p_a	79.97

5 mins. 120°C					
t	p	t	p	t	p
28	0.54	44	26.52	63	71.39
30	0.98	46	33.52	66	74.07
32	1.79	49	43.77	70	76.73
34	3.10	51	49.64	75	78.55
36	5.33	53	54.70	80	79.43
38	8.77	55	59.45		
40	13.54	57	63.07	p_f	80.00
42	19.67	60	68.08	p_a	108.2

TABLE 7.24 contd.

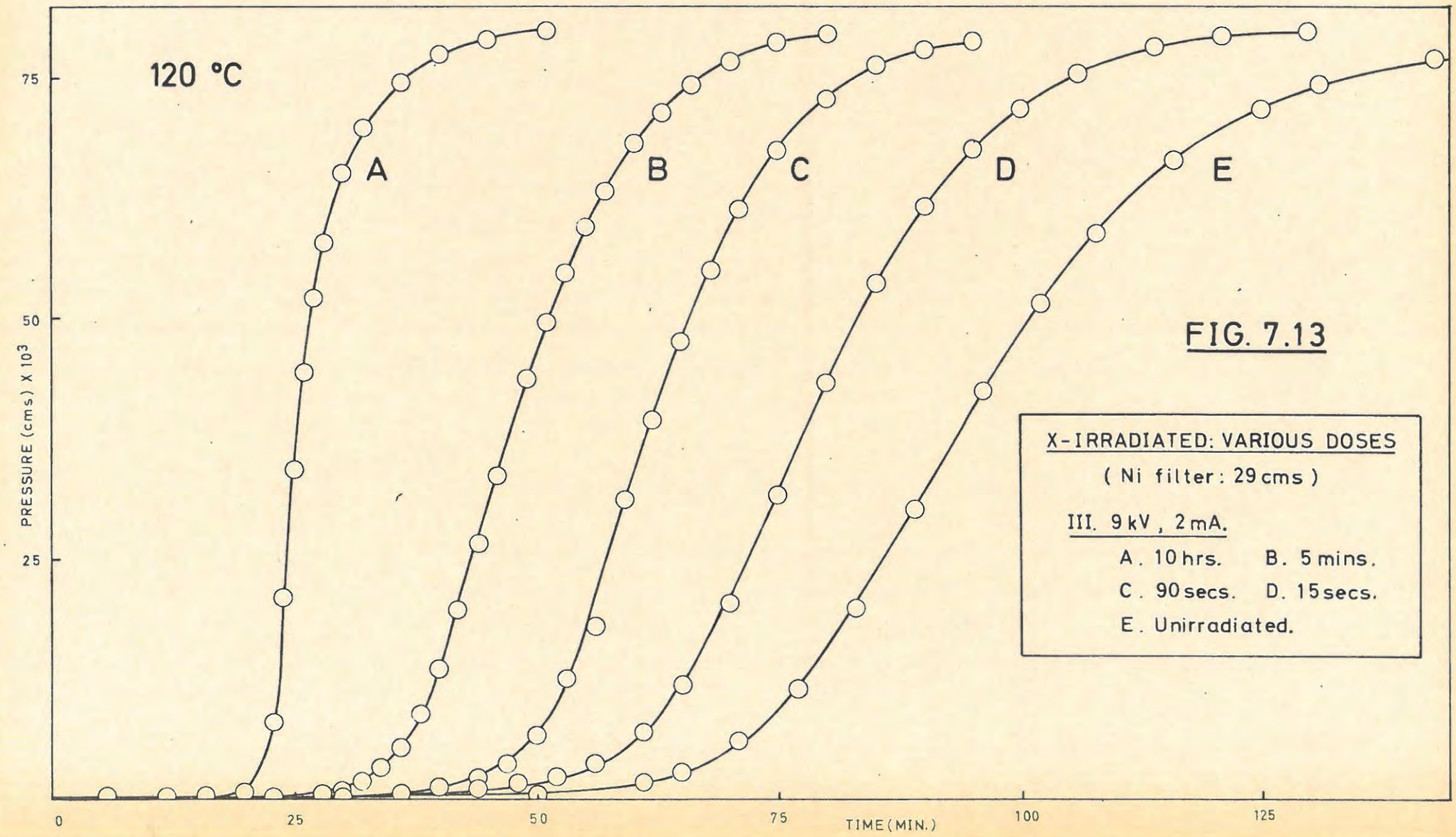
120 °C
A
B
C
D
E
PRESSURE (cms) X 10³
75
50
25
0
25
50
75
100
125
TIME (MIN.)
X-IRRADIATED: VARIOUS DOSES
(Ni filter : 29 cms)
III. 9 kV , 2 mA.
A . 10 hrs. B . 5 mins.
C . 90 secs. D . 15 secs.
E . Unirradiated.

FIG. 7.13

TABLE 7.24 contd.

90 secs. 120°C					
t	p	t	p	t	p
6	0.08	50	6.84	75	67.39
15	0.22	53	12.50	80	72.92
23	0.33	56	22.99	85	76.24
30	0.44	59	31.03	90	77.79
36	0.74	62	39.43	95	78.96
40	1.21	65	47.47		
44	2.29	68	55.02	p_f	80.00
47	3.89	71	61.39	p_a	60.7

15 secs. 120°C					
t	p	t	p	t	p
19	0.55	56	3.71	95	67.63
29	0.70	61	6.98	100	71.94
32	0.76	65	11.77	106	75.54
36	0.87	70	20.48	114	78.10
40	1.03	75	31.59	121	79.14
44	1.28	80	43.29	130	79.91
48	1.70	85	53.71	p_f	80.00
52	2.43	90	61.76	p_a	78.42

Once again the extent of fit of the power law (7.4) was not affected by increasing doses of X-rays. No linear relationship was found between the length of the induction period and the dose, or log (dose).

7.3.9.3. The Effect of Temperature.

Samples of material that had received an exposure of 10 mins. at 13 cms, in the filtered (Ni) beam of the X-ray generator, operating at 9kV and 2mA, were decomposed at various temperatures in the range 100°C to 120°C. The runs are tabulated in TABLE 7.25.

TABLE 7.25/...

TABLE 7.25

X-IRRADIATED CaN_6				100°C	
t	p	t	p	t	p
20	0.04	135	9.66	215	67.53
68	0.18	142	13.72	223	70.47
80	0.29	147	17.15	234	74.10
88	0.45	154	22.52	244	76.15
98	0.87	161	28.52	255	78.15
107	1.62	169	35.50	265	79.19
113	2.47	179	44.34	275	79.52
118	3.39	191	53.81		
123	4.76	196	57.06	p_f	80.00
129	6.83	207	63.84	p_a	89.46

				105°C	
t	p	t	p	t	p
45	0.40	105	18.44	156	71.70
53	0.47	110	25.96	167	75.60
62	0.59	115	32.95	176	77.43
71	0.82	120	40.20	192	79.11
77	1.18	125	46.67	210	80.00
83	1.98	130	52.62		
90	4.12	135	57.75	p_f	80.00
95	7.09	141	62.76	p_a	90.0
100	11.96	148	67.68		

				110°C	
t	p	t	p	t	p
36	0.25	75	19.43	105	67.55
46	1.21	78	25.01	110	71.92
54	2.26	82	32.80	116	74.91
60	3.87	86	40.46	122	77.32
64	5.95	90	47.60	130	78.95
68	9.40	95	55.65	p_f	80.00
72	14.69	100	62.28	p_a	86.8

TABLE 7.25 contd.

TABLE 7.25 contd.

115°C					
t	p	t	p	t	p
20	0.57	54	14.40	74	68.46
26	0.76	56	20.58	78	72.89
32	0.97	58	27.67	83	76.70
38	1.28	60	35.29	90	80.09
41	1.55	62	42.09	95	80.09
45	2.22	64	48.59	100	79.84
48	3.35	66	54.01		
50	5.86	68	58.32	p_f	80.00
52	10.05	71	64.32	p_a	80.83

120°C					
t	p	t	p	t	p
8	0.17	35	8.13	48	66.20
14	0.27	37	15.23	51	71.75
18	0.34	39	27.00	54	74.18
22	0.43	40	33.68	59	78.29
27	0.80	41	40.20	67	79.55
29	1.25	42	46.09		
31	2.22	44	56.84	p_f	80.00
33	4.10	46	61.04	p_a	61.67

7.3.9.4. Mathematical Analysis.

A typical pressure-time plot for X-irradiated material is shown in FIGURE 7.14, curve B.

The analysis applied to both the unirradiated and the gamma-irradiated salt holds for the X-irradiated material. Over the acceleratory period:

$$(p - p_o)^{\frac{1}{3}} = k_1 t + C_1 \qquad \ldots\ldots\ldots \qquad (7.4)$$

holds for $0.013 < \alpha < 0.5$ FIGURE 7.14, curve A.

For the decay period:

$$1 - (1 - p/p_f)^{\frac{1}{3}} = k_2 t \qquad \ldots\ldots\ldots \qquad (7.5)$$

applies/...

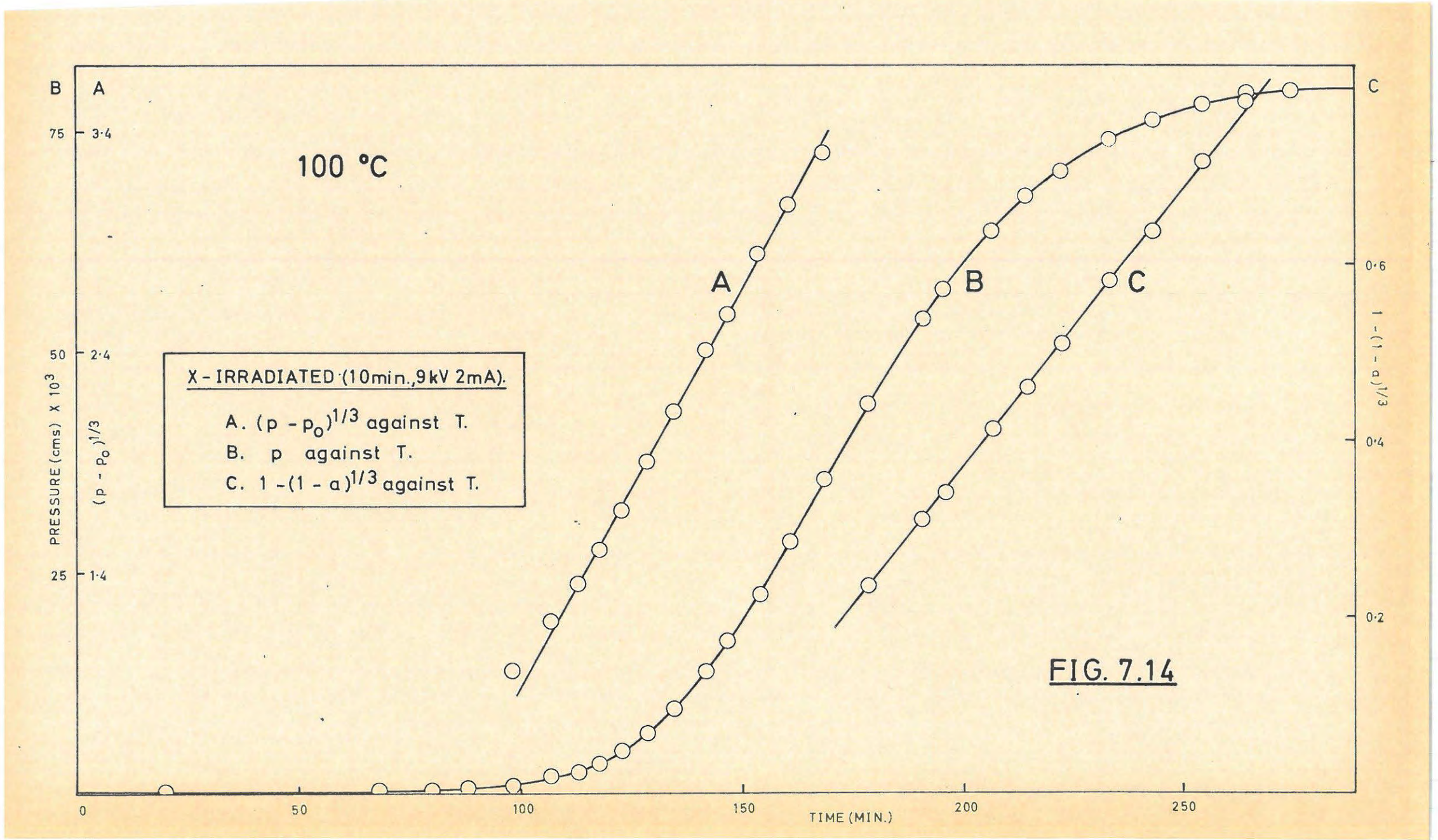
100 °C
X - IRRADIATED (10min., 9kV 2mA).
A. $(p - p_o)^{1/3}$ against T.
B. p against T.
C. $1 - (1 - a)^{1/3}$ against T.
A
B
C
PRESSURE (cms) X 10^3
$(p - p_o)^{1/3}$
$1 - (1 - a)^{1/3}$
TIME (MIN.)
75
50
25
3·4
2·4
1·4
0·6
0·4
0·2
0
50
100
150
200
250

FIG. 7.14

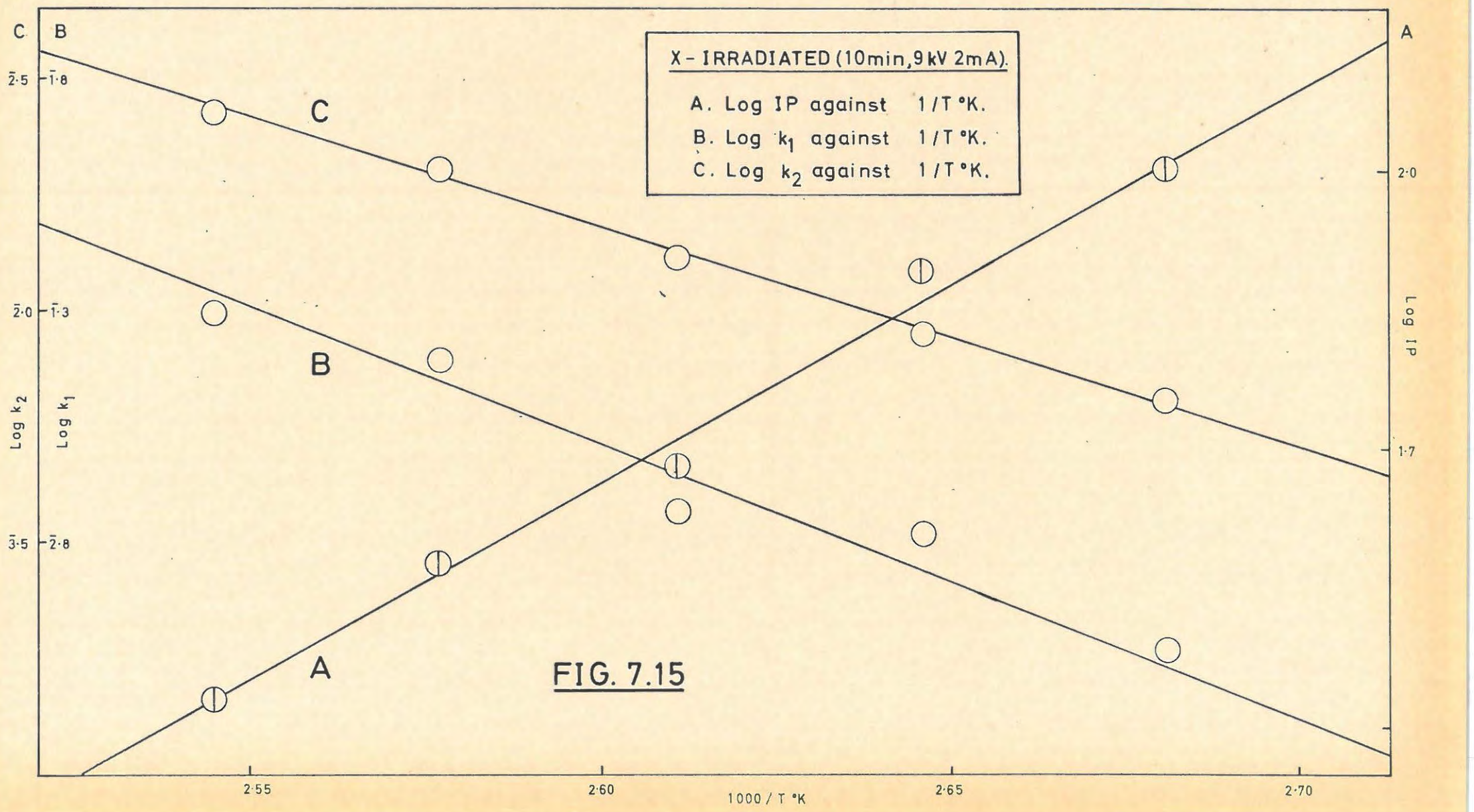
X - IRRADIATED (10min, 9 kV 2mA).
A. Log IP against 1/T °K.
B. Log k_1 against 1/T °K.
C. Log k_2 against 1/T °K.
C
B
A
Log k_2
Log k_1
Log IP
$\bar{2}\cdot5$
$\bar{1}\cdot8$
$\bar{2}\cdot0$
$\bar{1}\cdot3$
$\bar{3}\cdot5$
$\bar{2}\cdot8$
2·0
1·7
2·55
2·60
2·65
2·70
1000 / T °K

FIG. 7.15

applies from $\alpha = 0.5$ to $\alpha = 0.99$. FIGURE 7.14, curve C.

The values of k_1 and k_2, as well as the lengths of the induction periods at various temperatures are given in TABLE 7.26.

The values of log IP, log k_1 and log k_2 are plotted against $1/T^{o}K$ in FIGURE 7.15. The values of the activation energies obtained from these plots are:-

induction period : 19.2 kcal/mole.

acceleratory reaction: 27.1 kcal/mole.

decay reaction : 21.9 kcal/mole.

TABLE 7.26

X-IRRADIATED CaN_6			
Temp. ^{o}C	IP (Induction Period) (mins)	Acceleratory $k_1 \times 100$ (cms $Hg^{\frac{1}{3}}$ per min)	Decay $k_2 \times 1000$ (per min)
100	102	3.671	6.36
105	78	6.55	8.90
110	48	7.40	12.88
115	38	15.6	20.10
120	27	19.8	26.55

7.3.10. THE EFFECT OF PRE-IRRADIATION WITH ULTRA-VIOLET LIGHT.

7.3.10.1. Irradiation.

The UV-source was a Philips UV lamp 125W, Type 57202E/70. The conditions for irradiation are described in the next section.

7.3.10.2. Reproducibility and Handling Conditions.

Thinly spread samples, in sealed cellophane envelopes were irradiated at a distance of 24 cms from the lamp, for 16 hours. The atmosphere inside the envelope was:- air (Run 1); nitrogen (Run 2) and argon (Run 3). Samples of

each/...

each were decomposed at 120°C. The runs are given in TABLE 7.27.

The runs are almost superimposable, showing that air does not affect the irradiation.

Further irradiations were carried out in air at a distance of 13 cms from the lamp. The sample was placed in a porcelain dish and stirred during irradiation.

TABLE 7.27

UV-IRRADIATED	Run 1	AIR		120°C	
t	p	t	p	t	p
6	0.06	29	34.96	45	73.70
12	0.15	30	39.85	50	76.72
16	0.22	32	47.51	56	78.93
21	1.12	34	53.91		
24	3.43	36	58.57	p_f	80.00
26	11.44	39	64.57	p_a	52.0
28	29.12	42	69.36		

	Run 2	NITROGEN		120°C	
t	p	t	p	t	p
7	0.14	26	14.05	39	62.53
12	0.22	27	18.69	42	67.62
17	0.54	28	23.41	46	72.62
20	1.51	29	28.44	50	75.67
22	3.42	30	32.86	56	78.57
23	5.60	32	41.98	62	79.43
24	7.60	34	49.25	p_f	80.00
25	10.20	36	55.30	p_a	93.33

	Run 3	ARGON		120°C	
t	p	t	p	t	p
6	0.05	26	11.79	42	62.10
12	0.12	27	16.55	46	68.28
16	0.24	28	20.74	50	72.61

TABLE 7.27 contd.

TABLE 7.27 contd.

t	p	t	p	t	p
19	0.68	29	24.68	55	76.37
21	1.48	30	28.67	63	79.83
22	2.20	32	36.21	66	79.67
23	3.24	34	42.62	70	79.91
24	4.93	36	48.26	p_f	80.00
25	7.70	39	55.82	p_a	73.89

7.3.10.3. The Effect of Various Doses of UV-light.

Samples that had received doses, under the conditions described above, ranging from 430 mins. to 10 mins., were decomposed at 120°C. The results are listed in TABLE 7.28 and illustrated in FIGURE 7.16.

TABLE 7.28

UV-IRRADIATED		430 mins.		120°C	
t	p	t	p	t	p
5	0.30	25	32.39	38	74.92
10	0.55	26	38.50	42	77.81
14	0.87	27	44.12	46	79.10
17	1.61	28	49.22	50	79.79
19	3.12	29	53.68		
21	8.53	30	57.44	p_f	80.00
23	19.45	32	64.24	p_a	78.77
24	25.90	35	71.11		

		140 mins.		120°C	
t	p	t	p	t	p
11	0.23	29	27.10	45	75.13
16	0.50	31	37.14	50	78.57
20	1.50	33	46.09	55	79.94
23	3.86	35	54.15		
25	7.70	38	63.12	p_f	80.00
27	16.41	41	69.63	p_a	61.97

TABLE 7.28 contd.

TABLE 7.28 contd.

40 mins.				120°C	
t	p	t	p	t	p
11	0.01	37	23.34	60	73.13
18	0.10	40	33.27	65	77.03
23	0.68	43	42.44	70	78.94
28	2.87	46	50.60	75	79.66
30	4.82	49	57.52	80	79.76
32	7.87	52	62.84	p_f	80.00
35	16.88	56	68.90	p_a	70.77

20 mins.				120°C	
t	p	t	p	t	p
10	0.07	38	7.41	71	68.05
16	0.14	41	12.12	77	74.36
21	0.29	44	17.41	84	78.78
25	0.60	48	25.79	90	80.00
29	1.37	53	36.88		
32	2.45	59	49.16	p_f	80.00
35	4.31	65	59.80	p_a	67.01

10 mins.				120°C	
t	p	t	p	t	p
7	0.03	43	6.49	78	70.31
12	0.07	47	11.34	83	75.27
16	0.12	51	18.12	88	78.44
21	0.21	54	23.91	95	80.05
26	0.46	57	30.04	100	80.05
30	0.86	60	36.22		
34	1.64	64	45.07	p_f	80.00
37	2.60	68	53.00	p_a	82.05
40	4.14	73	62.62		

The/...

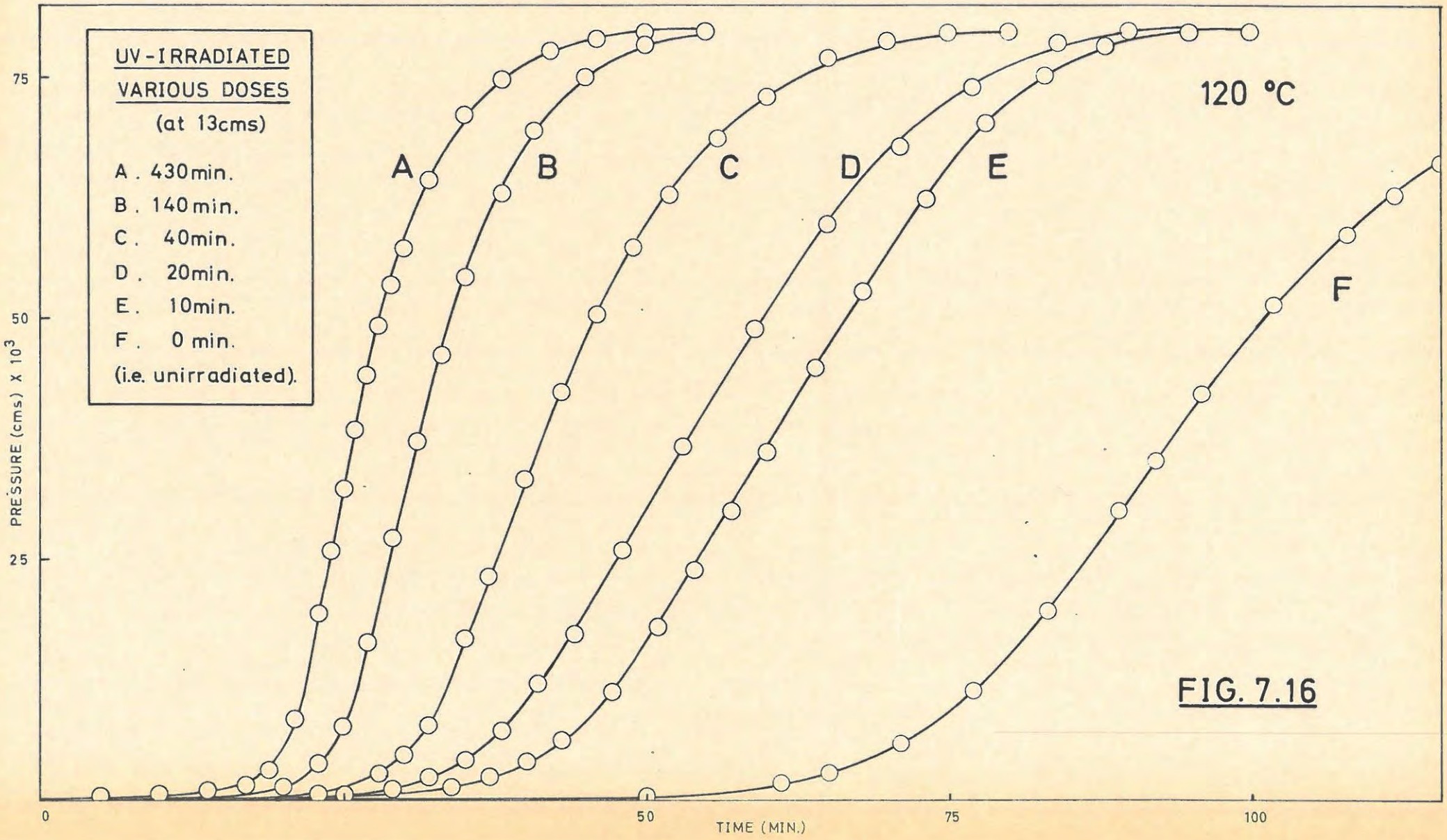
UV-IRRADIATED
VARIOUS DOSES
(at 13cms)
A . 430min.
B . 140 min.
C . 40min.
D . 20min.
E . 10min.
F . 0 min.
(i.e. unirradiated).
120 °C
A
B
C
D
E
F
PRESSURE (cms) X 10³
75
50
25
0
50
75
100
TIME (MIN.)

FIG. 7.16

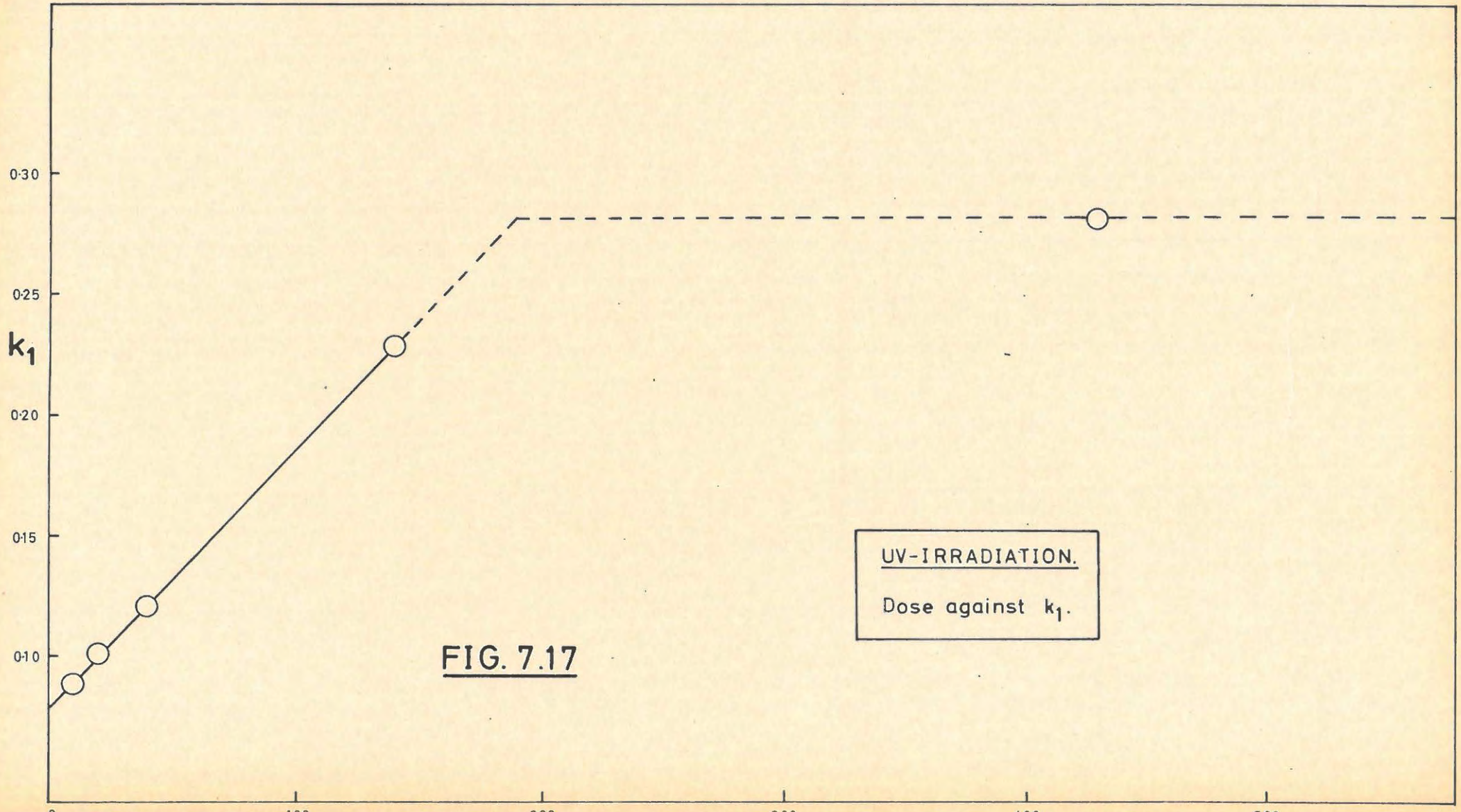
0·30
0·25
k_1
0·20
0·15
0·10
0
100
200
300
400
500
EXPOSURE (MINS).
UV-IRRADIATION.
Dose against k_1.

FIG. 7.17

The lengths of the induction periods (IP), and the values of k_1 for the acceleratory periods, are tabulated against the irradiation dose and log (dose) in TABLE 7.29. No linear relationship between the length of the induction period (IP) and the dose or log (dose) was found. A plot of k_1 against dose, FIGURE 7.17, is linear up to at least an exposure of 140 mins., and by 430 mins. k_1 has reached a "saturation" value.

Once again the extent of fit of the $p^{\frac{1}{3}}$ plot (Equation 7.4) over the acceleratory period was not affected by increasing irradiation dose, and remained constant at up to $\alpha \approx 0.5$.

TABLE 7.29

UV-IRRADIATED		120°C	
DOSE (d) (mins)	log d	IP (mins)	k_1 ($cm^{\frac{1}{3}}$ per min)
10	1.000	32	0.0885
20	1.301	26	0.1005
40	1.602	23	0.1205
140	2.146	19	0.2290
430	2.634	16	0.2814

7.3.10.4. The Effect of Temperature.

Samples from a batch of material that had received an exposure of 430 mins. at 13 cms from the UV-lamp, with stirring in air, were decomposed at various temperatures in the range 100°C to 125°C. The runs are tabulated in TABLE 7.30.

TABLE 7.30/...

TABLE 7.30

UV-IRRADIATED				100°C	
t	p	t	p	t	p
11	0.01	80	12.81	166	67.49
20	0.05	86	17.22	178	71.32
32	0.21	95	24.63	190	74.15
40	0.45	103	31.18	196	75.47
48	1.01	107	34.27	204	76.23
54	1.82	115	40.32	220	78.51
59	2.86	125	47.63	240	79.88
66	5.20	135	53.91	p_f	80.00
70	6.88	145	58.96	p_a	74.02
75	9.62	155	63.35		

				110°C	
t	p	t	p	t	p
6	0.07	42	9.87	70	61.34
12	0.40	44	13.93	75	66.56
15	0.52	46	17.85	80	70.34
20	0.72	48	21.87	86	74.05
24	0.94	51	28.21	92	76.15
27	1.16	54	34.82	100	78.04
30	1.50	57	41.33	110	79.78
33	2.05	60	46.84		
36	2.98	63	52.12	p_f	80.00
39	5.09	66	56.21	p_a	92.77

				115°C	
t	p	t	p	t	p
8	0.05	29	10.87	51	65.85
12	0.10	30	13.57	54	69.27
16	0.20	31	16.71	57	72.27
18	0.37	32	20.02	61	75.11
20	0.72	34	26.42	65	77.42
21	1.00	36	33.14	70	79.00
23	1.90	39	42.20	75	79.68
24	2.59	41	47.60	80	80.05
25	3.50	43	52.41		
27	6.28	45	56.36	p_f	80.00
28	8.35	48	61.91	p_a	103.07

TABLE 7.30 contd.

TABLE 7.30 contd.

120°C					
t	p	t	p	t	p
5	0.30	25	32.39	38	74.92
10	0.55	26	38.50	42	77.81
14	0.87	27	44.12	46	79.10
17	1.61	28	49.22	50	79.79
19	3.12	29	53.68		
21	8.53	30	57.44	p_f	80.00
23	19.45	32	64.24	p_a	78.77
24	25.90	35	71.11		

125°C 3.1 mg.					
t	p	t	p	t	p
5	0.17	20	28.35	30	75.79
8	0.25	21	38.02	32	77.44
11	0.38	22	46.77	35	78.95
14	0.88	23	54.33	40	79.98
16	2.31	24	59.68	45	80.00
17	4.62	25	64.47		
18	8.86	26	67.61	p_f	80.00
19	18.50	28	72.71	p_a	92.70

7.3.10.5. Mathematical Analysis.

A typical p/t plot for the decomposition of UV-irradiated material is shown in FIGURE 7.18, curve B. Once again the same analyses as for the unirradiated decomposition, apply. Over the acceleratory period:

$$(p - p_o)^{\frac{1}{3}} = k_1 t + C_1 \quad \ldots\ldots\ldots \quad (7.4)$$

holds for $0.010 < \alpha < 0.39$. FIGURE 7.18, curve A.

The contracting sphere equation:

$$1 - (1 - p/p_f)^{\frac{1}{3}} = k_2 t \quad \ldots\ldots\ldots \quad (7.5)$$

applies to the decay from $\alpha = 0.42$ to $\alpha = 0.98$. FIGURE 7.18, curve C.

This/...

This analysis thus holds for the unirradiated salt and for material irradiated with gamma-rays, with X-rays and with UV-light.

The values of k_1 and k_2, as well as the lengths of the induction periods at various temperatures, are tabulated in TABLE 7.31.

The values of log IP, log k_1 and log k_2 are plotted against $1/T^{o}K$ in FIGURE 7.19. The values of the activation energies obtained from these plots are:-

Induction period : 16.2 kcal/mole.
Acceleratory reaction: 27.4 kcal/mole.
Decay reaction : 25.7 kcal/mole.

TABLE 7.31

UV-IRRADIATED CaN_6			
Temp. ^{o}C	IP (Induction Period) mins.	Acceleratory $k_1 \times 100$ (cm $Hg^{\frac{1}{3}}$ per min)	Decay $k_2 \times 1000$ (per min)
100	48	4.20	4.983
110	27	7.83	12.56
115	20	17.38	17.23
120	16	29.00	30.15
125	12	44.40	48.30

7.3.11. Comparison of Activation Energies.

TABLE 7.32

COMPARISON OF ACTIVATION ENERGIES (kcal/mole).			
	INDUCTION PERIOD	ACCELERATORY	DECAY
UNIRRADIATED	18.2	27.1	18.8
γ-IRRADIATED	19.8	28.1	22.5
X-IRRADIATED	19.2	27.1	21.9
UV-IRRADIATED	16.2	27.4	25.7

7.3.11./...

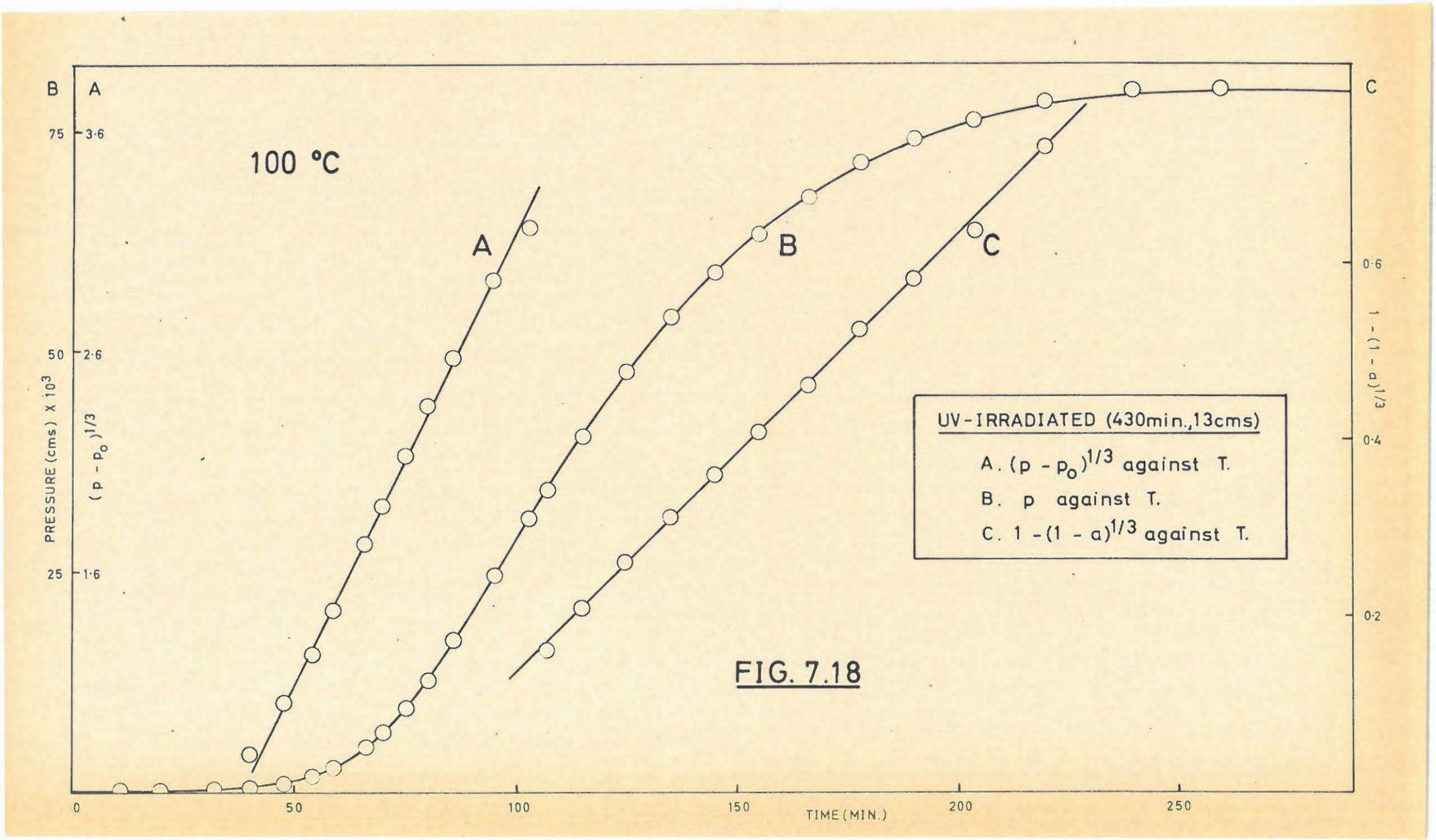
B
A
C
75
50
25
3·6
2·6
1·6
0·6
0·4
0·2
100 °C
A
B
C
PRESSURE (cms) X 10³
(p - p₀)^1/3
1 - (1 - a)^1/3
UV-IRRADIATED (430min.,13cms)
A. (p - p₀)^1/3 against T.
B. p against T.
C. 1 - (1 - a)^1/3 against T.
0
50
100
150
200
250
TIME (MIN.)

FIG. 7.18

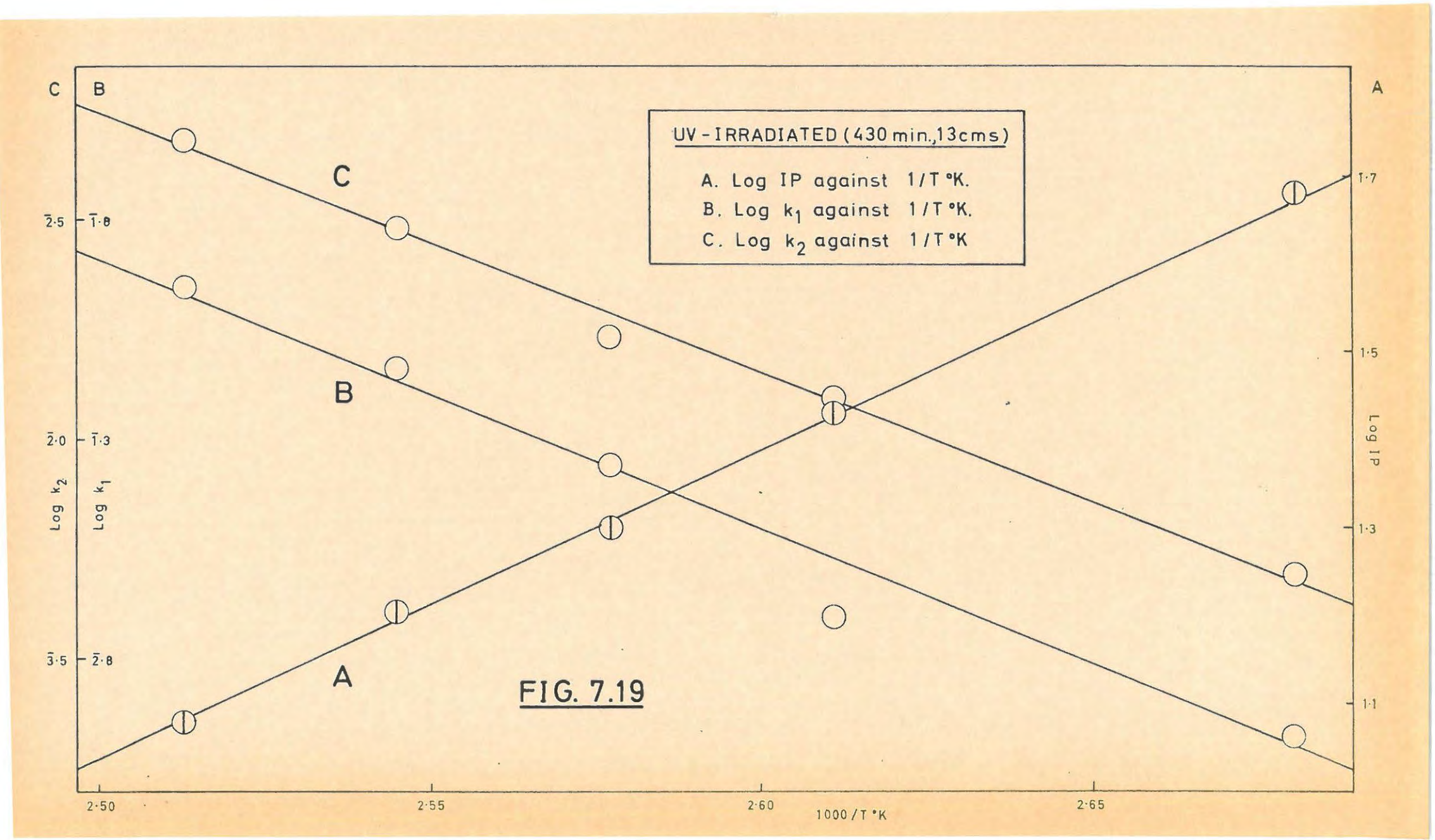
UV - IRRADIATED (430 min., 13cms)
A. Log IP against 1/T °K.
B. Log k_1 against 1/T °K.
C. Log k_2 against 1/T °K
C
B
A
$\bar{2}\cdot5$
$\bar{1}\cdot8$
$\bar{2}\cdot0$
$\bar{1}\cdot3$
$\bar{3}\cdot5$
$\bar{2}\cdot8$
Log k_2
Log k_1
1·7
1·5
1·3
1·1
Log IP
2·50
2·55
2·60
2·65
1000 / T °K

FIG. 7.19

7.3.12. Percentage Decomposition.

(a) Line Volume.

Known pressures of dry nitrogen were expanded from the calibrated bulb of the McLeod gauge into the evacuated decomposition system and the resulting pressure measured after thermal equilibrium had been reached. The volume of the system was then calculated using the gas laws.

With the liquid-air trap in position the line volume was found to be 1040 ml.

The volume of the liquid-air trap was 180 ml.

The temperature of the trap was 79°K giving it an "effective volume" at 25°C (298°K) of 680 ml.

The effective volume at 25°C of the decomposition system is then 1540 ml.

(b) Possible Reactions.

(i) $CaN_6 = Ca + 3N_2$

1 mg. $p_f = 29.7 \times 10^{-3}$ cm Hg at 25°C

(ii) $3\ CaN_6 = Ca_3N_2 + 8\ N_2$

1 mg. $p_f = 26.4 \times 10^{-3}$ cm Hg at 25°C

Calculations of the percentage decomposition based on equation (ii) above, generally gave values exceeding 100%.

Calculated values based on equation (i) are given in TABLE 7.33.

Pre-irradiation produced no detectable change in the percentage decomposition.

TABLE 7.33/...

TABLE 7.33

PERCENTAGE DECOMPOSITION CaN_6			
Temp. °C	Sample Wt. mg.	p_f cm Hg x 10^3	% Decomposition
UNIRRADIATED			
105	3.4	94.3	93.3
110	2.9	76.8	89.2
110	2.9	84.0	97.6
115	3.6	98.1	91.9
120	3.4	95.0	93.9
120	3.6	107	100.0
125	3.7	97.7	88.9
130	3.1	85.0	92.3
GAMMA-IRRADIATED		0.25 Mrad	
100	2.0	56.0	94.3
UV-IRRADIATED			
120	4.0	110.4	92.9

The Average Percentage Decomposition (Unirradiated) = 93.4%.

7.4. DISCUSSION/...

7.4. DISCUSSION.

7.4.1. Unirradiated CaN_6.

7.4.1.1. General Characteristics.

Reproducibility of results for the isothermal decomposition was highly satisfactory and better than had been achieved by previous workers. The p/t plots showed a very slow initial reaction with little gas evolved, followed by an acceleratory period obeying a third power law, and finally a decay period fitted by the contracting sphere formula. The degree of fit of the mathematical equations was the same at all temperatures, and there was no change in the value of α_i, the fractional decomposition corresponding to the inflexion point in the p/t plots.

7.4.1.2. The Physical Nature of the Nuclei and their Mode of Growth.

The one-third power in the equation (7.4) can be ascribed to:-

(i) the two-dimensional growth of nuclei increasing in number, linearly with time;

(ii) three-dimensional growth of nuclei from a fixed number of centres; or

(iii)one-dimensional nuclei, increasing in number with the square of time. Possibility (iii) is unlikely because of the relatively high value of α_i, and the applicability of the contracting sphere formula in the decay region.

The effect of interrupting the run before the decay period, destroying the surface nuclei by the admission of water vapour, and then continuing the run, is to reproduce the "induction period" and reduce the rate constant k_1. These results contradict possibility (ii), since destruction of the fixed number of nuclei should destroy the reaction,

or/...

or at least cause any new rate to be very different from the original value, i.e. if nuclei form at the interface of the product of the water + nucleus reaction. Nuclei are not present at the commencement of heating since admission of water vapour at t = 0, had no effect on the subsequent decomposition.

For reasons that will be given when dealing with the irradiated salt, it is supposed that the nuclei are mainly surface ones. With surface nuclei and single crystals, α_i should be fairly small. The value of $\alpha_i \approx 0.50$, obtained, is due, no doubt, to the very small particle size of the ground material.

The fall in k_1 after interruption and admission of water vapour, can be attributed to the 'de-activation' of certain areas of the particle surface. k_1 is dependent on the number of nuclei at the start of the acceleration and a decrease in this number will thus reduce the value of k_1.

The decay period commences when the surface nuclei touch, and the reaction proceeds inwards with the reactant/product interface taking the form of a contracting envelope.

7.4.1.3. The Mechanism of Formation and Growth of Nuclei.

The decomposition of solids is governed by the formation and growth of nuclei and these have often been observed and photographed. They are formed on the external surface and, to a lesser extent, within the crystal. Clustering may be observed, or the distribution of the nuclei may suggest places where formation is preferred. These preferred positions are likely to be localities on the surface of the particle, such as surface cracks or lines of strain, where disorganisation or mechanical damage has taken place and there is a higher thermodynamic instability, and unsaturation of cohesive forces.

Examination/...

Examination of the activation energies obtained for the thermal decomposition, suggests that the same rate-determining process is occurring during the "induction period" and the decay stage, since the energies are approximately the same (18.2 kcal/mole and 18.8 kcal/mole respectively). The value for the acceleratory reaction (27.1 kcal/mole), is considerably higher and is consistent with the value of 26.9 kcal/mole, obtained on a second preparation which had received similar grinding.

FIGURE 7.1, curve D, shows that what has been called the "induction period", is really a slow reaction. As in BaN_6 [361], there is assumed to be a slow surface decomposition when N_2 is liberated as follows:-

$$2N_3^- \longrightarrow 3N_2 + 2e \qquad \ldots\ldots\ldots \quad (7.9)$$

Calcium atoms will be formed as calcium ions combine with the freed electrons. These Ca atoms will be initially at the interatomic spacing in CaN_6, but when a critical concentration is reached, they will recrystallise to form Ca metal and thus a metal speck, with the associated electronic properties of a metal, will be formed. Work on the structure and properties of thin films of metals [362], indicates that the structure of a metal in a thin film is that of the bulk metal, and that pseudomorphism is not shown except by elements with a high degree of homopolar bonding e.g. Bi and Ge. Films are formed by lateral growth of nuclei and may become continuous at thicknesses as low as 50Å. The character of the conductivity of such metal films corresponds very closely to that of the massive metal.

The slow step is assumed to be (7.9) above, and the activation energy obtained (18.2 kcal/mole) is for this reaction. As with BaN_6, a portion of the evolved N_2 will be absorbed on the powder.

The/...

The acceleratory period commences when the metal nuclei are formed. N_2 is evolved by the mechanism suggested for BaN_6, namely the elevation of an electron from an azide ion into the conduction band of the metal, followed by the reaction of an adjacent azide ion and the azide radical when the former receives sufficient thermal energy. N_2 will be produced by this reaction. The results of Heal [363] on the decomposition of NaN_3 by X-rays, suggested that single azide ions do not break up to any extent by the mechanism.

$$N_3^- \longrightarrow N_2 + N + e \qquad \ldots\ldots\ldots \qquad (7.10)$$

(Activation Energy 37 kcal/mole), since the resulting nitrogen atoms would capture electrons from the conduction band to give N^{-3}. Reaction probably occurs between pairs of azide ions or radicals (either member, or both members, of a pair being excited), giving molecular nitrogen directly.

$$2N_3^- \longrightarrow 3N_2 + 2e \qquad \ldots\ldots\ldots \qquad (7.11)$$

$$2N_3 \longrightarrow 3N_2 \qquad \ldots\ldots\ldots \qquad (7.12)$$

$$N_3^- + N_3 \longrightarrow 3N_2 + e \qquad \ldots\ldots\ldots \qquad (7.13)$$

This last reaction is unimolecular as far as positive holes are concerned, and was hence suitable for explaining the observed increase in decomposition with the first power of the X-ray intensity. Heal stated that the activation energy for the reaction must be very low, for otherwise the steady-state concentration of trapped holes would have risen so high that extensive recombination with conduction electrons would have been caused, leading to decomposition rates proportional to less than the first power of the intensity.

F-centres will also be formed and on their collapse, the resulting Ca atoms will add on to the growing nucleus. The rate-determining step for the N_2 evolution is assumed to be the first one i.e. the transfer of an electron to the conduction band. The energy for this transfer, which is the

activation/...

activation energy for the acceleratory reaction, is 27 kcal/mole, which is almost the same as the activation energies for the acceleratory periods of BaN_6 (26.8 kcal/mole) [364] and SrN_6 (25.0 kcal/mole) [365]. The essential role played by the Ca metal nucleus is demonstrated by the fact that destruction of such nuclei by the admission of water vapour, causes the reaction to begin afresh.

The decay reaction commences when the surface nuclei touch and reaction takes place at the contracting interface. The mechanism here, is similar to that occurring during the "induction period", since the activation energies are approximately the same. The metal sheath around the azide particle will exert compressive stresses on the azide lattice. Distortion of adjacent azide ions at the reactant/product interface will be a maximum. In this region of strain the azide ions will interact. It is reasonable to expect this compressive effect as the cell parameters for CaN_6 (orthorhombic) are [366]:

$$a = 11.62\text{Å},\quad b = 10.92\text{Å},\quad c = 5.66\text{Å};$$

while for Ca metal (cubic) [367]:

$$a = 5.565\text{Å}$$

Another possible means by which strain may be created at the reactant/product interface, is by the pressure exerted on the azide lattice by the evolved N_2 if escape is not easy.

During the acceleratory period this strain should be slight since the nucleus is in effect a thin film of metal spreading laterally.

7.4.2. Pre-irradiated (γ-rays) CaN_6.

Irradiation of a solid with high-energy γ-rays is, in effect, an internal bombardment by electrons varying in velocity from very fast to very slow, and the possible

reactions/...

reactions in the solid are numerous. The following changes are possible in CaN_6 during irradiation.

$$N_3^- \longrightarrow N_3 + e^-$$

$$N_3 + e^- \longrightarrow N_3^-$$

$$N_3 + N_3^{-*} \longrightarrow 3N_2 + \boxed{A} + F$$

$$A + e^- \longrightarrow F$$

$$N_3 + F \longrightarrow N_3^- + \boxed{A}$$

$$N_3 + C + N_3 \longrightarrow 3N_2 + \boxed{C} + 2\boxed{A}$$

where $\boxed{A}$ = anion vacancy,

$\boxed{C}$ = cation vacancy,

F = F-centre,

N_3^{-*} = excited state (internal excitation or an exciton)

Thus the CaN_6 after irradiation, may contain N_2, cation and anion vacancies and F-centres. The absence of any colouration after irradiation suggests that F-centres are not produced in an appreciable amount.

The effect of the aggregation at the surface, of the vacancies which are produced, will be to alter the surface topography and thus create additional centres at which strained azide radicals will decompose, (cf. unirradiated CaN_6 during the "induction period"). Thus, at a particular temperature, the time taken to reach the critical concentration of Ca atoms for recrystallisation to a metal nucleus, will be considerably reduced i.e. the "induction period" will be shortened. At the start of the acceleration, reaction proceeds from many more centres and consequently k_1 will be increased. The accompanying increase in k_2 indicates that nucleation occurs at internal surfaces, probably grain boundaries, so that when the growing nuclei touch, there will be a number of "contracting envelopes", both external and internal, and the rate of evolution of N_2 will be increased.

At/...

At 110°C the "induction period" of a 0.25 Mrad γ-irradiated sample was decreased to 15% of the unirradiated value, while k_1 and k_2 were increased by 1750% and 380% respectively.

The admission of water vapour will destroy the metal nuclei. On recommencing the reaction, the centres of product of the Ca/H_2O reaction will act as vacancy traps and thus the nuclei will form earlier at these points than before interruption. Consequently the "induction period" will become shorter but k_1 will fall as a result of the decrease in the number of available vacancies i.e. a depletion of the "vacancy reservoir" will have occurred during the first phase of the decomposition. Interruption in the decay will lead to a greatly reduced, but not eliminated, reaction since the available vacancies will have been largely used up.

The runs involving interruption of the thermal decomposition of an unirradiated specimen, followed by irradiation (FIGURE 7.9), show that the vacancies produced on irradiation can accelerate the decomposition even in the decay period. The acceleration at this stage in the decomposition must arise from internal nuclei which are only generated in pre-irradiated material. The saturation effect in k_1 and k_2 is due to the fact that only a limited number of reaction envelopes is possible.

7.4.3. Pre-irradiated (X-rays) CaN_6.

The effects were similar to those for γ-rays. This is to be expected as here again the effect of X-rays will be the creation of vacancies.

7.4.4. Pre-irradiated (UV-light) CaN_6.

Effects similar to those in 7.4.2. and 7.4.3. above, were obtained. Again it appears that internal nucleation occurs.

7.4.5./...

7.4.5. General.

During the writing of this work, a paper by Tompkins and Young [368] has appeared which must be commented on, since some of the findings reported here are at variance with their results.

Tompkins and Young, using fine crystals of calcium azide, precipated with absolute alcohol, studied the thermal decomposition of freshly prepared, aged, and annealed material before and after irradiation with UV-light.

Ionic conductivity measurements on unirradiated material suggested that the ageing and the annealing processes consisted essentially of the aggregation, or diffusion to boundary sinks, of vacancies, present in fresh material in excess of their equilibrium number at room temperature. Annealing commenced within the temperature range of measurable decomposition (70 - 130°C), and the temperature at which this equilibrium concentration of vacancies is reached is stated to be 97°C. On cooling the ionic conductivity associated with a normal equilibrium concentration of single vacancies was measured.

The acceleratory period in the thermal decomposition of fresh unirradiated material was fitted by the cubic power law:-

$$\alpha = k^3(t - t_o)^3$$

for ($0.05 < \alpha < 0.4$). This was interpreted as three-dimensional growth of a constant number of nuclei. Activation energies of 35 kcal/mole for individual runs, and 18 kcal/mole for split runs, were obtained. 18 kcal/mole was taken to be the "true" activation energy of radial growth, while the "apparent" activation energy of 35 kcal/mole was said to include a term allowing for the variation of the pre-exponential factor with temperature. This factor

contains/...

the number of active growth nuclei, and this number was thus assumed to vary with temperature.

The mechanism proposed was that during the period t_o, annealing of excess vacancies within the surface region occurs. These diffuse to the surface to form clusters or potential nucleus-forming sites, which become active growth nuclei on trapping an electron or F-centre. No explanation of the source of these electrons was given further than to say that the rate of capture is largely controlled by the slow rate of production of electrons. A detailed mechanism in terms of the chemical reactions occurring, was not put forward and, in particular, the mode of growth of nuclei was not postulated. As soon as the clusters become active growth nuclei, few new growth nuclei are created. No mention is made of the effect of ageing on the induction period, t_o, nor was the decay reaction studied.

Increasing the initial temperature in split runs below 97°C, had the effect of stripping a greater depth of surface region of vacancies and hence forming more clusters, but with increasing temperature in a given split run, the number of growing nuclei was constant. Thus the variation in the pre-exponential factor disappeared and the "true" activation energy of 18 kcal/mole was obtained.

For aged or annealed salt, cluster formation should be virtually complete and hence the number of growth nuclei would be approximately constant for any initial temperature. Thus the 18 kcal/mole value should be obtained for split or individual runs. This was found to be so.

Above 97°C, a second type of growth nucleus arises from aggregation of 'bulk' vacancies into clusters. Split runs with $T_1 < 97°C$ and $T_2 > 97°C$, meant that while the number of growth nuclei in the surface region was fixed by

T_1/...

T_1, at T_2 'bulk' nuclei made a contribution. Above 112°C, the number of 'bulk' nuclei was fixed. In individual runs above 97°C (up to 112°C), the nucleus population was fixed by the temperature of the run and an apparent activation energy of 35 kcal/mole was obtained. Above 112°C, the "true" value was obtained.

The thermal decomposition, below 97°C, of CaN_6 pre-irradiated with UV-light, showed differences between the aged and the freshly-prepared material. The cubic rate constant, k, increased with dose up to a saturation value, which was higher for fresh material. The explanation given for the increase in k, was that the number of growth nuclei is larger since irradiation produces both additional anion vacancies and electrons for activation of clusters. For fresh material, 'bulk' clusters within the radiation/exciton penetration range are activated, increasing the total number of active nuclei.

The period t_o decreases similarly with dose for both fresh and aged material. This period was regarded as being related to the slow growth of clusters, and irradiation was thought to cause growth of clusters as well as formation.

For aged material the range of applicability of the cubic power law decreased with dose. This was explained as being due to earlier coalescence of the increased concentration of surface nuclei. In fresh material, however, this range was increased and it was stated that this was caused by the influence of 'bulk' nuclei, thought to be located at topographical sites which made overlap or coalescence improbable.

For individual runs above 97°C, on pre-irradiated fresh material, the range of the cubic power law decreases virtually to zero with increasing dose.

In/...

In lightly irradiated material above 97°C, the increased number of nuclei in the surface region was large in comparison with the number of 'bulk' nuclei and the power law held with an activation energy of 18 kcal/mole.

At higher doses the number of 'bulk' nuclei is large too, and the growth mechanism changes as clusters form 'contracting' envelopes. The activation energy was still 18 kcal/mole.

Much of the reasoning of Tompkins and Young hinges on plots in region A, i.e. temperatures below 97°C, where 3 to 5 points are used to define a line. Conclusions are then drawn from the velocity constants, regarding the change in magnitude of the pre-exponential factor as the initial temperature in split runs is altered. This does not seem possible in view of the irreproducibility from one interrupted run to another.

The mechanism put forward to explain the third power law analysis, was that of three-dimensional growth of a fixed number of nuclei. However, as reported in this thesis, the effect of water vapour on a partially decomposed specimen discounts this.

For runs above 112°C, Tompkins and Young state that for all specimens and both types of run, individual and interrupted (split), an activation energy of 18 kcal/mole should be obtained. Later, however, this is contradicted in that it is stated that individual runs above 97°C lead to an activation energy of 35 kcals/mole, while for lightly irradiated material above 97°C, an activation energy of 18 kcal/mole will result.

The activation energy was not ascribed to any particular process.

No/...

No ageing effect was observed in the preparation used in the present study. A specimen that had been stored for 12 months in vacuum over P_2O_5 in the dark, was annealed in a vacuum for 24 hours at 60°C. The variation of velocity constants over the same temperature range as before (105 - 130°C), led to activation energies, with values from the "fresh" material in brackets for comparison, of: [369]

Induction Period : 20.6 kcal/mole (18.2 kcal/mole).
Acceleratory Reaction: 26.9 kcal/mole (27.1 kcal/mole).
Decay Reaction : 21.0 kcal/mole (18.8 kcal/mole).

In addition the activation energy for the acceleratory period was determined using the above 12 month old specimen and the "split-run" method. The value obtained was 26.4 kcals/mole [369]. According to the paper of Tompkins and Young, the value should have been $\sim$ 18 kcal/mole.

Andreev [355] worked over the temperature range 60 - 150°C and apparently obtained a high proportion of nitride as decomposition product. He reported irreproducibility of rate constants and proceeded to determine the activation energy for the acceleratory reaction, using split runs and defining a line with two points. His values varied from 20.8 kcal/mole (81 - 61°C) to 27 kcal/mole (106 - 93°C). The latter value is in agreement with the value of 27.1 kcal/mole obtained in the present study.

Marke [356] also reported irreproducibility using a ground sample. His plots of log k_1 and log k_2 against $1/T^{\circ}K$, lie in a broad band, from which, by the method of least squares, he obtained values of 18 kcal/mole for the acceleratory reaction and 19 kcal/mole for the decay reaction. (Over the range 84 - 98°C).

Garner and Reeves [357] using a split run method and material in the form of whole agglomerates, found activation energies, over the range 82 - 102°C, of 18.5 kcal/mole (acceleratory reaction) and 17.8 kcal/mole (decay reaction). These values were in agreement with those found by Marke. Again, reproducibility for the whole agglomerates was not good. Although a study of the effect of UV-irradiation on the thermal decomposition was made, no activation energies for the reactions involving the irradiated material, were reported.

It is not possible, with the available explanation to find a reason for the discrepancies which occur in the evaluation of the activation energy of the acceleratory period. However it seems that perhaps the method of preparation of the azide may determine the value obtained - it is significant that Tompkins and Young used material which had been precipitated by the addition of alcohol. Work is to be undertaken in these laboratories to study this possibility.

8. S U M M A R Y.

One of the primary objects of this research was to determine, if possible, the nature of the radiation damage prior to thermal decomposition. The X-ray study has not wholly achieved this although more information has been derived from it than from similar work on $AgMnO_4$. However, the diffuse reflections obtained do indicate, quite strongly, the creation of point defects during irradiation. This is of value since such assumptions have been made in the explanation of the kinetics of decomposition of a number of irradiated solids (BaN_6,CaN_6). In addition the X-ray work has suggested future research which should produce useful information; namely, a precise study of the diffuse reflections.

Another object of the research was to attempt to determine what characteristics, if any, of the kinetics of the decomposition of an unirradiated solid would predetermine a marked irradiation effect. It is obvious that the type of nuclear growth which occurs e.g. branching chain, or power law, does not characterise a substance with regard to a possible irradiation effect. The photosensitivity, or otherwise, also does not determine whether there will be an irradiation effect. However, the one property that the substances which have been studied, have in common, is a polyatomic anion, but here again ammonium dichromate does not show an acceleration of the decomposition after irradiation. Consequently it is considered that it is not possible to say, a priori, whether a solid will undergo an accelerated decomposition after irradiation. Each new solid, unless it belongs to a particular class e.g. the alkaline earth azides, must be considered afresh.

Nevertheless/...

Nevertheless it does appear that the irradiation effect can take two forms:-

(i) the production of an unstable compound e.g. nickel oxalate, the decomposition of which affects the normal pyrolysis; and

(ii) the production of point defects which determine the nature of the subsequent thermal decomposition e.g. CaN_6. It is possible that the effect requires an interaction of the created point defects with the existing line defects.

9. B I B L I O G R A P H Y.

1. Wischin - Proc. Roy. Soc. A 172 (1939) 314
2. Young and Tompkins - Trans. Far. Soc. 52 (1956) 1245
3. Bartlett, Tompkins and Young - J. Chem. Soc.(1956) 3323
4. Fischbeck and Spengler - Z. Anorg. Chem. 241 (1939) 209
5. Garner and Hailes - Proc. Roy. Soc. A 139 (1933) 576
6. Finch, Jacobs and Tompkins - J. Chem. Soc.(1954)2053
7. Hill - Trans. Far. Soc. 54 (1958) 685
8. Prout and Tompkins - Trans. Far. Soc. 40 (1944)488
9. Herley and Prout - J. Phys. Chem. 66 (1962) 961
10. Prout and Tompkins - Trans. Far. Soc. 42 (1946) 482
11. Avrami - J. Chem. Phys. 7 (1939) 1103; 8 (1940) 212; 9 (1941) 177
12. Jacobs and Tompkins - Chemistry of the Solid State - Ed. Garner - (Butterworths 1955)p208
13. Erofeyev - C.R. Acad. Sci. URSS 52 (1946) 511
14. Hume and Colvin - Proc. Roy. Soc. A 125 (1929) 635
15. Jacobs and Tompkins - Chemistry of the Solid State - Ed. Garner - (Butterworths 1955)p203
16. Bradley, Colvin and Hume - Phil. Mag. 14 (1932)1102; Proc. Roy. Soc. A 137 (1932)531
17. Trout and Tompkins - Trans. Far. Soc. 40 (1944) 488
18. Garner and Tanner - J. Chem. Soc. (1930) 47
19. Jacobs and Tompkins - Chemistry of the Solid State - Ed. Garner - (Butterworths 1955)Ch.3
20. Fergusson - Phys. Rev. 66 (1944) 220
21. Frenkel - Phys. Rev. 37 (1931) 17, 276
22. Seitz - Rev. Mod. Phys. 26 (1954) 17
23. Knox - Theory of Excitons (Academic Press 1963)
24. Pohl - Proc. Phys. Soc. Lond. 49 (1937) 3
25. De Boer - Rec. Trav. Chim. Pays-Bas. 56 (1937) 301
26. Spinks and Woods - An Introduction to Radiation Chemistry (Wiley 1964) Ch.3
27. Seitz - Disc. Far. Soc. 5 (1949) 271
28. Huntingdon - Phys. Rev. 93 (1954) 1414

29/...

29. Kohn - Phys. Rev. 94 (1954) 1409

30. Brown and Augustyniak - Bull. Am. Phys. Soc. 2 (1957) 156

31. Gibson, Goland, Milgram and Vineyard - Phys. Rev. 120 (1960) 1229

32. Dienes - Reactivity of Solids - Ed. De Boer - (Elsevier 1961) p.416

33. Vineyard - Disc. Far. Soc. 31 (1961) 10

34. Vineyard - Radiation Damage in Solids - Ed. Billington (Academic Press 1962) p.291

35. Erginsoy - ASTM Spec. Tech. Publ. No.359 (1964) p.79

36. Seitz - Phys. Rev. 61 (1942) 315

37. Kinchin and Pease - Rept. Prog. Phys. 18 (1955) 1

38. Silsbee - J. Appl. Phys. 28 (1957) 1246

39. Bartlett and Dienes - Phys. Rev. 89 (1953) 848

40. Damask, Dienes and Weizer - Phys. Rev. 113 (1959) 781

41. Seitz and Kohler - Solid State Physics 2 (1956) 305

42. Dienes and Vineyard - Radiation Effects in Solids (Interscience 1957) p.17

43. Dienes and Vineyard - ibid. p.48

44. Cleland, Crawford and Holmes - Bull. Am. Phys. Soc. 1 (1956) 135

45. Seitz - Rev. Mod. Phys. 26 (1954) 1

46. Knox - Theory of Excitons - Solid State Physics Suppl. 5 (1963) 172

47. Bauer and Gordon - J. Appl. Phys. 33 (1962) 672

48. Varley - Nature 174 (1954) 886

49. Varley - J. Nucl. Energy 1 (1954) 130

50. Varley - Progress in Nuclear Energy (Pergamon 1956) Vol. 1, Ch. 8

51. Dexter - Phys. Rev. 118 (1960) 934

52. Froelich - Proc. Roy. Soc. A74 (1959) 643

53. Mitchell, Wiegand and Smoluchowski - Phys. Rev. 117 (1960) 442

54. Nowick - Phys. Rev. 111 (1958) 16

55. Howard, Vosko and Smoluchowski - Phys. Rev. 122 (1961) 1406

56. Smoluchowski and Wiegand - Disc. Far. Soc. 31 (1961) 151

57. Durup and Platzman - Disc. Far. Soc. 31 (1961) 156

58/...

58. Bethe and Ashkin - Experimental Nuclear Physics - Ed. Segré - (Wiley 1953) Vol. 1, p.166

59. Burhop - The Auger Effect (C.U.P. 1952)

60. Massey and Burhop - Electronic and Ionic Impact Phenomena - (O.U.P. 1952) Ch.10

61. Sharma and Smoluchowski - Bull. Am. Phys. Soc. 7 (1962) 178

62. Ritz - Proc. of Int. Symp. on Colour Centres in the Alkali Halides - (Stuttgart 1962)

63. Royce - ASTM Spec. Tech. Publ. No.359 (1963) p.98

64. Klick - Phys. Rev. 120 (1960) 760

65. Vineyard - Disc. Far. Soc. 31 (1961) 22

66. Etzel - Phys. Rev. 87 (1952) 906

67. Etzel and Allard - Phys. Rev. Letters 2 (1959) 452

68. Hayes and Nichols - Phys. Rev. 117 (1960) 993

69. Crawford and Nelson - Phys. Rev. Letters 5 (1960) 314

70. van Bueren - Imperfections in Crystals - (North-Holland 1960)

71. Kröger - The Chemistry of Imperfect Crystals (North-Holland 1964) Chap. 8

72. Billington and Crawford - Radiation Damage in Solids (Oxford 1961) Ch. 8

73. Dienes - J. Chem. Phys. 16 (1948) 620

74. Mott and Littleton - Trans. Far. Soc. 34 (1938) 485

75. Keyes - J. Chem. Phys. 29 (1958) 467

76. Mott and Gurney - Electronic Processes in Ionic Crystals - (O.U.P. 1946) p.50

77. Billington and Crawford - Radiation Damage in Solids - (Oxford 1961) Ch. 3

78. Mapother - Phys. Rev. 89 (1953) 1231

79. Cunnel and Schneider - Phys. Rev. 95 (1954) 598

80. Christy and Harte - Phys. Rev. 109 (1958) 710

81. Hacke - Z. Physik 155 (1959) 628

82. Nelson, Sproull and Caswell - Phys. Rev. 90 (1953) 364

83. Seitz - Rev. Mod. Phys. 26 (1954) 7

84. Smoluchowski - Proc. Int. Conf. on Peaceful Uses of Atomic Energy (UNO 1956) Vol. 7 p.676

85. Kobayashi - Phys. Rev. 102 (1956) 348

86. Watkins - Phys. Rev. 113 (1959) 91

87/...

87. Purley - The Hall Effect and Related Phenomena (Butterworths 1960)

88. Delbecq, Smaller and Yuster - Phys. Rev. 111 (1958) 1235

89. Klick and Compton - J. Phys. Chem. Solids 7 (1958) 170

90. Levy - ASTM Spec. Tech. Publ. No.359 (1964) 3

91. Bube - Photoconductivity of Solids (Wiley 1960)

92. Bowers - J. Phys. Chem. Solids 8 (1959) 206

93. Krumhansl - J. Appl. Phys. 30 (1959) 1183

94. O'Reilly - Adv. Catalysis 12 (1960) 31

95. Ludwig and Woodbury - Solid State Physics 13 (1962) 223

96. Portis, Kip, Kittel and Brattain - Phys. Rev. 90 (1953) 988

97. Castner and Känzig - J. Phys. Chem. Solids 3 (1957) 178

98. Feher - Phys. Rev. 103 (1956) 834

99. Feher - Phys. Rev. 105 (1957) 1122

100. Seidel - Z. Physik 165 (1961) 218, 239

101. Lax and Mavroides - Solid State Physics 11 (1960) 261

102. Griffiths, Owen and Ward - Report of the Bristol Conference on Defects in Crystalline Solids (Phys. Soc. London 1955) p.81

103. Gross and Wolf - Naturwissen 48 (1961) 299

104. Ohkura and Murase - J. Phys. Soc. Japan 16 (1961) 2076

105. Sonder - Bull. Am. Phys. Soc. 6 (1961) 114

106. Krumhansl - J. Phys. Chem. Solids 8 (1959) 343

107. Mielczarek and Frederikse - Phys. Rev. 115 (1959) 888

108. Gebhardt - J. Phys. Chem. Solids 23 (1962) 1123

109. Lin - Phys. Rev. 102 (1956) 968

110. Rabin - Phys. Rev. 116 (1961) 1381

111. Esterman, Leivo and Stern - Phys. Rev. 75 (1949) 627

112. Witt - Nachr. Göttingen Nr. 4 (1952) 17

113. Wiegand - Proc. Int. Symp. on Colour Centres in Alkali Halides (Stuttgart, Germany 1962)

114. Nadeau - Bull. Am. Phys. Soc. 7 (1962) 210

115. Müller - Reactivity of Solids - Ed. De Boer - (Elsevier 1961) p.682

116. Mehmed - J. Chem. Phys. 38 (1963) 607

117. Allen - J. Phys. Chem, Solids 19 (1961) 87

118/...

118. Guinier - X-ray Diffraction (Freeman 1963) p.152

119. James - The Optical Principles of the Diffraction of X-rays
- The Crystalline State Vol.2 (Bell 1962) Ch.5

120. Wooster - Diffuse X-ray Reflections from Crystals
- (C.U.P. 1962) Ch.1,2,3

121. Wooster - Ibid Ch.4

122. Wilson - Acta Cryst. 5 (1952) 318

123. Willis - Proc. Roy. Soc. A239 (1957) 184

124. Suzuki and Willis - Nature 177 (1956) 712

125. Wilson - Nuovo Cimento 1 (1955) 277

126. Vassamillet - Nuovo Cimento 13 (1959) 1133

127. Webb - Direct Observation of Imperfections in Crystals
Ed. Newkirk and Wernick (Interscience 1961) p.29

128. Azaroff - Advanced Methods of Crystallography -
Ed. Ramachandran - (Academic Press 1964) p.256

129. Zachariasen - Theory of X-ray Diffraction in Crystals
(Wiley 1945) p.213

130. Huang - Proc. Roy. Soc. A190 (1947) 102

131. Eshelby - J. Appl. Phys. 25 (1954) 255

132. Sampson and Tucker - Phys. Rev. 105 (1957) 1117

133. Ekstein - Phys. Rev. 68 (1945) 120

134. Matsubara - J. Phys. Soc. Japan 7 (1952) 270

135. Cochran - Acta Cryst. 9 (1956) 259

136. Cochran and Kartha - Acta Cryst. 9 (1956) 941, 944

137. Kanzaki - J. Phys. Chem. Solids 2 (1957) 24, 107

138. Chang - J. Phys. Chem. Solids 25 (1964) 1081

139. Warren, Averbach and Roberts - J. Appl. Phys. 22 (1951) 1493

140. Herbstein, Borie and Averbach - Acta Cryst. 9 (1956) 466

141. Borie - Acta Cryst. 10 (1957) 89

142. Dienes and Vineyard - Radiation Effects in Solids
- (Interscience 1957) p.114

143. Crawford and Wittels - Proc. of the Int. Conference on the
Peaceful Uses of Atomic Energy
(UNO 1956) Vol.7 p.654

144. Guinier - X-ray Diffraction - (Freeman 1963) p.161

145. Guinier - Ibid Ch. 6

146. Wooster - Advanced Methods of Crystallography
- Ed. Ramachandran - (Academic Press 1964) p.121

147/...

147. Lipson and Taylor - Acta Cryst. 4 (1951) 261, 458

148. Tucker and Senio - Acta Cryst. 7 (1954) 456

149. Tucker and Senio - Acta Cryst. 8 (1955) 371

150. Tucker and Senio - Phys. Rev. 99 (1955) 1777

151. Herbstein and Averbach - Acta Metallurg. 4 (1956) 407

152. Primak - Phys. Rev. 92 (1953) 1064; 95 (1954) 837

153. Keating - Phys. Rev. 98 (1955) 1859

154. Weissman and Nakajuma - J. Appl. Phys. 34 (1963) 611

155. Estermann, Leivo and Stern - Phys. Rev. 75 (1949) 627

156. Sakaguchi and Suita - Technol. Repts. Osaka Univ. 2 (1952)177

157. Berry - Phys. Rev. 98 (1955) 934, 1540

158. Wiegand - Phys. Rev. Letters 9 (1962) 201

159. Rabin - Phys. Rev. 116 (1959) 1381

160. Peisl - Z. Angew. Physik. 14 (1962) 529

161. Seitz - Rev. Mod. Phys. 26 (1954) 7-94

162. Lin - Phys. Rev. 102 (1956) 968

163. Primak, Delbecq and Yuster - Phys. Rev. 98 (1955) 1708

164. Wiegand and Smoluchowski - Phys. Rev. 110 (1958) 991

165. Merriam, Wiegand and Smoluchowski - J. Phys. Chem. Solids 25 (1964) 273

166. Etzel - Phys. Rev. 100 (1955) 1643

167. Chynoweth - Phys. Rev. 113 (1959) 159

168. Okada - J. Phys. Soc. Japan 15 (1960) 363

169. Toyoda, Shimada and Tanaka - J. Phys. Soc. Japan 15 (1959) 536

170. Boutin and Frazer - J. Phys. Chem. Solids 24 (1963) 341

171. Krueger, Cook, Sartain and Yockey - J. Appl. Phys. 34 (1963) 218

172. Cook and Cushing - Acta Met. 1 (1953) 539

173. Blewitt and Coltmann - Acta Met. 2 (1954) 549

174. Adam, Green and Dugdale - Phil. Mag. 43 (1952) 1216

175. Krause - Z. Krist. 115 (1961) 413

176. Krause - J. Chem. Phys. 39 (1963) 1706

177. Keating and Kasner - J. Phys. Chem. Solids 20 (1961) 150

178/...

178. Aźaroff - Crystallography and Crystal Perfection - Ed. Ramachandran (Academic Press 1963) p.109

179. Aźaroff - Progress in Solid State Chemistry (Pergamon 1963) Vol. 1. p.347

180. Schwuttke - Direct Observations of Imperfections in Crystals - Ed. Newkirk and Wernick (Interscience 1961) p.497

181. Int. Conference on Crystal Physics - Rev. Mod. Phys. 30 (1958) 47-68

182. Cochran - Ibid - p.47

183. Attard and Azároff - J. Appl. Phys. 34 (1963) 774

184. Mohanty and Azároff - J. Chem. Phys. 35 (1961) 1268

185. Mohanty and Azároff - Phys. Rev. 120 (1960) 1224

186. Azároff - Advanced Methods of Crystallography - Ed. Ramachandran - (Academic Press 1964) p.251

187. Woods - M.Sc. Thesis (Rhodes University 1962)

188. Prout and Woods - ASTM Spec. Tech. Publ. No.359 (1964)p.50

189. Boldyrev and Bystrykh - Russian Chem. Rev. 32 (1963) 426

190. Forty - Brit. J. Appl. Phys. 14 (1963) 3

191. Herley and Prout - J. Am. Chem. Soc. 82 (1960) 1540

192. Flanagan - J. Phys. Chem. 66 (1962) 416

193. Prout - J. Inorg. Nucl. Chem. 7 (1958) 368

194. Dienes and Vineyard - Radiation Effects in Solids (Interscience 1957) p.144

195. Fletcher and Brown - Phys. Rev. 92 (1953) 585

196. Prout and Herley - J. Phys. Chem. 66 (1962) 961

197. Simpson and Taylor - J. Chem. Soc. (1958) 2378

198. Boldyriev and Oblivantsev - Kinetika i Kataliz - Akad. Nauk. SSSR, Moskva 3 (1962)887

199. Boldyriev - Russian Chem. Rev. 32 (1963) 426

200. Boldyriev - Izd. Akad. Nauk. SSSR (1962) 42

201. Freeman and Anderson - ASTM. Spec. Tech. Publ. No.359 (1964) p.58

202. Galwey and Jacobs - Proc. Roy. Soc. A254 (1960) 455

203. Galwey and Jacobs - J. Chem. Soc. (1959) 837

204. Freeman, Anderson and Campisi - J. Phys. Chem. 64 (1960) 1727

205. Bircumshaw and Newman - Proc. Roy. Soc. A227 (1955) 228

206/...

206. Freeman and Anderson - ASTM. Spec. Tech. Publ. No.359 (1964) p.65

207. Freeman and Anderson - J. Phys. Chem. 65 (1961) 1662

208. Zirkind and Freeman - Nature 199 (1963) 1280

209. Hyde and Freeman - J. Phys. Chem. 65 (1961) 1636

210. Cole - J. Chem. Phys. 35 (1961) 1169

211. Petricciani, Wiberley, Bauer and Clapper - J. Phys. Chem. 64 (1960) 1309

212. Cassel and Liebman - J. Chem. Phys. 34 (1961) 343

213. Jach - Reactivity of Solids - Ed. De Boer - (Elsevier 1961) p.334

214. Cobble and Boyd - J. Phys. Chem. 63 (1959) 919

215. Harty and Moulton - Phys. Rev. 116 (1959) 1459

216. Haynes and Young - Disc. Far. Soc. 31 (1961) 229

217. Boldyriev - Doklady Akad. Nauk. SSSR 129 (1959) 365

218. Sviridov and Branitskii - Khim. i. Khim. Tekhnol 7 (1964)691

219. Boldyriev - Izd. Akad. Nauk. SSSR. (1962) 42

220. Herley and Prout - Nature 184 (1959) 445

221. Young - J. Chem. Soc. (1960) 4533

222. Evans, Yoffe and Gray - Chem. Rev. 59 (1959) 515

223. Gray - Quart. Rev. 17 (1963) 441

224. Bowden and Yoffe - Endeavour 21 (1962) 125

225. Garner and Moon - J. Chem. Soc. (1933) 1398

226. Maggs - Trans. Far. Soc. 35 (1939) 433

227. Garner and Reeves - Ibid 51 (1955) 694

228. Jacobs and Tompkins - Proc. Roy. Soc. A215 (1952) 265

229. Bowden and Singh - Ibid A227 (1954) 22

230. Prout - Nature 183 (1959) 884

231. Boldyriev and Skorik - Fiz. Shchelochnogaliodnykh Kristallov, Riga (1961) 527

232. Jach - Trans. Far. Soc. 59 (1963) 947

233. Prout and Moore - Nature 203 (1964) 860

234. Prout and Moore - Nature 205 (1965) 1209

235. Prout - Nature 183 (1959) 884

236. Jacobs, Tompkins and Young - Disc. Far. Soc. 28 (1959) 234

237/...

237. Boldyriev - Russian Chem. Rev. 32 (1963) 426

238. Seitz - Rev. Mod. Phys. 26 (1954) 17

239. Kalm and Kittel - Phys. Rev. 89 (1953) 315

240. Mott - Proc. Roy. Soc. A172 (1939) 326

241. Mott and Gurney - Electronic Processes in Ionic Crystals 2nd Edn. (O.U.P. 1948) p.231, 265

242. Mott and Schneider - Photographic Sensitivity (Butterworths 1951) p.13

243. Mitchell - Chemistry of the Solid State - Ed. Garner - (Butterworths 1955) p.321

244. Grimley and Mott - Disc. Far. Soc. 1 (1947) 3

245. Burrow and Mitchell - Phil. Mag. 45 (1954) 208

246. Thomas and Tompkins - Proc. Roy. Soc. A209 (1951) 550

247. Thomas and Tompkins - J. Chem. Phys. 20 (1952) 662

248. Jacobs and Tompkins - Proc. Roy. Soc. A215 (1952) 254

249. Heal - Canad. J. Chem. 31 (1953) 91

250. Heal - Canad. J. Chem. 31 (1953) 1153

251. Jacobs, Tompkins and Young - Disc. Far. Soc. 28 (1959) 234

252. Baidins - Disc. Far. Soc. 28 (1959) 248

253. Deb - J. Chem. Phys. 35 (1961) 2122

254. Jacobs, Tompkins and Pai Verneker - J. Phys. Chem. 66 (1962) 1113

255. Tompkins and Young - Proc. Roy. Soc. A236 (1956) 10

256. Cunningham and Tompkins - Proc. Roy. Soc. A251 (1959) 27

257. Dodd - J. Chem. Phys. 35 (1961) 1815

258. Miller - J. Chem. Phys. 40 (1964) 2371

259. Carlson - J. Chem. Phys. 39 (1963) 1206

260. Johnson - ASTM Spec. Tech. Publ. No.359 (1964) 71

261. Chen and Johnson - J. Phys. Chem. 66 (1962) 2248

262. Allen and Ghormley - J. Chem. Phys. 15 (1947) 208

263. Doigan and Davis - J. Phys. Chem. 56 (1952) 764

264. Hennig, Lees and Matheson - J. Chem. Phys. 21 (1953) 664

265. Prince - Thesis, Stephens Institute of Technology, Hoboken N.J.

266. Cunningham and Heal - Trans. Far. Soc. 54 (1958) 1334

267. Hochandel and Davis - J. Chem. Phys. 27 (1957) 333

268/...

268. Johnson and Forten - Disc. Far. Soc. 31 (1961) 238

269. Boyd, Graham and Larson - J. Phys. Chem. 66 (1962) 300

270. Boldyrev, Oblivantsev and Lykhin - Dokl. Akad. Nauk. SSSR 159 (1964) 1113

271. Logan and Moore - J. Phys. Chem. 67 (1963) 1042

272. Zeldes and Livingston - J. Chem. Phys. 35 (1961) 563

273. Prout - Unpublished work.

274. Simpson and Taylor - J. Chem. Soc. (1958) 2378

275. Prout and Tompkins - Trans. Far. Soc. 40 (1944) 488

276. Prout - J. Inorg. Nucl. Chem. 7 (1958) 368

277. Prout and Herley - Nature 188 (1960) 717

278. Herley - Ph.D. Thesis (Rhodes University 1961)

279. Prout and Woods - ASTM. Special Technical Publication No.359 (1964) p.50

280. Woods - M.Sc. Thesis (Rhodes University 1962)

281. Prout and Tompkins - Trans. Far. Soc. 42 (1946) 482

282. Jacobs and Tompkins - Chemistry of the Solid State - Ed. Garner (Butterworths 1955) p.196

283. Mooney - Phys. Rev. 37 (1935) 1306

284. James and Wood - Proc. Roy. Soc. A109 (1925) 598

285. Basche and Mark - Ziets. f. Krist. 64 (1926) 1

286. Wyckoff - The Structure of Crystals (Reinhold 1935) p.72

287. Wyckoff - Crystal Structures (Interscience 1951) Vol. II, Table VIII A, 10

288. Int. Tables of X-ray Crystallography, Vol. I. - Ed. Lonsdale (Kynoch 1952) p.63,370

289. Ramaseshan, Venkatesan and Mani - Proc. Indian Acad. Sci. A46 (1957) 95

290. Int. Tables for X-ray Crystallography, Vol. I - Ed. Lonsdale (Kynoch 1952) p.151

291. Buerger - Crystal Structure Analysis - (Wiley 1960) pp. 288, 441, 462, 473

292. Int. Tables for X-ray Crystallography, Vol. I - Ed. Lonsdale (Kynoch 1952) p.63,370

293. Nassimbeni - M.Sc. Thesis (Rhodes University 1963)

294. Dawton - Proc. Phys. Soc. 50 (1938) 419

295. Buerger - Crystal Structure Analysis (Wiley 1960) p.596

296. Ibid. p.105

297/...

297. Wiebenga and Smits - Acta Cryst. 3 (1950) 265

298. Monteath Robertson - J. Sci. Instr. 20 (1943) 175

299. Woods - M.Sc. Thesis (Rhodes University 1962) p.50

300. Buerger - Crystal Structure Analysis (Wiley 1960) p.130

301. Buerger - X-ray Crystallography (Wiley 1942) p.256, Fig. 140A

302. Bullen - Acta Cryst. 6 (1953) 825

303. Jeffrey and Rose - Acta Cryst. 17 (1964) 343

304. Lange - Handbook of Chemistry (McGraw Hill 10th Edn.1961) p.292

305. Buerger - Crystal Structure Analysis (Wiley 1960) p.206

306. Int. Tables for X-ray Crystallography, Vol. II, - Ed. Lonsdale (Kynoch 1959) p.295

307. Waller - Ann. Physik 83 (1927) 153

308. Buerger - Crystal Structure Analysis (Wiley 1960) p.231

309. Nassimbeni - M.Sc. Thesis (Rhodes University 1963) p.101

310. Int. Tables for X-ray Crystallography, Vol. II - Ed. Lonsdale (Kynoch 1959) p.241

311. Buerger - Crystal Structure Analysis (Wiley 1960) p.554

312. Buerger - Vector Space (Wiley 1959) Ch.2

313. Beevers and Lipson - Phil. Mag. 17 (1934) 855
Nature 137 (1936) 825
Proc. Phys. Soc. Lond. 48 (1936) 772

314. Buerger - Crystal Structure Analysis (Wiley 1960) p.495

315. Nassimbeni - M.Sc. Thesis (Rhodes University 1963)

316. Int. Tables for X-ray Crystallography - Ed. Lonsdale - Vol.III (1962) p.204

317. Ibid. Vol. II (1959) p.382

318. Lange - Handbook of Chemistry - (Mcgraw-Hill-10th Edn.1961) p.108

319. Buerger - The Precession Method - (Wiley 1964) p.58

320. Buerger - X-ray Crystallography (Wiley 1942) p.426

321. Henry, Lipson and Wooster - The Interpretation of X-ray Diffraction Photographs (Macmillan 2nd Edn. 1963) Ch.13 p.194

322. Nassimbeni - M.Sc. Thesis (Rhodes University 1963) p.63

323. Bradley and Jay - Proc. Phys. Soc. 44 (1932) 563; 45 (1933) 507

324. Buerger - X-ray Crystallography (Wiley 1942) p.414

325/...

325. Taylor and Sinclair - Proc. Phys. Soc. 57 (1944) 126

326. Parrish - Acta Cryst. 13 (1960) 838

327. Nelson and Riley - Proc. Phys. Soc. 57 (1945) 160

328. Lonsdale - Acta Cryst. 3 (1950) 400

329. James - The Optical Principles of the Diffraction of X-rays - Crystalline State, Vol.2 (Bell 1962) p.245

330. Bunn - Chemical Crystallography - (Oxford 2nd Edn. 1961)p.110

331. Lonsdale and Smith - Proc. Roy. Soc. A179 (1941) 27

332. Kanazaki - J. Phys. Chem. Solids 2 (1957) 107

333. Herley - M.Sc. Thesis (Rhodes University 1959)

334. Prout and Herley - J. Chem. Ed. 37 (1960) 643

335. Jacobs and Kureishy - Reactivity of Solids - Ed. De Boer - (Elsevier 1961) p.352

336. Avrami - J. Chem. Phys. 9 (1941) 177

337. Erofeyev - Compt. Rend. Acad. Sci. URSS 52 (1946) 511

338. Allen and Scaife - J. Phys. Chem. 58 (1954) 667

339. Danes and Ponec - Coll. Czech. Chem. Comm. 23 (1958) 858

340. Prout and Tompkins - Trans. Far. Soc. 40 (1944) 488

341. Tompkins - South African Inductrial Chemist 17 (1963) 62

342. Jagodzinski - Advanced Methods of Crystallography - Ed. Ramachandran - (Academic Press 1964) p.181

343. Bragg - The Crystalline State, Vol.I - (Bell 1955) p.202

344. Moles and Gonzalez - Anales Fis. Quim. 21 (1923) 204

345. Ball - J. Chem. Soc. (1909) 87

346. Harbard and King - J. Chem. Soc. (1938) 955

347. Fischbeck and Springler - Z. Anorg. Chem. 235 (1938) 183; 241 (1939) 209

348. Jacobs and Tompkins - Chemistry of the Solid State - Ed. Garner - (Butterworths 1955) p.201

349. Taylor - J. Chem. Soc. (1955) 1033

350. Simpson and Taylor - J. Chem. Soc. (1958) 2378

351. Prout and Tompkins - Trans. Far. Soc. 40 (1944) 488

352. Bartlett, Tompkins and Young - J. Chem. Soc. (1956) 3323

353. Tompkins and Young - Disc. Far. Soc. 23 (1957) 202

354. Erofeyev - Reactivity of Solids - Ed. De Boer - (Elsevier 1961) p.273

355/...

355. Andreev - Physik. Z. Soviet Union 6 (1934) 1121

356. Marke - Trans. Far. Soc. 33 (1937) 770

357. Garner and Reeves - Trans. Far. Soc. 51 (1955) 694

358. Tompkins and Young - Disc. Far. Soc. 23 (1957) 202

359. Inorganic Syntheses, Vol. I - Ed. Booth - (McGraw-Hill 1939) p.77

360. Vogel - Quantitative Inorganic Analysis - (Longmans 3rd Edn. 1961) p.473

361. Prout and Moore - ASTM Symposium on "The Effects of High Energy Radiation on Inorganic Solids". - Seattle, 1965

362. Nuegebauer-(Ed) - The Structure and Properties of Thin Films - (Wiley 1959) pp.39,53,244

363. Heal - Trans. Far. Soc. 53 (1957) 210

364. Prout and Moore - Nature 203 (1964) 860

365. Prout and Moore - Nature 205 (1965) 1209

366. Gray - Quart. Rev. 17 (1963) 453

367. Wyckoff - Crystal Structures - (Interscience 1948) Vol. I, Ch. II, Table p.5

368. Tompkins and Young - Trans. Far. Soc. 61 (1965) 1470

369. Private Communication from D.J. Moore, Rhodes University.